TECHNISCHE UNIVERSITÄT MÜNCHEN

TUM School of Engineering and Design

Methodological and Application-Oriented Advances in Sensitivity Analysis with a Focus on Structural Engineering

Martin Fußeder

Vollständiger Abdruck der von der TUM School of Engineering and Design der Technischen Universität München zur Erlangung eines

Doktors der Ingenieurwissenschaften (Dr.-Ing.)

genehmigten Dissertation.

Vorsitz:

Prof. Dr. Daniel Straub

Prüfer der Dissertation:

1. Prof. Dr.-Ing. Kai-Uwe Bletzinger
2. Prof. Dr.-Ing. habil. Manfred Bischoff
3. Prof. Dr.-Ing. Tim Ricken

Die Dissertation wurde am 18.03.2024 bei der Technischen Universität München eingereicht und durch die TUM School of Engineering and Design am 31.05.2024 angenommen.

Schriftenreihe des Lehrstuhls für Statik
TU München

Band 64

Martin Fußeder

Methodological and Application-Oriented Advances in Sensitivity Analysis with a Focus on Structural Engineering

München 2024

Veröffentlicht durch

Kai-Uwe Bletzinger
Lehrstuhl für Statik
Technische Universität München
Arcisstr. 21
80333 München

Telefon: +49(0)89 289 22422
Telefax: +49(0)89 289 22421
E-Mail: kub@tum.de
Internet: www.cee.ed.tum.de/st/startseite/

ISBN: 978-3-943683-75-2

Abstract

This thesis addresses methodological developments of sensitivity analysis. While sensitivity analysis is an established field of research and is successfully employed in use cases such as gradient-based optimization, there are only a few applications and associated research concerning structural engineering. To exploit the great potential of sensitivity analysis also in this application field, the advancements presented in the dissertation are developed with a particular focus on structural engineering. For this purpose, the work considers analysis approaches and special simulation cases specific to structural engineering.
The influence function approach, a well-known technique in structural analysis, is closely related to adjoint sensitivity analysis. Based on this connection, the thesis shows how the method of influence functions can be generalized. The outcome is an engineering tool for sensitivity analysis, which can consider various kinds of responses, parameters, structures, and physics. The relationship between influence functions and adjoint sensitivity analysis is discussed in detail. It is demonstrated how influence functions can be identified as part of the adjoint sensitivity equations. Furthermore, the thesis explores the significance of the generalized influence function method in the case of general responses and parameters in different structures. This highlights the potential of the approach but also its limitations and particularities. Finally, the concepts developed for structural mechanics are applied to steady state heat transfer to investigate their generalizability.
Another introduced methodological advance is the application of sensitivity analysis to sequenced simulation processes. In structural engineering, these are necessary for conducting construction stage analysis or for the multi-stage design process of lightweight structures. The thesis investigates how sensitivity analysis needs to be extended to account for the transition from one analysis stage to the next. On this basis, the sensitivity equations are adapted for construction stage analysis and the design process of lightweight structures. It can be seen in both cases that the complexity of the sensitivity equations and the computational effort required to evaluate them is significantly higher than in a one-step analysis.
Finally, the application of sensitivity analysis as a tool for structural design is demonstrated. For this purpose, the thesis discusses the processing and interpretation of sensitivities for practical use. On this basis, analysis models of real-world engineering structures are examined. The examples show how sensitivity analysis can support structural design in a valuable and goal-oriented way.

Kurzfassung

Diese Arbeit befasst sich mit methodischen Weiterentwicklungen der Sensitivitätsanalyse. Obwohl Sensitivitätsanalysen ein etabliertes Forschungsgebiet sind und in Anwendungsfällen wie der gradientenbasierten Optimierung erfolgreich eingesetzt werden, finden diese in der Tragwerksplanung bisher kaum Beachtung. Auch gibt es nur wenige Forschungsarbeiten mit diesem Anwendungsschwerpunkt. Um das große Potential der Sensitivitätsanalyse für die Tragwerksplanung stärker zu erschließen und aufzuzeigen, beschäftigt sich diese Arbeit mit der Weiterentwicklung von Sensitivitätsanalysen mit speziellem Fokus auf die Tragwerksberechnung. Dies spiegelt sich durch den Einbezug baustatischer Methoden und der Berücksichtigung von speziell in der Tragwerksplanung verwendeten Modellierungsansätzen wider.

Die Technik der Einflussfunktionen ist eine etablierte Berechnungsmethode der Statik und ist eng mit der adjungierten Sensitivitätsanalyse verbunden. Auf der Grundlage dieser Beziehung diskutiert die Arbeit, wie die Methode der Einflussfunktionen zu einem Berechnungswerkzeug für Sensitivitäten verallgemeinert werden kann. Der klassische baustatische Ansatz wird so für verschiedenste Antwortgrößen, Parameter, Strukturen und physikalische Probleme erweitert. Die Beziehung zwischen Einflussfunktionen und adjungierter Sensitivitätsanalyse wird im Detail diskutiert. Insbesondere wird gezeigt, wie die Einflussfunktion als Zwischenergebnis der adjungierten Sensitivitätsanalyse identifiziert werden kann. Darüber hinaus wird die Anwendung der Methode der verallgemeinerten Einflussfunktionen für generelle Antwortgrößen und Parameter in verschiedenen Strukturen untersucht. Dabei zeigt sich der Nutzen und die Aussagekraft des Ansatzes, aber auch seine Grenzen und Besonderheiten. Abschließend werden die auf einer strukturmechanischen Basis entwickelten Konzepte auf stationäre Wärmeübertragungsprobleme angewendet, um deren Verallgemeinerbarkeit zu demonstrieren.

Im Allgemeinen werden Bauwerke in einer Vielzahl von aufeinanderfolgenden Bauabschnitten errichtet. In der statischen Berechnung kann der Bauablauf durch Baufortschrittsmodelle berücksichtigt werden, die einen sequenziellen Simulationsprozess erfordern. Ähnliche mehrstufige Analysen finden auch beim Entwurfsprozess von Leichtbaustrukturen Anwendung. In dieser Arbeit wird untersucht, wie die Sensitivitätsanalyse zur Berücksichtigung von sequenziellen Simulationsprozessen adaptiert werden muss. Ausgehend von grundlegenden Erweiterungen der Sensitivitätsanalyse für den Übergang von einer Analysestufe zur nächsten werden die Sensitivitätsgleichungen für Baufortschrittsmodelle und den Entwurfsprozess von Leichtbaustrukturen angepasst. In beiden Anwendungsfällen zeigt sich, dass die Komplexität der Sensitivitätsgleichungen und der Rechenaufwand zu ihrer Lösung deutlich höher ist als bei einer einstufigen Analyse.

Abschließend setzt sich die Arbeit mit der Anwendung von Sensitivitätsanalysen in der Planung und Bemessung von Tragwerken auseinander. Hierfür wird die weitere Aufbereitung und Interpretation von Sensitivitäten für den praktischen Einsatz diskutiert. Auf dieser Grundlage werden Berechnungsmodelle von realen Ingenieurbauwerken untersucht. Die Beispiele zeigen, wie Sensitivitätsanalysen die Tragwerksplanung zielführend unterstützen können.

Acknowledgements

This thesis was written from 2018 to 2024 during my time as a research and teaching associate at the Chair of Structural Analysis (Lehrstuhl für Statik) at the Technical University of Munich.
First of all, I would like to express my gratitude to Prof. Dr.-Ing. Kai-Uwe Bletzinger for the opportunity to work in his group. I want to thank him not only for the chance to research in the rewarding field of sensitivity analysis but also for his support, the numerous inspiring discussions, his confidence to work with a high level of freedom, and the opportunity to teach with him. My time at the chair has significantly contributed to my academic and personal development. I am very grateful to Prof. Bletzinger for the excellent working environment.
I would like to thank Prof. Dr.-Ing. habil. Manfred Bischoff and Prof. Dr.-Ing. Tim Ricken for completing my board of examiners and Prof. Dr. Daniel Straub for the organization. Their interest in my work is gratefully acknowledged.
I would like to thank Prof. Dr.-Ing. habil. Roland Wüchner for many valuable discussions that have enriched this work. Furthermore, I would like to acknowledge Dr.-Ing. Christian Mühlbauer for being my mentor during my time as a doctoral candidate. Thanks also to Dr.-Ing. Frank Breinlinger for providing analysis models of real structures in order to examine them with sensitivity analysis.
I would like to thank all my colleagues at the Chair of Structural Analysis for our friendly environment and pleasant time together. Among them, I want to acknowledge my teaching assistant colleagues Veronika Singer, Dr.-Ing. Ann-Kathrin Goldbach, and Dr.-Ing. Klaus B. Sautter for their excellent cooperation. Furthermore, there are Manuel Meßmer, Philipp Bucher, and Dr.-Ing. Thomas Oberbichler, who made my time very pleasant by having good conversations about technical issues and private matters. I want also like to mention my longtime roommate Stefan Grabke. Thank you, Stefan, for the great time we spent together! Thanks also to Max Teichgräber for the fruitful collaboration on the GruSiBau project and our joint publications.
My deepest gratitude goes to my family, especially my parents Marianne and Johann Fußeder, who have supported me through all chapters of my life.

Thank you!

Martin Fußeder
Munich
July, 2024

Contents

Chapter 1

Introduction

The civil engineer and computer pioneer *Konrad Zuse* began his developments with the motivation to carry out time-consuming static calculations with machines. Today, this vision is a reality: combining powerful computers and numerical techniques such as the finite element method makes it possible to analyze complex structures. This has led to modeling and model evaluation becoming key parts of structural design as computers carry out the calculations. A deep understanding of the used model is therefore essential. Knowledge of the effects of changes in load, stiffness, or boundary conditions on the phenomena of a structure, such as displacements or stresses, is required, or, in abstract terms, the relationship between the input parameters and the output quantities of a model needs to be examined. However, these relationships often cannot be evaluated using engineering knowledge for structures with complex load-bearing behavior. Instead, parameter studies are commonly carried out through repeated analyses with different parameter values. Since this procedure is cumbersome and computationally intensive, systematic and powerful computer methods are of interest.

Sensitivity analysis

Sensitivity analyses are systematic approaches to study the effects of varied input parameters on the variation of output quantities ($\hat{=}$ responses) of models. Regarding the design process of structures, common tasks of sensitivity analysis are (i) to identify and evaluate the importance of parameters in the modeling process, (ii) to investigate and quantify the effects of parameter changes for the design and optimization of structures, or (iii) to support the model assessment by providing information of the characteristics of the model. Sensitivity analysis is no unique approach. Rather, it is the collective term for various methods that differ regarding informative value and computational effort. A distinction is typically made between local and global approaches. Refer to Saltelli et al. [126] for an overview of different methods.
Global methods are commonly used prior to uncertainty analysis to investigate which of the uncertain model parameters have a low or high contribution

to the uncertainty of the output variable. To perform a global sensitivity analysis, probabilistic properties of the parameters (i.e., their probability density function) are required. Global sensitivity measures include realizations of the parameter values in the entire parameter space and are not constrained to reference values. In addition, global sensitivity measures can also describe interactions between different input variables. The *Sobol' indices* (Sobol' [132]) or the α-sensitivity factors (Hohenbichler et al. [89]) are exemplary global sensitivity measures. Refer to Iooss et al. [92] for an overview and further information on global approaches.

Local methods usually characterize the relation between an input parameter s and a response J by the derivative dJ/ds. As the derivatives are calculated based on reference values of the model parameters, local sensitivity measures are dependent on those. In addition, the first order derivatives dJ/ds do not provide information on the interaction between different parameters. The informative value of local sensitivity measures is consequently lower than that of global sensitivity analyses. However, calculating local sensitivities does not require probabilistic properties of the parameters, which are often unknown in structural design practice. Combined with the significantly lower computational effort, this is a striking argument explaining why local methods are of interest for everyday structural engineering.

Research on local sensitivity analyses has a long history. Refer to Kelley [93] or Tomović [134] for contributions on sensitivity theory at an early stage published in the 1960s. Local sensitivity analyses became particularly interesting as a derivative supplier in gradient-based structural optimization. In this context, it was recognized that the main computational effort of the entire optimization procedure can be attributed to the gradient determination. This circumstance drove the research and development of systematic and efficient computer-based local sensitivity analyses in the 1970s and 1980s. The publications by Haug et al. [84], Arora et al. [7], or Belegundu [15] are examples of that period. The high level of research activity was particularly evident when *NASA* organized the 1986 "*Sensitivity Analysis in Engineering*" symposium, see Adelman et al. [2]. In addition, Haug et al. [85] published a comprehensive textbook on the topic in the same year. The review papers Adelman et al. [3] and Haftka et al. [80] also prove that sensitivity analysis was already a well-established field of research at that time.

While the initial focus was on discrete, linear problems concerning size parameters (e.g., cross-sectional area or thickness), various aspects of structural mechanics have been considered over time. To name a few examples: There is research on variational shape sensitivity analysis (Arora [6], Tortorelli et al. [135], or Barthold et al. [10]), non-linear structural problems (Ryu et al. [125], or Cardoso et al. [32]), follower loads (Poldneff et al. [120]), path-dependent responses in the presence of material non-linearity (Schwarz [128] or Liedmann et al. [100]), or non-linear transient problems (Fernandez et al. [57]). Research papers on the implementation of sensitivity analysis that try to find a trade-off between performance, accuracy, and implementation effort can be found. Refer to Poldneff et al. [121] on the implementation in a non-linear finite element code, to Bischof et al. [19] or Wujek et al. [138] for the use of automatic differentiation techniques and to Cheng et al. [35]

or Bletzinger et al. [23] for semi-analytical methods that try to overcome tedious derivations of element quantities by finite difference approximations. In addition to structural mechanics, research on local sensitivity analysis can be found in various application areas. For instance, Giles et al. [70] shows the sensitivity analysis for compressible flows, Errico [53] for meteorology problems, Cacuci et al. [31] for cooling towers of power plants, Santos [127] for heat transfer problems, Henning et al. [87] for geotechnical engineering, or Heimbach et al. [86] for glaciology. The literature provides more than methodologically oriented work on local sensitivity analysis. A large number of publications also deal with the utilization of sensitivity analysis as a gradient-supplier. In addition to the optimization already mentioned, applications in model updating (Mottershead et al. [115] or Airaudo et al. [4]), uncertainty analysis (Cacuci et al. [30] or Luo et al. [106]), or the construction of response surfaces (Chung et al. [39]) can be found.

In summary, sensitivity analysis for structural mechanics problems is highly advanced after a long research period. That includes powerful sensitivity calculations, applicability to advanced mechanical models, and a wide range of application areas. Recent publications confirm this to be the case. For example, Antonau et al. [5] shows that large-scale industrial optimization problems with up to millions of parameters can be solved with gradient-based approaches using highly efficient computational sensitivity analyses. The extension to advanced mechanical models, including material non-linearity or damage mechanisms, is demonstrated by Liedmann et al. [100] or Guhr et al. [78]. The importance of sensitivity analysis for research trends such as digital twins is demonstrated by the work Airaudo et al. [4], in which gradient-based algorithms are used to identify weaknesses in structures. Ehre et al. [49] presents a novel application of sensitivities in Bayesian updating.

Despite the high level of research activity described above and the advanced knowledge gained, sensitivity analysis has not been integrated into everyday structural engineering practice. Furthermore, there is limited research in this direction. Henning et al. [87] shows the development and practical application in geotechnical engineering. The work of Prof. *Friedel Hartmann*'s research group at the University of Kassel is also worth mentioning. Based on Green's functions ($\hat{=}$ influence functions in structural analysis), the group developed a sensitivity analysis approach for reanalysis. It is used to make predictions of the impact of stiffness changes in structural analysis models. Refer to Hartmann et al. [83], Kunow [97], Carl [33], Carl et al. [34], and Hartmann et al. [82] for respective works.

Goals of the thesis

This dissertation aims to develop sensitivity analysis further, focusing on applications in structural engineering. As noted above, there is little research in this direction, but interest in this topic is recognizable. For example, Hertle [88] recently rated sensitivity analysis as an essential tool for investigating the causes of structural failures. To support the application and acceptance of sensitivity analysis, this thesis presents methodological developments that relate specifically to structural engineering. Since structural engineering is a

far-reaching subject in which sensitivity analysis could be used for various objectives, the work is consequently limited to selected aspects. Adjoint sensitivity analysis is the methodological basis of most of the developments presented. The adjoint method enables the efficient calculation of the sensitivities of a selected response with respect to a large number of parameters. This feature holds great potential for structural design. Even in complex analysis models, the most influential parameters can be determined by efficiently providing a large amount of sensitivity information per response. A valuable introduction to adjoint sensitivity analysis is given by Giles et al. [71].

A novel methodical development presented in this dissertation is the generalization of the influence function method for sensitivity analysis. The influence functions approach is a traditional and well-known technique in structural analysis. By combining this established method with the efficiency of numerical sensitivity analysis and its versatile possibilities, a valuable tool for structural engineering practice is presented. It is known from the literature that the adjoint variable (intermediate result of adjoint sensitivity analysis) can be identified as the influence function concerning the response. Refer to Belegundu [14, 16, 17], which are the first research papers to report on this relationship. Prof. Hartmann's earlier mentioned research group has also recognized the connection, which is documented in Kunow [97] and Hartmann et al. [82]. The publications by Belegundu and the Hartmann group have in common that they concentrate on identifying the adjoint variable as influence function. Furthermore, the Hartmann group proposed a method to determine sensitivities concerning parameters influencing the structural stiffness based on Green's function (cf. Hartmann et al. [82]). These findings are used and continued accordingly in this thesis. The research goal is to investigate how and to what extent the influence function method can be generalized for sensitivity analysis. In this context, the generalization concerning various kinds of (i) responses, (ii) parameters, and (iii) physics is studied.

Engineering structures cannot be built in one single piece. Instead, they result from a construction process during which deformations occur due to their self-weight. Considering such aspects in the simulation is called construction stage analysis, which comprises a sequence of simulation stages. Since construction phase models have not yet been extensively established in structural design and are generally complex, a systematic investigation and assessment of them is of interest. In that regard, the literature only covers classic parameter studies used to investigate construction stage models. Refer to Kurc et al. [98] or Laggner et al. [99] as exemplary works. However, applying systematic computer-aided sensitivity analyses to sequential simulation processes is a new and previously unexplored field of application. Hence, the research goal is to investigate how sensitivity analysis can be applied to sequenced simulation processes.

In addition to the methodological developments mentioned above, the dissertation deals with applying sensitivity analysis in structural engineering. For this purpose, sensitivity analysis is considered as a stand-alone engineering tool and not as a gradient supplier for other methods. The research goal is to demonstrate sensitivity analysis as a supporting means for structural design.

Outline of the thesis

CHAPTER 2 introduces the fundamentals of structural mechanics and steady state heat transfer. These are the underlying physics to which sensitivity analysis is applied in the thesis. The consideration of steady state heat transfer is required to demonstrate the generalization of the influence functions approach for another physics.

CHAPTER 3 introduces the basics of adjoint sensitivity analysis, which are necessary for the methodological developments in the dissertation. The sensitivity equations are derived in discrete and variational formulations for structural mechanics and steady state heat transfer. Furthermore, the influence function approach is presented.

CHAPTER 4 presents investigations on the generalization of the method of influence functions for sensitivity analysis. The connection of the adjoint variable and the influence function is discussed from different viewpoints. Subsequently, it is demonstrated how the influence function for significant practice-relevant responses as displacements, stress resultants, or support forces can be identified in adjoint sensitivity analysis. On that basis, the thesis proposes how the influence function method can be extended for general responses and parameters. In that regard, the extendability of the graphical solution procedure of the classical influence functions method is also considered. A further focus is the discussion of the significance of the influence function in general cases and the limitations of the generalization approach. Finally, the validity of the proposed concept is demonstrated along steady state heat transfer for a different physical phenomenon.

CHAPTER 5 presents investigations on the required extensions of sensitivity analysis for sequenced simulation processes. It is discussed how analysis models can be initialized for the subsequent simulation stage and the necessary adjustments for sensitivity analysis. Based on these findings, additional extensions for sensitivity analysis in the case of construction stage analysis and the sequenced simulation process of lightweight structures are investigated. An essential issue of the chapter is also the critical assessment of the additional computational costs of sensitivity analysis for sequenced simulation processes.

CHAPTER 6 demonstrates the use of sensitivity analysis in structural design. Application-oriented aspects such as the graphical processing and the interpretation of sensitivities are discussed. Subsequently, concepts for the systematic use of sensitivities are proposed. The final focus is to demonstrate the described concepts and methods on real-world analysis models of engineering structures.

CHAPTER 7 concludes the thesis and provides an outlook for possible future research.

Kratos Multiphysics

All sensitivity analyses presented in this dissertation are conducted with the open-source[1] simulation framework *Kratos Multiphysics*. Information can be found in Dadvand et al. [43], Dadvand et al. [44], and Ferrándiz et al. [58]. The research code is structured in a core and applications. The core defines the framework and provides basic functionalities. The applications contain specific implementations and are available for various use cases such as structural mechanics, fluid dynamics, or optimization. Furthermore, different numerical approaches, such as the finite element method or particle-based methods, are implemented. For this dissertation, the *StructuralMechanicsApplication* is used for examples from structural engineering and the *ConvectionDiffusion-Application* for steady state heat transfer simulations. The sensitivity analysis for structural problems is part of the StructuralMechanicsApplication and was implemented by the author of this dissertation. In contrast, the sensitivity analysis in the ConvectionDiffusionApplication was already available for shape parameters. For this work, the existing implementation was extended for various other parameters and the proposed generalized influence function approach.

[1] GitHub repository: https://github.com/KratosMultiphysics/Kratos

Chapter 2

Structural mechanics and heat transfer

2.1 Preliminaries

Gâteaux derivatives and variations

Gâteaux or *directional derivatives* provide information about the changing behavior of scalar, vector, or tensor-valued fields concerning a selected argument in an arbitrary direction $(\bullet)$. The Gâteaux derivative of a function $\Phi(\boldsymbol{u})$ with respect to $\boldsymbol{u}$ in direction of $(\bullet)$ is defined as

$$\Phi'_{\boldsymbol{u}}\left(\boldsymbol{u};(\bullet)\right) = D_{(\bullet)}\Phi(\boldsymbol{u}) = \frac{d}{d\varepsilon}\Phi\left(\boldsymbol{u}+\varepsilon(\bullet)\right)|_{\varepsilon=0} \tag{2.1}$$

where $D_{(\bullet)}$ denotes the Gâteaux operator. The Gâteaux derivative of Φ in direction of $\delta\boldsymbol{u}$ is equivalent to the *variation* $\delta\Phi$ due to variation $\delta\boldsymbol{u}$ of argument $\boldsymbol{u}$:

$$\delta\Phi = \delta_{\boldsymbol{u}}\Phi = \Phi'_{\boldsymbol{u}}\left(\boldsymbol{u};\delta\boldsymbol{u}\right) = D_{\delta\boldsymbol{u}}\Phi(\boldsymbol{u}) = \frac{d}{d\varepsilon}\Phi\left(\boldsymbol{u}+\varepsilon\delta\boldsymbol{u}\right)|_{\varepsilon=0} \tag{2.2}$$

The relation of Gâteaux derivative and gradient is given by

$$D_{\delta\boldsymbol{u}}\Phi(\boldsymbol{u}) = \frac{\partial\Phi(\boldsymbol{u})}{\partial\boldsymbol{u}}\cdot\delta\boldsymbol{u} \tag{2.3}$$

as a result of applying the chain rule. If a quantity $\Phi(\boldsymbol{u},\boldsymbol{s})$ depends on several arguments, the *partial variations* $\delta_{\boldsymbol{u}}\Phi = \Phi'_{\boldsymbol{u}}$ and $\delta_{\boldsymbol{s}}\Phi = \Phi'_{\boldsymbol{s}}$ can be computed with respect to one argument by Equation (2.1) if the other argument is held fixed. On that basis, the *total variation*

$$\Phi' = \Phi'_{\boldsymbol{u}}(\boldsymbol{u},\boldsymbol{s}) + \Phi'_{\boldsymbol{s}}(\boldsymbol{u},\boldsymbol{s}) \tag{2.4}$$

can be determined. If the argument $\boldsymbol{u}$ depends on $\boldsymbol{s}$, the *total partial variation* of $\Phi(\boldsymbol{u}(\boldsymbol{s}),\boldsymbol{s})$ with respect to $\boldsymbol{s}$ reads

$$\mathcal{D}_s\Phi(\boldsymbol{u},\boldsymbol{s})\cdot\delta\boldsymbol{s} = \frac{\partial\Phi}{\partial\boldsymbol{s}}\cdot\delta\boldsymbol{s} + \frac{\partial\Phi}{\partial\boldsymbol{u}}\frac{d\boldsymbol{u}}{d\boldsymbol{s}}\cdot\delta\boldsymbol{s} \tag{2.5}$$

using the chain rule.

Variational forms

Variational or *weak forms* of the underlying physical problem (e.g., structural mechanics or heat transfer) are the basis for numerical approaches such as the *finite element method* (FEM). The variational form

$$\begin{aligned} A(\boldsymbol{u},\boldsymbol{v}) = a(\boldsymbol{u},\boldsymbol{v}) - F(\boldsymbol{v}) = 0 \quad \forall \boldsymbol{v} \in \mathcal{V} \\ \text{with} \quad a(\boldsymbol{u},\boldsymbol{v}) : \mathcal{U} \times \mathcal{V} \to \mathbb{R} \quad \text{and} \quad F(\boldsymbol{v}) : \mathcal{V} \to \mathbb{R} \end{aligned} \tag{2.6}$$

is concerned with determining the state field $\boldsymbol{u}$ in a solution space $\mathcal{U}$ and utilizes a test field $\boldsymbol{v} \in \mathcal{V}$ whereby $\mathcal{V}$ is called weighting space. The spaces $\mathcal{U}$ and $\mathcal{V}$ are defined as

$$\begin{aligned} \mathcal{U} &= \{\boldsymbol{u} \in \mathcal{H}^m(\Omega) \ : \ \boldsymbol{u} = \hat{\boldsymbol{u}} \text{ on } \Gamma_D\} \\ \mathcal{V} &= \{\boldsymbol{v} \in \mathcal{H}^m(\Omega) \ : \ \boldsymbol{v} = \boldsymbol{0} \text{ on } \Gamma_D\} \end{aligned} \tag{2.7}$$

where $\hat{\boldsymbol{u}}$ are prescribed values of the state field on the *Dirichlet* boundary Γ_D of a domain Ω. In contrast, the test field fulfills homogeneous boundary conditions on Γ_D. Information about the *Sobolev*-space $\mathcal{H}^m$ can be found by Adams et al. [1]. The order m of $\mathcal{H}$ is defined by the highest derivative order of the test function $\boldsymbol{v}$ in the weak form.
The *functional* $F(\boldsymbol{v})$ operates on the test function $\boldsymbol{v}$. Frequently occurring functionals in the context of Equation (2.6) are in the shape

$$F(\boldsymbol{v}) = (\boldsymbol{p},\boldsymbol{v}) = \int_\Omega \boldsymbol{p} \cdot \boldsymbol{v} \, d\Omega \tag{2.8}$$

for a given $\boldsymbol{p}$ (e.g., distributed load or heat source). Forms and functionals may depend on several arguments simultaneously. To separate non-linear from linear arguments, a semicolon is used. For instance, the form $a(\boldsymbol{u},\boldsymbol{s};\boldsymbol{v},\boldsymbol{w})$ and the functional $F(\boldsymbol{u},\boldsymbol{s};\boldsymbol{v},\boldsymbol{w})$ are non-linear in $\boldsymbol{u}$ and $\boldsymbol{s}$ but linear with respect to $\boldsymbol{v}$ and $\boldsymbol{w}$. If $a(\boldsymbol{u},\boldsymbol{v})$ is linear in both arguments, the form is denoted *bilinear*. Otherwise, the case $a(\boldsymbol{u};\boldsymbol{v})$ is designated as *semilinear*.
In structural mechanics, the weak form equates to the *principle of virtual work* or more precisely the *principle of virtual displacements*. Therefore, the test function $\boldsymbol{v}$ is interpreted as *virtual displacement*, which is typically denoted by $\delta\boldsymbol{u}$. With the internal virtual work $\delta W_{\text{int}}(\boldsymbol{u},\delta\boldsymbol{u}) = -a(\boldsymbol{u},\delta\boldsymbol{u})$ and external virtual work $\delta W_{\text{ext}}(\delta\boldsymbol{u}) = F(\delta\boldsymbol{u})$ the weak form can written as:

$$\delta W = \delta W_{\text{int}}(\boldsymbol{u},\delta\boldsymbol{u}) + \delta W_{\text{ext}}(\delta\boldsymbol{u}) = 0 \tag{2.9}$$

For instance, the virtual work expressions read

$$\begin{aligned} \delta W_{\text{int}}(w,\delta w) = -a(w,\delta w) = -\int_0^l EIw'' \cdot \delta w'' \, dx \quad \text{and} \\ \delta W_{\text{ext}}(\delta w) = F(\delta w) = (p,\delta w) = \int_0^l p \cdot \delta w \, dx \end{aligned} \tag{2.10}$$

in the case of an Euler-Bernoulli beam with length l (cf. Appendix B.1).

Finite element discretization and solution procedure

In the previous section, variational problems $A(\boldsymbol{u}, \boldsymbol{v})$ were introduced. However, the utilized solution and weighting space (cf. Equation (2.7)) contain an infinite number of linearly independent functions whereby the solution of Equation (2.6) is practically not possible. Approximate solution techniques as the finite element method restrict the solution and weighting space to finite dimensional sub-spaces $\mathcal{U}_h \subset \mathcal{U}$ and $\mathcal{V}_h \subset \mathcal{V}$. Hence, the problem

$$A(\boldsymbol{u}_h, \boldsymbol{v}_h) = a(\boldsymbol{u}_h, \boldsymbol{v}_h) - F(\boldsymbol{v}_h) = 0 \quad \forall \boldsymbol{v}_h \in \mathcal{V}_h \tag{2.11}$$

is treated to solve for $\boldsymbol{u}_h \in \mathcal{U}_h$. A further characteristic of the finite element method is separating the domain Ω into sub-domains Ω^e, i.e., into the name-giving elements. Within the elements, the state field and test function are interpolated in terms of shape functions $\boldsymbol{N}$ as

$$\boldsymbol{u}_h^e(\boldsymbol{\xi}) = \boldsymbol{N}(\boldsymbol{\xi})\boldsymbol{u}^e \quad \text{and} \quad \boldsymbol{v}_h^e(\boldsymbol{\xi}) = \boldsymbol{N}(\boldsymbol{\xi})\boldsymbol{v}^e \tag{2.12}$$

with the nodal values of state field $\boldsymbol{u}^e$ and test function $\boldsymbol{v}^e$, respectively. In general, Equation (2.11) is non-linear concerning the unknown state field $\boldsymbol{u}_h$ and must be solved iteratively. For the solution with the *Newton Raphson* scheme, the variational form is linearized as

$$A(\boldsymbol{u}_h; \boldsymbol{v}_h) + A'_{\boldsymbol{u}_h}(\boldsymbol{u}_h; \boldsymbol{v}_h, \Delta\boldsymbol{u}_h) + \mathcal{O} = 0 \tag{2.13}$$

where $A'_{\boldsymbol{u}_h}(\bullet)$ denotes the Gâteaux derivative with respect to $\boldsymbol{u}_h$ in the direction of the state field increment $\Delta\boldsymbol{u}_h$. The higher order terms are designated by $\mathcal{O}$ and are neglected subsequently. Hence, the linear problem

$$A'_{\boldsymbol{u}_h}(\boldsymbol{u}_h; \boldsymbol{v}_h, \Delta\boldsymbol{u}_h) = -A(\boldsymbol{u}_h; \boldsymbol{v}_h) \tag{2.14}$$

must be solved in every iteration step to determine the increment $\Delta\boldsymbol{u}_h$.

2.2 Structural mechanics

This section briefly introduces the fundamentals of structural mechanics. The focus is on linear and geometrically non-linear static problems. For more in-depth information, please refer to the literature, e.g., the textbooks by Başar et al. [11], Bonet et al. [26], Borst et al. [27], and Holzapfel [90] are recommended.

2.2.1 Kinematics

Subsequently, it is necessary to distinguish the reference configuration (undeformed) and the current configuration (deformed) of the structural domain. Capital letters are used for variables in the reference configuration, and lowercase letters are employed for those in the current configuration.
The displacement $\boldsymbol{u}$ is determined by the difference of the position vector of a material point in the reference and current configuration (cf. Figure 2.1):

$$\boldsymbol{u} = \boldsymbol{x} - \boldsymbol{X} \tag{2.15}$$

A parametric geometry description based on curvilinear coordinates θ^i can be utilized to represent the position vectors by

$$\boldsymbol{X} = X^j\left(\theta^1,\theta^2,\theta^3\right)\mathbf{e}_j \quad \text{and} \quad \boldsymbol{x} = x^j\left(\theta^1,\theta^2,\theta^3\right)\mathbf{e}_j \tag{2.16}$$

where $\mathbf{e}_j$ are the base vectors of a global Cartesian coordinate system. Based on the position vectors, local bases in co- and contravariant manner can be determined. These are defined as

$$\boldsymbol{G}_i = \frac{\partial \boldsymbol{X}}{\partial \theta^i}, \quad \boldsymbol{G}^i = \frac{\partial \theta^i}{\partial \boldsymbol{X}}, \quad \boldsymbol{g}_i = \frac{\partial \boldsymbol{x}}{\partial \theta^i}, \quad \text{and} \quad \boldsymbol{g}^i = \frac{\partial \theta^i}{\partial \boldsymbol{x}} \tag{2.17}$$

in reference and current configuration, respectively. The co- and contravariant bases can be transformed in each other by metrics as listed in Table 2.1.

Table 2.1: Transformation of co- and contravariant bases by metrics.

configuration	reference	current
covariant metric	$G_{ij} = \boldsymbol{G}_i \cdot \boldsymbol{G}_j$	$g_{ij} = \boldsymbol{g}_i \cdot \boldsymbol{g}_j$
contravariant metric	$G^{ij} = \boldsymbol{G}^i \cdot \boldsymbol{G}^j$	$g^{ij} = \boldsymbol{g}^i \cdot \boldsymbol{g}^j$
covariant bases	$\boldsymbol{G}_i = G_{ij}\boldsymbol{G}^j$	$\boldsymbol{g}_i = g_{ij}\boldsymbol{g}^j$
contravariant bases	$\boldsymbol{G}^i = G^{ij}\boldsymbol{G}_j$	$\boldsymbol{g}^i = g^{ij}\boldsymbol{g}_j$

The *deformation gradient* $\boldsymbol{\mathcal{F}}$ describes the mapping of an infinitesimal fiber $d\boldsymbol{X}$ in the reference configuration to the deformed fiber $d\boldsymbol{x}$ in the current configuration

$$d\boldsymbol{x} = \boldsymbol{\mathcal{F}} \cdot d\boldsymbol{X} \tag{2.18}$$

and can be determined by

$$\boldsymbol{\mathcal{F}} = \frac{d\boldsymbol{x}}{d\boldsymbol{X}} = \boldsymbol{g}_i \otimes \boldsymbol{G}^i. \tag{2.19}$$

Non-linear strain measures can be introduced using the deformation gradient. The *Green-Lagrange* (GL) strain tensor $\boldsymbol{E}$ is defined as

$$\boldsymbol{E} = \frac{1}{2}\left(\boldsymbol{\mathcal{F}}^T \cdot \boldsymbol{\mathcal{F}} - \boldsymbol{I}\right) = \frac{1}{2}\left(g_{ij} - G_{ij}\right)\boldsymbol{G}^i \otimes \boldsymbol{G}^j \tag{2.20}$$

and the *Euler-Almansi* (EA) strain tensor $\boldsymbol{e}$ as

$$\boldsymbol{e} = \frac{1}{2}\left(\boldsymbol{I} - \boldsymbol{\mathcal{F}}^{-T} \cdot \boldsymbol{\mathcal{F}}^{-1}\right) = \frac{1}{2}\left(g_{ij} - G_{ij}\right)\boldsymbol{g}^i \otimes \boldsymbol{g}^j \tag{2.21}$$

where $\boldsymbol{I}$ denotes the identity tensor. For other non-linear strain measures, refer to the literature, e.g., Holzapfel [90] or Başar et al. [11]. Usually, the coefficients of constitutive equations refer to a local Cartesian basis. Therefore, the strains in Equation (2.20) can be transformed by

$$\bar{\boldsymbol{E}}_{\gamma\delta} = \frac{1}{2}(g_{ij} - G_{ij})(\mathbf{e}_\gamma \cdot \boldsymbol{G}^i)(\boldsymbol{G}^j \cdot \mathbf{e}_\delta) \tag{2.22}$$

where $\mathbf{e}_\gamma$, $\mathbf{e}_\delta$ denote the base vectors of a Cartesian frame. A bar $\bar{\bullet}$ is utilized to denote that the strains refer to a Cartesian reference frame.

2.2.2 Constitutive equations and stresses

Constitutive equations relate strains and stresses using a material law. In non-linear structural mechanics, several strain and stress measures are established. In Section 2.2.1, the Green-Lagrange and the Euler-Almansi strain are introduced. Their energetically conjugated stress measure is the *Second Piola-Kirchhoff* (PK2) stress tensor $\boldsymbol{S}$ and the *Cauchy* stress tensor $\boldsymbol{\sigma}$, respectively. In the context of this thesis, only problems with large displacements but small strains are considered in the case of non-linear analyses. Hence, a linear relation between strains and stresses described by the *Saint Venant-Kirchhoff* material law is used. The chosen material law is characterized by the strain-energy function

$$\begin{aligned} \boldsymbol{\Psi}(\boldsymbol{E}) &= \frac{1}{2}\lambda \left(tr\left(\boldsymbol{E}\right)\right)^2 + \mu \; tr\left(\boldsymbol{E}^2\right) \\ \lambda = \frac{E\nu}{(1+\nu)(1-2\nu)}, &\quad \mu = \frac{E}{2(1+\nu)} \end{aligned} \tag{2.23}$$

with the Lamé constants λ and μ, Young's modulus E, Poisson's ratio ν, and the trace operator $tr\left(\bullet\right)$ (cf., e.g., Holzapfel [90] for details). The PK2 stress tensor can be determined based on the strain energy function $\boldsymbol{\Psi}$ by:

$$\boldsymbol{S} = \frac{\partial \boldsymbol{\Psi}}{\partial \boldsymbol{E}} \tag{2.24}$$

The material tensor $\mathbb{C}$ is defined as

$$\mathbb{C} = \frac{\partial^2 \boldsymbol{\Psi}}{\partial \boldsymbol{E}^2} = \frac{\partial \boldsymbol{S}}{\partial \boldsymbol{E}} \tag{2.25}$$

to describe the relation between strains and stresses, which is linear in the case of the Saint Venant-Kirchhoff model:

$$\boldsymbol{S} = \mathbb{C} : \boldsymbol{E} \tag{2.26}$$

The PK2 stress tensor $\boldsymbol{S}$ can be transformed into alternative stress tensors. The relation with the *First Piola-Kirchhoff* (PK1) stress tensor $\boldsymbol{P}$ is given by

$$\boldsymbol{P} = \boldsymbol{\mathcal{F}} \cdot \boldsymbol{S} \tag{2.27}$$

and with the Cauchy stress tensor $\boldsymbol{\sigma}$ through

$$\boldsymbol{\sigma} = \frac{1}{\det \boldsymbol{\mathcal{F}}} \boldsymbol{\mathcal{F}} \cdot \boldsymbol{S} \cdot \boldsymbol{\mathcal{F}}^T \tag{2.28}$$

where $\boldsymbol{\mathcal{F}}$ is the deformation gradient according to Equation (2.19). Please note that only the Cauchy stresses allow a meaningful physical interpretation among the introduced stress types. Analogously to the linear case, the components of the Cauchy stress can be interpreted as forces per unit area in the deformed configuration.

2.2.3 Governing equation

The equilibrium of internal and external forces gives the governing equation in structural mechanics. The equilibrium can be formulated in reference or current configuration (cf. Figure 2.1). For static problems in which dynamic effects are neglected, the equilibrium in the reference state (indicated by subscript "0") can be expressed as

$$\mathrm{div}\boldsymbol{P} + \boldsymbol{p}_0 = \boldsymbol{0} \tag{2.29}$$

by means of the PK1 stress tensor $\boldsymbol{P}$ and the distributed volume forces $\boldsymbol{p}_0$ (commonly referred to as body forces). In addition to the equilibrium requirement, boundary conditions must be met. In the following it is assumed that the boundary Γ_0 of the domain Ω_0 is composed of a *Dirichlet* part Γ_{D0} and *Neumann* part Γ_{N0} with the following properties:

$$\Gamma_0 = \Gamma_{D0} \cup \Gamma_{N0} \quad \text{and} \quad \Gamma_{D0} \cap \Gamma_{N0} = \emptyset \tag{2.30}$$

On Γ_{D0} the structural displacements $\boldsymbol{u}$ have to be equivalent to predefined values $\hat{\boldsymbol{u}}$. In contrast, on Γ_{N0}, external forces $\hat{\boldsymbol{t}}_0$ are specified, which must be in equilibrium with the internal forces. Hence, the boundary conditions read

$$\boldsymbol{u} = \hat{\boldsymbol{u}} \qquad \text{on } \Gamma_{D0} \tag{2.31a}$$

$$\boldsymbol{n}\boldsymbol{P} = \hat{\boldsymbol{t}}_0 \qquad \text{on } \Gamma_{N0} \tag{2.31b}$$

where $\boldsymbol{n}$ is a unit normal vector on the domain boundary. The combination of Equations (2.29) and (2.31) represent the *strong form* of the boundary value problem of elastostatics. The respective formulation in the current configuration can be found in the literature (e.g., Holzapfel [90]).

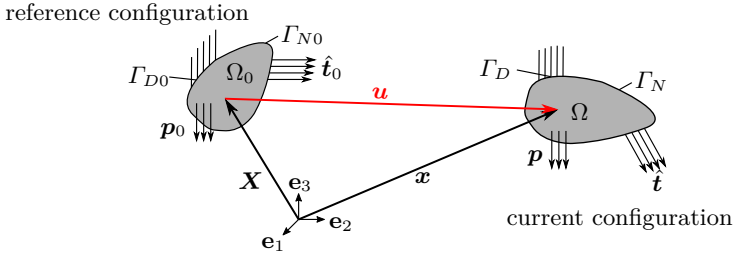

Figure 2.1: Domain in the reference and current configuration with Dirichlet and Neumann boundary conditions.

2.2.4 Weak form

The direct determination of the displacements $\boldsymbol{u}$ by the analytical solution of the static boundary value problem defined in Section 2.2.3 is generally impossible. To apply approximate solution techniques such as the finite

element method, the weak form of the boundary value problem is required. Therefore, Equation (2.29) is multiplied by an arbitrary test function $\boldsymbol{v} \in \mathcal{V}$ (cf. Section 2.1). Subsequent integration over Ω_0 gives:

$$\int_{\Omega_0} (\operatorname{div}(\boldsymbol{P}) + \boldsymbol{p}_0) \cdot \boldsymbol{v} \, d\Omega_0 = 0 \tag{2.32}$$

By application of Cauchy's theorem and the divergence theorem ($\hat{=}$ Gauß's theorem) to Equation (2.32), and subsequent substitution of the PK2 stress tensor by means of Equation (2.27), the weak form of the boundary value problem of elastostatics is obtained:

$$\begin{aligned} A(\boldsymbol{u};\boldsymbol{v}) &= a(\boldsymbol{u};\boldsymbol{v}) - F(\boldsymbol{u};\boldsymbol{v}) = 0 \quad \text{with} \\ a(\boldsymbol{u};\boldsymbol{v}) &= \int_{\Omega_0} \boldsymbol{S} : D_{\boldsymbol{v}}\boldsymbol{E}(\boldsymbol{u}) \, d\Omega_0 \quad \text{and} \\ F(\boldsymbol{u};\boldsymbol{v}) &= \int_{\Omega_0} \boldsymbol{p}_0 \cdot \boldsymbol{v} \, d\Omega_0 + \int_{\Gamma_{N0}} \hat{\boldsymbol{t}}_0 \cdot \boldsymbol{v} \, d\Gamma_{N0} \end{aligned} \tag{2.33}$$

If the test function $\boldsymbol{v}$ is considered as virtual displacement $\delta\boldsymbol{u}$, the variational form in Equation (2.33) can be recognized as the principle of virtual work

$$\begin{aligned} \delta W &= \delta W_{\text{int}} + \delta W_{\text{ext}} = 0 \quad \text{with} \\ \delta W_{\text{int}} &= -\int_{\Omega_0} \boldsymbol{S} : \delta\boldsymbol{E} \, d\Omega_0 \quad \text{and} \\ \delta W_{\text{ext}} &= \int_{\Omega_0} \boldsymbol{p}_0 \cdot \delta\boldsymbol{u} \, d\Omega_0 + \int_{\Gamma_{N0}} \hat{\boldsymbol{t}}_0 \cdot \delta\boldsymbol{u} \, d\Gamma_{N0} \end{aligned} \tag{2.34}$$

with the internal virtual work $\delta W_{\text{int}}(\boldsymbol{u};\delta\boldsymbol{u}) = -a(\boldsymbol{u};\delta\boldsymbol{u})$ and external virtual work $\delta W_{\text{ext}}(\boldsymbol{u};\delta\boldsymbol{u}) = F(\boldsymbol{u};\delta\boldsymbol{u})$, respectively.

2.2.5 Finite element based solution procedure

The equilibrium state given in terms of the principle of virtual work in Equation (2.34) can be expressed as

$$\delta W = \frac{\partial W}{\partial \boldsymbol{u}} \delta\boldsymbol{u} = 0 \tag{2.35}$$

if the relation of Gâteaux derivative and gradient as introduced by Equation (2.3) is considered. Finite element discretization of Equation (2.35) (cf. Section 2.1) gives

$$\delta W = \frac{\partial W}{\partial \boldsymbol{u}_h} \delta\boldsymbol{u}_h = -\boldsymbol{r} \cdot \delta\boldsymbol{u}_h = 0 \tag{2.36}$$

where $\boldsymbol{r}$ denotes the vector of unbalanced forces. The vector $\boldsymbol{r}$ is computed by

$$\boldsymbol{r}(\boldsymbol{u}_h) = -\frac{\partial W_{\text{int}}}{\partial \boldsymbol{u}_h} - \frac{\partial W_{\text{ext}}}{\partial \boldsymbol{u}_h} = \boldsymbol{f}_{\text{int}}(\boldsymbol{u}_h) - \boldsymbol{f}_{\text{ext}}(\boldsymbol{u}_h) = \boldsymbol{0} \tag{2.37}$$

and can be interpreted as the equilibrium of internal forces $\boldsymbol{f}_{\text{int}}$ and external forces $\boldsymbol{f}_{\text{ext}}$. Moreover, the equilibrium state defined by Equation (2.37) represents the discrete state equation of non-linear structural problems.
Equation (2.37) is non-linear concerning $\boldsymbol{u}_h$ and cannot solved directly. An iterative solution procedure such as the Newton Raphson scheme can be used instead (cf. Section 2.1 or Borst et al. [27] for detailed information). Therefore, Equation (2.37) is linearized. The result is the linear problem

$$\boldsymbol{K}_T \Delta \boldsymbol{u}_h = -\boldsymbol{r} \tag{2.38}$$

which has to be solved in every iteration step of the Newton Raphson algorithm. The tangential stiffness matrix $\boldsymbol{K}_T$ in Equation (2.38) can be computed by

$$\boldsymbol{K}_T(\boldsymbol{u}_h) = \frac{\partial \boldsymbol{r}}{\partial \boldsymbol{u}_h} = \frac{\partial \boldsymbol{f}_{\text{int}}}{\partial \boldsymbol{u}_h} - \frac{\partial \boldsymbol{f}_{\text{ext}}}{\partial \boldsymbol{u}_h}. \tag{2.39}$$

2.2.6 Linear elasticity theory

The governing equation to determine the structural displacements $\boldsymbol{u}$ on the basis of linear elasticity theory is given by

$$-\mathcal{L}\boldsymbol{u} = -\left[\mu\Delta + (\lambda+\mu)\,\nabla\text{div}\right]\boldsymbol{u} = \boldsymbol{p} \qquad \text{in } \Omega \tag{2.40a}$$

$$\boldsymbol{u} = \hat{\boldsymbol{u}} \qquad \text{on } \Gamma_D \tag{2.40b}$$

$$\boldsymbol{\sigma}\boldsymbol{n} = \hat{\boldsymbol{t}} \qquad \text{on } \Gamma_N \tag{2.40c}$$

with the Lamé operator $\mathcal{L}$, the Lamé constants μ and λ as defined by Equation (2.23) and the distributed volume forces $\boldsymbol{p}$. Additionally, displacements $\hat{\boldsymbol{u}}$ and traction forces $\hat{\boldsymbol{t}}$ are prescribed on the Dirichlet and Neumann boundary. The respective weak form reads

$$\begin{aligned} A(\boldsymbol{u},\boldsymbol{v}) &= a(\boldsymbol{u},\boldsymbol{v}) - F(\boldsymbol{v}) = 0 \quad \text{with} \\ a(\boldsymbol{u},\boldsymbol{v}) &= \int_\Omega \boldsymbol{\sigma}(\boldsymbol{u}) : \boldsymbol{\epsilon}(\boldsymbol{v})\, d\Omega \quad \text{and} \\ F(\boldsymbol{v}) &= \int_\Omega \boldsymbol{p}\cdot\boldsymbol{v}\, d\Omega + \int_{\Gamma_N} \hat{\boldsymbol{t}}\cdot\boldsymbol{v}\, d\Gamma_N \end{aligned} \tag{2.41}$$

where $\boldsymbol{\sigma}(\boldsymbol{u}) = \mathbb{C} : \boldsymbol{\epsilon}(\boldsymbol{u})$ is the Cauchy stress tensor based on the linear strain tensor

$$\boldsymbol{\epsilon}(\boldsymbol{u}) = \frac{1}{2}\left(\nabla\boldsymbol{u} + \nabla\boldsymbol{u}^T\right) \tag{2.42}$$

and the material tensor $\mathbb{C}$. If $\boldsymbol{v}$ is interpreted as virtual displacement $\delta\boldsymbol{u}$, the variational form in Equation (2.41) can be recognized as the principle of virtual work with the internal virtual work $\delta W_{\text{int}}(\boldsymbol{u},\delta\boldsymbol{u}) = -a(\boldsymbol{u},\delta\boldsymbol{u})$ and external virtual work $\delta W_{\text{ext}}(\delta\boldsymbol{u}) = F(\delta\boldsymbol{u})$, respectively.
After finite element discretization of Equation (2.41), the discrete state equation for linear structural problems

$$\boldsymbol{r}(\boldsymbol{u}_h) = \boldsymbol{K}\boldsymbol{u}_h - \boldsymbol{F} = \boldsymbol{0} \tag{2.43}$$

with the symmetric stiffness matrix $\boldsymbol{K} = \boldsymbol{K}^T$ and load vector $\boldsymbol{F}$ is received.

2.3 Steady state heat transfer

Steady state heat transfer problems are only used to demonstrate the generalizability of the proposed sensitivity analysis approach for another physics in Chapter 4 and are not within the main focus of this thesis. The underlying physics is therefore kept as simple as possible. For example, only state-independent material properties are assumed. For further reading and background information, refer to the literature like the comprehensive textbook Lienhard et al. [101]. Please note that the following derivations are mainly based on Huang et al. [91] and Zienkiewicz et al. [139].

2.3.1 Governing equation

The theoretical basis for steady state heat transfer is *Fourier's law of heat conduction* (Fourier [60]), which relates the heat flow rate per unit area q, i.e., the heat flux, with the gradient of the temperature ϕ by

$$q = -\kappa \cdot \frac{d\phi}{dx} \tag{2.44}$$

where the constant κ denotes the material-dependent thermal conductivity. See Lienhard et al. [101, Appendix A] for a comprehensive list of thermal conductivity values for various materials. In a three-dimensional setting, Equation (2.44) can be generalized in Cartesian coordinates as

$$\boldsymbol{q} = \begin{pmatrix} q_x \\ q_y \\ q_z \end{pmatrix} = -\boldsymbol{\kappa} \boldsymbol{\nabla} \phi \tag{2.45}$$

with the matrix $\boldsymbol{\kappa}$ containing the conductivity properties of the body. For isotropic materials, the matrix $\boldsymbol{\kappa}$ can be written as $\boldsymbol{\kappa} = \kappa \cdot \boldsymbol{I}$, where $\boldsymbol{I}$ is the identity matrix. In the presence of a heat source Q (heat generated per unit volume), the heat flow equilibrium

$$\frac{\partial q_x}{\partial x} + \frac{\partial q_y}{\partial y} + \frac{\partial q_z}{\partial z} = \boldsymbol{\nabla} \cdot \boldsymbol{q} = Q. \tag{2.46}$$

must be fulfilled. Finally, by substitution of Equation (2.45) into Equation (2.46) the governing equation for the temperature ϕ is obtained:

$$-\boldsymbol{\nabla} \cdot (\boldsymbol{\kappa} \boldsymbol{\nabla} \phi) = Q \tag{2.47}$$

2.3.2 Boundary conditions

In the following it is assumed that the boundary Γ of the domain Ω is composed of a Dirichlet part Γ_D and Neumann part Γ_N with the following properties:

$$\Gamma = \Gamma_D \cup \Gamma_N \quad \text{and} \quad \Gamma_D \cap \Gamma_N = \emptyset \tag{2.48}$$

Dirichlet boundary conditions
On the Dirichlet boundary Γ_D the temperature is specified:

$$\phi = \hat{\phi} \tag{2.49}$$

Neumann boundary conditions
On the Neumann boundary Γ_N the heat flow in the normal direction of the surface is assigned by

$$\boldsymbol{q}^T \boldsymbol{n} = -\left(\boldsymbol{\kappa} \boldsymbol{\nabla} \phi\right)^T \boldsymbol{n} = q_N \tag{2.50}$$

where $\boldsymbol{n}$ is the unit normal vector of the domain boundary. The introduced boundary heat flow variable q_N can include different conditions, which are:

- The boundary heat inflow can be fixed by a prescribed value $\hat{q}$:

$$q_N = -\hat{q} \tag{2.51}$$

- Convection boundary conditions can be considered by *Newton's law of cooling* defined as

$$q_N = \alpha(\phi - \phi_a) \tag{2.52}$$

  where α denotes the heat transfer coefficient and ϕ_a is the ambient temperature. For exemplary values of the heat transfer coefficient α and for a discussion on its temperature dependency, refer to Lienhard et al. [101].

- Radiation boundary conditions can be considered by

$$q_N = \sigma\epsilon\left(\phi^4 - \phi_a^4\right) \tag{2.53}$$

  where σ is the *Stefan-Boltzmann constant* ($5.67 \cdot 10^{-8} W/m^2K^4$) and ϵ is the emissivity of the boundary. For details on radiation, refer to Balaji [8].

2.3.3 Weak form

Multiplication of Equation (2.47) by an arbitrary test function $v \in \mathcal{V}$ (cf. Section 2.1) and integration over Ω gives:

$$\int_\Omega v \cdot \left(\boldsymbol{\nabla} \cdot \left(\boldsymbol{\kappa} \boldsymbol{\nabla} \phi\right) + Q\right) d\Omega = 0 \tag{2.54}$$

Through integration by parts of Equation (2.54) and subsequent incorporation of the Neumann boundary conditions (Equations (2.50)-(2.53)), the weak form

$$A(\phi; v) = a(\phi; v) - F(v) = 0 \quad \text{with} \tag{2.55a}$$

$$a(\phi; v) = \int_\Omega \left(\boldsymbol{\nabla} v\right)^T \boldsymbol{\kappa} \boldsymbol{\nabla} \phi \, d\Omega + \int_{\Gamma_N} v\left(\alpha\phi + \sigma\epsilon\phi^4\right) d\Gamma_N \tag{2.55b}$$

$$F(v) = \int_\Omega vQ \, d\Omega + \int_{\Gamma_N} v\left(\alpha\phi_a + \sigma\epsilon\phi_a^4 + \hat{q}\right) d\Gamma_N \tag{2.55c}$$

of steady state heat transfer problems is obtained. It shall be noted that convection and radiation boundary conditions add additional parts to the stiffness matrix (second integral in Equation (2.55b)) if the problem is further discretized. Furthermore, a non-linear occurrence of the temperature ϕ in Equation (2.55b) due to radiation can be observed. For details on the iterative solution procedure of non-linear steady state heat transfer problems, refer to Bathe [12] and Milka [113].

2.3.4 One-dimensional linear case

The equations derived in the previous chapters are subsequently applied to the one-dimensional case. Thereby, a rod with length l where heat conduction occurs in x-direction is assumed. Additionally, heat convection at the circumferential surface of the rod as proposed by Liu et al. [103] is considered. The differential equation and applied boundary conditions read

$$\frac{d}{dx}\left(\kappa A \cdot \frac{d\phi}{dx}\right) + Q - \alpha U\left(\phi - \phi_a\right) = 0 \qquad \phi(0) = \hat{\phi},\ q(l) = 0 \tag{2.56}$$

where A is the cross-sectional area, and U is the perimeter of the rod. Based on Equation (2.56), the weak form

$$\int_0^l \frac{dv}{dx}\kappa A\frac{d\phi}{dx}dx + \int_0^l v\alpha U\left(\phi - \phi_a\right)dx - \int_0^l vQdx = 0 \tag{2.57}$$

can be derived. It should be noted that the governing equation and the weak form correspond to the respective equations of a linear truss.

Chapter 3

Adjoint sensitivity analysis and influence functions

3.1 Introduction to duality approaches

Adjoint sensitivity analysis and the method of influence functions rely on the principle of duality. The motivation behind dual approaches is to replace the solution of a linear system of equations (discrete case) or a partial differential equation (continuous case) by the solution of the corresponding dual ($\hat{=}$ adjoint) problem. For explanation, the quantity of interest J

$$J = \boldsymbol{g}^T \boldsymbol{u} \tag{3.1}$$

is considered. The vector $\boldsymbol{u}$ is the solution of the *primal problem*

$$\boldsymbol{K}\boldsymbol{u} = \boldsymbol{F} \tag{3.2}$$

with a matrix $\boldsymbol{K}$ and a right-hand side vector $\boldsymbol{F}$. To omit the solution of Equation (3.2), the *adjoint problem*

$$\boldsymbol{K}^T \boldsymbol{\eta} = \boldsymbol{g} \tag{3.3}$$

with the adjoint variable $\boldsymbol{\eta}$ is introduced. If Equation (3.3) is substituted into Equation (3.1)

$$J = \boldsymbol{g}^T \boldsymbol{u} = \left(\boldsymbol{K}^T \boldsymbol{\eta}\right)^T \boldsymbol{u} = \boldsymbol{\eta}^T \boldsymbol{K}\boldsymbol{u} = \boldsymbol{\eta}^T \boldsymbol{F} \tag{3.4}$$

the dual form to determine J is found. The dual form becomes advantageous if J must be determined based on $n > 1$ different vectors $\boldsymbol{F}$. In this case, solving Equation (3.2) n-times can be circumvented by evaluating Equation (3.3) once. In adjoint sensitivity analysis, this property is used to decouple the computational effort from the number of parameters for which sensitivities must be computed (cf. Section 3.2). The influence function method uses the

advantage by efficiently evaluating the value of a specific structural response due to different load cases (cf. Section 3.4).

REMARK I: In the case of a symmetric matrix $\boldsymbol{K}$, the system matrix of the adjoint and primal problem are the same since $\boldsymbol{K}^T = \boldsymbol{K}$ applies. Such problems are called *self-adjoint*.

REMARK II: In linear structural analysis, the matrix $\boldsymbol{K}$ is symmetric and Equation (3.4) can be identified as *Betti's theorem*. Furthermore, the dual solution equates the influence function of the quantity of interest J. For a detailed description, refer to Hartmann et al. [82].

3.2 Discrete adjoint sensitivity analysis

Subsequently, response functions J (e.g., stresses) are considered, which depend on model input parameters $\boldsymbol{s}$ (e.g., Young's modulus) and on the state variables $\boldsymbol{u}$ (e.g., displacements of the finite element nodes), that are also dependent on $\boldsymbol{s}$:

$$J(\boldsymbol{s}, \boldsymbol{u}(\boldsymbol{s})) \tag{3.5}$$

To determine the derivative of the response function concerning an input parameter $s_i \in \boldsymbol{s}$, the chain rule of differentiation has to be employed:

$$\frac{dJ}{ds_i} = \frac{\partial J}{\partial s_i} + \left[\frac{\partial J}{\partial \boldsymbol{u}}\right]^T \cdot \frac{d\boldsymbol{u}}{ds_i} \tag{3.6}$$

The *state derivative* $d\boldsymbol{u}/ds_i$ is determined by deriving the state equation

$$\boldsymbol{r}(\boldsymbol{s}, \boldsymbol{u}(\boldsymbol{s})) = \boldsymbol{0} \tag{3.7}$$

with respect to parameter s_i

$$\frac{d\boldsymbol{r}}{ds_i} = \frac{\partial \boldsymbol{r}}{\partial s_i} + \frac{\partial \boldsymbol{r}}{\partial \boldsymbol{u}} \cdot \frac{d\boldsymbol{u}}{ds_i} = \boldsymbol{0} \Longrightarrow \frac{d\boldsymbol{u}}{ds_i} = \left[\frac{\partial \boldsymbol{r}}{\partial \boldsymbol{u}}\right]^{-1} \cdot \left[-\frac{\partial \boldsymbol{r}}{\partial s_i}\right] = \left[\frac{\partial \boldsymbol{r}}{\partial \boldsymbol{u}}\right]^{-1} \cdot \boldsymbol{F}^* \tag{3.8}$$

where $\partial \boldsymbol{r}/\partial \boldsymbol{u}$ equates to the stiffness matrix $\boldsymbol{K}$ in structural mechanics. The right-hand side $-\partial \boldsymbol{r}/\partial s_i$ is referred to as *pseudo-load* $\boldsymbol{F}^*$. The insertion of Equation (3.8) into Equation (3.6) leads to

$$\frac{dJ}{ds_i} = \frac{\partial J}{\partial s_i} + \left[\frac{\partial J}{\partial \boldsymbol{u}}\right]^T \cdot \left[\frac{\partial \boldsymbol{r}}{\partial \boldsymbol{u}}\right]^{-1} \cdot \left[-\frac{\partial \boldsymbol{r}}{\partial s_i}\right] \tag{3.9}$$

as sensitivity equation. If Equation (3.9) is evaluated from right to left, i.e., by solving Equation (3.8) first, the inverse matrix-vector multiplication with $\partial \boldsymbol{r}/\partial \boldsymbol{u}$ needs to be carried out for each parameter. This is because the right-hand side $-\partial \boldsymbol{r}/\partial s_i$ of the linear system of equations depends on s_i. Hence, the number of required solutions of linear systems containing the stiffness matrix is linearly dependent on the number of parameters but independent of the number of responses. Starting the sensitivity analysis with the solution

of Equation (3.8) is known as *direct sensitivity analysis*, which is favored in cases where the relationship between fewer parameters than responses needs to be investigated.
For opposite problems, where the number of parameters exceeds the number of responses, it is advantageous to change the calculation order by introducing the *adjoint variable* $\boldsymbol{\eta}$ as the solution of the linear system of equations

$$\boldsymbol{\eta}^T = \left[\frac{\partial J}{\partial \boldsymbol{u}}\right]^T \cdot \left[\frac{\partial \boldsymbol{r}}{\partial \boldsymbol{u}}\right]^{-1} \Leftrightarrow \left[\frac{\partial \boldsymbol{r}}{\partial \boldsymbol{u}}\right]^T \boldsymbol{\eta} = \frac{\partial J}{\partial \boldsymbol{u}} \tag{3.10}$$

where the right-hand side $\partial J/\partial \boldsymbol{u}$ is denoted as *adjoint load*. Equation (3.10) is the adjoint problem as introduced in Section 3.1. If Equation (3.10) is solved first, instead of the state derivative given by Equation (3.8), the number of necessary system solutions is determined by the number of responses and is at the same time decoupled from the number of parameters. By inserting the adjoint variable into Equation (3.9), the expression for *adjoint sensitivity analysis* is obtained:

$$\frac{dJ}{ds_i} = \frac{\partial J}{\partial s_i} + \boldsymbol{\eta}^T \cdot \left[-\frac{\partial \boldsymbol{r}}{\partial s_i}\right] = \frac{\partial J}{\partial s_i} + \boldsymbol{\eta}^T \boldsymbol{F}^* \tag{3.11}$$

It is worth emphasizing that the determination of the partial derivatives $\partial J/\partial s_i$, $\partial \boldsymbol{r}/\partial s_i$ and the dot product of the latter and the adjoint variable requires less computational effort than the solution of the linear system in Equation (3.10). Thus, adjoint sensitivity analysis is a method that enables the calculation of sensitivities concerning a large number of parameters with the effort of only one system evaluation per response.

REMARK I: For the method proposed in Chapter 4, the contrary dependencies of adjoint variable and pseudo-load are essential. According to Equation (3.10), the adjoint variable depends on the considered response J and, in the case of a non-linear response concerning $\boldsymbol{u}$, also on the state variables $\boldsymbol{u}$. However, the adjoint variable is independent of the parameters $\boldsymbol{s}$. In contrast, the pseudo-load $-\partial \boldsymbol{r}(\boldsymbol{s}, \boldsymbol{u})/\partial s_i$ is independent of the response but is determined by the parameters $\boldsymbol{s}$ and the state $\boldsymbol{u}$. Only the partial derivative $\partial J/\partial s_i$ simultaneously depends on response and parameter. Section 4.2 demonstrates that $\partial J/\partial s_i$ vanishes for significant responses in structural engineering. In these cases, the overall contribution of the response to the sensitivity is described by the adjoint variable and the entire contribution of the parameters by the pseudo-load. Hence, the individual analysis of the adjoint variable and pseudo-load provides additional sensitivity information. For instance, the adjoint variable indicates zones of a structure where parameter variations could have a minor or significant effect on the response.

REMARK II: The Lagrangian approach is an alternative to the shown derivation of adjoint sensitivity analysis. In Section 3.3.1, a Lagrangian approach is utilized in the case of variational adjoint sensitivity analysis. This thesis does not show the equivalent procedure for discrete formulations, but it can be found in the literature (e.g., Belegundu [15]).

3.2.1 Linear structural problems

The derived general sensitivity equations are applied to linear structural problems. The respective state equation

$$\boldsymbol{r}(\boldsymbol{s}, \boldsymbol{u}(\boldsymbol{s})) = \boldsymbol{K}(\boldsymbol{s})\boldsymbol{u}(\boldsymbol{s}) - \boldsymbol{F}(\boldsymbol{s}) = \boldsymbol{0} \tag{3.12}$$

is derived in Section 2.2.6. The insertion of Equation (3.12) in Equation (3.10) leads to

$$\boldsymbol{\eta}^T = \left[\frac{\partial J}{\partial \boldsymbol{u}}\right]^T \boldsymbol{K}^{-1} \Leftrightarrow \underbrace{\boldsymbol{K}^T}_{=\boldsymbol{K}} \boldsymbol{\eta} = \frac{\partial J}{\partial \boldsymbol{u}} \tag{3.13}$$

as an adjoint problem. Since the stiffness matrix is symmetric, the problem is self-adjoint. According to Equation (3.13), the adjoint variable $\boldsymbol{\eta}$ is the solution of a linear static problem. Hence, the components of $\boldsymbol{\eta}$ can be interpreted as the nodal displacements of a system that is stressed by the adjoint load. The negative partial derivative of Equation (3.12) concerning the parameter, i.e., the pseudo-load $\boldsymbol{F}^*$, can be evaluated by:

$$-\frac{\partial \boldsymbol{r}}{\partial s_i} = \boldsymbol{F}^* = \frac{\partial \boldsymbol{F}}{\partial s_i} - \frac{\partial \boldsymbol{K}}{\partial s_i}\boldsymbol{u} \tag{3.14}$$

The insertion of Equation (3.14) in Equation (3.11) finally leads to

$$\frac{dJ}{ds_i} = \frac{\partial J}{\partial s_i} + \boldsymbol{\eta}^T \left[\frac{\partial \boldsymbol{F}}{\partial s_i} - \frac{\partial \boldsymbol{K}}{\partial s_i}\boldsymbol{u}\right] \tag{3.15}$$

as adjoint sensitivity equation for linear structural problems.

REMARK I: The pseudo-load in Equation (3.14) accounts only for the dependencies of the load vector and stiffness matrix on the parameter s_i. However, the components of the displacement vector $\boldsymbol{u}$ can also directly depend on the parameters. Prescribed displacements to model support settlements are an example. Section 6.6 shows how the pseudo-load must be adapted for such parameters.

3.2.2 Non-linear structural problems

The derived general sensitivity equations are applied to non-linear structural problems. The respective state equation

$$\boldsymbol{r}(\boldsymbol{s}, \boldsymbol{u}(\boldsymbol{s})) = \boldsymbol{f}_{\text{int}}(\boldsymbol{s}, \boldsymbol{u}(\boldsymbol{s})) - \boldsymbol{f}_{\text{ext}}(\boldsymbol{s}, \boldsymbol{u}(\boldsymbol{s})) = \boldsymbol{0} \tag{3.16}$$

is derived in Section 2.2.5 and represents the equilibrium of internal and external forces. The insertion of Equation (3.16) in Equation (3.10) leads to the adjoint problem

$$\boldsymbol{\eta}^T = \left[\frac{\partial J}{\partial \boldsymbol{u}}\right]^T \left[\frac{\partial \boldsymbol{f}_{\text{int}}}{\partial \boldsymbol{u}} - \frac{\partial \boldsymbol{f}_{\text{ext}}}{\partial \boldsymbol{u}}\right]^{-1} \Leftrightarrow \left[\boldsymbol{K}_T(\boldsymbol{u})\right]^T \boldsymbol{\eta} = \frac{\partial J}{\partial \boldsymbol{u}} \tag{3.17}$$

where the tangential stiffness matrix $\boldsymbol{K}_T$ as introduced by Equation (2.39) can be identified. It shall be noted that Equation (3.17) is based on a certain pre-computed equilibrium state $\boldsymbol{u}$. Consequently, the adjoint variable $\boldsymbol{\eta}$ is also the solution of a linear system of equations in the case of non-linear analysis. The negative partial derivative of the state Equation (3.16) with respect to the parameter can be determined by:

$$-\frac{\partial \boldsymbol{r}}{\partial s_i} = \boldsymbol{F}^* = \frac{\partial \boldsymbol{f}_{\text{ext}}}{\partial s_i} - \frac{\partial \boldsymbol{f}_{\text{int}}}{\partial s_i} \tag{3.18}$$

The insertion of Equation (3.18) in Equation (3.11) finally leads to

$$\frac{dJ}{ds_i} = \frac{\partial J}{\partial s_i} + \boldsymbol{\eta}^T \left[\frac{\partial \boldsymbol{f}_{\text{ext}}}{\partial s_i} - \frac{\partial \boldsymbol{f}_{\text{int}}}{\partial s_i} \right] \tag{3.19}$$

as adjoint sensitivity equation for non-linear structural problems.

REMARK I: In the case of conservative systems, the tangential stiffness matrix $\boldsymbol{K}_T$ is the symmetric Hessian of the potential energy (cf. Belytschko et al. [18]), and the adjoint problem is self-adjoint. In non-conservative systems, the tangential stiffness matrix is generally unsymmetrical. A reason for non-conservatism in structural mechanics can be deformation-dependent loads. In such cases, the tangential stiffness matrix must be extended by an additional contribution $\partial \boldsymbol{f}_{\text{ext}}/\partial \boldsymbol{u}$ from the external load called load stiffness matrix. For details in evaluating the load stiffness matrix and its symmetry properties, refer, e.g., to Mok et al. [114], Rumpel et al. [124], and Schweizerhof et al. [129]. The references show that depending on the utilized formulation of the load field, the load stiffness matrix can be symmetrical or unsymmetrical. Hence, in the case of deformation-dependent loads, the tangential stiffness matrix can also be symmetric, leading to self-adjoint problems.

REMARK II: The shown derivation within this section is only valid for path-independent responses. For opposite cases, refer to the literature, e.g., Schwarz [128] investigated path-dependent sensitivity analysis in the presence of elastoplastic material behavior.

3.2.3 Computational aspects

The pseudo-load $\boldsymbol{F}^*$ consists of partial derivatives of the system stiffness matrix and load vector (cf. Equation (3.14)) and the internal and external forces (cf. Equation (3.18)), respectively. These receive their contributions from the elements and boundary conditions (Neumann and Dirichlet) of the finite element model. The global stiffness matrix $\boldsymbol{K}$, for instance, is constructed by assembling the element stiffness matrices $\boldsymbol{k}^e$ of all m finite elements in the domain by

$$\boldsymbol{K} = \mathcal{A}_m \boldsymbol{k}^e \tag{3.20}$$

where $\mathcal{A}$ denotes the assembly operator. However, typical parameters only influence some entries of $\boldsymbol{K}/\boldsymbol{F}$ or $\boldsymbol{f}_{\text{int}}/\boldsymbol{f}_{\text{ext}}$. If the observed parameter affects

merely a subdomain consisting of $n \subset m$ elements, only these n elements assemble a contribution to the partial derivative of the stiffness matrix:

$$\frac{\partial \boldsymbol{K}}{\partial s_i} = \mathcal{A}_n \frac{\partial \boldsymbol{k}^e}{\partial s_i} \tag{3.21}$$

In such cases, $\boldsymbol{F}^*$ is a sparse vector. For reasons of computational efficiency, an element-wise or boundary condition-wise evaluation of Equations (3.15) and (3.19) (further characterized by the superscript letter e) is recommended instead of assembling and operating with system matrices and vectors. From the system vector $\boldsymbol{\eta}$, which is solved by Equation (3.10), the adjoint displacements of member e are extracted to form the adjoint variables $\boldsymbol{\eta}^e$ related to the elements and boundary conditions. Eventually, the sensitivities can be calculated by summing the contributions of the n elements and conditions affected by a given s_i:

$$\frac{dJ}{ds_i} = \frac{\partial J}{\partial s_i} + \sum_n \left\{ [\boldsymbol{\eta}^e]^T \left(\frac{\partial \boldsymbol{f}^e}{\partial s_i} - \frac{\partial \boldsymbol{k}^e}{\partial s_i} \boldsymbol{u}^e \right) \right\} \tag{3.22a}$$

$$\frac{dJ}{ds_i} = \frac{\partial J}{\partial s_i} + \sum_n \left\{ [\boldsymbol{\eta}^e]^T \left(\frac{\partial \boldsymbol{f}^e_{\text{ext}}}{\partial s_i} - \frac{\partial \boldsymbol{f}^e_{\text{int}}}{\partial s_i} \right) \right\} \tag{3.22b}$$

Additional computational simplifications can be achieved by replacing the analytic derivatives of the components of the pseudo-load with finite difference approximations

$$\frac{dJ}{ds_i} = \frac{\partial J}{\partial s_i} + \sum_n \left\{ [\boldsymbol{\eta}^e]^T \left(\frac{\Delta \boldsymbol{f}^e}{\Delta s_i} - \frac{\Delta \boldsymbol{k}^e}{\Delta s_i} \boldsymbol{u}^e \right) \right\} \tag{3.23a}$$

$$\frac{dJ}{ds_i} = \frac{\partial J}{\partial s_i} + \sum_n \left\{ [\boldsymbol{\eta}^e]^T \left(\frac{\Delta \boldsymbol{f}^e_{\text{ext}}}{\Delta s_i} - \frac{\Delta \boldsymbol{f}^e_{\text{int}}}{\Delta s_i} \right) \right\} \tag{3.23b}$$

which is known as *semi-analytic sensitivity analysis* (cf. e.g., Bletzinger et al. [23] and Cheng et al. [35]). The approach is easy to implement and can be used for any parameter s_i and any element or boundary condition. This is advantageous in the case of complex finite element formulations where the analytic derivative can be very extensive to deduce and implement. Furthermore, the semi-analytic approach is competitive to the pure analytic procedure regarding computational time. Refer to Masching [108] for investigations of the numerical efficiency of the semi-analytic procedure.
The non-exactness of the semi-analytic approach is a disadvantage. For too small disturbance values Δs_i, rounding errors can occur, and too large values for Δs_i lead to approximation errors. Hence, a compromise between the two error sources must be found when choosing Δs_i. For an illustrative discussion of that issue and an exemplary determination of optimal disturbance values, refer to Masching [108]. Despite this disadvantage, the semi-analytic approach according to Equation (3.23) is implemented in *Kratos Multiphysics* (cf. Section 1) due to its generality. To judge the suitability of the utilized disturbance value, convergence studies were carried out in all examples contained in this thesis.

3.3 Variational adjoint sensitivity analysis

Discrete sensitivity analysis, as derived in Section 3.2, computes derivatives of a response concerning scalar model parameters of a discretized finite element model. In contrast, variational sensitivity analysis determines sensitivities for parameters distributed throughout the domain as functions.
In contrast to discrete sensitivity analysis, a methodical distinction has to be made concerning the observed parameters. On the one hand, some parameters explicitly appear in the weak form of the underlying physics and the response functional but do not influence the domain shape. In the literature (e.g., Choi et al. [38]), these parameter types refer to *variational sizing sensitivity analysis*, which is characterized by the fact that the integration can be performed over a fixed domain. Typical parameters are cross-sectional dimensions, thickness variables, material properties, or load parameters. For example, derivations of variational sizing sensitivity equations are given by Cho et al. [36], Choi et al. [38], and Haug et al. [85]. On the other hand, there are parameters that influence the shape of the domain. These are handled by *variational shape sensitivity analysis* approaches. A well-known method is the material derivative approach (cf. Arora [6]), in which the shape evolution is described in terms of pseudo time and design velocity. The sensitivity analysis is then conducted by application of the material derivative concept of continuum mechanics. Furthermore, the domain parametrization approach (cf. Tortorelli et al. [135]) is worth mentioning. That method utilizes the transformation of the underlying equations to a fixed reference configuration. Both approaches are compared and critically assessed by Barthold [9]. Another noteworthy method is presented in Barthold et al. [10], which uses an enhanced description of the kinematics in the continuum mechanical formulation.
From a mathematical point of view, shape sensitivity analysis is more sophisticated. As this section shall serve as an introduction to the topic, the derivations in Sections 3.3.2, 3.3.3, and 3.3.4 are limited to parameters that do not influence the integration domain. For derivations of variational shape sensitivity equations, refer to the mentioned literature. Please note that the general procedure shown in Section 3.3.1 applies to both sizing and shape parameters.

3.3.1 Basic principle

For variational sensitivity analysis, the functional

$$J(\boldsymbol{u}, \boldsymbol{s}) : \mathcal{U} \times \mathcal{S} \to \mathbb{R} \tag{3.24}$$

is used to express the response for which sensitivities shall be computed. The functional operates on a state field $\boldsymbol{u}$ and extracts a scalar response value. The aim is to determine the sensitivities of J concerning a design parameter function $\boldsymbol{s} \in \mathcal{S}$ where $\mathcal{S}$ is a space of admissible designs. The variational form $A(\boldsymbol{u}, \boldsymbol{s}; \boldsymbol{v})$ describes the primal problem that solves the state field $\boldsymbol{u}$. For generality, it is assumed that the response functional and the underlying variational problem are non-linear concerning $\boldsymbol{u}$ and $\boldsymbol{s}$. Refer to Section 2.1 for an introduction to forms and variations.

According to Belegundu [15], the Lagrangian approach is a systematic procedure to set up adjoint sensitivity analysis. The variational form $A(\bullet)$ is used as a constraint in the Lagrangian function, i.e., the sensitivities are computed by enforcing that the equilibrium in its weak formulation is fulfilled. Based on this setting, the Lagrangian function reads

$$L(\boldsymbol{u}, \boldsymbol{s}; \boldsymbol{\eta}) = J(\boldsymbol{u}, \boldsymbol{s}) - A(\boldsymbol{u}, \boldsymbol{s}; \boldsymbol{\eta}) \quad \forall \boldsymbol{\eta} \in \mathcal{V} \tag{3.25}$$

whereby $\boldsymbol{\eta}$ indicates the Lagrange multiplier. The total directional derivative (cf. Section 2.1) of the Lagrangian in Equation (3.25) is given by

$$L'(\boldsymbol{u}, \boldsymbol{s}; \boldsymbol{\eta}, \delta\boldsymbol{s}, \delta\boldsymbol{u}, \delta\boldsymbol{\eta}) = L'_s(\boldsymbol{u}, \boldsymbol{s}; \boldsymbol{\eta}, \delta\boldsymbol{s}) + L'_u(\boldsymbol{u}, \boldsymbol{s}; \boldsymbol{\eta}, \delta\boldsymbol{u}) + L'_\eta(\boldsymbol{u}, \boldsymbol{s}; \boldsymbol{\eta}, \delta\boldsymbol{\eta}) \tag{3.26}$$

with

$$L'_s(\boldsymbol{u}, \boldsymbol{s}; \boldsymbol{\eta}, \delta\boldsymbol{s}) = J'_s(\boldsymbol{u}, \boldsymbol{s}; \delta\boldsymbol{s}) - A'_s(\boldsymbol{u}, \boldsymbol{s}; \boldsymbol{\eta}, \delta\boldsymbol{s}) \tag{3.27a}$$

$$L'_u(\boldsymbol{u}, \boldsymbol{s}; \boldsymbol{\eta}, \delta\boldsymbol{u}) = J'_u(\boldsymbol{u}, \boldsymbol{s}; \delta\boldsymbol{u}) - A'_u(\boldsymbol{u}, \boldsymbol{s}; \boldsymbol{\eta}, \delta\boldsymbol{u}) \tag{3.27b}$$

$$L'_\eta(\boldsymbol{u}, \boldsymbol{s}; \boldsymbol{\eta}, \delta\boldsymbol{\eta}) = -A'_\eta(\boldsymbol{u}, \boldsymbol{s}; \boldsymbol{\eta}, \delta\boldsymbol{\eta}) = -A(\boldsymbol{u}, \boldsymbol{s}; \delta\boldsymbol{\eta}) = 0. \tag{3.27c}$$

Note that the Gâteaux derivative $A'_\eta(\bullet)$ equates to the initial variational problem because $A(\boldsymbol{u}, \boldsymbol{s}; \boldsymbol{\eta})$ is linear concerning $\boldsymbol{\eta}$. Hence, Equation (3.27c) is zero if the equilibrium requirement is fulfilled. The Lagrange multiplier is chosen such that Equation (3.27b) vanishes. Therefore,

$$A'_u(\boldsymbol{u}, \boldsymbol{s}; \boldsymbol{\eta}, \delta\boldsymbol{u}) = J'_u(\boldsymbol{u}, \boldsymbol{s}; \delta\boldsymbol{u}) \quad \forall \delta\boldsymbol{u} \in \mathcal{V} \tag{3.28}$$

defines the variational adjoint problem to determine the adjoint variable $\boldsymbol{\eta}$. Note that the Gâteaux derivatives $A'_u(\bullet)$ and $J'_u(\bullet)$ are based on a fixed primal state $\boldsymbol{u}$. Hence, Equation (3.28) is a linear problem concerning $\boldsymbol{\eta}$, which is based on a given solution $\boldsymbol{u}$ determined by the variational primal problem $A(\bullet)$. Finally, Equation (3.26) simplifies to

$$L'(\boldsymbol{u}, \boldsymbol{s}; \boldsymbol{\eta}, \delta\boldsymbol{s}) = L'_s(\boldsymbol{u}, \boldsymbol{s}; \boldsymbol{\eta}, \delta\boldsymbol{s}) = J'_s(\boldsymbol{u}, \boldsymbol{s}; \delta\boldsymbol{s}) - A'_s(\boldsymbol{u}, \boldsymbol{s}; \boldsymbol{\eta}, \delta\boldsymbol{s}) \tag{3.29}$$

and is equal to the total partial variation of the response J

$$\mathcal{D}_s J(\boldsymbol{u}, \boldsymbol{s}) \cdot \delta\boldsymbol{s} = J'_s(\boldsymbol{u}, \boldsymbol{s}; \delta\boldsymbol{s}) - A'_s(\boldsymbol{u}, \boldsymbol{s}; \boldsymbol{\eta}, \delta\boldsymbol{s}) \quad \forall \delta\boldsymbol{s} \in \mathcal{S} \tag{3.30}$$

where $J'_s(\bullet)$ represents the explicit partial variation and $A'_s(\bullet)$ accounts for the implicit dependency on $\boldsymbol{s}$ through the state field $\boldsymbol{u}(\boldsymbol{s})$. In summary, variational adjoint sensitivity analysis can be written as

$$\mathcal{D}_s J(\boldsymbol{u}, \boldsymbol{s}) \cdot \delta\boldsymbol{s} = J'_s(\boldsymbol{u}, \boldsymbol{s}; \delta\boldsymbol{s}) - A'_s(\boldsymbol{u}, \boldsymbol{s}; \boldsymbol{\eta}, \delta\boldsymbol{s}) \quad \forall \delta\boldsymbol{s} \in \mathcal{S} \tag{3.31a}$$

subjected to

$$\left\{ \begin{matrix} J'_u(\boldsymbol{u}, \boldsymbol{s}; \delta\boldsymbol{u}) - A'_u(\boldsymbol{u}, \boldsymbol{s}; \boldsymbol{\eta}, \delta\boldsymbol{u}) \\ A(\boldsymbol{u}, \boldsymbol{s}; \delta\boldsymbol{\eta}) \end{matrix} \right\} = \boldsymbol{0} \quad \forall \{\delta\boldsymbol{u},\ \delta\boldsymbol{\eta}\} \in \mathcal{V} \times \mathcal{V} \tag{3.31b}$$

and consists in analogy to the discrete procedure described in Section 3.2 of the solution of the primal problem, the adjoint problem (both in Equation (3.31b)), and the final sensitivity post-processing (Equation (3.31a)).

3.3.2 Linear structural problems

Subsequently, variational adjoint sensitivity analysis is derived for linear elasticity problems. To create the Lagrangian functional on the basis of Equation (3.25), the variational problem $A(\bullet)$ given by Equation (2.41) is utilized. On that basis, the Lagrangian functional

$$L(\boldsymbol{u};\boldsymbol{\eta}) = J(\boldsymbol{u}) - \int_\Omega \boldsymbol{\sigma}(\boldsymbol{u}) : \boldsymbol{\epsilon}(\boldsymbol{\eta})\, d\Omega + \int_\Omega \boldsymbol{p}\cdot\boldsymbol{\eta}\, d\Omega + \int_{\Gamma_N} \hat{\boldsymbol{t}}\cdot\boldsymbol{\eta}\, d\Gamma_N \tag{3.32}$$

is received. The adjoint problem (Equation (3.28)) is determined by the Gâteaux derivative of Equation (3.32) with respect to $\boldsymbol{u}$ in direction of $\delta\boldsymbol{u}$:

$$\int_\Omega \boldsymbol{\sigma}(\delta\boldsymbol{u}) : \boldsymbol{\epsilon}(\boldsymbol{\eta})\, d\Omega = J'_u(\boldsymbol{u};\delta\boldsymbol{u}). \tag{3.33}$$

The Lagrange multiplier $\boldsymbol{\eta}$ and $\delta\boldsymbol{u}$ can be exchanged within the integral on the left side in Equation (3.33), which leads to the variational problem

$$\int_\Omega \boldsymbol{\sigma}(\boldsymbol{\eta}) : \boldsymbol{\epsilon}(\delta\boldsymbol{u})\, d\Omega = J'_u(\boldsymbol{u};\delta\boldsymbol{u}) \tag{3.34}$$

to solve for the adjoint variable $\boldsymbol{\eta}$. Finally, the sensitivities can be computed by Equation (3.31a). For non-shape parameters, only the Cauchy stress tensor $\boldsymbol{\sigma}$, the distributed force $\boldsymbol{p}$, and the surface traction $\hat{\boldsymbol{t}}$ can be potentially influenced by the parameters. Thus, the total partial variation of the response finally reads

$$\begin{aligned}\mathcal{D}_s J(\boldsymbol{u},\boldsymbol{s})\cdot\delta\boldsymbol{s} = J'_s(\boldsymbol{u},\boldsymbol{s};\delta\boldsymbol{s}) &- \int_\Omega D_{\delta\boldsymbol{s}}\boldsymbol{\sigma}(\boldsymbol{u}) : \boldsymbol{\epsilon}(\boldsymbol{\eta})\, d\Omega \\ &+ \int_\Omega D_{\delta\boldsymbol{s}}\boldsymbol{p}\cdot\boldsymbol{\eta}\, d\Omega + \int_{\Gamma_N} D_{\delta\boldsymbol{s}}\hat{\boldsymbol{t}}\cdot\boldsymbol{\eta}\, d\Gamma_N\end{aligned} \tag{3.35}$$

where $\delta\boldsymbol{s}$ denotes the variation of $\boldsymbol{s}$.

3.3.3 Non-linear structural problems

Subsequently, variational adjoint sensitivity analysis is derived for non-linear structural problems. To create the Lagrangian functional based on Equation (3.25), the variational problem $A(\bullet)$ given by Equation (2.33) is utilized. On that basis, the Lagrangian functional

$$\begin{aligned}L(\boldsymbol{u};\boldsymbol{\eta}) = J(\boldsymbol{u}) &- \int_{\Omega_0} \boldsymbol{S}(\boldsymbol{E}(\boldsymbol{u})) : D_{\boldsymbol{\eta}}\boldsymbol{E}(\boldsymbol{u})\, d\Omega_0 \\ &+ \int_{\Omega_0} \boldsymbol{p}_0\cdot\boldsymbol{\eta}\, d\Omega_0 + \int_{\Gamma_{N0}} \hat{\boldsymbol{t}}_0\cdot\boldsymbol{\eta}\, d\Gamma_{N0}\end{aligned} \tag{3.36}$$

is received. The adjoint problem (Equation (3.28)) is determined by the Gâteaux derivative of Equation (3.36) with respect to $\boldsymbol{u}$ in direction of $\delta\boldsymbol{u}$

$$\begin{aligned}\int_{\Omega_0} [\boldsymbol{S}(\boldsymbol{E}(\boldsymbol{u})) : D_{\delta\boldsymbol{u}\boldsymbol{\eta}}\boldsymbol{E}(\boldsymbol{u}) + D_{\boldsymbol{\eta}}\boldsymbol{E}(\boldsymbol{u}) : \mathbb{C} : D_{\delta\boldsymbol{u}}\boldsymbol{E}(\boldsymbol{u})]\, d\Omega_0 \\ - \int_{\Omega_0} D_{\delta\boldsymbol{u}}\boldsymbol{p}_0 \cdot \boldsymbol{\eta}\, d\Omega_0 - \int_{\Gamma_{N0}} D_{\delta\boldsymbol{u}}\hat{\boldsymbol{t}}_0 \cdot \boldsymbol{\eta}\, d\Gamma_{N0} = J'_u(\boldsymbol{u}; \delta\boldsymbol{u})\end{aligned} \tag{3.37}$$

where $\mathbb{C} = \partial\boldsymbol{S}(\boldsymbol{E})/\partial\boldsymbol{E}$ denotes the elasticity tensor (cf. Equation (2.25)). The left-hand side part of Equation (3.37) is equivalent to the linearization of the variational form, which is needed for the iterative computation with the Newton Raphson scheme (cf. Section 2.1). In that regard, the vector $\delta\boldsymbol{u}$ is equivalent to the incremental displacement field $\Delta\boldsymbol{u}$ for which it has to be solved in the Newton Raphson algorithm. The discretization of the left-hand side part of Equation (3.37) results in the tangential stiffness matrix $\boldsymbol{K}_T$ (cf. Equation (2.39)).

For the sake of simplicity, it is subsequently assumed that $\boldsymbol{p}_0$ and $\hat{\boldsymbol{t}}_0$ are independent of the displacement field $\boldsymbol{u}$. It follows that the Gâteaux derivatives

$$D_{\delta\boldsymbol{u}}\boldsymbol{p}_0 = 0 \quad \text{and} \quad D_{\delta\boldsymbol{u}}\hat{\boldsymbol{t}}_0 = 0 \tag{3.38}$$

vanish, which reduces Equation (3.37) to:

$$\int_{\Omega_0} [\boldsymbol{S}(\boldsymbol{E}(\boldsymbol{u})) : D_{\delta\boldsymbol{u}\boldsymbol{\eta}}\boldsymbol{E}(\boldsymbol{u}) + D_{\boldsymbol{\eta}}\boldsymbol{E}(\boldsymbol{u}) : \mathbb{C} : D_{\delta\boldsymbol{u}}\boldsymbol{E}(\boldsymbol{u})]\, d\Omega_0 = J'_u(\boldsymbol{u}; \delta\boldsymbol{u}) \tag{3.39}$$

The adjoint variable $\boldsymbol{\eta}$ and $\delta\boldsymbol{u}$ can be interchanged in Equation (3.39) without changing the result of the integral (cf. Holzapfel [90]). By rewriting Equation (3.39), the adjoint problem

$$\int_{\Omega_0} [\boldsymbol{S}(\boldsymbol{E}(\boldsymbol{u})) : D_{\boldsymbol{\eta}\delta\boldsymbol{u}}\boldsymbol{E}(\boldsymbol{u}) + D_{\delta\boldsymbol{u}}\boldsymbol{E}(\boldsymbol{u}) : \mathbb{C} : D_{\boldsymbol{\eta}}\boldsymbol{E}(\boldsymbol{u})]\, d\Omega_0 = J'_u(\boldsymbol{u}; \delta\boldsymbol{u}) \tag{3.40}$$

to solve for $\boldsymbol{\eta}$ is received. Finally, the sensitivities can be computed using Equation (3.31a). For non-shape parameters, only the Second Piola-Kirchhoff stress tensor $\boldsymbol{S}$, the body force $\boldsymbol{p}_0$, and the surface traction $\hat{\boldsymbol{t}}_0$ can be potentially influenced by the parameters. Thus, the total partial variation of the response finally reads

$$\begin{aligned}\mathcal{D}_s J(\boldsymbol{u}, \boldsymbol{s}) \cdot \delta\boldsymbol{s} = J'_s(\boldsymbol{u}, \boldsymbol{s}; \delta\boldsymbol{s}) - \int_{\Omega_0} D_{\delta\boldsymbol{s}}\boldsymbol{S}(\boldsymbol{E}(\boldsymbol{u})) : D_{\boldsymbol{\eta}}\boldsymbol{E}(\boldsymbol{u})\, d\Omega_0 \\ + \int_{\Omega_0} D_{\delta\boldsymbol{s}}\boldsymbol{p}_0 \cdot \boldsymbol{\eta}\, d\Omega_0 + \int_{\Gamma_{N0}} D_{\delta\boldsymbol{s}}\hat{\boldsymbol{t}}_0 \cdot \boldsymbol{\eta}\, d\Gamma_{N0}\end{aligned} \tag{3.41}$$

where $\delta\boldsymbol{s}$ denotes the variation of $\boldsymbol{s}$.

3.3.4 Steady state heat transfer problems

Besides structural mechanics, variational adjoint sensitivity analysis is derived for steady state heat transfer problems. To create the Lagrangian functional based on Equation (3.25), the variational problem $A(\bullet)$ given by Equation (2.55) is utilized. On that basis, the Lagrangian functional

$$\begin{aligned} L(\phi;\eta) = J(\phi) - \int_\Omega (\boldsymbol{\nabla}\eta)^T \boldsymbol{\kappa}\boldsymbol{\nabla}\phi \, d\Omega - \int_{\Gamma_N} \eta \left(\alpha\phi + \sigma\epsilon\phi^4\right) d\Gamma_N \\ + \int_\Omega \eta Q \, d\Omega + \int_{\Gamma_N} \eta \left(\alpha\phi_a + \sigma\epsilon\phi_a^4 + \hat{q}\right) d\Gamma_N \end{aligned} \tag{3.42}$$

is received. The adjoint problem (Equation (3.28)) is determined by the Gâteaux derivative of Equation (3.42) with respect to ϕ in direction of $\delta\phi$:

$$\int_\Omega (\boldsymbol{\nabla}\eta)^T \boldsymbol{\kappa}\boldsymbol{\nabla}\delta\phi \, d\Omega + \int_{\Gamma_N} \eta \left(\alpha + \sigma\epsilon \cdot 4\phi^3\right) \delta\phi \, d\Gamma_N = J'_\phi(\phi;\delta\phi) \tag{3.43}$$

The Lagrange multiplier η and $\delta\phi$ can be exchanged within the integral on the left side in Equation (3.43), which leads to the variational problem

$$\int_\Omega (\boldsymbol{\nabla}\delta\phi)^T \boldsymbol{\kappa}\boldsymbol{\nabla}\eta \, d\Omega + \int_{\Gamma_N} \delta\phi \left(\alpha + \sigma\epsilon \cdot 4\phi^3\right) \eta \, d\Gamma_N = J'_\phi(\phi;\delta\phi) \tag{3.44}$$

to solve for the adjoint variable η. Finally, the sensitivities can be computed using Equation (3.31a). The total partial variation of the response with respect to all non-shape parameters reads

$$\begin{aligned} \mathcal{D}_s J(\phi, \boldsymbol{s}) \cdot \delta\boldsymbol{s} = & J'_s(\phi, \boldsymbol{s}; \delta\boldsymbol{s}) - \int_\Omega (\boldsymbol{\nabla}\eta)^T D_{\delta\boldsymbol{s}}\boldsymbol{\kappa}\boldsymbol{\nabla}\phi \, d\Omega \\ & - \int_{\Gamma_N} \eta \cdot D_{\delta\boldsymbol{s}} \left(\alpha\phi + \sigma\epsilon\phi^4\right) d\Gamma_N + \int_\Omega \eta \cdot D_{\delta\boldsymbol{s}} Q \, d\Omega \\ & + \int_{\Gamma_N} \eta \cdot D_{\delta\boldsymbol{s}} \left(\alpha\phi_a + \sigma\epsilon\phi_a^4 + \hat{q}\right) d\Gamma_N \end{aligned} \tag{3.45}$$

where $\delta\boldsymbol{s}$ denotes the variation of $\boldsymbol{s}$.

3.4 Influence functions in structural analysis

The method of influence lines and surfaces (or more general influence functions) is a well-established structural analysis approach. The influence function describes the impact of a load at an arbitrary position in a analysis model on a specifically selected response (stress resultant or displacement) by a displacement field. As the approach is a well-known and established method in structural analysis, information can be found in many publications. For

instance, detailed and theory-focused descriptions of the method are given by Hartmann [81], Hartmann et al. [82], and Melnikov [111]. In contrast, Ghali et al. [69] and Marti [107] provide brief and application-orientated instructions.

3.4.1 Fundamentals

The method of influence functions consists of two analysis phases. In the first step, the influence function $\boldsymbol{\eta}$ for the chosen response J at a position $\boldsymbol{x}$ has to be evaluated as the structural displacement by application of the *dual load*. The dual load can be described by the generalized Dirac delta function, which fulfills the properties

$$\boldsymbol{\delta}_i^j(\boldsymbol{y}-\boldsymbol{x}) = \mathbf{0} \quad \text{for} \quad \boldsymbol{y} \neq \boldsymbol{x} \quad \text{and} \quad \int_\Omega \boldsymbol{f}(\boldsymbol{y}) \cdot \boldsymbol{\delta}_i^j(\boldsymbol{y}-\boldsymbol{x}) d\Omega_{\boldsymbol{y}} = \partial^i f_j(\boldsymbol{x}) \tag{3.46}$$

where $\partial^i f_j(\boldsymbol{x})$ denotes a partial differential operator of order i which acts on a function f at $\boldsymbol{x}$ in the jth direction (cf. Grätsch [73] for more information). Employing the Dirac delta, the influence function can be computed by the dual problem

$$-\boldsymbol{\mathcal{L}}_{\boldsymbol{y}} \boldsymbol{\eta}_i(\boldsymbol{y}, \boldsymbol{x}) = \boldsymbol{\delta}_i^j(\boldsymbol{y} - \boldsymbol{x}) \quad \text{in } \Omega \tag{3.47}$$

which satisfies homogeneous boundary conditions at $\Gamma = \partial\Omega$. Note that the subscript on $\boldsymbol{\mathcal{L}}$ indicates that the differential operator acts on $\boldsymbol{y}$. In the case of a displacement as a response, the Dirac function in Equation (3.47) can be interpreted as unity point load in j-direction applied at $\boldsymbol{x}$. In the case of force quantities (internal or support forces), a unity displacement at the response location $\boldsymbol{x}$ has to be applied according to *Land's theorem* and *Müller-Breslau's principle*. The Dirac delta can be interpreted as a unity jump or kink at $\boldsymbol{x}$, which can be realized by a pre-deformation load case in practice. Common dual load cases are illustrated in Figure 3.1. For further information, refer to Hartmann et al. [82].
In the second step, the functional value of J due to a distributed load $\boldsymbol{p}$ can be determined using the influence function. The procedure can be motivated if the reciprocal external work of the primal problem ($\hat{=}$ governing equation of linear elasticity theory according to Equation (2.40)) and dual problem (Equation (3.47)) is related by *Betti's theorem*

$$\int_\Omega \boldsymbol{u}(\boldsymbol{y}) \cdot \boldsymbol{\delta}_i^j(\boldsymbol{y} - \boldsymbol{x}) d\Omega_{\boldsymbol{y}} - \int_\Omega \boldsymbol{\eta}_i(\boldsymbol{y}, \boldsymbol{x}) \cdot \boldsymbol{p}(\boldsymbol{y}) d\Omega_{\boldsymbol{y}} = 0 \tag{3.48}$$

where $\boldsymbol{u}$ is assumed to be $\mathbf{0}$ on Γ. Finally, Equation (3.48) can be reformulated as

$$1 \cdot \partial^i u_j(\boldsymbol{x}) = 1 \cdot J = \int_\Omega \boldsymbol{\eta}_i(\boldsymbol{y}, \boldsymbol{x}) \cdot \boldsymbol{p}(\boldsymbol{y}) d\Omega_{\boldsymbol{y}} \tag{3.49}$$

in order to compute the response value $J = \partial^i u_j(\boldsymbol{x})$. In the case of a discrete problem, the response value is evaluated by the dot product

$$1 \cdot J = \boldsymbol{\eta}^T \boldsymbol{F} \tag{3.50}$$

of the discrete influence function $\boldsymbol{\eta}$ and load vector $\boldsymbol{F}$. The comparison with Equation (3.4) shows that Equation (3.50) is the dual form for calculating the response value J.
The multiplier "1" on the left-hand side of Equations (3.49) and (3.50) can be interpreted as the energetic conjugated dual load concerning the response. Hence, the equations contain work expressions on both sides. Since the "1" is mathematically not necessary, it is only written explicitly in the thesis in cases where it is essential to recognize that the method of influence functions is based on a work balance.
To illustrate the meaning of the generalized Dirac delta and the corresponding left-hand side part in Equation (3.49), an Euler Bernoulli beam (cf. Appendix B.1) is considered. The Dirac delta function of order i has, in this case, the following filtering properties for the displacement w:

$$\int_0^l \delta_i(y-x)\, w(y)\, dy = \begin{cases} 1 \cdot w(x) & (i=0) \\ 1 \cdot w'(x) & (i=1) \\ 1 \cdot M(x) = -EIw''(x) \cdot 1 & (i=2) \\ 1 \cdot V(x) = -EIw'''(x) \cdot 1 & (i=3) \end{cases} \tag{3.51}$$

The Dirac deltas and the corresponding "1" can be interpreted as

$$\begin{aligned} &\delta_0: \text{ load } \bar{P}=1 && \delta_1: \text{ moment } \bar{M}=1 \\ &\delta_2: \text{ kink } \Delta\bar{w}'=1 && \delta_3: \text{ jump } \Delta\bar{w}=1 \end{aligned} \tag{3.52}$$

which are the dual loads shown in Figure 3.1. For further reading on the meaning of the Dirac delta function in the context of the influence function approach, please refer to Hartmann et al. [82].

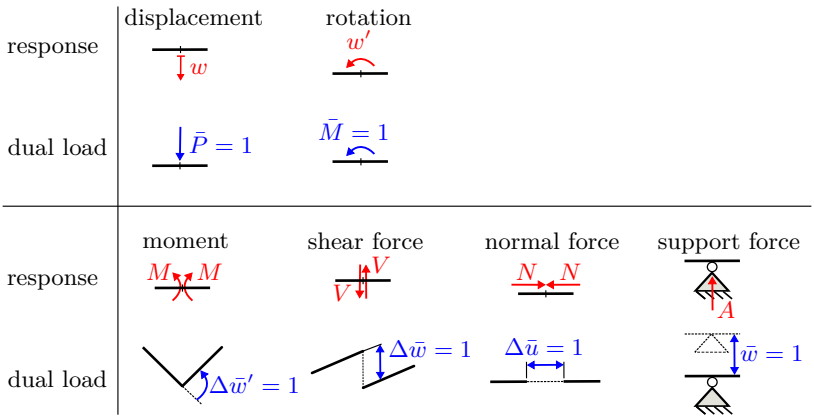

Figure 3.1: Dual loads (blue) for generating influence functions of displacement and force quantities as responses (red).

3.4.2 Practical relevance

The determination of the influence function $\boldsymbol{\eta}$ represents the main effort of the entire approach. Once the influence function $\boldsymbol{\eta}$ has been predetermined, the evaluation of the response value using Equations (3.49) and (3.50) is simple and can be carried out with minimal computational effort. Hence, the method of influence functions is an efficient tool to deal with various load cases regarding selected responses. This feature can be beneficially employed to find critical positions of moving loads or to identify critical load cases. This is why influence functions are highly relevant, especially when designing bridges or crane runways.
The practical benefits can be further enhanced if influence functions are used as a graphical tool. For illustration, Figure 3.2 shows the influence function of the bending moment M_m at location x_m (center of right span). The structure is subjected to three different load cases. The task is to find the critical loading concerning M_m. Load case 3 is identified as decisive since a line load with higher intensity coincides with a region of the influence function with dominant functional values. The intuitive solution of such tasks by graphical means is a significant benefit of influence functions and can be seen as the reason for their importance in structural analysis.

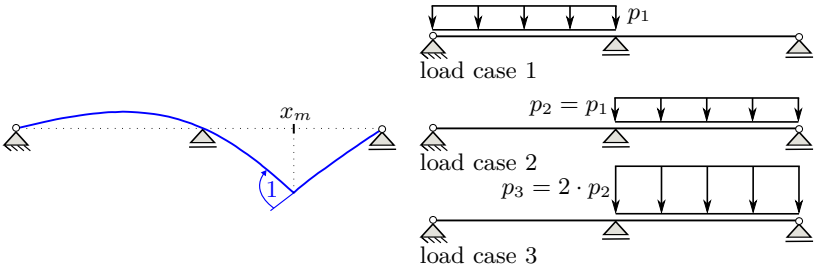

Figure 3.2: Influence function of bending moment M_m at location x_m (left) and three different load cases (right).

3.4.3 Relation to Green's function

The *Green's function* approach is a well-established method in the mathematics of differential equations. There is a large number of publications and books dealing with this topic. Comprehensive mathematical descriptions can be found at Stakgold et al. [133] or Cabada [29]. Rother [123] provides a discussion of the topic in physics, and Melnikov [111] focuses on Green's function for problems in structural mechanics. There is a close relationship between the Green's function approach and the influence function method.
In the following, the linear, inhomogeneous differential equation (boundary value problem)

$$-\boldsymbol{\mathcal{L}}\boldsymbol{u}(\boldsymbol{x}) = \boldsymbol{p}(\boldsymbol{x}) \quad \text{in } \Omega \tag{3.53}$$

is considered where $\boldsymbol{\mathcal{L}}$ denotes the differential operator and $\boldsymbol{u}$ and $\boldsymbol{p}$ are functions which are defined in the domain Ω. If Equation (3.53) must be solved for different right-hand side terms $\boldsymbol{p}(\boldsymbol{x})$, it is beneficial to determine the unknown function $\boldsymbol{u}(\boldsymbol{x})$ by

$$\boldsymbol{u}(\boldsymbol{x}) = \int_{\Omega} \boldsymbol{G}_0(\boldsymbol{x}, \boldsymbol{y}) \boldsymbol{p}(\boldsymbol{y}) d\Omega_{\boldsymbol{y}} \tag{3.54}$$

instead. The kernel $\boldsymbol{G}_0(\boldsymbol{x}, \boldsymbol{y})$ of the integral operator given in Equation (3.54) is called *Green's function*. A unique Green's function $\boldsymbol{G}_0(\boldsymbol{x}, \boldsymbol{y})$ exists if the homogeneous differential equation $\boldsymbol{\mathcal{L}u}(\boldsymbol{x}) = \boldsymbol{0}$ corresponding to Equation (3.53) has only the trivial (zero) solution. See e.g., Melnikov [111] or Stakgold et al. [133] for more information. Furthermore, a Green's function has to satisfy

$$-\boldsymbol{\mathcal{L}}_{\boldsymbol{x}} \boldsymbol{G}_0(\boldsymbol{x}, \boldsymbol{y}) = \boldsymbol{\delta}_0^j(\boldsymbol{x} - \boldsymbol{y}) \tag{3.55}$$

where the subscript on $\boldsymbol{\mathcal{L}}$ indicates that the differential operator acts on $\boldsymbol{x}$. The function $\boldsymbol{\delta}_0^j(\boldsymbol{x} - \boldsymbol{y})$ denotes the Dirac delta as introduced by Equation (3.46). In structural mechanics, the Dirac delta in Equation (3.55) can be interpreted as a unity point load acting at $\boldsymbol{y}$ in direction j and the Green's function as the resultant structural displacement. Similar interpretations are also possible for other physics. In steady state heat transfer problems the Green's function equates the temperature corresponding to a unit heat source applied at $\boldsymbol{y}$. As the Dirac delta in the Green's function approach equates the dual load, the influence function $\boldsymbol{\eta}_i$ in structural analysis can be identified as Green's function $\boldsymbol{G}_i$. However, the aims and applications of the two approaches differ slightly. The goal of Green's function approach is to determine the unknown function $\boldsymbol{u}(\boldsymbol{x})$ for a given $\boldsymbol{p}$ based on Equation (3.54). In contrast, the method of influence function is concerned with a specific response at a fixed position $\boldsymbol{x}$. This can seen by the exchanged arguments $\boldsymbol{x}$ and $\boldsymbol{y}$ in Equations (3.47) and (3.49) compared to Equations (3.54) and (3.55).

Chapter 4

The method of generalized influence functions

The literature shows a strong relationship between adjoint sensitivity analysis and the method of influence functions. Refer to Chapter 1 for an overview of essential references. Based on the knowledge about this methodical connection, this chapter investigates how and to what extent the method of influence functions can be generalized based on adjoint sensitivity analysis. The goal is to extend the traditional influence functions approach as a tool for sensitivity analysis, which compromises various kinds of (i) responses (also other than deflections and stress resultants), (ii) parameters (also other than load position and intensity), (iii) and underlying physics (also other than structural mechanics). Consequently, the methodical enhancement is denoted as the *method of generalized influence functions*.

The relation between general responses and parameters is commonly non-linear. In such cases, the superposition principle is invalid, so the response value cannot be evaluated for a given value of a general parameter using the influence function. In a generalized perception, the task of the influence function is to identify the parts of a structure where parameter variations could significantly affect the response. Hence, the method of generalized influence functions aims to provide the derivatives instead of the response value in the case of general responses and parameters. This understanding also extends the influence functions approach to non-linear structural analysis. Please note that Kunow [97] or Estep et al. [54] use the denotation *generalized influence function* to generate influence functions for various responses and not in the context of sensitivity analysis.

This chapter is organized as follows: Section 4.1 provides a fundamental discussion about the connection of the adjoint variable and the influence function. Section 4.2 derives influence functions for significant practice-relevant responses as displacements, stress resultants, or support forces based on adjoint sensitivity analysis. Subsequently, Section 4.3 investigates how the method of influence functions can be extended for general responses and parameters and what limitations exist. Therefore, a mechanically interpretable

extension that can be linked to the work expressions based on *Betti's theorem* is investigated. Another objective of the section is to examine how the graphical procedure, for which the classical influence functions approach is well known, can be extended for various parameters. The application of the concept to another physics is demonstrated in Sections 4.4.
It shall be noted that the concept of generalizing the method of influence functions by adjoint sensitivity analysis and some parts of this chapter have been pre-published in Fußeder et al. [63, 66, 67]. For readability reasons, these sources are not always explicitly referred to below.

4.1 Equivalence of adjoint variable and influence function

The crucial requisite for the method of generalized influence functions is the appearance of the influence function as part of the adjoint approach. As outlined in Chapter 1, the adjoint variable can be identified as influence function. In the following, different approaches to identify the influence function as the adjoint variable are reviewed and discussed.

4.1.1 Connection through load sensitivities

Influence functions are typically used to determine worst-case positions of movable loads or for efficient evaluation of response values due to various load cases (cf. Section 3.4.2). From another perspective, an influence function can also be seen as a provider of sensitivities concerning the parameters "load intensity" and "load position." Figure 4.1 illustrates the influence function of the bending moment at the position x_m of a two-span, which is subjected to a point load at x_m and x_n, respectively.

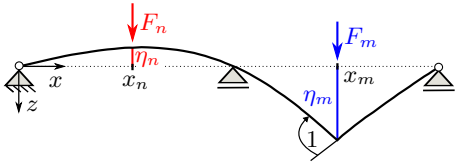

Figure 4.1: Influence function of bending moment at location at x_m. Single forces are evaluated at x_m and x_n.

Due to $|\eta_m| > |\eta_n|$, a variation of the load at x_m has a more significant influence on the bending moment as the same variation of the load at x_n. This becomes apparent when Equation (3.49) is applied to the given problem and then differentiated concerning the load intensities in order to calculate the sensitivities:

$$\left|\frac{dM_m}{dF_m}\right| = |\eta_m| > |\eta_n| = \left|\frac{dM_m}{dF_n}\right| \text{ with } M_m = \eta_m F_m + \eta_n F_n \qquad (4.1)$$

Equation (4.1) indicates that the sensitivity is equal to the functional value of the influence function at the position of the load. Thus, the graphical influence function can be seen as a sensitivity map for the parameter "loading," which allows a graphical assessment of the impact of a change in load intensity or position solely by examining the ordinate of the influence function. A more general term for sensitivity calculations concerning a load parameter s_i can be found in discrete formulation by deriving Equation (3.50):

$$\frac{dJ}{ds_i} = \boldsymbol{\eta}^T \frac{\partial \boldsymbol{F}}{\partial s_i} \tag{4.2}$$

Equation (4.2) states that the sensitivity analysis for load parameters corresponds to the evaluation of an artificial load vector $\partial \boldsymbol{F}/\partial s_i$ on the influence function. Hence, the sensitivity analysis is formally equivalent to the evaluation of physical loads $\boldsymbol{F}$ according to the Equation (3.50). If the parameter s_i is the intensity F_j of the jth component of $\boldsymbol{F}$, Equation (4.2) reduces to the jth component η_j of the discrete influence function

$$\frac{dJ}{dF_j} = \boldsymbol{\eta}^T \frac{\partial \boldsymbol{F}}{\partial F_j} = \boldsymbol{\eta}^T \boldsymbol{e}_j = \eta_j \cdot 1 \tag{4.3}$$

where $\boldsymbol{e}_j$ is the jth unit vector. Based on that finding and on the basis of Equation (4.1), the derivative $dJ/d\boldsymbol{F}$ can be identified as discrete influence function:

$$\frac{dJ}{d\boldsymbol{F}} = \boldsymbol{\eta} \tag{4.4}$$

Belegundu [14] was the first researcher who wrote about the methodical connection. The basis of his argumentation is the understanding that influence functions are the direct carriers of load sensitivities as indicated by Equation (4.4). In detail, Belegundu [14] computes sensitivities with respect to the components of the load vector $\boldsymbol{F}$ of a response $J(\boldsymbol{u}(\boldsymbol{F}))$ by applying the chain rule of differentiation

$$\left[\frac{dJ}{d\boldsymbol{F}}\right]^T = \left[\frac{\partial J}{\partial \boldsymbol{u}}\right]^T \cdot \frac{d\boldsymbol{u}}{d\boldsymbol{F}} \tag{4.5}$$

which can be reformulated by using $d\boldsymbol{u}/d\boldsymbol{F} = \boldsymbol{K}^{-1}$ and by considering the symmetry of the stiffness matrix $\boldsymbol{K}$ to

$$\boldsymbol{K}\frac{dJ}{d\boldsymbol{F}} = \frac{\partial J}{\partial \boldsymbol{u}}. \tag{4.6}$$

Equation (4.6) is equal to the adjoint problem defined in Equation (3.13) if the derivative $dJ/d\boldsymbol{F}$ is replaced by the adjoint variable $\boldsymbol{\eta}$. Based on Equation (4.4), which identifies the derivative $dJ/d\boldsymbol{F}$ as influence function, it can be concluded that the adjoint variable must be the discrete influence function.

REMARK I: The shown derivation of Belegundu only considers the implicit dependency of J on $\boldsymbol{F}$ through the state $\boldsymbol{u}$. However, there are also

responses with an explicit dependency concerning $\boldsymbol{F}$, i.e., $J(\boldsymbol{F}, \boldsymbol{u}(\boldsymbol{F}))$ should be used correctly. This would require adding the partial derivative $\partial J/\partial \boldsymbol{F}$ to Equation (4.5) whereby, as a consequence, the relation with the adjoint problem cannot be directly established. Section 4.2 examines the importance of explicit parameter dependencies for determining influence functions in adjoint sensitivity analysis.

REMARK II: In Belegundu [16, 17], influence functions for a support force and a bending moment are determined based on Equation (4.6) without justification of the support shift and the kink by a value of "1." Section 4.2 shows how the discontinuities of the influence functions can be originated based on the complete sensitivity equation.

4.1.2 Connection through the Lagrangian approach

Section 3.3.1 describes the Lagrangian approach as a systematic way to derive adjoint sensitivity analysis. The traditional method of influence functions requires the validity of the principle of superposition. To show the equivalence of adjoint variable and influence function, a functional $J(\boldsymbol{s}; \boldsymbol{u}) : \mathcal{S} \times \mathcal{U} \to \mathbb{R}$ which linearly operates on the unknown function $\boldsymbol{u} \in \mathcal{U}$ must be considered. Furthermore, let $\boldsymbol{u}$ be the result of a given linear variational problem

$$A(\boldsymbol{u}, \boldsymbol{v}) = a(\boldsymbol{u}, \boldsymbol{v}) - (\boldsymbol{p}, \boldsymbol{v}) = 0 \quad \forall \boldsymbol{v} \in \mathcal{V} \tag{4.7}$$

where $a(\boldsymbol{u}, \boldsymbol{v}) : \mathcal{U} \times \mathcal{V} \to \mathbb{R}$ represents a symmetric bilinear form and $(\boldsymbol{p}, \boldsymbol{v}) = F(\boldsymbol{v}) : \mathcal{V} \to \mathbb{R}$ a functional concerning load $\boldsymbol{p}$ (see Section 2.1 for information). Furthermore, it is assumed that $\boldsymbol{u}$ fulfills homogeneous boundary conditions ($\boldsymbol{u} = \boldsymbol{0}$ on Γ_D) whereby the spaces $\mathcal{U}$ and $\mathcal{V}$ coincide (cf. Equation (2.7)). Based on the Lagrangian functional

$$L(\boldsymbol{s}; \boldsymbol{u}, \boldsymbol{\eta}) = J(\boldsymbol{s}; \boldsymbol{u}) - A(\boldsymbol{s}; \boldsymbol{u}, \boldsymbol{\eta}) \quad \forall \boldsymbol{\eta} \in \mathcal{V} \tag{4.8}$$

with the Lagrange multiplier $\boldsymbol{\eta} \in \mathcal{V}$, variational adjoint sensitivity analysis according to Equation (3.31) can be established:

$$\mathcal{D}_s J(\boldsymbol{s}; \boldsymbol{u}) \delta \boldsymbol{s} = J'_s(\boldsymbol{s}; \boldsymbol{u}, \delta \boldsymbol{s}) - A'_s(\boldsymbol{s}; \boldsymbol{u}, \boldsymbol{\eta}, \delta \boldsymbol{s}) \quad \forall \delta \boldsymbol{s} \in \mathcal{S} \tag{4.9a}$$

subjected to

$$\left\{ \begin{matrix} J'_u(\boldsymbol{s}; \boldsymbol{u}, \delta \boldsymbol{u}) - A'_u(\boldsymbol{s}; \boldsymbol{u}, \boldsymbol{\eta}, \delta \boldsymbol{u}) \\ A(\boldsymbol{s}; \boldsymbol{u}, \delta \boldsymbol{\eta}) \end{matrix} \right\} = \boldsymbol{0} \quad \forall \{\delta \boldsymbol{u},\ \delta \boldsymbol{\eta}\} \in \mathcal{V} \times \mathcal{V} \tag{4.9b}$$

Under consideration of the assumed linearity of A and J concerning $\boldsymbol{u}$ and $\boldsymbol{\eta}$, Equation (4.9b) simplifies to

$$\left\{ \begin{matrix} J(\delta \boldsymbol{u}) - a(\delta \boldsymbol{u}, \boldsymbol{\eta}) \\ a(\boldsymbol{u}, \delta \boldsymbol{\eta}) - (\boldsymbol{p}, \delta \boldsymbol{\eta}) \end{matrix} \right\} = \boldsymbol{0} \quad \forall \{\delta \boldsymbol{u},\ \delta \boldsymbol{\eta}\} \in \mathcal{V} \times \mathcal{V} \tag{4.10}$$

where the dependency with respect to $\boldsymbol{s}$ is dropped for improved readability. Based on the assumption of linearity of the functional and the variational

problem, the dual problem can be solved independently from the primal solution, i.e., without pre-computation of $\boldsymbol{u}$. The adjoint and primal problem in Equation (4.10) share the identical symmetrical bilinear form and their solution is contained in the same solution space. Hence, the arguments of $a(\cdot,\cdot)$ in Equation (4.10) are exchangeable and the dual and primal problem can be combined:

$$a(\boldsymbol{u},\boldsymbol{\eta}) = (\boldsymbol{p},\boldsymbol{\eta}) = J(\boldsymbol{u}) \tag{4.11}$$

Equation (4.11) reveals that the functional $J(\boldsymbol{u})$ can be evaluated by the scalar product of the adjoint variable $\boldsymbol{\eta}$ and the right-hand side $\boldsymbol{p}$ of the underlying boundary value problem (cf. Equation (2.40)):

$$J(\boldsymbol{u}) = (\boldsymbol{p},\boldsymbol{\eta}) = \int_\Omega \boldsymbol{\eta}\cdot\boldsymbol{p}\,d\Omega \tag{4.12}$$

As the equivalence of Equations (4.12) and (3.49) is obvious, the adjoint variable $\boldsymbol{\eta}$ can be interpreted as the influence function related to the response defined by the functional $J(\boldsymbol{u})$. It is worth mentioning that also Grätsch et al. [74] identifies the dual-solution as influence function.
To illustrate the meaning of Equations (4.10) and (4.11), the variational form of an Euler-Bernoulli beam given by Equation (B.5) is observed. Based on the response functional

$$J(w) = \int_0^l w\cdot\delta_i(x-y)\,dx \tag{4.13}$$

according to Equation (3.51), the variational forms in Equation (4.10) read:

$$\int_0^l \delta w\cdot\delta_i(x-y)\,dx - \int_0^l EI\delta w''\cdot\eta''\,dx = 0 \tag{4.14a}$$

$$\int_0^l EIw''\cdot\delta\eta''\,dx - \int_0^l \delta\eta\cdot p\,dx = 0 \tag{4.14b}$$

By replacing δw with w in Equation (4.14a) and $\delta\eta$ with η in Equation (4.14b), both variational forms are still fulfilled and share the same bilinear form $a(w,\eta)$. Thus, the sum of Equation (4.14a) and (4.14b) with replaced arguments is

$$\int_0^l w\cdot\delta_i(x-y)\,dx - \int_0^l \eta\cdot p\,dx = 0 \quad\Rightarrow\quad J(w) = \int_0^l \eta\cdot p\,dx \tag{4.15}$$

which equates Betti's theorem as used in Equation (3.48) to derive the influence functions approach.

REMARK I: Hartmann et al. [83] and Kunow [97] apply a Lagrangian function as a systematic approach to show the existence of a Green's function ($\hat{=}$ influence function, see Section 3.4.3) for various kinds of functionals $J(\boldsymbol{u})$. Therefore, they consider the Lagrangian functional

$$L(\boldsymbol{u},\boldsymbol{\eta}) = J(\boldsymbol{u}) - (a(\boldsymbol{u},\boldsymbol{\eta}) - (\boldsymbol{p},\boldsymbol{\eta})) = J(\boldsymbol{u}) - A(\boldsymbol{u},\boldsymbol{\eta}) \quad \forall \boldsymbol{\eta} \in \mathcal{V} \tag{4.16}$$

without consideration of a dependence with respect to $\boldsymbol{s}$ whose total directional derivative

$$L'(\boldsymbol{u},\boldsymbol{\eta},\delta\boldsymbol{u},\delta\boldsymbol{\eta}) = L'_u(\boldsymbol{u},\boldsymbol{\eta},\delta\boldsymbol{u}) + L'_\eta(\boldsymbol{u},\boldsymbol{\eta},\delta\boldsymbol{\eta}) \tag{4.17}$$

is a reduced version of Equation (3.26). Nevertheless, the same stationary conditions can be derived based on Equation (4.17) as those from adjoint sensitivity analysis (Equation (4.9b)). Hence, the same findings can be drawn as with Equation (4.11). Since the Lagrangian approach is not limited to linear responses and linear variational problems, Kunow [97] utilizes the adjoint problem to determine influence functions for non-linear functionals and non-linear problems and consequently denotes the adjoint variable as *generalized Green's function*.
Although the reduced Lagrangian (Equation (4.16)) leads to the same adjoint variable as based on Equation (4.8), the consideration of the dependency on $\boldsymbol{s}$ has the advantage that the influence function is systematically and consistently embedded to sensitivity analysis in terms of Equation (4.9a). This advantage will be used when the influence function approach is generalized for various parameters in Section 4.3.

REMARK II: In the literature, generalized Green's or influence functions are defined differently. Grätsch et al. [74] relates the term basically to any but linear quantity of interests. Kunow [97] uses the notion also for non-linear responses within non-linear problems.

4.1.3 Connection of adjoint variable and finite element influence functions

The adjoint variable is identified as influence function in Sections 4.1.1 and 4.1.2. This thesis mainly focuses on numerical sensitivity analysis based on finite element models. Therefore, it is essential to classify the solution of the discrete adjoint problem given by Equation (3.13).
It can be shown that the discrete adjoint variable is equivalent to the so-called *finite element influence function*. The finite element influence function is the projection of the exact influence function onto the finite element subspace $\mathcal{V}_h \subset \mathcal{V}$ (cf. Section 2.1), i.e., it is the influence function which can be represented by the finite element mesh and its shape functions. Projected influence functions were investigated in detail by Grätsch [73] and can be computed as follows.
A linear functional J concerning $\boldsymbol{u}$ defined as

$$J(\boldsymbol{u}) = \int_\Omega \boldsymbol{\delta}_i^j(\boldsymbol{y}-\boldsymbol{x})\boldsymbol{u}(\boldsymbol{y})\, d\Omega_{\boldsymbol{y}} \tag{4.18}$$

is considered. $\boldsymbol{\delta}_i^j$ is the generalized Dirac delta which extracts the quantity of interest J from the solution $\boldsymbol{u}$ (cf. Equation (3.46)). According to Grätsch [73], the projected influence function is defined as the solution $\boldsymbol{\eta}_h \in \mathcal{V}_h \subset \mathcal{V}$ of the variational form

$$a(\boldsymbol{\eta}_h, \boldsymbol{v}_h) = (\boldsymbol{\delta}_i^j, \boldsymbol{v}_h) \quad \forall \boldsymbol{v}_h \in \mathcal{V}_h \subset \mathcal{V}. \tag{4.19}$$

An essential property of finite element influence functions is that the same value of $J(\boldsymbol{u}_h)$ as the primary finite element analysis would deliver can also be computed by the evaluation of the right-hand side of the governing differential equation $\boldsymbol{p}$ on the projected influence function:

$$J(\boldsymbol{u}_h) = \int_\Omega \boldsymbol{\eta}_h(\boldsymbol{y}, \boldsymbol{x}) \cdot \boldsymbol{p}(\boldsymbol{y})\, d\Omega_{\boldsymbol{y}} \tag{4.20}$$

Refer to Grätsch [73] for the proof. Hence, according to Equation (4.20), the accuracy of $J(\boldsymbol{u}_h)$ is directly related to how well the finite element program can approximate the influence function. Consequently, the projected influence function has been applied to establish goal-orientated error estimation of finite element calculations, see Cirak et al. [41], Grätsch et al. [74, 76], and Pierce et al. [119].

In order to compute $\boldsymbol{\eta}_h$ with the finite element method, the right-hand side of Equation (4.19) has to be converted into equivalent nodal forces using the shape functions $\boldsymbol{N}$ (cf. Section 2.1). Subsequently, the Dirac delta is assumed to be located within element e. According to Grätsch [73], the kth equivalent nodal force corresponding to the kth degree of freedom (DOF) can be computed by:

$$f_k = \int_{\Omega^e} \boldsymbol{\delta}_i^j(\boldsymbol{y} - \boldsymbol{x}) \boldsymbol{N}_k(\boldsymbol{y})\, d\Omega_{\boldsymbol{y}}^e \tag{4.21}$$

In consideration of Equation (4.18), Equation (4.21) can be rewritten as

$$f_k = J(\boldsymbol{N}_k) \tag{4.22}$$

whereby $\boldsymbol{N}_k$ describes the elemental displacement if the kth DOF is set to one and all other DOFs to zero. Hence, the equivalent nodal force f_k in Equation (4.22) corresponds to the value of the functional J due to the kth unit displacement.

It can be shown that the result of Equation (4.22) is equivalent to the adjoint load $\partial J / \partial \boldsymbol{u}$ (cf. Equation (3.13)). Therefore, the finite element solution with n DOFs of the linear functional

$$J(\boldsymbol{u}_h) = J\left(\sum_{i=1}^{n} u_i \boldsymbol{N}_i\right) = \sum_{i=1}^{n} u_i \cdot J\left(\boldsymbol{N}_i\right) \tag{4.23}$$

which operates on $\boldsymbol{u}_h$ is considered. The kth entry of the adjoint load of response J

$$\frac{\partial J}{\partial u_k} = \frac{\partial}{\partial u_k}\left[\sum_{i=1}^{n} u_i \cdot J\left(\boldsymbol{N}_i\right)\right] = J(\boldsymbol{N}_k) \tag{4.24}$$

is the same as the equivalent nodal force f_k. Consequently, the adjoint variable must be the finite element influence function.
To illustrate the findings, stresses, which are typical post-processing results of finite element analyses, are considered. Stresses can be recovered on the element level (denoted by index e) by the elastic constitutive equation

$$\boldsymbol{\sigma}^e = \boldsymbol{C}^e \boldsymbol{\epsilon}^e \tag{4.25}$$

with the elasticity matrix $\boldsymbol{C}^e$. Usually, the stresses are evaluated at the nodes or the Gauß points of the element (cf. Felippa [56] for a brief description). The strain vector $\boldsymbol{\epsilon}^e$ can be recovered by

$$\boldsymbol{\epsilon}^e = \boldsymbol{B}^e \boldsymbol{u}^e \tag{4.26}$$

where $\boldsymbol{B}^e$ is the strain-displacement matrix, cf. Zienkiewicz et al. [139] for instance. The jth component of the stress vector $\boldsymbol{\sigma}^e$

$$J = \boldsymbol{e}_j^T \boldsymbol{\sigma}^e = \boldsymbol{e}_j^T \boldsymbol{C}^e \boldsymbol{B}^e \boldsymbol{u}^e \tag{4.27}$$

is considered as response J where $\boldsymbol{e}_j$ is the jth unity vector which extracts the scalar response. The partial derivative of Equation (4.27) with respect to the kth displacement $u_k \in \boldsymbol{u}^e$ reads

$$\frac{\partial J}{\partial u_k} = \boldsymbol{e}_j^T \boldsymbol{C}^e \boldsymbol{B}^e \boldsymbol{e}_k. \tag{4.28}$$

If Equation (4.27) is compared with (4.28), it can be observed that the adjoint load component $\partial J / \partial u_k$ equates the response value due to the kth unit displacement described by the kth unity vector $\boldsymbol{e}_k$. Hence, the adjoint load is equal to the load case to generate the finite element influence function of response J by Equation (4.22).

REMARK I: In the numerical analysis of beam and truss structures, post-processing results (e.g., displacement field or course of stress resultant) consists typically of a homogeneous and a particular (local) solution (cf., e.g., Ghali et al. [69] or Hartmann et al. [82]). For instance, the particular solution of a beam element corresponds to the displacement, bending moment, or shear force of a clamped-clamped beam due to a transverse line load. Analogously, a local solution $\boldsymbol{\eta}_{ls}$ can be added to the finite element influence function as Hartmann et al. [82] proposes:

$$\boldsymbol{\eta} = \boldsymbol{\eta}_h \; + \; \boldsymbol{\eta}_{ls} \tag{4.29}$$

In Sections 4.2.2, 4.2.3, and 4.2.4, it is shown that the local solution can be systematically derived within adjoint sensitivity analysis.

4.2 Influence functions in adjoint sensitivity analysis

This section aims to determine influence functions for various responses based on adjoint sensitivity analysis. In particular, the responses of the traditional

approach are observed. Although these were already briefly examined by Belegundu [16, 17], the novelty of the subsequent investigations is that not only the adjoint variable is analyzed. Instead, the complete sensitivity equations are considered, which enables specific modifications of the adjoint variable. Parts of this section have been directly taken from the pre-published journal paper Fußeder et al. [67] and can thus be understood as quotations.

4.2.1 Nodal displacements

The jth nodal displacement $u_j \in \boldsymbol{u}$ is considered as response:

$$J = u_j \tag{4.30}$$

To compute the adjoint variable with Equation (3.10), the response formulation in Equation (4.30) needs to derived with respect to $\boldsymbol{u}$:

$$\frac{\partial J}{\partial \boldsymbol{u}} = \boldsymbol{e}_j \tag{4.31}$$

The result of Equation (4.31) corresponds to the jth unit vector $\boldsymbol{e}_j$ and can be interpreted as unity force applied at the jth degree of freedom. Hence, the adjoint load $\partial J/\partial \boldsymbol{u}$ equates the dual load for a nodal displacement (cf. Figure 3.1) and $\boldsymbol{\eta}$ has to be the influence function. This was also shown before by, e.g., Hartmann et al. [83]. As the response according to Equation (4.30) has no explicit dependency on parameter s_i, the derivative $\partial J/\partial s_i$ is zero.

4.2.2 Support forces

To obtain a mathematical formulation of a support force as response, the entire state equation with n degrees of freedom, which also contains the m degrees of freedom of the supports, must be considered:

$$\underbrace{\begin{bmatrix} \boldsymbol{K}_{11} & \boldsymbol{K}_{12} \\ \boldsymbol{K}_{21} & \boldsymbol{K}_{22} \end{bmatrix}}_{\boldsymbol{K}\ (n\times n)} \underbrace{\begin{bmatrix} \boldsymbol{u}_1 \\ \boldsymbol{u}_2 \end{bmatrix}}_{\boldsymbol{u}\ (n\times 1)} = \underbrace{\underbrace{\begin{bmatrix} \boldsymbol{F}_1 \\ \boldsymbol{F}_2 \end{bmatrix}}_{\boldsymbol{F}_L} + \begin{bmatrix} \boldsymbol{0} \\ \boldsymbol{F}_A \end{bmatrix}}_{\boldsymbol{F}(n\times 1)} \tag{4.32}$$

The vector of state variables $\boldsymbol{u} \in \mathbb{R}^n$ in the equilibrium condition according to Equation (4.32) is composed of the unknown nodal displacements $\boldsymbol{u}_1 \in \mathbb{R}^{n-m}$ and the prescribed displacements $\boldsymbol{u}_2 \in \mathbb{R}^m$, which have a given value (0 for a fixed support or $\neq 0$ for a support settlement). The total vector of nodal forces $\boldsymbol{F}_L \in \mathbb{R}^n$ encompasses the vectors $\boldsymbol{F}_1 \in \mathbb{R}^{n-m}$ and $\boldsymbol{F}_2 \in \mathbb{R}^m$ of the equivalent nodal forces from different load cases. The vector $\boldsymbol{F}_A \in \mathbb{R}^m$ contains the support forces. Additional explanations are given by Ghali et al. [69].
As response J, the support force $F_{A,j}$ in the jth row ($n - m + 1 \leq j \leq n$) of the load vector $\boldsymbol{F} \in \mathbb{R}^n$ is chosen. It can be extracted from Equation (4.32)

with the auxiliary vector $\boldsymbol{\eta}_0 \in \mathbb{R}^n$ by

$$\begin{aligned} F_{A,j} &= \boldsymbol{\eta}_0^T \left(\boldsymbol{F}_L - \boldsymbol{K}\boldsymbol{u}\right) \\ \boldsymbol{\eta}_0^T &= \begin{bmatrix} 0 & \cdots & \underbrace{-1}_{j} & \cdots & 0 \end{bmatrix} \end{aligned} \tag{4.33}$$

where the value of "-1" contained in $\boldsymbol{\eta}_0$ is necessary for a later simplification of the derivation. In order to calculate sensitivities according to Equation (3.15) regarding the response $F_{A,j}$, the adjoint variable $\boldsymbol{\eta} \in \mathbb{R}^n$ needs to be computed in advance. For this purpose, the derivative $\partial F_{A,j}/\partial \boldsymbol{u} \in \mathbb{R}^n$ is required (cf. Equation (3.13)). The derivative of Equation (4.33) with respect to the kth displacement $u_k \in \boldsymbol{u}$

$$\frac{\partial F_{A,j}}{\partial u_k} = \frac{\partial}{\partial u_k}\left(\boldsymbol{\eta}_0^T \left(\boldsymbol{F}_L - \boldsymbol{K}\boldsymbol{u}\right)\right) = K_{jk} \tag{4.34}$$

is the entry in the jth row and kth column of $\boldsymbol{K} \in \mathbb{R}^{n\times n}$. Thus, $\partial F_{A,j}/\partial \boldsymbol{u}$ (column vector) is according to Equation (4.34) the transposed jth row $\boldsymbol{K}_{(j;\ n)}$ or due to the symmetry of the stiffness matrix the jth column $\boldsymbol{K}_{(n;\ j)}$ of $\boldsymbol{K}$:

$$\frac{\partial F_{A,j}}{\partial \boldsymbol{u}} = \boldsymbol{K}_{(j;\ n)}^T = \boldsymbol{K}_{(n;\ j)} \tag{4.35}$$

The substitution of Equation (4.35) into Equation (3.13) yields the adjoint problem:

$$\underbrace{\begin{bmatrix} \boldsymbol{K}_{11} & \boldsymbol{K}_{12} \\ \boldsymbol{K}_{21} & \boldsymbol{K}_{22} \end{bmatrix}}_{\boldsymbol{K}} \underbrace{\begin{bmatrix} \boldsymbol{\eta}_1 \\ \boldsymbol{\eta}_2 \end{bmatrix}}_{\boldsymbol{\eta}} = \boldsymbol{K}_{(n;\ j)} = \begin{bmatrix} \boldsymbol{K}_{(1..n-m;\ j)} \\ \boldsymbol{K}_{(n-m+1..n;\ j)} \end{bmatrix} \tag{4.36}$$

Since homogeneous boundary conditions $\boldsymbol{\eta}_2 = \boldsymbol{0}$ $(m \times 1)$ have to be assumed when solving the adjoint problem (see e.g., Giles et al. [71]), the adjoint displacements $\boldsymbol{\eta}_1 \in \mathbb{R}^{n-m}$, which are still unknown in Equation (4.36), result from solving the linear system of equations:

$$\boldsymbol{K}_{11}\boldsymbol{\eta}_1 = \boldsymbol{K}_{(1..n-m;\ j)} \tag{4.37}$$

According to Equation (4.36), the adjoint variable $\boldsymbol{\eta}$ of $F_{A,j}$ is the displacement vector of a static problem in which the jth column of $\boldsymbol{K}$ is the load vector. This load case corresponds to a prescribed displacement of the jth degree of freedom by a value of "-1." Please note that support forces typically have the same direction as the corresponding degrees of freedom in a finite element analysis. Thus, the adjoint load case is equivalent to the dual load for generating the influence function of a support force: a unity displacement against the force direction (cf. Figure 3.1). However, since the solution of $\boldsymbol{\eta}_1$ by Equation (4.37) is based on the assumption of homogeneous boundary conditions, the support corresponding to the response remains in its initial position ($\eta_j = 0$). Hence, $\boldsymbol{\eta}$ differs in its jth entry from the influence function of the response function $F_{A,j}$. The discrepancy between the adjoint displacement $\boldsymbol{\eta}$ and the influence

function is shown comparatively in Figure 4.2 using the example of the vertical support force $F_{A,4z}$ (right support at node 4) of a two-span which is discretized by 3 Euler-Bernoulli beam elements (see element numbers in Figure 4.2). The graphical comparison shows that the two deformation figures differ only in the vertical displacement degree of freedom η_{4z} of the right support node.

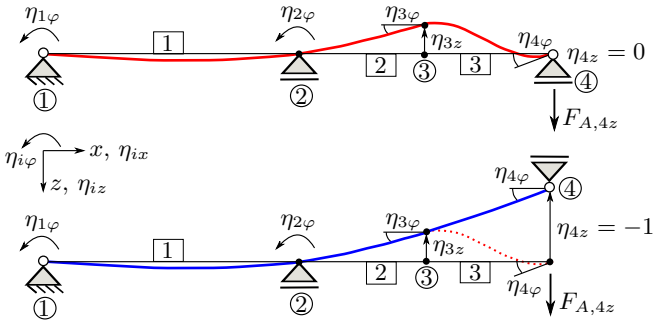

Figure 4.2: Adjoint displacement (red line) of the vertical support force $F_{A,4z}$ as response and the corresponding influence function (blue line). Adapted from Fußeder et al. [67].

The required displacement of the support node to adapt $\boldsymbol{\eta}$ to the influence function is determined by the partial derivative $\partial F_{A,j}/\partial s_i$ which is obtained by differentiating Equation (4.33) with respect to s_i:

$$\frac{\partial F_{A,j}}{\partial s_i} = \frac{\partial}{\partial s_i}\left(\boldsymbol{\eta}_0^T\left(\boldsymbol{F}_L - \boldsymbol{K}\boldsymbol{u}\right)\right) = \boldsymbol{\eta}_0^T\left[\frac{\partial \boldsymbol{F}_L}{\partial s_i} - \frac{\partial \boldsymbol{K}}{\partial s_i}\boldsymbol{u}\right] \tag{4.38}$$

The bracket term in Equation (4.38) can be identified as the pseudo-load $\boldsymbol{F}^*$. Thus, $\boldsymbol{\eta}$ can be merged with $\boldsymbol{\eta}_0$ when Equation (4.38) is substituted in Equation (3.15):

$$\begin{aligned}\frac{dF_{A,j}}{ds_i} &= \underbrace{\boldsymbol{\eta}_0^T\left[\frac{\partial \boldsymbol{F}_L}{\partial s_i} - \frac{\partial \boldsymbol{K}}{\partial s_i}\boldsymbol{u}\right]}_{\partial F_{A,j}/\partial s_i} + \boldsymbol{\eta}^T\left[\frac{\partial \boldsymbol{F}_L}{\partial s_i} - \frac{\partial \boldsymbol{K}}{\partial s_i}\boldsymbol{u}\right] \\ &= \left(\boldsymbol{\eta}_0^T + \boldsymbol{\eta}^T\right)\left[\frac{\partial \boldsymbol{F}_L}{\partial s_i} - \frac{\partial \boldsymbol{K}}{\partial s_i}\boldsymbol{u}\right]\end{aligned} \tag{4.39}$$

The analysis of the sum contained in Equation (4.39)

$$\begin{aligned}\boldsymbol{\eta}_0^T + \boldsymbol{\eta}^T &= \begin{bmatrix} \eta_1 & \cdots & \eta_{j-1} & (\eta_j - 1) & \eta_{j+1} & \cdots & \eta_n \end{bmatrix} \\ &= \begin{bmatrix} \eta_1 & \cdots & \eta_{j-1} & -1 & \eta_{j+1} & \cdots & \eta_n \end{bmatrix}\end{aligned} \tag{4.40}$$

indicates that the jth entry of $\boldsymbol{\eta}$ is modified by the value "-1" according to the definition of $\boldsymbol{\eta}_0$ in Equation (4.33). Consequently, the sum of $\boldsymbol{\eta}$ and $\boldsymbol{\eta}_0$ represents the influence function. It shall be noted that $\boldsymbol{\eta}_0$ equates the local solution, which corrects the finite element influence function (cf. Section 4.1.3 and Equation (4.29)).

4.2.3 Stress resultants

Stress resultants are post-processing quantities of finite element analyses computed locally by the elements. Thus, the sensitivity derivations must be made on the element level (indicated by superscript e in the following). The jth stress resultant $S_j \in \boldsymbol{S}^e$ as the observed response can be extracted from the element residual equation $\boldsymbol{r}^e$ (containing the element stiffness matrix $\boldsymbol{k}^e$, the element nodal force vector $\boldsymbol{f}^e$, and element displacement vector $\boldsymbol{u}^e$) with the auxiliary vector $\boldsymbol{\eta}_0^e$ by

$$\begin{aligned} S_j &= [\boldsymbol{\eta}_0^e]^T \, [-\boldsymbol{r}^e] = [\boldsymbol{\eta}_0^e]^T \, (\boldsymbol{f}^e - \boldsymbol{k}^e \boldsymbol{u}^e) \\ \boldsymbol{\eta}_0^e &= \begin{bmatrix} 0 & \cdots & 0 & \underbrace{-1}_{j} & 0 & \cdots & 0 \end{bmatrix}^T \end{aligned} \tag{4.41}$$

where the value of "-1" contained in $\boldsymbol{\eta}_0^e$ is negative to facilitate similar simplifications as for the response function "support force" in Section 4.2.2. To set up Equation (3.13) for the response, the derivative $\partial S_j / \partial \boldsymbol{u}$ needs to be computed first. The derivative of Equation (4.41) with respect to the kth displacement $u_k \in \boldsymbol{u}^e$

$$\frac{\partial S_j}{\partial u_k} = \frac{\partial}{\partial u_k} \left([\boldsymbol{\eta}_0^e]^T \, (\boldsymbol{f}^e - \boldsymbol{k}^e \boldsymbol{u}^e) \right) = k_{jk}^e \tag{4.42}$$

is the entry in the jth row and kth column of the element stiffness matrix. According to Equation (4.42), $\partial S_j / \partial \boldsymbol{u}^e$ corresponds to the transposed jth row or jth column of the symmetric element stiffness matrix:

$$\frac{\partial S_j}{\partial \boldsymbol{u}^e} = \left[\boldsymbol{k}_{(j;\, n)}^e \right]^T = \boldsymbol{k}_{(n;\, j)}^e \tag{4.43}$$

The adjoint element load vector $\partial S_j / \partial \boldsymbol{u}^e$ needs to be assembled in the system adjoint load vector $\partial S_j / \partial \boldsymbol{u}$ to solve Equation (3.13) on system level and can be interpreted as the load case of a negative unit pre-deformation of the degree of freedom where the response S_j is to be determined. Again, the adjoint load is equivalent to the dual load for generating the influence function (cf. Figure 3.1). Nevertheless, the displacement field $\boldsymbol{\eta}$ contains no exact representation of the proper influence function's characteristic discontinuity (kink or jump). For illustration, the adjoint variable $\boldsymbol{\eta}$ for the response "bending moment M_3 at node 3" of the example shown in Figure 4.3 is solved by Equation (3.13) with the result of Equation (4.43) as applied adjoint load. The adjoint displacement field is then generated by interpolating the discrete $\boldsymbol{\eta}$-values with cubic shape functions as shown by a red line in Figure 4.3. Therefore, the two-span beam is discretized with 3 Euler-Bernoulli beam elements (see element numbers in Figure 4.3) where the specific traced response is the bending moment at the right node of element 2. It becomes evident that the adjoint displacement of elements 1 and 3 already conforms with the influence function. The discrepancy is limited to element 2, where the response variable is located and can be attributed to the elemental degree of freedom corresponding to the traced moment. To generate the discontinuity, the rotation $\eta_{3\varphi}$ at the

right node of element 2 needs to be corrected by the value "-1" locally at the element level to fit the adjoint displacement field with the influence function as indicated with a blue line in Figure 4.3.

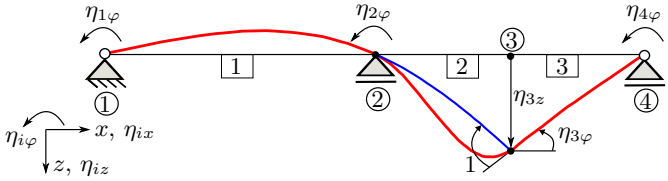

Figure 4.3: Adjoint displacement of the response bending moment at node 3 (red line) and its discrepancy to the influence function in element 2 (blue line). Adapted from Fußeder et al. [67].

The modification of the jth elemental degree of freedom can be justified by the partial derivative with respect to s_i

$$\frac{\partial S_j}{\partial s_i} = \frac{\partial}{\partial s_i}\left([\boldsymbol{\eta}_0^e]^T\left(\boldsymbol{f}^e - \boldsymbol{k}^e\boldsymbol{u}^e\right)\right) = [\boldsymbol{\eta}_0^e]^T \underbrace{\left(\frac{\partial \boldsymbol{f}^e}{\partial s_i} - \frac{\partial \boldsymbol{k}^e}{\partial s_i}\boldsymbol{u}^e\right)}_{\boldsymbol{f}^{e*}} \tag{4.44}$$

in which the element contribution of the pseudo-load $\boldsymbol{f}^{e*}$ can be identified. Thus, $\boldsymbol{\eta}^e$ can be merged with $\boldsymbol{\eta}_0^e$, when Equation (4.44) is substituted in the element-wise sensitivity term of Equation (3.22):

$$\begin{aligned}\frac{dS_j}{ds_i} &= \underbrace{[\boldsymbol{\eta}_0^e]^T\left(\frac{\partial \boldsymbol{f}^e}{\partial s_i} - \frac{\partial \boldsymbol{k}^e}{\partial s_i}\boldsymbol{u}^e\right)}_{\partial S_j/\partial s_i} + \sum_n \left\{[\boldsymbol{\eta}^e]^T\left(\frac{\partial \boldsymbol{f}^e}{\partial s_i} - \frac{\partial \boldsymbol{k}^e}{\partial s_i}\boldsymbol{u}^e\right)\right\} \\ &= \sum_n \left\{\left([\boldsymbol{\eta}_0^e]^T + [\boldsymbol{\eta}^e]^T\right)\left(\frac{\partial \boldsymbol{f}^e}{\partial s_i} - \frac{\partial \boldsymbol{k}^e}{\partial s_i}\boldsymbol{u}^e\right)\right\}\end{aligned} \tag{4.45}$$

The vector $\boldsymbol{\eta}_0^e$ in Equation (4.45) is always a zero vector except for the element in which the observed stress resultant is located. There $\boldsymbol{\eta}_0^e$ contains the value "-1" at its jth entry. Thus, the discrepancy between the adjoint variable and the influence function is fixed by $\boldsymbol{\eta}_0^e$. It shall be noted that $\boldsymbol{\eta}_0^e$ equates the local solution which corrects the finite element influence function (cf. Section 4.1.3 and Equation (4.29)).

REMARK I: The vector $\boldsymbol{\eta}_0^e$ is a local modification of $\boldsymbol{\eta}^e$ at element level. Hence, $\boldsymbol{\eta}_0^e$ comes only into play in the case of sensitivity analysis with respect to parameters that have explicit influence at the element where the response is located. For illustration, the two-span example shown in Figure 4.3 is considered. Sensitivities shall be computed for response M_3 concerning the Young's modulus of element 2 (E_2) and the intensity of an external bending

moment acting at node 3 ($\hat{M}_L$, not shown in the figure). The sensitivity with respect to E_2 can be computed with Equation (4.45) by:

$$\frac{dM_3}{dE_2} = \left([\boldsymbol{\eta}_0^e]^T + [\boldsymbol{\eta}^e]^T\right)\left(-\frac{\partial \boldsymbol{k}^e}{\partial E_2}\boldsymbol{u}^e\right) \tag{4.46}$$

In contrast, $\hat{M}_L$ is no parameter of element 2. Hence, the sensitivity is determined by

$$\frac{dM_3}{d\hat{M}_L} = \boldsymbol{\eta}^T \frac{\partial \boldsymbol{F}}{\partial \hat{M}_L} = \eta_{3\varphi} \cdot 1 \tag{4.47}$$

with the adjoint variable $\boldsymbol{\eta}$ on system level.

REMARK II: In the utilized response formulation according to Equation (4.41), the direction of action of the stress resultants conforms with the orientation of the corresponding degrees of freedom. Thus, the orientation does not match the usual sign convention for some of the stress resultants. To adjust the signs of the stress resultants, a diagonal matrix $\boldsymbol{H}_0^e$ with "-1" or "+1" on the main diagonal can be introduced:

$$\boldsymbol{S}^e = \boldsymbol{H}_0^e\,(\boldsymbol{f}^e - \boldsymbol{k}^e\boldsymbol{u}^e) \tag{4.48}$$

Hence, $\boldsymbol{\eta}_0^e$ equates the transposed jth row of $\boldsymbol{H}_0^e$. For example, in case of a truss with two degrees of freedom as shown in Figure 4.4 the sign transformation matrix reads:

$$\boldsymbol{H}_0^e = \begin{bmatrix} +1 & 0 \\ 0 & -1 \end{bmatrix} \tag{4.49}$$

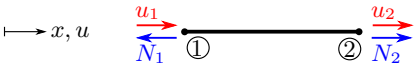

Figure 4.4: Orientation of the degrees of freedom u (red) and the normal forces N (blue) of a one-dimensional truss element.

REMARK III: No distinction between global and local orientation was made to keep the derivations as clearly laid out as possible. However, stress resultants of a beam or truss are typically computed based on the local orientation of the element. If it is assumed that the elemental residual $\boldsymbol{k}^e\boldsymbol{u}^e - \boldsymbol{f}^e$ is given in a global frame, the response formulation (Equation (4.41)) must supplemented by a transformation matrix $\boldsymbol{T}$, which transforms the elemental residual from a global to a local frame:

$$S_{\text{local},\,j} = [\boldsymbol{\eta}_0^e]^T\,\boldsymbol{T}\,(\boldsymbol{f}^e - \boldsymbol{k}^e\boldsymbol{u}^e) \tag{4.50}$$

Please note that all interpretations with respect to the influence function in this section can also be made based on Equation (4.50).

4.2.4 Residual-based responses

The influence function of stress resultants and support forces contains a discontinuity (jump or kink). Sections 4.2.2 and 4.2.3 show how the discontinuity can be derived within the framework of adjoint sensitivity analysis. In brief, the response formulations of stress resultants and support forces have in common that they are components of the elemental residual $\boldsymbol{r}^e$ and system residual $\boldsymbol{r}$, respectively. Furthermore, to select a specific component of the residual, an auxiliary vector $\boldsymbol{\eta}_0$ is introduced. Based on these response formulations, the pseudo-load can be identified as part of the partial derivative $\partial J/\partial s_i$. Hence, the adjoint variable $\boldsymbol{\eta}$ can be merged with $\boldsymbol{\eta}_0$, which justifies the discontinuity. Subsequently, it is shown how the procedure can be adapted to other residual-based responses. A general vector $\boldsymbol{\eta}_0(s_i)$ is introduced which extracts the response from the residual through

$$J = [\boldsymbol{\eta}_0(s_i)]^T [-\boldsymbol{r}] \quad \text{or} \quad J = [\boldsymbol{\eta}_0^e(s_i)]^T [-\boldsymbol{r}^e] \tag{4.51}$$

whereby explicit parameter dependencies of $\boldsymbol{\eta}_0$ are assumed to be as general as possible. In structural mechanics, the residual $\boldsymbol{r}$ is the state equation (equilibrium condition) given by Equations (2.37) (non-linear case) and (2.43) (linear case). The element residual $\boldsymbol{r}^e$ denotes the contribution which is assembled by a finite element to the state equation (e.g., in the linear case $\boldsymbol{r}^e = \boldsymbol{k}^e\boldsymbol{u}^e - \boldsymbol{f}^e$ consisting of stiffness matrix, nodal force vector, and displacement vector of element e). The partial derivatives based on Equation (4.51) read

$$\frac{\partial J}{\partial s_i} = \left[\frac{\partial \boldsymbol{\eta}_0}{\partial s_i}\right]^T \underbrace{[-\boldsymbol{r}]}_{=\boldsymbol{0}} + [\boldsymbol{\eta}_0(s_i)]^T \left[-\frac{\partial \boldsymbol{r}}{\partial s_i}\right] = [\boldsymbol{\eta}_0(s_i)]^T \underbrace{\left[-\frac{\partial \boldsymbol{r}}{\partial s_i}\right]}_{\boldsymbol{F}^*} \tag{4.52a}$$

$$\frac{\partial J}{\partial s_i} = \left[\frac{\partial \boldsymbol{\eta}_0^e}{\partial s_i}\right]^T [-\boldsymbol{r}^e] + [\boldsymbol{\eta}_0^e(s_i)]^T \underbrace{\left[-\frac{\partial \boldsymbol{r}^e}{\partial s_i}\right]}_{\boldsymbol{f}^{e*}} \tag{4.52b}$$

in which the pseudo-load $\boldsymbol{F}^*$ or $\boldsymbol{f}^{e*}$ can be identified. Hence, the final sensitivity terms simplify to

$$\frac{dJ}{ds_i} = \left(\boldsymbol{\eta}_0^T + \boldsymbol{\eta}^T\right) \cdot \boldsymbol{F}^* \tag{4.53a}$$

$$\frac{dJ}{ds_i} = \left[\frac{\partial \boldsymbol{\eta}_0^e}{\partial s_i}\right]^T [-\boldsymbol{r}^e] + \sum_n \left\{\left([\boldsymbol{\eta}_0^e]^T + [\boldsymbol{\eta}^e]^T\right) \cdot \boldsymbol{f}^{e*}\right\} \tag{4.53b}$$

if the partial derivatives of Equation (4.52) are substituted in Equations (3.11) and (3.22), respectively. Equation (4.53) shows that the partial derivative $\partial J/\partial s_i$ can be replaced by a local modification of $\boldsymbol{\eta}$ which can be interpreted as discontinuity of the influence function. However, the partial derivative is not completely compensable in cases where $\boldsymbol{\eta}_0^e$ explicitly depends on s_i.

Internal force of geometrically non-linear spatial truss element

Geometrically non-linear spatial trusses are usually derived under the assumption of constant strains within the element. Moreover, a structural truss system is assumed to be subjected only to node forces (cf., e.g., Borst et al. [27] and Krenk [96]). Hence, the elemental residual equation consists merely of the internal force vector

$$\boldsymbol{r}^e = \boldsymbol{f}^e_{\text{int}} = A \cdot \frac{l}{L} \cdot \sigma_{\text{PK2}} \cdot \frac{\partial l}{\partial \boldsymbol{u}} \tag{4.54}$$

where the orientation of internal forces is related to the degrees of freedom $\boldsymbol{u}$. The derivation of the elemental residual equation can be found in Appendix B.2. Based on Equation (4.54), the element contribution to the pseudo-load reads:

$$\boldsymbol{f}^{e*} = -\frac{\partial \boldsymbol{r}^e}{\partial s_i} = -\frac{\partial \boldsymbol{f}^e_{\text{int}}}{\partial s_i} \tag{4.55}$$

A specific response formulation of an internal force N in local element orientation can be generated by introducing a transformation matrix $\boldsymbol{T}$ (transforms from global to local frame) and the auxiliary vector $\boldsymbol{\eta}_0$. In analogy to Equation (4.41), the latter contains either "-1" or "$+1$" at its jth entry depending on whether the local element degree of freedom corresponds to the direction of action of the force or not. Hence, the response formulation reads:

$$\begin{aligned} N_j &= [\boldsymbol{\eta}^e_0]^T \boldsymbol{T} \, (-\boldsymbol{f}^e_{\text{int}}) \\ \boldsymbol{\eta}^e_0 &= \begin{bmatrix} 0 & \cdots & 0 & \underbrace{\pm 1}_{j} & 0 & \cdots & 0 \end{bmatrix}^T \end{aligned} \tag{4.56}$$

As Equation (4.56) represents an elemental residual-based response, the formulations according to Equation (4.52b) and (4.53b) can be applied. Hence, the final element-wise sensitivity term is

$$\frac{dN_j}{ds_i} = \sum_n \left\{ \left([\boldsymbol{\eta}^e_0]^T \boldsymbol{T} + [\boldsymbol{\eta}^e]^T \right) \cdot \boldsymbol{f}^{e*} \right\} \tag{4.57}$$

whereby the matrix-vector product $[\boldsymbol{\eta}^e_0]^T \boldsymbol{T}$ transforms $\boldsymbol{\eta}^e_0$ into the global frame. The result of Equation (4.57) is in analogy to normal forces of linear trusses (cf. Section 4.2.3). Also, in the case of a non-linear truss, a local modification of the adjoint variable of $|1|$ at the position of the traced internal force is received.

Normal stress in beam element

In the case of a two-dimensional beam problem, the normal stress at the outer cross-sectional edges can be computed by

$$\sigma = \frac{N}{A} \pm \frac{M}{W} \tag{4.58}$$

with normal force N, bending moment M, cross-sectional area A, and section modulus W. Equation (4.58) can be computed based on the elemental residual equation through

$$\begin{aligned} \sigma &= [\boldsymbol{\eta}_0^e]^T \left(\boldsymbol{f}^e - \boldsymbol{k}^e \boldsymbol{u}^e\right) \\ \boldsymbol{\eta}_0^e &= \begin{bmatrix} 0 & \cdots & \underbrace{\pm\frac{1}{A}}_{i} & \cdots & \underbrace{\pm\frac{1}{W}}_{j} & \cdots & 0 \end{bmatrix}^T \end{aligned} \tag{4.59}$$

where the indices i and j correspond to the position of the normal force and the bending moment in the element residual. As the response formulation of Equation (4.59) is an extended version of Equation (4.41), the interpretations for stress resultants in Section 4.2.3 can be straight forward applied for normal stress response. Hence, the adjoint load represents simultaneous pre-deformations with intensity "$1/A$" and "$1/W$" of the degrees of freedom corresponding to N and M. In the case of the partial derivative $\partial\sigma/\partial s_i$, Equation (4.52b) and the final sensitivity Equation (4.53b) are fully applicable. The local modifications of $\boldsymbol{\eta}^e$ by $\boldsymbol{\eta}_0^e$ can be interpreted as a jump $|1/A|$ and a kink $|1/W|$ of the influence function. Refer to Figure 4.5 as an example. It can be concluded that the influence function of normal stress is the superposition of the scaled influence functions of a normal force and a bending moment. Please note the existence of $\partial\boldsymbol{\eta}_0^e/\partial s_i$ if s_i is either A or W of the element in which the considered stress is located.

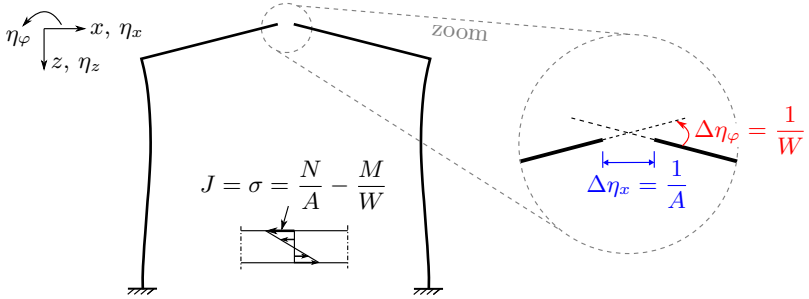

Figure 4.5: Influence function of the normal stress on the upper edge in the center of the rafter as response J. At the position of the response, a longitudinal jump of $|1/A|$ and a kink of $|1/W|$ can be observed.

4.3 Sensitivity analysis considering various parameters and responses

4.3.1 Preliminary remarks

Identifying the adjoint variable as influence function embeds the latter systematically into sensitivity analysis and allows the generation of influence functions for general responses. This provides a possible basis for generalizing the method of influence functions based on adjoint sensitivity analysis. Furthermore, a comparable computational sequence of the method of influence functions and adjoint sensitivity analysis can be identified. The formal equivalence can be seen as the requirement to extend the method for various parameters. The comparison in Table 4.1 illustrates that both methods are comparable two-step approaches. In the first step, the influence function is computed. Secondly, a kind of post-processing is performed. In the case of the classical method, physical loads are evaluated on the influence function ($\boldsymbol{\eta}^T\boldsymbol{F}$, cf. Equation (3.50)). In contrast, the parameter-dependent pseudo-load has to be used in an adjoint sensitivity analysis ($\boldsymbol{\eta}^T\boldsymbol{F}^*$, cf. Equation (3.11)). The only difference is the partial derivative $\partial J/\partial s_i$. Hence, the equivalent computational sequence allows the interpretation of the adjoint approach as the extension of the method of influence functions for sensitivity analysis. This becomes additionally visible if Equation (4.2) is compared with (3.15)

$$\frac{dJ}{ds_i} = \boldsymbol{\eta}^T \cdot \underbrace{\frac{\partial \boldsymbol{F}}{\partial s_i}}_{\substack{\text{limited to} \\ \text{load parameters}}} \tag{4.60a}$$

$$\frac{dJ}{ds_i} = \boldsymbol{\eta}^T \cdot \left[\frac{\partial \boldsymbol{F}}{\partial s_i} - \underbrace{\frac{\partial \boldsymbol{K}}{\partial s_i}\boldsymbol{u}}_{\substack{\text{additional terms for} \\ \text{general parameters}}}\right] + \frac{\partial J}{\partial s_i} \tag{4.60b}$$

where it can be observed how sensitivity analysis for load parameters based on influence functions is extended by the adjoint approach. However, Equation (4.60b) reveals that not the whole parameter effect is evaluated on the influence function. Instead, the partial derivative $\partial J/\partial s_i$ must be added. The latter expresses the explicit parameter dependency of the response. The expressiveness of the influence function is, in a general case, consequently lower as it contributes only to the implicit parameter dependency. This issue is further discussed in Section 4.3.4. However, Section 4.2 shows that $\partial J/\partial s_i$ is for some of the most important practice-relevant responses (e.g., displacement, stress resultant, and support force) either nonexistent or can be replaced. In these cases, sensitivity analysis reduces to evaluating the pseudo-load on the influence function and has thus an identical computation sequence as the classical influence functions method.

Table 4.1: Comparison of the method of influence functions and the adjoint approach.

#	classical method	adjoint method
1. step	determination of influence function $\boldsymbol{\eta}$ by	
	application of dual load (see Figure 3.1) independent of load $\boldsymbol{F}$	solution of adjoint problem (according to Equation (3.10)) independent of parameters $\boldsymbol{s}$
2. step	evaluation of physical loads: $\boldsymbol{\eta}^T \boldsymbol{F}$ /	evaluation of pseudo-loads: $\boldsymbol{\eta}^T \boldsymbol{F}^*$ $+\partial J/\partial s_i$
result	functional value of response J due to $\boldsymbol{F}$	derivative of response J with respect to parameter s_i

4.3.2 Adjoint work

As noticed in Section 4.3.1, the method of influence functions can be numerically extended by considering the full pseudo-load and by adding $\partial J/\partial s_i$. This section aims to propose a mechanically more interpretable viewpoint. Therefore, the work expression of the traditional influence functions approach, based on Betti's theorem, is considered. Section 3.4.1 explains how Betti's theorem establishes the influence functions approach for the traditional responses (i.e., stress resultants and displacement quantities). The result of that derivation can be written generally for response J as

$$1 \cdot J = \int_\Omega \boldsymbol{p} \cdot \boldsymbol{\eta} \, d\Omega \tag{4.61}$$

where the "1" on the left-hand side represents the dual load to generate the influence function (cf. Figure 3.1). Since the dual load is the energetic conjugated counterpart of the response, work expressions on both sides of Equation (4.61) can be observed. Therefore, $\boldsymbol{\eta}$ has to be considered as displacement. Based on Equation (4.61), the variational sensitivity term

$$1 \cdot \frac{dJ}{d\boldsymbol{s}} \cdot \delta \boldsymbol{s} = \int_\Omega D_{\delta \boldsymbol{s}} \boldsymbol{p} \cdot \boldsymbol{\eta} \, d\Omega \tag{4.62}$$

can be derived with Gâteaux operator D (cf. Equation (2.1)) where $\boldsymbol{s}$ represents a parameter function which affects exclusively the load $\boldsymbol{p}$. It can be observed that the sensitivity term in Equation (4.62) also contains work expressions on both sides since the additional units due to $\boldsymbol{s}$ cancel. In the analogy of adjoint sensitivity analysis and to express that the work expressions are part of a sensitivity term, the variation of $\boldsymbol{p}$ is denoted as *pseudo-load* and the work of the latter with the influence function as external *adjoint work*. Hence, Equation (4.62) shows how the work balance of the classical influence function technique is extended for sensitivity analysis with respect to load

parameters. The adjoint work expression can be smoothly extended by employing variational adjoint sensitivity analysis that encloses the influence function. However, the identification of Equations (4.61) and (4.62) as work expressions requires the presence of the dual load "1" and the assumption of the influence function as displacement. The sensitivity equations derived in Section 3.3 do not fulfill the requirements. The unit of the influence function computed by the adjoint problem given in Equation (3.10) is [response unit] / [force unit]. This becomes especially visible if the influence function is interpreted as a carrier of the sensitivity with respect to the load vector, i.e., $dJ/d\boldsymbol{F} = \boldsymbol{\eta}$ (cf. Equation (4.4)). Furthermore, the dual load "1" appears not as a multiplier of the sensitivity equations. Both deficits can be resolved if the adjoint sensitivity analysis expressions are multiplied by the energetic conjugated dual load "1." Hence, in the case of linear structural analysis, the complete adjoint work reads

$$1 \cdot \frac{dJ}{d\boldsymbol{s}} \cdot \delta\boldsymbol{s} = 1 \cdot J'_s(\boldsymbol{s}; \boldsymbol{u}, \delta\boldsymbol{s}) + W^*_{\text{int}} + W^*_{\text{ext}} \quad \text{with} \tag{4.63a}$$

$$W^*_{\text{int}} = -\int_\Omega D_{\delta\boldsymbol{s}}\boldsymbol{\sigma}(\boldsymbol{u}) : (1 \cdot \boldsymbol{\epsilon}(\boldsymbol{\eta}))\ d\Omega \tag{4.63b}$$

$$W^*_{\text{ext}} = \int_\Omega D_{\delta\boldsymbol{s}}\boldsymbol{p} \cdot 1 \cdot \boldsymbol{\eta}\ d\Omega + \int_{\Gamma_N} D_{\delta\boldsymbol{s}}\hat{\boldsymbol{t}} \cdot 1 \cdot \boldsymbol{\eta}\ d\Gamma_N \tag{4.63c}$$

on the basis of Equation (3.35). All parts of Equation (4.63) can be identified as work expressions. These can be seen as generalized adjoint work. Equation (4.63b) represents the internal adjoint work W^*_{int} of pseudo-stress ($\hat{=}$ variation of the Cauchy stress tensor with respect to $\boldsymbol{s}$) and the adjoint strain ($\hat{=}$ linear strain of the influence function). In contrast, Equation (4.63c) can be interpreted as the external adjoint work W^*_{ext} of influence function and pseudo-forces ($\hat{=}$ variation of the distributed volume and traction force with respect to $\boldsymbol{s}$). Hence, the method of influence functions can be generalized for sensitivity analysis by an extended work balance expression. Apart from $J'_{\boldsymbol{s}}$, the work of the influence function or its strain with an energetically conjugated pseudo-quantity can be identified. Hence, the influence function and its strain indicate zones in a structure where parameter variations could have a minor or large effect on the response.

A general response may be defined based on a non-linear structural analysis. There, the adjoint work expressions are obtained by employing the variational adjoint sensitivity equation

$$1 \cdot \frac{dJ}{d\boldsymbol{s}} \cdot \delta\boldsymbol{s} = 1 \cdot J'_s(\boldsymbol{u}, \boldsymbol{s}; \delta\boldsymbol{s}) + W^*_{\text{int}} + W^*_{\text{ext}} \quad \text{with} \tag{4.64a}$$

$$W^*_{\text{int}} = -\int_{\Omega_0} D_{\delta\boldsymbol{s}}\boldsymbol{S}(\boldsymbol{E}(\boldsymbol{u})) : (1 \cdot D_{\boldsymbol{\eta}}\boldsymbol{E}(\boldsymbol{u}))\ d\Omega_0 \tag{4.64b}$$

$$W^*_{\text{ext}} = \int_{\Omega_0} D_{\delta\boldsymbol{s}}\boldsymbol{p}_0 \cdot 1 \cdot \boldsymbol{\eta}\ d\Omega_0 + \int_{\Gamma_{N0}} D_{\delta\boldsymbol{s}}\hat{\boldsymbol{t}}_0 \cdot 1 \cdot \boldsymbol{\eta}\ d\Gamma_{N0} \tag{4.64c}$$

on the basis of Equation (3.41). Compared to the linear case, the most significant differences can be found in the internal adjoint work (Equation (4.64b))

originated from the work conjugate pair Green-Lagrange strain tensor and Second Piola-Kirchhoff stress tensor. Firstly, the Second Piola-Kirchhoff pseudo-stress $D_{\delta \boldsymbol{s}} \boldsymbol{S}(\boldsymbol{E}(\boldsymbol{u}))$ is obviously non-linear with respect to $\boldsymbol{u}$. Secondly, the energetic conjugated adjoint strain is not a strain in a proper sense. Instead, it is the variation, i.e., the Gâteaux derivative of the Green-Lagrange strain tensor concerning the primal solution $\boldsymbol{u}$ in the direction of the influence function $\boldsymbol{\eta}$ at a specific $\boldsymbol{u}$. Hence, a simultaneous dependency of the adjoint strain on the primal solution $\boldsymbol{u}$ and the influence function $\boldsymbol{\eta}$ can be observed. As the solution of $\boldsymbol{\eta}$ depends according to Equation (3.40) also on $\boldsymbol{u}$, a pronounced dependency of the adjoint strain on the primal solution can be noticed.

REMARK I: Equations (4.63) and (4.64) are derived for non-shape parameters (cf. Section 3.3). The consequences of shape parameters to the described procedure are discussed in Section 4.3.5.1.

REMARK II: Equations (4.63) and (4.64) are multiplied by the energetic conjugated dual load "1". Table 4.2 summarizes how the units of the original adjoint variables of the traditional responses are adjusted towards a displacement unit. It becomes obvious that the unit of "1" is [work unit] / [response unit] in each case.

Table 4.2: Summary of units of the adjoint variable $\boldsymbol{\eta}$, the dual load "1," and of the combination of both. Used unit abbreviations: length or displacement $[L]$, force $[F]$, and unit-less [-].

response J	$\boldsymbol{\eta}$	1	$1 \cdot \boldsymbol{\eta}$
displacement w	$[L] \,/\, [F]$	$[F]$	
rotation $\varphi = -w'$	[-] / $[F]$	$[F \cdot L]$	
normal force N	$[F] \,/\, [F]$	$[L]$	$[L]$
shear force V	$[F] \,/\, [F]$	$[L]$	
bending moment M	$[F \cdot L] \,/\, [F]$	[-]	

REMARK III: The multiplication with the dual load "1" adjusts the sensitivity equations to work expressions. However, the adjoint load $\partial J / \partial \boldsymbol{u}$ of general responses is not related to dual loads with intensity "1." This becomes obvious if, for example, the adjoint load of linear strain energy (Equation (4.83)) or an eigenvalue (Equation (4.91)) is observed. Even though a "1," which properly adjusts the dimensions, can be found for general responses, its meaning is artificial. In addition, the units' adjustment is not necessary to determine spatial distributions of the sensitivity $dJ/d\boldsymbol{s}$ and their composition. For this reason, the multiplier "1" is omitted from the notation below.

4.3.3 Extension of graphical analysis procedure

A significant strength of the traditional method of influence functions is its graphical analysis procedure. Based on the visualization of the influence function as a displacement field, decisive or even critical load cases can be intuitively identified (cf. Section 3.4.2). This section discusses which graphical means can be served by the method of generalized influence functions. The aim is to support sensitivity analysis by a graphical analysis procedure that provides ancillary information concerning the composition of the resulting sensitivities and their spatial distribution. It can be observed that the integrands of the internal and external adjoint work in Equations (4.63b) and (4.63c) can be separated into two parts each. As these quantities are related to typical post-processing results such as strains, stresses, displacements, and external forces, they are suitable for visualization. Furthermore, the internal and external adjoint work components show contrary dependencies. The pseudo-quantities reflect the observed parameter contribution and the primal state independently from the response. In contrast, the second part of the integrands corresponds to the influence function, which notifies the response contribution independently from the parameters. Hence, the individual visualization of the two parts gives insights into the composition of the sensitivities. Please note that a complete separation of the parameter and response contribution to the final sensitivity is generally impossible. The reason is the partial variation $J'_s(\cdot)$, which depends on the observed parameter and response simultaneously. Refer to Section 4.3.4 for a discussion concerning the influence of the partial variation $J'_s(\cdot)$ on the concept. The subsequent demonstration is restricted to examples with vanishing $J'_s(\cdot)$.

4.3.3.1 Exemplary demonstration for beam structures

For a two-sided clamped Euler-Bernoulli beam as introduced in Appendix B.1, the variational sensitivity expression reads

$$\frac{dJ}{ds} \cdot \delta s = J'_s(s, u; \delta s) + W^*_{\text{int}} + W^*_{\text{ext}} \quad \text{with} \tag{4.65a}$$

$$W^*_{\text{int}} = -\int_0^l \delta s \cdot \frac{\partial M(x)}{\partial s} \cdot \kappa_\eta(x)\, dx = -\int_0^l \delta s \cdot M^*_s(x) \cdot \kappa_\eta(x)\, dx \tag{4.65b}$$

$$W^*_{\text{ext}} = \int_0^l \delta s \cdot \frac{\partial p(x)}{\partial s} \cdot \eta(x)\, dx = \int_0^l \delta s \cdot p^*_s(x) \cdot \eta(x)\, dx \tag{4.65c}$$

where Equation (4.65b) describes the internal adjoint work W^*_{int} of the curvature of the influence function $\kappa_\eta = -\eta''$ ($\hat{=}$ adjoint curvature) and the pseudo-moment M^*_s. In contrast, Equation (4.65c) contains the external adjoint work W^*_{ext} of pseudo-line load p^*_s and the influence function.
The aim is to compute sensitivities dJ/ds. Therefore, providing a variation δs is not required. Instead, it is sufficient to determine and visualize the

multipliers of δs in Equation (4.65). In that regard, several sensitivity maps can be provided. If the complete multiplier is visualized, the map represents the distributed sensitivity course along the beam. This map displays at a point x the derivative of a specific response (e.g., the bending moment at a fixed position) concerning the parameter at point x (e.g., the bending stiffness $EI(x)$). Further sensitivity information can be provided if the partitions of the multiplier, namely the influence function, its curvature, the pseudo-line load, and the pseudo-moment, are visualized.

Example 1: two-span

The graphical analysis is applied to the example shown in Figure 3.2 for response M_m at x_m. Sensitivities are computed with respect to the intensities p_{1-3} of the constant line loads. Therefore, Equation (4.65) reduces to the external adjoint work

$$\frac{dM_m}{dp_i} \cdot \delta p_i = \int_0^l \delta p_i \cdot \frac{\partial p(x)}{\partial p_i} \cdot \eta(x)\, dx = \int_0^l \delta p_i \cdot 1 \cdot \eta(x)\, dx \tag{4.66}$$

with a constant pseudo-line load $p^*_{p_i}(x) = 1$ for each p_i. The coefficient (multiplicative combination of $\eta(x)$ and $p^*_{p_i}(x)$) of δp_i is plotted along the beam in Figure 4.6. The map displays at a point x the derivative of the bending moment M_m (fixed at point x_m, cf. Figure 4.6) concerning an infinitesimal line load segment at x. As the pseudo-loads are constant with intensity "1," the final sensitivity courses equate pieces of the influence function. This is obvious as the influence function is the carrier of load sensitivities (cf. Section 4.1.1). It can observed that the pseudo-loads of p_2 and p_3 coincide with larger influence function values compared to the pseudo-load of p_1. Hence, the pure graphical inspection reveals that the sensitivities with respect to p_2 and p_3 have to be equal and larger as in the case of p_1.

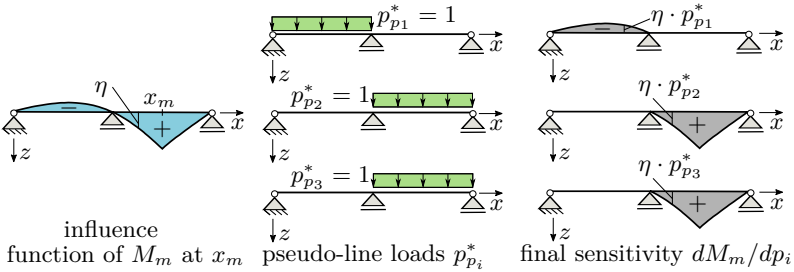

Figure 4.6: The point-wise multiplication of influence function η (left) and pseudo-line load $p^*_{p_i}$ (middle) lead to the sensitivity distribution (right). The analysis is performed for response M_m with respect to the intensities p_i of the three load cases defined in Figure 3.2.

In analogy, the sensitivities of response M_m with respect to the bending stiffness EI can be computed. For that setting, sensitivity analysis based on Equation (4.65) reduces to

$$\frac{dM_m}{dEI} \cdot \delta EI = -\int_0^l \delta EI \cdot \frac{\partial M(x)}{\partial EI} \cdot \kappa_\eta(x)\, dx$$
$$\text{with } \frac{\partial M(x)}{\partial EI}(x) = \frac{\partial}{\partial EI}\{EI\} \cdot \kappa(x) = 1 \cdot \kappa(x) = M^*_{EI}(x) \tag{4.67}$$

which is the internal adjoint work of the curvature of the influence function κ_η and the pseudo-moment M^*_{EI}. The latter equates the curvature $\kappa = -w''$ of the primal bending deflection w due to load case p_i. The adjoint work components and their point-wise multiplicative combination, i.e., the final sensitivity courses, are shown in Figure 4.7. The final sensitivity maps display at a point x the derivative of the bending moment M_m (fixed at point x_m, cf. Figure 4.7) with respect to the bending stiffness at x. The influence function of response M_m is independent of the load case. Thus, its curvature can be utilized for the three sensitivity analyses based on p_{1-3}. For the piecewise cubic influence function, a symmetric bi-linear course of its curvature is received. Hence, combining the mirrored pseudo-moments for load cases 1 and 2 ($p_1 = p_2$) leads to mirrored sensitivity distributions. As $p_3 = 2 \cdot p_2$ is applied, the pseudo-moment and sensitivities of load case 3 are twice the values of load case 2. Significant sensitivities concerning the bending stiffness appear near the mid-support and the respective loaded field for all three load cases.

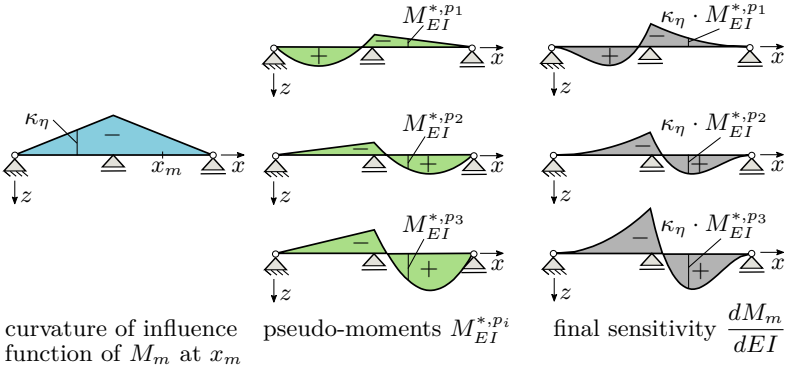

Figure 4.7: The combination of the curvature of influence function κ_η (left) and pseudo-moment $M^*_{EI}(x)$ (middle) lead to the sensitivity distribution (right). The analyses are performed for response M_m and are based on the three load cases defined in Figure 3.2.

In the graphical analysis in Figure 4.7, the curvature of one influence function is applied to different pseudo-moments. Subsequently, a reverse execution is conducted and the pseudo-moment M_{EI}^{*,p_1} based on load case p_1 is applied to the adjoint curvature of the nodal displacements w_1 (J_1), w_2 (J_2), and strain energy (J_3) as responses. The location of the displacement responses, the final sensitivity courses, and incorporated adjoint work components are visualized in Figure 4.8. The adjoint curvature of w_1 and w_2 are mirrored. However, the maximal adjoint curvature values of w_1 coincide with the maximal values of the pseudo-moment. Hence, significantly higher maximal sensitivities for w_1 can be observed. In the case of strain energy, the analysis is performed based on Equation (4.84a) where the partial derivative $\partial J_3/\partial EI$ is vanishing. Furthermore, the adjoint curvature of strain energy is a scaled version of the pseudo-moment since $\eta = 0.5 \cdot w$ (cf. Equation (4.83a)). As the adjoint curvature of w_1 and strain energy are similar in their course, similar final sensitivity courses based on the same pseudo-moment are received.

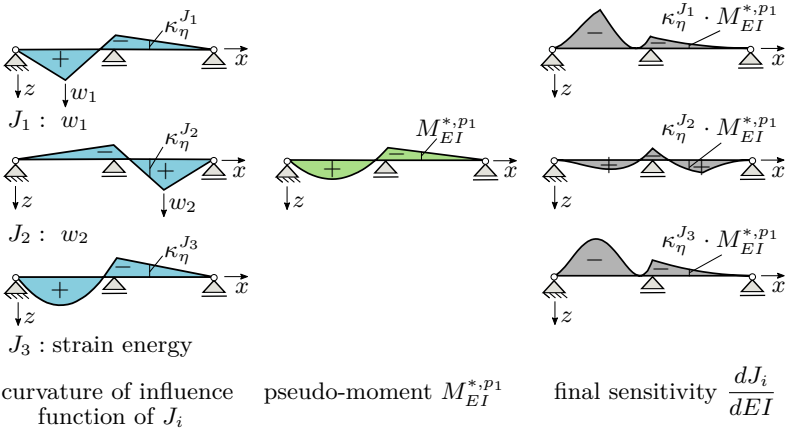

Figure 4.8: The combination of the curvature of influence function $\kappa_\eta^{J_i}$ (left) and pseudo-moment M_{EI}^{*,p_1} (middle) lead to the sensitivity distribution (right). The analysis is performed based on load case 1 (cf. Figure 3.2).

Example 2: two story building

The pseudo-quantities and their adjoint counterparts act on each other like a filter. Only regions where noticeable values of both quantities coincide show high sensitivities. Consequently, the individual judgment of all sensitivity partitions has the advantage that potentially critical zones can be identified. An example of how to use that extra sensitivity information for the structural design of a two-story concrete building is given in Figure 4.9. The response of interest is the normal force N_n of a column at a fixed x_n whose influence function is shown in the top left of Figure 4.9. The goal is to determine the

course of sensitivity with respect to the bending stiffness EI_y of down-stand beams and columns (highlighted by black lines). In analogy to the previous example, the final sensitivity comprises the pseudo-moment and the influence function's curvature, shown on the right side of Figure 4.9. Zooming into a selected column clearly shows the benefit of additional information. Because of the high curvature of the influence function, a potentially critical zone can be identified. However, the small values of the pseudo-moments indicate that the variation of parameter EI_y in that area is of minor effect. The final sensitivity resulting from the combination of that contradictory information is consequently also of minor importance. As the pseudo-moment is a scaled version of the moment of the primal analysis (cf. Equation (4.67)), another load case could lead to a larger pseudo-moment in this region and, accordingly, to higher sensitivities. This capability can be identified by observation of the influence function's curvature. Please note that in real-world problems, the procedure might be repeated for stiffness parameters influencing bending around the other axis or torsion. Therefore, respective pseudo and adjoint fields have to be observed.

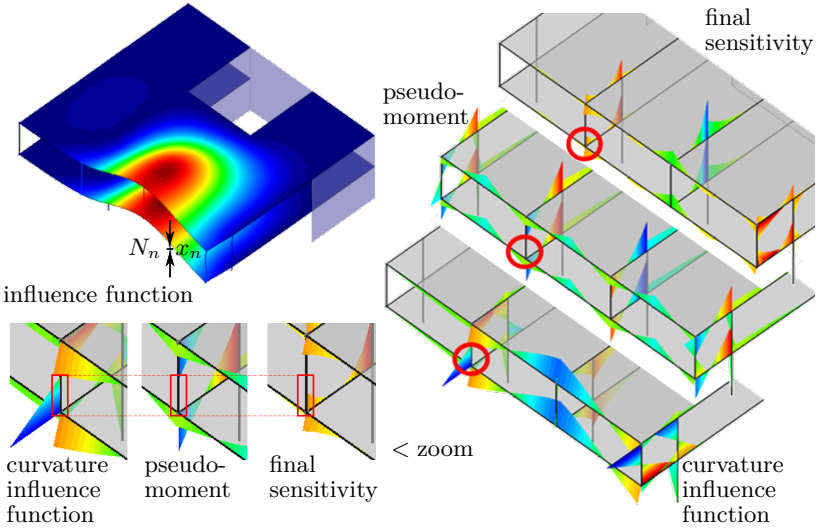

Figure 4.9: Sensitivity analysis of normal force N_n with respect to the bending stiffness EI_y of the beam construction members. The combination of the curvature of influence function and pseudo-moment leads to the final sensitivity distribution.

Example 3: arch-type bridge

In the previous examples, only the adjoint work related to bending around one axis had to be incorporated. Subsequently, an arch-type bridge is con-

sidered and the sensitivities of the main girder normal force N_n at a fixed x_n with respect to the Young's modulus of the beam construction members are computed. Appendix A.3 provides a detailed description of the structure. The adjoint work for the problem reads

$$\begin{aligned}\frac{dN_n}{dE}\delta E = &- \int_0^l \delta E \frac{\partial M_y(x)}{\partial E}\kappa_{\eta,y}(x)\,dx - \int_0^l \delta E \frac{\partial M_z(x)}{\partial E}\kappa_{\eta,z}(x)\,dx \\ &- \int_0^l \delta E \frac{\partial M_x(x)}{\partial E}\gamma_{\eta,x}(x)\,dx - \int_0^l \delta E\ \frac{\partial N(x)}{\partial E}\epsilon_\eta(x)\,dx\end{aligned} \tag{4.68}$$

since the bridge is stressed by multiaxial bending and longitudinal action. The bending moments around the y- and z-axis are denoted by M_y and M_z, the twisting moment by M_x, and the normal force by N. $\kappa_{\eta,y}$ and $\kappa_{\eta,z}$ denote the curvature concerning the y- and z-axis, $\gamma_{\eta,x}$ the torsional shear strain, and ϵ_η the longitudinal strain of the influence function η.

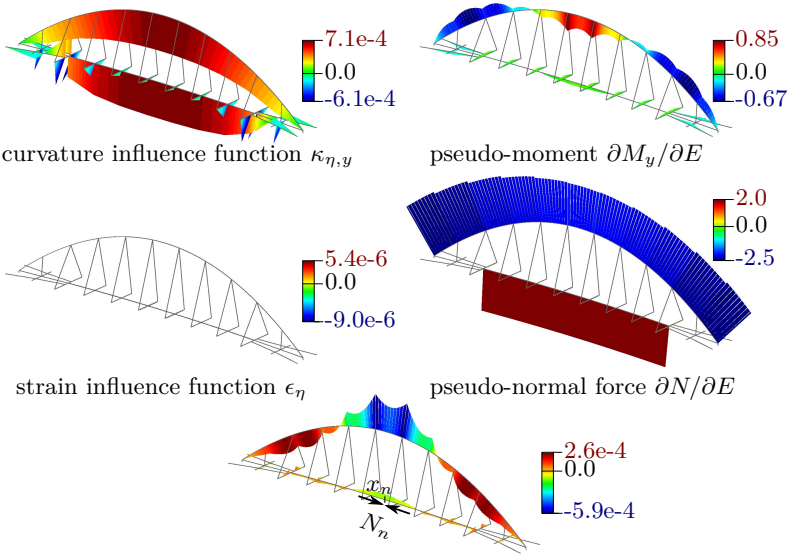

Figure 4.10: Sensitivity analysis of normal force N_n with respect to the Young's modulus of the beam construction members. Only the adjoint work components significantly contributing to the final sensitivity are shown.

The main load-bearing behavior is due to bending around the y-axis and longitudinal action. Torsion and bending around the z-axis are of minor importance for the overall sensitivity course and are not shown in Figure 4.10. Adjoint curvature/strain and pseudo-moment/normal force are plotted with the same scaling factor. Since the values of the adjoint strain ϵ_η are much smaller compared to those of the adjoint curvature $\kappa_{\eta,y}$, they are not visible in Figure 4.10. Hence, it becomes obvious that the final sensitivity course, which is the result of combining the coefficients of δE in the integrals in Equation (4.68), is dominated by the y-bending part of the adjoint work. The significant pseudo-normal force values are irrelevant because they are multiplied with minor adjoint strain values. Since the adjoint curvature $\kappa_{\eta,y}$ changes evenly along the arch and main girder, the waviness of the pseudo-moment is directly reflected in the final sensitivity course. The pseudo-moment $\partial M_y(x)/\partial E = I_y \cdot \kappa_y(x)$ is a scaled version of the primal bending moment $M_y(x)$. Hence, it can be observed that the sensitivity course is mainly determined by the bending around the strong y-axis. The example shows how the graphical analysis of the adjoint work components can assist in identifying the mechanical causes of the final sensitivity courses.

4.3.3.2 Numerical implementation

Variational adjoint sensitivity analysis is utilized to identify adjoint and pseudo-fields for the graphical solution procedure. However, the discrete adjoint approach is used to perform the sensitivity computations for this thesis (cf. Section 3.2.3).
Equivalent to the recovery of displacements, strains, and stresses of finite element analyses (cf. standard textbooks concerning the finite element method as Bathe [12] and Zienkiewicz et al. [139]), the adjoint and pseudo-fields can be generated as post-processing results. Once the discrete adjoint variable $\boldsymbol{\eta}$ is computed by Equation (3.10), the shape functions $\boldsymbol{N}$ are utilized in analogy to Equation (2.12) to recover the value of the adjoint displacement field within element e at location $\boldsymbol{\xi}$

$$\boldsymbol{\eta}_h^e(\boldsymbol{\xi}) = \boldsymbol{N}(\boldsymbol{\xi})\boldsymbol{\eta}^e \tag{4.69}$$

where $\boldsymbol{\eta}^e$ are the adjoint displacement values at the element nodes. The adjoint strain within the element at location $\boldsymbol{\xi}$ is recovered by

$$\boldsymbol{\epsilon}_h^e(\boldsymbol{\eta})(\boldsymbol{\xi}) = \boldsymbol{B}^e(\boldsymbol{\xi})\boldsymbol{\eta}^e \tag{4.70}$$

where $\boldsymbol{B}^e$ is the strain-displacement matrix. The corresponding pseudo-stress concerning a non-shape parameter s_i is obtained by

$$\frac{\partial \boldsymbol{\sigma}_h^e(\boldsymbol{u})}{\partial s_i}(\boldsymbol{\xi}) = \frac{\partial \boldsymbol{C}^e}{\partial s_i}\boldsymbol{B}^e(\boldsymbol{\xi})\boldsymbol{u}^e \tag{4.71}$$

including the partial derivative of the elasticity matrix $\boldsymbol{C}^e$ and the nodal displacements $\boldsymbol{u}^e$ of the primal problem. For non-shape parameters, only $\boldsymbol{C}^e$ must be derived within Equation (4.71).

To demonstrate the relation of discrete and variational sensitivity analysis, Equations (4.69), (4.70), and (4.71) are inserted into the internal and external adjoint work given by Equation (4.63) (the formulation is regarding the element domain $\Omega^e \subset \Omega$ with Neumann boundary Γ_N^e and the variation δs_i is dropped). The result

$$\begin{aligned} W_{\text{int}}^{e*} &= -\int_{\Omega^e} \boldsymbol{\epsilon}_h^e(\boldsymbol{\eta}) \cdot \frac{\partial \boldsymbol{\sigma}_h^e(\boldsymbol{u})}{\partial s_i}\, d\Omega^e = -\int_{\Omega^e} [\boldsymbol{B}^e \boldsymbol{\eta}^e]^T \cdot \frac{\partial \boldsymbol{C}^e}{\partial s_i} \boldsymbol{B}^e \boldsymbol{u}^e\, d\Omega^e \\ &= -[\boldsymbol{\eta}^e]^T \frac{\partial \boldsymbol{k}^e}{\partial s_i} \boldsymbol{u}^e \\ W_{\text{ext}}^{e*} &= \int_{\Omega^e} \boldsymbol{\eta}_h^e \cdot \frac{\partial \boldsymbol{p}^e}{\partial s_i}\, d\Omega^e + \int_{\Gamma_N^e} \boldsymbol{\eta}_h^e \cdot \frac{\partial \hat{\boldsymbol{t}}^e}{\partial s_i}\, d\Gamma_N^e \\ &= \int_{\Omega^e} [\boldsymbol{N}^e \boldsymbol{\eta}^e]^T \cdot \frac{\partial \boldsymbol{p}^e}{\partial s_i}\, d\Omega^e + \int_{\Gamma_N^e} [\boldsymbol{N}^e \boldsymbol{\eta}^e]^T \cdot \frac{\partial \hat{\boldsymbol{t}}^e}{\partial s_i}\, d\Gamma_N^e \\ &= [\boldsymbol{\eta}^e]^T \frac{\partial \boldsymbol{f}^e}{\partial s_i} \end{aligned} \tag{4.72}$$

equates the element-wise dot product of the influence function and the pseudo-load (cf. Equation (3.22a)) where the definitions

$$\begin{aligned} \boldsymbol{k}^e &= \int_{\Omega^e} [\boldsymbol{B}^e]^T \boldsymbol{C}^e \boldsymbol{B}^e\, d\Omega^e \\ \boldsymbol{f}^e &= \int_{\Omega^e} [\boldsymbol{N}^e]^T \boldsymbol{p}^e\, d\Omega^e + \int_{\Gamma_N^e} [\boldsymbol{N}^e]^T \hat{\boldsymbol{t}}^e\, d\Gamma_N^e \end{aligned} \tag{4.73}$$

of the element stiffness matrix and load vector are applied.

REMARK I: In the case of residual-based responses, it is recommended to include the local modification $\boldsymbol{\eta}_0^e$ (cf. Section 4.2.4) for the recovery of the adjoint strain:

$$\boldsymbol{\epsilon}_h^e(\boldsymbol{\eta})(\boldsymbol{\xi}) = \boldsymbol{B}^e(\boldsymbol{\xi})\,(\boldsymbol{\eta}_0^e + \boldsymbol{\eta}^e) \tag{4.74}$$

On the one hand, $\boldsymbol{\eta}_0^e$ replaces $\partial J/\partial s_i$. On the other hand, it prevents distortion of the adjoint strain. For illustration, the adjoint curvature of the two-span example in Figure 4.3 is recreated without consideration of $\boldsymbol{\eta}_0^e$. The structure is discretized with three Euler-Bernoulli beam elements. Adjoint displacement and influence function are created as described in Section 4.2.3. Figure 4.11 shows the adjoint displacement, influence function, and the respective adjoint curvature courses. Element 2 (response location) is highly stressed by bending through the additional unity rotation of its right node in the case of the adjoint displacement. Hence, the adjoint curvature in element 2 is much higher than for the influence function. It differs by $2EI/l_2 \cdot 1/EI$ and $4EI/l_2 \cdot 1/EI$ at the nodes of element 2. Please note that using the adjoint curvature without $\boldsymbol{\eta}_0^e$ is not wrong if $\partial J/\partial s_i$ is considered. However, the intuitive understanding of the adjoint field is severely limited.

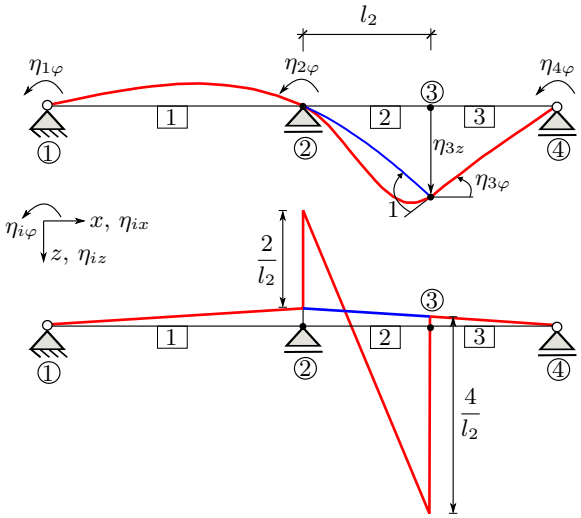

Figure 4.11: Top figure: Adjoint displacement of the bending moment at node 3 as response (red line) and its discrepancy to the influence function in element 2 (blue line). Bottom figure: Adjoint curvature based on adjoint displacement (red line) and its discrepancy to the curvature of the influence function in element 2 (blue line).

4.3.4 Significance in the case of general responses

Section 4.1.1 discusses the influence function as a provider of sensitivities concerning load parameters. The corresponding sensitivity analysis can be interpreted as the work of a pseudo-load with the influence function, denoted as external adjoint work. If the considered parameter is the load intensity, the external adjoint work equates evaluating a pseudo-load with intensity "1" on the influence function (cf. Equation (4.66)). In the case of more general parameters (e.g., parameters influencing the elastic stiffness), the sensitivity analysis is complemented by the internal adjoint work where the strain of the influence functions appears. The inspection of the influence function and its strain allows, thus, the identification of zones in a structure where parameter variations could significantly impact the response. Hence, the influence function and its strain are essential for the resulting sensitivities. The significance of the influence function and its strain might decrease for general responses with a non-vanishing partial derivative $\partial J/\partial s_i$. Furthermore, $\partial J/\partial s_i$ is an essential formal difference between the method of influence functions and adjoint sensitivity analysis (cf. discussion in Section 4.3.1). Hence, it is pertinent to investigate the significance of the partial derivative and the internal/external adjoint work for cases where both contribute to the resulting sensitivities. This section explores the issue through an exemplary discussion of responses with different characteristics of $\partial J/\partial s_i$. Therefore, local (locally defined at a finite element node or integration point) and global responses (performance measures of a complete model) are considered.

4.3.4.1 Local element stresses

Sensitivity equation

The generation of influence functions of local post-processing results as responses is well documented in the literature. Especially in the context of adaptivity and error analysis of finite element calculations, influence functions of local quantities are derived and applied. Refer to Cirak [40] and Grätsch et al. [74, 75, 77] for example. In addition, the significance of the influence function is subsequently investigated in the context of sensitivity analysis.
Section 4.1.3 derives the adjoint load of local element stresses based on linear structural analysis. A more general approach to recover local stresses in a finite element analysis can be established on the continuum mechanical relations derived in Section 2.2. These are executed element-wise (denoted by index e) in a discretized formulation. Based on Equation (2.22), the Green-Lagrange strains in a local Cartesian basis (denoted with bar $\bar{\bullet}$) can be recovered through

$$\bar{\boldsymbol{E}}^e_{\gamma\delta} = \frac{1}{2}(g^e_{ij} - G^e_{ij})(\boldsymbol{e}_\gamma \cdot \boldsymbol{G}^{i,e})(\boldsymbol{G}^{j,e} \cdot \boldsymbol{e}_\delta) \tag{4.75}$$

where the underlying base vectors are determined by

$$\boldsymbol{G}^e_i = \frac{\partial \boldsymbol{N}}{\partial \theta^i}\boldsymbol{X}^e \quad \text{and} \quad \boldsymbol{g}^e_i = \frac{\partial \boldsymbol{N}}{\partial \theta^i}(\boldsymbol{X}^e + \boldsymbol{u}^e) \tag{4.76}$$

in terms of shape functions $\boldsymbol{N}$ and primal displacement values $\boldsymbol{u}^e$ at the element nodes. For the subsequent stress recovery, the components of strain tensor $\bar{\boldsymbol{E}}^e_{\gamma\delta}$ are assembled into the elemental strain vector $\bar{\boldsymbol{E}}^e$ in terms of Voigt notation. The strains are connected with the Second Piola-Kirchhoff (PK2) stresses by the elastic constitutive equation

$$\bar{\boldsymbol{S}}^e = \bar{\boldsymbol{C}}^e \bar{\boldsymbol{E}}^e + \bar{\boldsymbol{S}}^e_0 \tag{4.77}$$

with elasticity matrix $\bar{\boldsymbol{C}}^e$ and prestress $\bar{\boldsymbol{S}}^e_0$. The jth component of stress vector $\bar{\boldsymbol{S}}^e$ is considered as response

$$J = \boldsymbol{e}_j^T \bar{\boldsymbol{S}}^e \tag{4.78}$$

where $\boldsymbol{e}_j$ is the jth unity vector which extracts the scalar response. The partial derivatives of Equation (4.78) with respect to kth displacement $u_k \in \boldsymbol{u}^e$ and the parameter s_i read

$$\frac{\partial J}{\partial u_k} = \boldsymbol{e}_j^T \bar{\boldsymbol{C}}^e \frac{\partial \bar{\boldsymbol{E}}^e}{\partial u_k} \quad \text{and} \tag{4.79a}$$

$$\frac{\partial J}{\partial s_i} = \boldsymbol{e}_j^T \frac{\partial \bar{\boldsymbol{C}}^e}{\partial s_i} \bar{\boldsymbol{E}}^e + \boldsymbol{e}_j^T \bar{\boldsymbol{C}}^e \frac{\partial \bar{\boldsymbol{E}}^e}{\partial s_i} + \boldsymbol{e}_j^T \frac{\partial \bar{\boldsymbol{S}}^e_0}{\partial s_i} \tag{4.79b}$$

where the partial derivatives of the Green-Lagrange strains $\bar{\boldsymbol{E}}^e$ can be determined by applying the chain rule of differentiation to Equation (4.75). Finally, the final sensitivity term

$$\frac{dJ}{ds_i} = \boldsymbol{e}_j^T \frac{\partial \bar{\boldsymbol{C}}^e}{\partial s_i} \bar{\boldsymbol{E}}^e + \boldsymbol{e}_j^T \bar{\boldsymbol{C}}^e \frac{\partial \bar{\boldsymbol{E}}^e}{\partial s_i} + \boldsymbol{e}_j^T \frac{\partial \bar{\boldsymbol{S}}^e_0}{\partial s_i} + \boldsymbol{\eta}^T \boldsymbol{F}^* \tag{4.80}$$

is obtained for a local element stress if $\partial J / \partial s_i$ is inserted in Equation (3.11).

REMARK I: Cauchy stresses in a Cartesian coordinate system are required for meaningful physical stress results. Therefore, the observed response in Equation (4.77) based on PK2 stresses has to be further transformed. Refer to Section 2.2.2 concerning the connection of Cauchy and PK2 stresses. Furthermore, Kiendl [94] can be recommended for a comprehensive description of the recovery of Cauchy stresses. The sensitivity equations of Cauchy stress as response are not presented here because they provide the same observations concerning the existence of $\partial J / \partial s_i$.

Significance of influence function and external adjoint work

The partial derivative $\partial J / \partial s_i$ vanishes according to Equation (4.79b) for external load parameters. Hence, load sensitivities can be solely computed by the external adjoint work of influence function and pseudo-load. To illustrate the influence function as a provider of load sensitivities, the four-point sail, described in more detail in Appendix A.2, is considered. The membrane is a very flexible structure that has to be analyzed by geometrically non-linear

analysis. Hence, the influence function based on Equation (3.17) is state-dependent. The maximal Cauchy stress σ_{mem} in the membrane surface under the simultaneous action of prestress and a snow load is chosen as the response (cf. Figure A.2 for the stress course). The influence function based on a snow load intensity of 0.5 kN/m^2 is shown in Figure 4.12 (left). The observed stress is orientated in warp direction (see Figure 4.12). It can be observed that the maximum values of the influence function are locally concentrated at the point where the traced stress is located. Furthermore, zones with negative sensitivities are identified. If the load in these parts increases, the observed stress decreases. The shown z-values of the influence function are integrated across the membrane surface. The result is 3 180 and equates the sensitivity with respect to the intensity of the applied uniformly distributed snow load p_s in the z-direction. The normalized sensitivity according to Equation (6.1) is 0.29%, i.e., the stress increases approximately 0.29% if the load is increased by 1.0% (cf. Section 6.2 for information on sensitivity normalization).

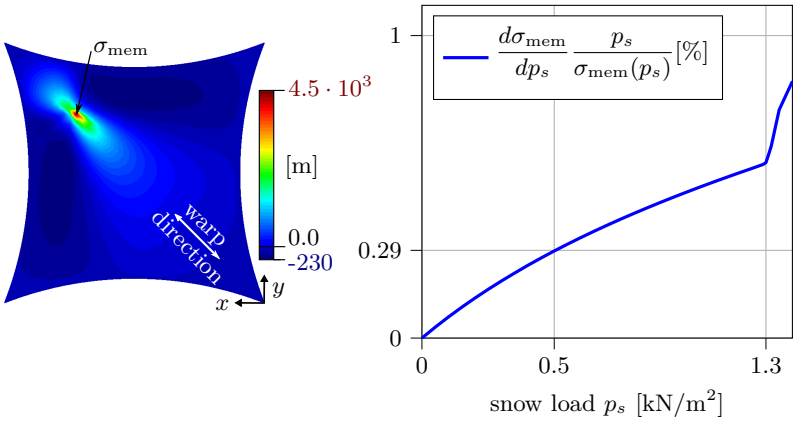

Figure 4.12: Influence function of the local Cauchy stress σ_{mem} in warp direction under a snow load of p_s=0.5 kN/m^2 (left). The response location coincides with the highest values of the influence function. Shown are the adjoint displacement components in the z-direction. Normalized sensitivities with respect to p_s during load increasement (right).

To illustrate the state dependency of the influence function and the associated load sensitivities, Figure 4.12 (right) shows the course of the normalized load sensitivities while the snow load p_s is increased step-wise by increments of 0.05 kN/m^2. Starting at a load of approximately 1.3 kN/m^2, a substantial increase in the load sensitivity is identified. This circumstance is associated with the onset of wrinkling deformation due to tension loss in the direction between the low points. The changing structural behavior can be studied if the state-dependent influence function is analyzed before and shortly after the onset of wrinkling. Figure 4.13 (left) shows the z-components of the

influence function for 1.0 kN/m^2 and 1.35 kN/m^2 which look qualitatively similar to the influence function at 0.5 kN/m^2. At all three load stages, it can be observed that the highest values are locally restricted around the observed stress. Furthermore, similar regions with negative sensitivities can be identified. To make the substantial sensitivity increase visible, the difference in the influence function values between the actual and the preceding load step is plotted on the right side in Figure 4.13. At 1.0 kN/m^2, the influence function increment is similar to the influence function. This is not the case for 1.35 kN/m^2. A substantial increase in the influence function values on the connection arch between the low points can be realized (green-colored areas). This observation reflects the change in the load-bearing behavior due to the onset of wrinkling.

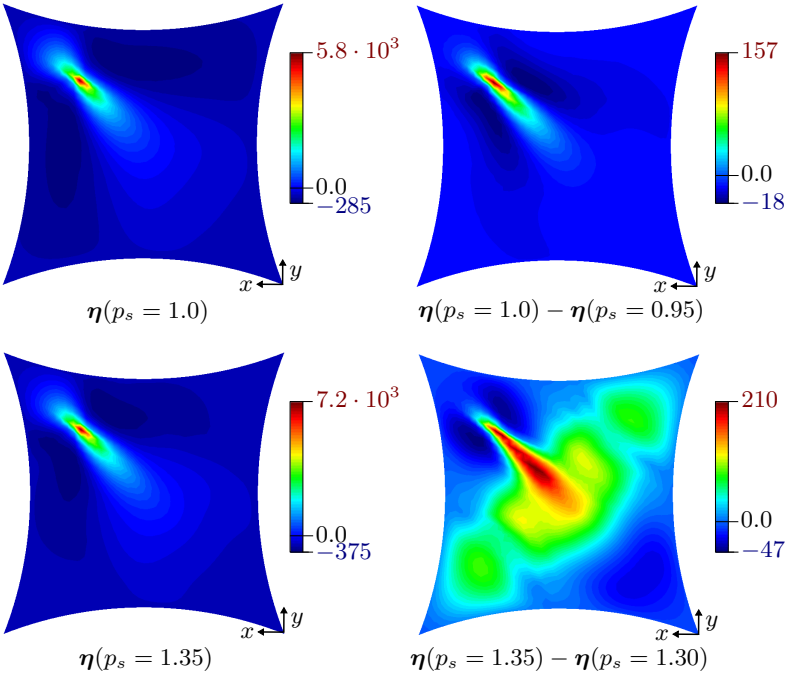

Figure 4.13: Influence function $\boldsymbol{\eta}$ (z-component) of σ_{mem} for p_s of 1.0 kN/m^2 and 1.35 kN/m^2 (left). Influence function difference between two consecutive load steps (right).

Significance of internal adjoint work

According to Equation (4.79b), the partial derivative $\partial J/\partial s_i$ does not vanish for the parameters that appear explicitly within the stress recovery of the

finite element e where the observed stress is located. For instance, these are material parameters such as Young's modulus or Poisson's ratio. Hence, $\partial J/\partial s_i$ exists for parameters that are also considered by the internal adjoint work. For this reason, it is impossible to calculate sensitivities using only the internal adjoint work for the element in which the response is located.

To study the significance of the explicit parameter influence $\partial J/\partial s_i$ and the internal adjoint work, the maximal Cauchy stress σ_{mem} in the four-point sail membrane structure under a snow load of p_s=0.5 kN/m^2 is again chosen as response (cf. Figure 4.12 for the location and the influence function of σ_{mem}). The element in which the response is located is further indicated with index j. As parameters, the Young's modulus of the membrane elements is considered. The sensitivity distribution, the course of the internal adjoint work, and the partial derivative are visualized in Figure 4.14. Please note that the figures show discrete sensitivity values for each element. Therefore, the internal adjoint work is computed element-wise in a discrete manner and added to the scalar value $\partial J/\partial E_i$. It can be observed that the overall sensitivity course (Sub-figures 4.14 (1) and (2)) is well presented by the internal adjoint work (Sub-figure 4.14 (3)). However, the partial derivative $\partial J/\partial E_j$ is of great significance for the sensitivity with respect to the Young's modulus of element j as the final sensitivity $dJ/dE_j = 1.9 \cdot 10^{-3}$ is composed of $\partial J/\partial E_j = 2.5 \cdot 10^{-3}$ and an internal adjoint work contribution of $-0.6 \cdot 10^{-3}$.

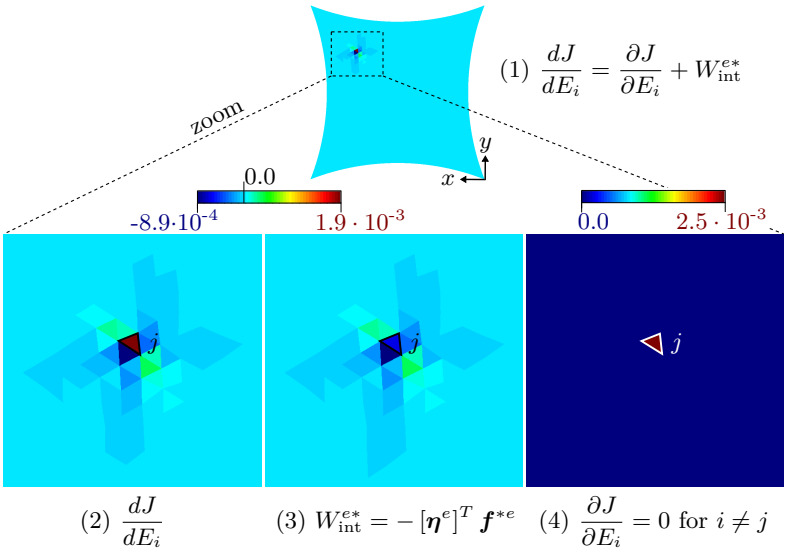

Figure 4.14: (1) Sensitivity distribution of Cauchy stress σ_{mem} located in element j concerning the Young's modulus of the elements, (2) zoom into sensitivity distribution, (3) discrete internal adjoint work, and (4) partial derivative.

The sensitivity of a parameter of a single finite element may only be of theoretical interest. Hence, sensitivities are subsequently calculated with respect to several parameters of the entire membrane. This can be realized by adding the discrete sensitivities of all membrane elements. The results are summarized in Table 4.3. A high significance of the partial derivative $\partial J/\partial s_i$ to the final sensitivity can be observed for all considered parameters. Although only element j contributes, the importance of $\partial J/\partial s_i$ is as significant as the internal adjoint work for which the entire membrane domain has to be considered.

Table 4.3: Composition of sensitivities of the local Cauchy stress σ_{mem} with respect to membrane parameters.

parameter s_i	dJ/ds_i	$\partial J/\partial s_i$	W^*_{int}
Young's modulus	0.0002	0.0025	-0.0023
Poisson's ratio	16.25	-550.75	567.00
isotropic prestress	0.41	1.00	-0.59

4.3.4.2 Linear strain energy

Sensitivity equation

The strain energy of a structure provides information about its stiffness. Hence, it is a frequently used objective function in structural optimization (e.g., Firl et al. [59] and Masching et al. [109]). In linear analysis, strain energy can be determined by two equivalent formulations:

$$E_{\text{lin}}(\boldsymbol{s}, \boldsymbol{u}(\boldsymbol{s})) = \frac{1}{2}\boldsymbol{u}(\boldsymbol{s})^T \boldsymbol{F}(\boldsymbol{s}) \quad \text{or} \tag{4.81a}$$

$$E_{\text{lin}}(\boldsymbol{s}, \boldsymbol{u}(\boldsymbol{s})) = \frac{1}{2}\boldsymbol{u}(\boldsymbol{s})^T \boldsymbol{K}(\boldsymbol{s})\boldsymbol{u}(\boldsymbol{s}) \tag{4.81b}$$

The sensitivity of $J = E_{\text{lin}}$ with respect to s_i is computed by

$$\begin{aligned} \frac{dJ}{ds_i} &= \frac{\partial J}{\partial s_i} + \left[\frac{\partial J}{\partial \boldsymbol{u}}\right]^T \frac{d\boldsymbol{u}}{ds_i} \\ &= \frac{1}{2}\boldsymbol{u}^T \frac{\partial \boldsymbol{F}}{\partial s_i} + \frac{1}{2}\boldsymbol{F}^T \boldsymbol{K}^{-1} \boldsymbol{F}^* \quad \text{or} \\ &= \frac{1}{2}\boldsymbol{u}^T \frac{\partial \boldsymbol{K}}{\partial s_i}\boldsymbol{u} + \boldsymbol{F}^T \boldsymbol{K}^{-1} \boldsymbol{F}^* \end{aligned} \tag{4.82}$$

wherein the definitions of state derivative and pseudo-load in Equations (3.8) and (3.14) are applied. The adjoint variable of strain energy can be identified in Equation (4.82) whose discrete values

$$\boldsymbol{\eta}_1 = \frac{1}{2}\boldsymbol{K}^{-1}\boldsymbol{F} = \frac{1}{2}\boldsymbol{u} \quad \text{or} \tag{4.83a}$$

$$\boldsymbol{\eta}_2 = \boldsymbol{K}^{-1}\boldsymbol{F} \quad = \boldsymbol{u} \tag{4.83b}$$

are directly obtained from the state variables $\boldsymbol{u}$ without additional solution of a system of equations. Finally, the sensitivities in an adjoint formulation can be computed by

$$\frac{dJ}{ds_i} = \frac{1}{2}\boldsymbol{u}^T\frac{\partial \boldsymbol{F}}{\partial s_i} + \boldsymbol{\eta}_1^T\left[\frac{\partial \boldsymbol{F}}{\partial s_i} - \frac{\partial \boldsymbol{K}}{\partial s_i}\boldsymbol{u}\right] \quad \text{or} \tag{4.84a}$$

$$\frac{dJ}{ds_i} = \frac{1}{2}\boldsymbol{u}^T\frac{\partial \boldsymbol{K}}{\partial s_i}\boldsymbol{u} + \boldsymbol{\eta}_2^T\left[\frac{\partial \boldsymbol{F}}{\partial s_i} - \frac{\partial \boldsymbol{K}}{\partial s_i}\boldsymbol{u}\right]. \tag{4.84b}$$

In principle, Equation (4.84) can be simplified to

$$\frac{dJ}{ds_i} = \boldsymbol{\eta}_1^T\left[2\cdot\frac{\partial \boldsymbol{F}}{\partial s_i} - \frac{\partial \boldsymbol{K}}{\partial s_i}\boldsymbol{u}\right] \quad \text{or} \tag{4.85a}$$

$$\frac{dJ}{ds_i} = \boldsymbol{\eta}_2^T\left[\frac{\partial \boldsymbol{F}}{\partial s_i} - \frac{1}{2}\cdot\frac{\partial \boldsymbol{K}}{\partial s_i}\boldsymbol{u}\right] \tag{4.85b}$$

taking into account that $\partial J/\partial s_i$ contains the influence function and parts of the pseudo-load. However, this operation creates a dependence of the pseudo-load on a specific response, which contradicts the concept of evaluating response-independent pseudo-loads on the influence function.

Significance of influence function and external adjoint work

The influence function of strain energy shows some remarkable properties. First, depending on whether Equation (4.81a) or (4.81b) is applied, a different influence function is received, where $\boldsymbol{\eta}_1 = 0.5\cdot\boldsymbol{\eta}_2$. Hence, there is no distinct influence function in the case of strain energy. Second, according to Equation (4.83), the influence function is instantaneous related to the load, which is a noteworthy difference from the traditional method of influence functions. For illustration, the steel hook presented by Geiser et al. [68] is considered, which is shown in Figure 4.15. The hook is subjected to two load cases. The direct relatedness of influence function and load cases becomes evident in the visualizations in Figure 4.15 (right).
The existence of $\partial J/\partial s_i$ concerning load parameters depends on the chosen influence function. If sensitivity analysis with $\boldsymbol{\eta}_1$ is used, $\partial J/\partial s_i$ is existent for parameters which affect the load vector $\boldsymbol{F}$. However, the partial derivative

$$\frac{\partial J}{\partial s_i} = \frac{1}{2}\boldsymbol{u}^T\frac{\partial \boldsymbol{F}}{\partial s_i} = \boldsymbol{\eta}_1^T\frac{\partial \boldsymbol{F}}{\partial s_i} \tag{4.86}$$

is identical to the discrete external adjoint work. To determine load sensitivities, the pseudo-load has to be evaluated with factor two (cf. Equation (4.85a)). Although the influence function is not immediately the provider of load sensitivities, its analysis is sufficient to get information concerning load sensitivities. In other words, significant values of the influence function indicate zones where load modifications are potentially influential. In the case of the hook shown in Figure 4.15, it can be observed that a variation of load case 2 has a larger impact on strain energy as the same variation of load case 1. If sensitivity analysis according to Equation (4.84b) is utilized, $\partial J/\partial s_i$ vanishes and the load sensitivities are directly the result of the external adjoint work.

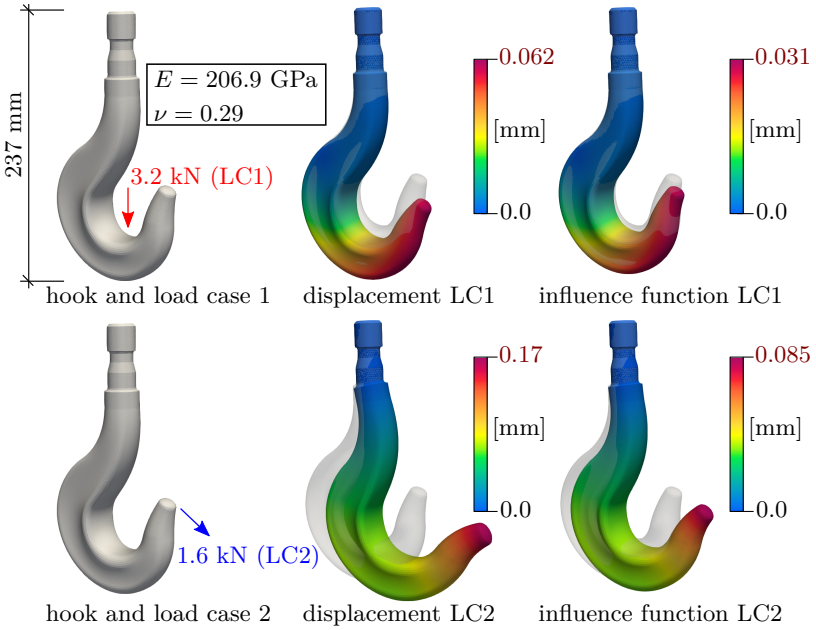

Figure 4.15: Primal displacement and influence function corresponding to load case 1 (LC1) and load case 2 (LC2). The influence function $\boldsymbol{\eta}_1$ is shown as defined in Equation (4.83a).

Significance of internal adjoint work

Parameters that only influence the stiffness matrix $\boldsymbol{K}$ are considered next. If Equation (4.84a) with $\boldsymbol{\eta}_1$ as influence function is applied, the partial derivative $\partial J/\partial s_i$ vanishes. The sensitivities are directly the result of the internal adjoint work. Otherwise, sensitivity analysis according to Equation (4.84b) requires $\partial J/\partial s_i$ which contains the partial derivative of the global stiffness matrix $\boldsymbol{K}$. If, for instance, the sensitivities with respect to the Young's modulus E^e of each element e of a finite element model is of interest, Equation (4.84b) can be executed element-wise by

$$\frac{dJ}{dE^e} = \underbrace{\frac{1}{2}\,[\boldsymbol{u}^e]^T\,\frac{\partial \boldsymbol{k}^e}{\partial E^e}\boldsymbol{u}^e}_{\partial J/\partial E^e} \underbrace{- [\boldsymbol{\eta}_2^e]^T\,\frac{\partial \boldsymbol{k}^e}{\partial E^e}\boldsymbol{u}^e}_{W_{\text{int}}^{*e}} \quad \text{with} \quad \boldsymbol{\eta}_2^e = \boldsymbol{u}^e. \tag{4.87}$$

Obviously, $\partial J/\partial E^e$ corresponds to half the dot product of influence function and pseudo-load ($\hat{=}$ element-wise discrete internal adjoint work, cf. result of Equation (4.72)). In the case of the graphical solution procedure, an additional map for the course of $\partial J/\partial E^e$ is required. This sensitivity map is a scaled version of the internal adjoint work. For visualization, the two-span

example in Figure 3.2 is discretized by 40 beam elements and loaded by load case 1 (line load with intensity p_1 on left field). The partial derivative and the discrete internal adjoint work are computed with respect to the Young's modulus E^e of each element. In the visualization in Figure 4.16, the scalar sensitivity partitions with respect to E^e are visualized constant along element e. The equivalence of partial derivative, the discrete internal adjoint work, and the final sensitivity course is intuitively visible. Hence, the graphical analysis of the internal adjoint work and its components is sufficient to receive qualitative information concerning the sensitivity composition. For instance, significant adjoint strain values indicate zones where stiffness modifications are potentially influential. This becomes visible in Figure 4.8 where the qualitative adjoint curvature of the considered strain energy response is visualized.

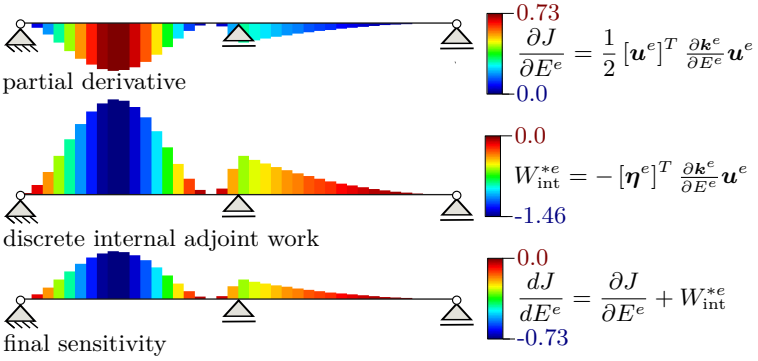

Figure 4.16: Composition of the sensitivity of the linear strain energy with respect to the Young's modulus of the beam elements.

4.3.4.3 Eigenvalue response of non-linear structural systems

Sensitivity equation

Subsequently, the eigenvalue problem

$$\left[\boldsymbol{K}_T\left(\tilde{\boldsymbol{u}}\right) - \alpha_k \boldsymbol{M}\left(\tilde{\boldsymbol{u}}\right)\right]\boldsymbol{\Phi}_k = \boldsymbol{0} \quad \text{where}$$

$$\boldsymbol{\Phi}_k^T \boldsymbol{M}\left(\tilde{\boldsymbol{u}}\right)\boldsymbol{\Phi}_l = \delta_{kl} \quad \text{with} \quad \delta_{kl} = \begin{cases} 1 \text{ if } k = l \\ 0 \text{ if } k \neq l \end{cases} \tag{4.88}$$

with eigenvalue α_k, eigenvector $\boldsymbol{\Phi}_k$, tangential stiffness matrix $\boldsymbol{K}_T$, and mass matrix $\boldsymbol{M}$ is considered. The system matrices $\boldsymbol{K}_T$ and $\boldsymbol{M}$ in Equation (4.88) depend on the state $\tilde{\boldsymbol{u}}$ which is determined by non-linear static analysis based on *operational conditions* related to static and pseudo-static external loading. Hence, the eigenvalue and eigenvector are state-dependent as well. Using operational conditions as the basis for eigenvalue problems is proposed by

Emiroğlu [51], where details on the formation of the loading are given. Using Equation (4.88) as the basis for sensitivity analysis and determining the associated equations are taken from Emiroğlu et al. [52]. Please note that the validity of the subsequent derivations presupposes symmetry of $\boldsymbol{K}_T$ and $\boldsymbol{M}$. As response for sensitivity analysis, the kth eigenvalue $J \triangleq \alpha_k$ is utilized. To apply the adjoint framework derived in Section 3.2.2, the partial derivatives $\partial J/\partial s_i$ and $\partial J/\partial \boldsymbol{u}$ are required. These can be determined by partial derivation of Equation (4.88) with respect to s_i and $\boldsymbol{u}$ which results in

$$\frac{\partial J}{\partial s_i} = \boldsymbol{\Phi}_k^T \left[\frac{\partial \boldsymbol{K}_T}{\partial s_i} - \alpha_k \frac{\partial \boldsymbol{M}}{\partial s_i} \right] \boldsymbol{\Phi}_k \tag{4.89}$$

and

$$\frac{\partial J}{\partial \boldsymbol{u}} = \boldsymbol{\Phi}_k^T \left[\frac{\partial \boldsymbol{K}_T}{\partial \boldsymbol{u}} - \alpha_k \frac{\partial \boldsymbol{M}}{\partial \boldsymbol{u}} \right] \boldsymbol{\Phi}_k. \tag{4.90}$$

If Equations (4.89) and (4.90) are substituted into Equations (3.17) and (3.19), respectively, the adjoint problem

$$\left[\boldsymbol{K}_T(\boldsymbol{u})\right]^T \boldsymbol{\eta}_k = \boldsymbol{\Phi}_k^T \left[\frac{\partial \boldsymbol{K}_T}{\partial \boldsymbol{u}} - \alpha_k \frac{\partial \boldsymbol{M}}{\partial \boldsymbol{u}} \right] \boldsymbol{\Phi}_k \tag{4.91}$$

and the adjoint sensitivity equation

$$\frac{dJ}{ds_i} = \boldsymbol{\Phi}_k^T \left[\frac{\partial \boldsymbol{K}_T}{\partial s_i} - \alpha_k \frac{\partial \boldsymbol{M}}{\partial s_i} \right] \boldsymbol{\Phi}_k + \boldsymbol{\eta}_k^T \left[\frac{\partial \boldsymbol{f}_{\text{ext}}}{\partial s_i} - \frac{\partial \boldsymbol{f}_{\text{int}}}{\partial s_i} \right] \tag{4.92}$$

are received for the kth eigenvalue as response. The relation of eigenfrequencies f_k and eigenvalues is given by

$$f_k = \frac{\sqrt{\alpha_k}}{2\pi} \tag{4.93}$$

on which basis the sensitivities

$$\frac{df_k}{ds_i} = \frac{1}{4\pi\sqrt{\alpha_k}} \cdot \frac{d\alpha_k}{ds_i} \tag{4.94}$$

of the kth eigenfrequency as the response can be determined.

Significance of influence function and external adjoint work

According to Equation (4.89), the partial derivative $\partial J/\partial s_i$ disappears for parameters that only influence the load vector $\boldsymbol{f}_{\text{ext}}$ and if the corresponding loads are deformation-independent, i.e., $\partial \boldsymbol{f}_{\text{ext}}/\partial \boldsymbol{u} = \boldsymbol{0}$. Hence, the influence function provides load sensitivities, i.e., the load sensitivities result from the external adjoint work. For illustration, the cable net bridge described in Appendix A.1 is considered. For the eigenvalue problem according to Equation (4.88), the bridge is subjected to dead load, prestress, and a uniform line load applied to the central bearer cables (cf. Figure A.1, right). On that basis, the first three eigenvalues and eigenmodes are computed, which are

shown in Figure 4.17 (left). The corresponding influence functions of the first three eigenvalues as responses are shown on the right of Figure 4.17. By their red-colored parts, the influence functions indicate zones of the bridge in which load variations have a maximal influence on the eigenvalues.
To interpret the comparatively large values of the influence functions shown in Figure 4.17, they are integrated along the central bearer cables. The results equate the force unit-dependent sensitivities with respect to the line load intensity. A line load sensitivity of 229 495 is received for the first eigenvalue as the response. According to Equation (6.1), the normalized sensitivity is 0.58%, i.e., the eigenvalue changes approximately 0.58% if the line load intensity of $9 \cdot 10^{-4}$ MN/m is increased by 1.0%. Please note that the normalized sensitivity of the equivalent eigenfrequency is with 0.29% only half. This can be determined if Equations (4.93) and (4.94) are applied to the normalized sensitivity of the eigenvalue. Refer to Section 6.2 for information concerning normalized sensitivities.

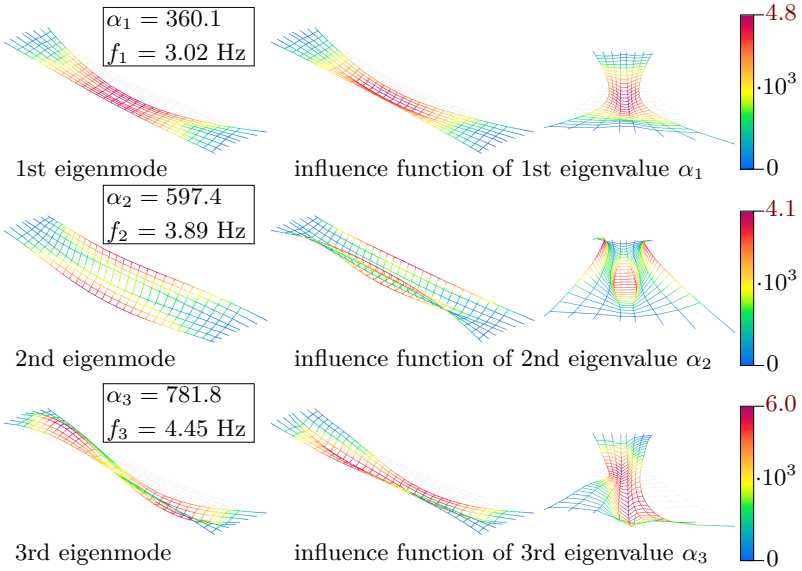

Figure 4.17: Left side: The first three eigenmodes. Right side: Influence functions of the eigenvalues α_{1-3} as responses shown from two perspectives.

Significance of internal adjoint work

The partial derivative of the eigenvalue response contains the global tangential stiffness and mass matrix (cf. Equation (4.89)). Consequently, all finite elements contribute whereby $\partial J / \partial s_i$ is potentially distributed across the

entire structural domain. The adjoint work thus only contributes a part to the resulting sensitivity distribution system-wide. For an exclusive parameter of the mass matrix $\boldsymbol{M}$, the final sensitivity is even equal to $\partial J/\partial s_i$. To investigate the significance of the partial derivative and the internal adjoint work, a stiffness parameter is considered that affects $\boldsymbol{K}_T$ and $\boldsymbol{f}_{\text{int}}$. Again, the cable net bridge presented in Appendix A.1 is observed. The sensitivity courses with respect to the Young's modulus of the elements are computed along the longitudinal cables. The sensitivity equation considering the Young's modulus of a single cable element as the parameter reads

$$\frac{d\alpha_k}{dE^e} = \underbrace{[\boldsymbol{\Phi}_k^e]^T \left[\frac{\partial \boldsymbol{k}_T^e}{\partial E^e}\right] \boldsymbol{\Phi}_k^e}_{\partial\alpha_k/\partial E^e} \underbrace{- \int_{L^e} A \cdot \varepsilon_{\text{GL}} \cdot \frac{\partial \varepsilon_{\text{GL}}}{\partial \boldsymbol{u}^e} \boldsymbol{\eta}_k^e \, dL^e}_{W_{\text{int}}^{*e}} \tag{4.95}$$

with the contribution of element e to the partial derivative and the internal adjoint work of adjoint strain $\partial\varepsilon_{\text{GL}}/\partial\boldsymbol{u}^e \cdot \boldsymbol{\eta}_k^e$ and PK2 pseudo-stress resultant $A \cdot \varepsilon_{\text{GL}}$. Information regarding the underlying variational formulation of the internal adjoint work can be found in Appendix B.2. The detailed visualization of the sensitivity analysis of the first eigenvalue α_1 is shown in Figure 4.18. Please note that the figures of internal adjoint work, partial derivative, and final sensitivity show discrete values for each element. Therefore, the integration of the internal adjoint work along the cable reference length L^e in Equation (4.95) has to be executed. The wavy course of the adjoint strain in combination with the constant pseudo-stress is directly reflected in a similarly wavy course of the internal adjoint work. In the case of the partial derivative, an equivalent waviness but with an opposite sign can be observed. Hence, the element-wise addition of partial derivative and internal adjoint work provides a constant sensitivity course. It should be noted that the assessment of the internal adjoint work and its components on the resulting sensitivity is not very significant: elements with comparably high or low absolute internal adjoint magnitudes (|-3.0e-7| vs. |-5.2e-6|) coincide with the same final sensitivity value of 6.4e-6. The numeric contribution of the partial derivative to the final sensitivity is higher than that from the internal adjoint work. However, the wavy course of the partial derivative $\partial\alpha_1/\partial E^e$ along the cables also does not match the resulting constant sensitivity course.

Similar conclusions can be drawn regarding the second eigenvalue α_2 as the response. Figure 4.19 shows the sensitivity components. In the internal adjoint work course, the zones of maximal absolute values of adjoint strain and pseudo-stress on the edge and central cables, respectively, become apparent. For instance, the maximal negative internal adjoint work values on the central bearer cables (blue-colored zones) can be explained by the comparable high pseudo-stresses prevailing there. However, the high internal adjoint work values on the central cables almost completely fade out due to similarly large but positive values of the partial derivative. It can be concluded that the courses of adjoint strain, pseudo-stress, and internal adjoint work are less significant as they provide only marginal indications of the final sensitivities. Even though the partial derivative values are not constantly distributed along the cables, they strongly dominate the final sensitivities. Thus, the partial

derivative and the final sensitivities show their maximum values at the edge cables. As in the case of α_1 as response (cf. Figure 4.18), constant sensitivities are obtained by the opposite waviness of internal adjoint work and partial derivative $\partial\alpha_2/\partial E^e$.

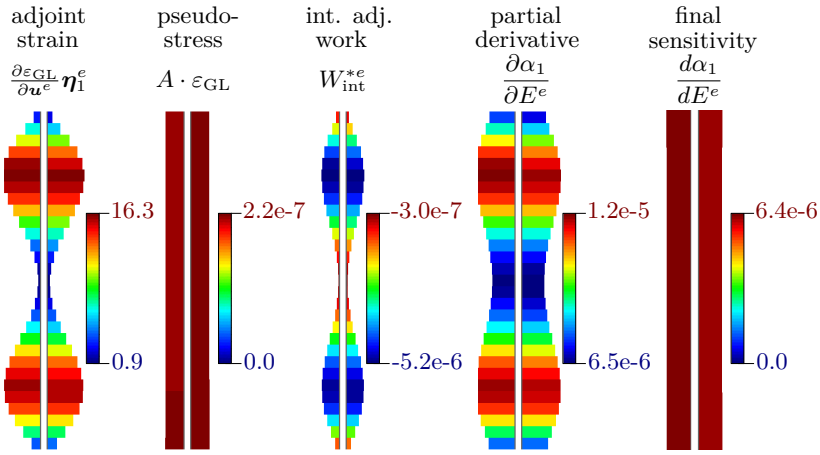

Figure 4.18: Composition of the sensitivity of the first eigenvalue α_1 of a cable net bridge with respect to the Young's modulus of the two central bearer cables.

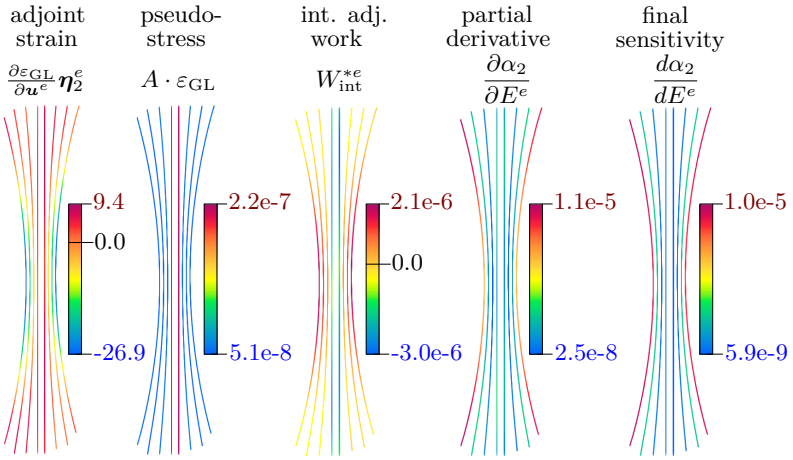

Figure 4.19: Composition of the sensitivity of the second eigenvalue α_2 of a cable net bridge with respect to the Young's modulus of the longitudinal cables.

4.3.4.4 Summary

The exemplary investigation of several responses shows that the properties and significance of $\partial J/\partial s_i$ differ strongly. It can be summarized as:

- In the case of local post-processing results like stresses, only the parameters of a single finite element contribute to $\partial J/\partial s_i$. Hence, the internal adjoint work course represents the final sensitivity course apart from the response element. The partial derivative does not exist for load parameters, and the sensitivities can be computed entirely by the external adjoint work. In this context, the state dependence of the influence function was discussed, showing that the analysis of the development of the influence function during the load increase can reveal changes in the load-bearing behavior.
- Since two sensitivity analysis options with different influence functions and $\partial J/\partial s_i$ are available, strain energy is a particular case. Depending on the option used, the partial derivative vanishes for parameters of the stiffness matrix or the load vector. In these cases, the computation of sensitivities reduces to evaluating the internal and external adjoint work, respectively. In the opposite cases, the partial derivative corresponds to a multiple of the internal and external adjoint work. Hence, the influence function, its strain, and the corresponding pseudo-quantities are sufficient to analyze the sensitivity courses.
- In the case of eigenvalues, the partial derivative vanishes for parameters that exclusively impact the external forces. Hence, the influence function as the provider of load sensitivities is significant. The partial derivative exists for parameters of the stiffness matrix and the mass matrix and is highly important for the final sensitivity. For this reason, the informative value of the influence function and its strain concerning the sensitivities is limited regarding these parameters.

In summary, the presence of $\partial J/\partial s_i$ is a drawback for the method of generalized influence functions. The significance of the influence function and its strain on the overall sensitivity is lower than for the examples discussed in Section 4.3.3. However, the expressiveness is quite different for the considered responses. This becomes obvious if local responses as stress within a single finite element and global responses as eigenvalues are compared. Furthermore, the graphical solution procedure is complicated since an additional partition of the sensitivity needs to be visualized and analyzed. Another difficulty is that $\partial J/\partial s_i$ is often a scalar value that refers to a finite element. Consequently, a discrete adjoint work value needs to be computed for the graphical and numerical comparison with $\partial J/\partial s_i$.

4.3.5 Limitations and particularities

4.3.5.1 Parameter dependent domains

Up to now, the discussion was limited to parameters that only affect the integrands in Equations (4.63) and (4.64) but not the shape of the domain. To examine the consequences if this precondition is not met, the variational sensitivity equations derived in Sections 3.3.2 - 3.3.4 must be extended for shape parameters. As noted in Section 3.3, different approaches for variational shape sensitivity analysis are known in the literature. For the subsequent discussion, the expressions presented in Materna [110] are used, but similar general conclusions can also be drawn with optional approaches, although the respective equations are different. According to Materna [110, Appendix B.2], the sensitivity equation in the case of linear elasticity theory is given as

$$\mathcal{D}_{\boldsymbol{s}} J(\boldsymbol{u}, \boldsymbol{s}) \cdot \delta\boldsymbol{s} = J'_{\boldsymbol{s}}(\boldsymbol{u}, \boldsymbol{s}; \delta\boldsymbol{s}) \tag{4.96a}$$

$$- \int_\Omega D_{\delta\boldsymbol{s}}\boldsymbol{\sigma}(\boldsymbol{u}) : \boldsymbol{\epsilon}(\boldsymbol{\eta}) d\Omega \tag{4.96b}$$

$$- \int_\Omega \boldsymbol{\sigma}(\boldsymbol{u}) : D_{\delta\boldsymbol{s}}\boldsymbol{\epsilon}(\boldsymbol{\eta}) d\Omega \tag{4.96c}$$

$$- \int_\Omega \boldsymbol{\sigma}(\boldsymbol{u}) : \boldsymbol{\epsilon}(\boldsymbol{\eta}) \left(d\Omega\right)'_{\boldsymbol{s}} + \int_\Omega \boldsymbol{p} \cdot \boldsymbol{\eta} \left(d\Omega\right)'_{\boldsymbol{s}} + \int_{\Gamma_N} \hat{\boldsymbol{t}} \cdot \boldsymbol{\eta} \left(d\Gamma_N\right)'_{\boldsymbol{s}} \tag{4.96d}$$

with $(d\Omega)'_{\boldsymbol{s}}$ and $(d\Gamma_N)'_{\boldsymbol{s}}$ denoting the variations of the domain and boundary elements. The design parameter $\boldsymbol{s}$ can be seen as a control function specifying the domain Ω. The constituents of Equation (4.96) are work expressions ($\boldsymbol{\eta}$ is assumed as displacement, refer to Section 4.3.2) and can be interpreted as extensions of the adjoint work introduced in Section 4.3.2. If Equation (4.96) is analyzed, the following observations can be made:

- Equation (4.96b) is equivalent to the internal adjoint work defined by Equation (4.63b). The integrand consists of a parameter dependent pseudo-stress $D_{\delta\boldsymbol{s}}\boldsymbol{\sigma}(\boldsymbol{u})$ and the linear strain of the influence function $\boldsymbol{\epsilon}(\boldsymbol{\eta})$. Hence, the response and parameter contributions to the sensitivity are separated by an adjoint and pseudo-quantity.
- Equation (4.96c) contains the variation $D_{\delta\boldsymbol{s}}\boldsymbol{\epsilon}(\boldsymbol{\eta})$ of the strain of the influence function with respect to $\boldsymbol{s}$. Hence, a quantity simultaneously dependent on response and parameter can be observed.
- The integrands in Equation (4.96d) contain either the influence function $\boldsymbol{\eta}$ or its strain $\boldsymbol{\epsilon}(\boldsymbol{\eta})$ to represent the response contribution to the sensitivity. However, the energetic conjugated force or stress quantity is independent of the specific $\boldsymbol{s}$ whereby no pseudo-quantity can be identified.

Even though Equation (4.96) can be seen as extended adjoint work, its constituents are not in each case the work of a pseudo-quantity and the energetically conjugated entity of the influence function. Instead, quantities

that are simultaneously dependent on response and parameter or that cannot be unambiguously assigned to either are observed. The concept of describing the composition of sensitivities by the interaction of response and parameter impact in terms of the influence function, its strain, and the corresponding pseudo-quantities is thus not applicable to shape parameters.

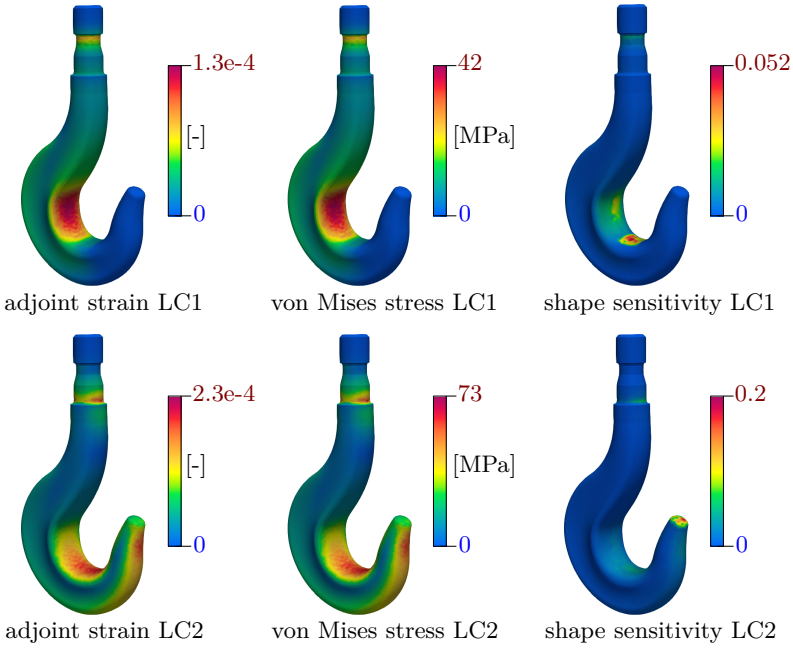

Figure 4.20: Considered is a hook which is subjected to two load cases (LC1 and LC2, see Figure 4.15). It can be observed that noticeable shape sensitivities coincide with noticeable high adjoint strains and primal von Mises stresses for both load cases. Observed response: linear strain energy.

The components of the integrands and their interaction can be analyzed and visualized to receive information concerning the sensitivity composition. Equation (4.96) depicts that the components of five integrals must be considered for a complete evaluation of the sensitivity composition. Given a practical sensitivity tool for problems in structural engineering, the added value of the analysis and assessment of this high amount of additional sensitivity information can be questioned. However, Equation (4.96) shows that sensitivities with respect to the shape are mainly driven by the influence function, its strain, and the the stress of the primal problem. Hence, qualitative assessment of these fields can provide at least partial insights into the sensitivities.
For illustration, the steel hook presented by Geiser et al. [68] shown in Figure 4.20 is studied. The hook is subjected to two load cases: a load at

the center (LC1) or the tip (LC2). The load cases and the resulting primal and adjoint displacement are shown in Figure 4.15. Linear strain energy (cf. Section 4.3.4.2) is chosen as response and sensitivities are computed with respect to the spatial position of the finite element nodes. Since the focus is on obtaining qualitative insights into the sensitivity composition, the von Mises stress of the primal state is used. The von Mises equation is also applied to the adjoint strain tensor. This bypasses the complete analysis of the entire set of stress and strain fields in the individual spatial directions or the principal stresses and strains. The sensitivity distributions in Figure 4.20 show that noticeable sensitivities can be found in the load application areas. Furthermore, high sensitivities are observed in zones where high values of primal stress and adjoint strain coincide. In the case of linear strain energy, the adjoint displacement equates according to Equation (4.83) the primal displacement. Hence, the primal stress and the adjoin strain are equally distributed within the hook, and high primal stresses perfectly fit zones with dominant adjoint strain. The mere consideration of primal stress or the adjoint strain is sufficient to gain qualitative insight. The example shows how analyzing the quantities, which are part of the variational sensitivity equation, can improve understanding of the reasons for the resulting sensitivity distributions. However, a complete and quantitative assessment of shape sensitivities is impossible merely by the strain of the influence function and the primal stress.

4.3.5.2 Graphical solution procedure of internal adjoint work

Section 4.3.3 proposes how the graphical solution procedure of the traditional influence functions approach can be extended employing pseudo-quantities and the energetically conjugated quantity of the influence function. In the case of beam structures, it was shown how sensitivity analysis can be beneficially supported by these graphical means. However, in the case of thin-walled and solid structures, the pseudo-stress and the strain of the influence function as part of the internal adjoint work in Equation (4.63) are tensor-valued quantities. In principle, the components of the tensors can be visualized individually. However, the feasibility and the benefit of the intuitive evaluation of the importance of the individual components and their interaction should be questioned critically.
The membrane structure presented in Appendix A.2 is considered to investigate and illustrate the issue. The sum of the displacements in the z-direction ($\hat{=}$ vertical) of all finite element nodes within a radius of 15 cm around the membrane center is chosen as response J. This response might be interesting to investigate the structure in terms of ponding. Prestressed membrane elements are briefly introduced in Appendix B.3. Based on the weak form given by Equation (B.15), the internal adjoint work

$$W_{\text{int}}^{*} = -\int_{A_0} D_{\delta \boldsymbol{s}} \left(\bar{\boldsymbol{n}}_{\text{el}} + \bar{\boldsymbol{n}}_0 \right) : \frac{\partial \bar{\boldsymbol{\epsilon}}}{\partial \boldsymbol{u}} \boldsymbol{\eta} \, dA_0 \tag{4.97}$$

of the pseudo-PK2 stress resultants and the adjoint strain ($\hat{=}$ variation of the Green-Lagrange strain) is received. Sensitivities are computed with respect to

the Poisson's ratio ν. Therefore, the sensitivity term reduces to the internal adjoint work

$$\frac{dJ}{d\nu} \cdot \delta\nu = -\int_{A_0} \delta\nu \cdot \frac{\partial \bar{\boldsymbol{n}}_{\mathrm{el}}}{\partial \nu} : \frac{\partial \bar{\boldsymbol{\epsilon}}}{\partial \boldsymbol{u}} \boldsymbol{\eta} \, dA_0 \quad \text{with} \quad \frac{\partial \bar{\boldsymbol{n}}_{\mathrm{el}}}{\partial \nu} = t \cdot \frac{\partial \bar{\boldsymbol{C}}^{\mathrm{iso}}}{\partial \nu} \cdot \bar{\boldsymbol{\epsilon}} \quad (4.98)$$

if Equation (4.97) is inserted in Equation (4.64). The partial variation $J'_s(\cdot)$ vanishes since $\partial J/\partial s_i$ is zero in the case of displacements as response (cf. Section 4.2.1). The pseudo-PK2 stress resultants are generated by applying a derived material matrix $\bar{\boldsymbol{C}}^{\mathrm{iso}}$ in the constitutive equation. This becomes obvious if the computation of $\partial \bar{\boldsymbol{n}}_{\mathrm{el}}/\partial \nu$ in Equation (4.98) is compared with Equation (B.13).
The pseudo-stress consists of two in-plane normal stress components and one in-plane shear stress quantity. Along with the corresponding adjoint strains, six maps are required to visualize the composition of the internal adjoint work. To support the graphical analysis, the partitions of the adjoint work computed by

$$W^*_{\mathrm{int},j} = -\int_{A_0} \delta\nu \cdot \frac{\partial \bar{n}_{\mathrm{el},j}}{\partial \nu} \cdot \frac{\partial \bar{\epsilon}_j}{\partial \boldsymbol{u}} \boldsymbol{\eta} \, dA_0 = -\int_{A_0} \delta\nu \cdot \partial_\nu \bar{n}_{\mathrm{el},j} \cdot \delta_{\boldsymbol{u}} \bar{\epsilon}_j \, dA_0 \quad (4.99)$$

are additionally plotted where the index $j = 1, 2, 3$ denotes the component of $\bar{\boldsymbol{n}}_{\mathrm{el}}$ and $\delta_{\boldsymbol{u}} \bar{\boldsymbol{\epsilon}}$. The final spatial sensitivity course equates the sum of the $\delta\nu$-multipliers in the integrand of $W^*_{\mathrm{int},j}$. The maps are shown together with the resulting sensitivity map ($\hat{=}$ course of the multiplier of $\delta\nu$ in the integral in Equation (4.98)) in Figure 4.21. The secondary significance of the shear part $W^*_{\mathrm{int},3}$ and the high relevance of $W^*_{\mathrm{int},1}$ can be identified. The distribution of $W^*_{\mathrm{int},1}$ is strongly driven by the adjoint strain component $\delta_{\boldsymbol{u}} \bar{\epsilon}_1$. This demonstrates the high relevance of $\delta_{\boldsymbol{u}} \bar{\epsilon}_1$ for the final sensitivity distribution. Due to the large amount of adjoint work constitutes, that have to be individually analyzed, the intuitive graphical analysis of the sensitivity course is more difficult than for the beam examples discussed in Section 4.3.3.1. In particular, adding the partitions $W^*_{\mathrm{int},j}$ complicates the graphical analysis. It is not only the coincidence of the components' maximum or minimum values that must be considered. In addition, their signs are of interest because maximum values with opposite signs can cancel each other out. Therefore, the point-wise quantitative graphical analysis of the sensitivity course through the entire set of adjoint work components can be classified as less significant for practical purposes. Rather, using the strain of the influence function and the pseudo-stress for a qualitative screening for potentially relevant zones in a structure can be recommended. In the case of the membrane structure, the coincidence of absolute maximum values of $\delta_{\boldsymbol{u}} \bar{\epsilon}_1$, $\delta_{\boldsymbol{u}} \bar{\epsilon}_2$, $\partial_\nu \bar{n}_{\mathrm{el},1}$, and $\partial_\nu \bar{n}_{\mathrm{el},2}$ in the center of the structure is a qualitative indicator of comparably high sensitivities prevailing there.

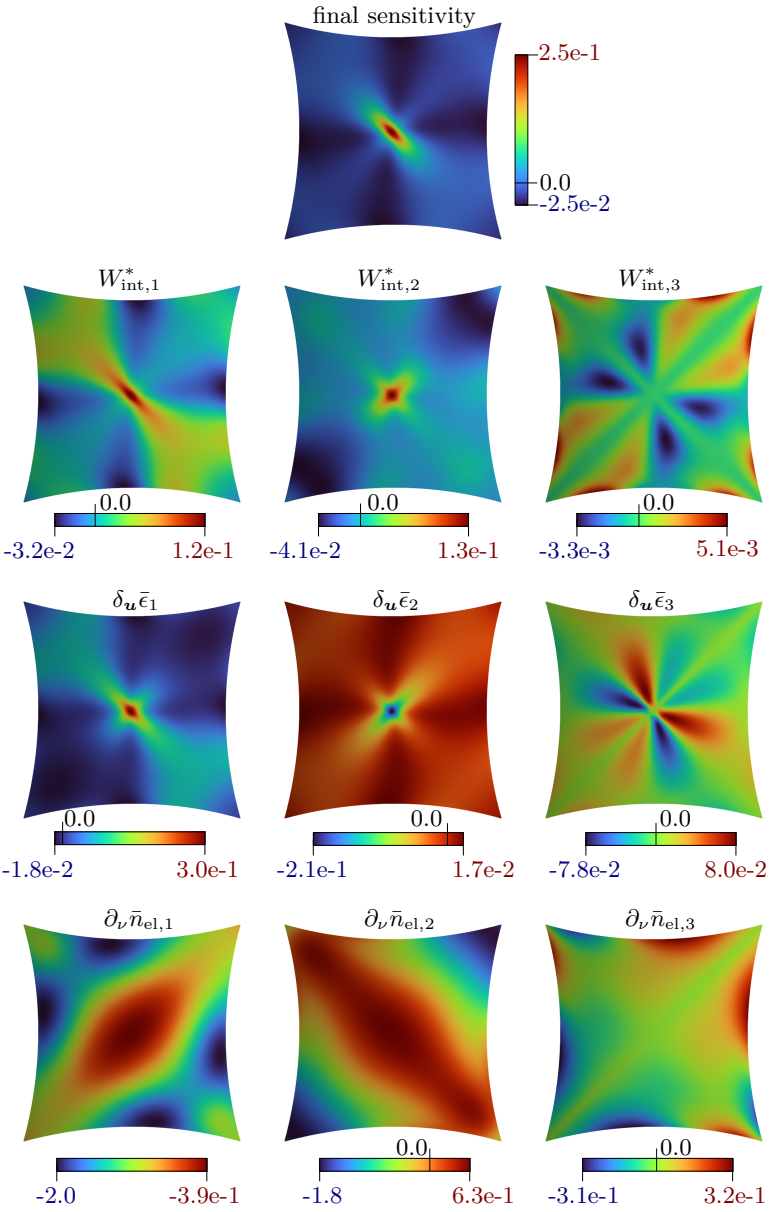

Figure 4.21: Sensitivity analysis of membrane center displacement with respect to Poisson's ratio ν. The final sensitivity is determined by the internal adjoint work consisting of adjoint strains $\delta_{\boldsymbol{u}}\bar{\epsilon}_j$ and pseudo-stresses $\partial_\nu \bar{n}_{\mathrm{el},j}$.

4.3.6 Connection to sensitivity analysis with Green's function method (SAGF)

Carl [33], Hartmann et al. [83], and Kunow [97] developed the sensitivity analysis with Green's functions method (SAGF), which is a computation technique to predict the consequences of local stiffness changes within a subdomain $\Omega_c \subset \Omega$. The SAGF approach strongly relates to the method of generalized influence functions. Subsequently, that methodical relatedness is discussed for the Euler-Bernoulli beam in more detail. The connection can be demonstrated analogously for other structural elements (e.g., truss, plate in bending or membrane action). Therefore, equivalent SAGF formulations of the references mentioned above can be utilized.

The SAGF approach compares the weak form of an initial structural status and that of a modified one in combination with Green's function ($\hat{=}$ influence function, cf. Section 3.4.3). For the exemplary case of an Euler-Bernoulli beam, the change of the bending moment $\Delta M(x_m)$ at $x = x_m$ due to a local modification of the bending stiffness ΔEI within the interval $[a, b] \subset [0, l]$ can be predicted by the SAGF method through

$$\begin{aligned} \Delta M(x_m) &\approx -\int_a^b \gamma_i \cdot M(x) \cdot M_\eta(x)\, dx \\ \text{with } \gamma_1 &= \frac{\Delta EI}{EI \cdot EI} \text{ (exemplary, for other } \gamma_i \text{ see Carl [33])} \end{aligned} \tag{4.100}$$

where $M(x)$ denotes the bending moment of the primal analysis, $M_\eta(x)$ is the bending moment of the Green's function of the response $M(x_m)$, and γ_i is a pre-factor which influences the quality of the approximation. According to Equation (4.100), the bending moment distribution of the primal analysis and the Green's function in the interval $[a, b]$ significantly decide the consequences of the stiffness modification. Hence, observing the two bending moment distributions reveals critical zones in a structure regarding stiffness alterations. Please note that in the same sense, the internal adjoint work of pseudo-moment and adjoint curvature can be used as discussed in Section 4.3.3.1.

Equation (4.100) is formulated with force quantities as primal variables. By using the denominator of γ_1, it is possible to reformulate Equation (4.100). Through the application of the inverse material law $\kappa = M/EI$, the expression

$$\Delta M(x_m) \approx -\int_a^b \Delta EI \cdot \kappa(x) \cdot \kappa_\eta(x)\, dx \tag{4.101}$$

is obtained. Equation (4.101) is equivalent to the total partial variation of the response $M(x_m)$ if the stiffness modification ΔEI is replaced by a respective

variation δEI

$$\begin{aligned} \mathcal{D}_{EI} M(x_m) \cdot \delta EI &= -\int_a^b \delta EI \cdot \kappa(x) \cdot \kappa_\eta(x)\, dx \\ &= -\int_a^b \delta EI \cdot M'_{EI}(x) \cdot \kappa_\eta(x)\, dx \\ &\text{with } M'_{EI} = \frac{\partial}{\partial EI}\{EI\} \cdot \kappa(x) = \kappa(x) \end{aligned} \tag{4.102}$$

or for a more general response J and a universal stiffness parameter s

$$\begin{aligned} \mathcal{D}_s J \cdot \delta s &= -\int_a^b \delta s \cdot M'_s(x) \cdot \kappa_\eta(x)\, dx \\ &\text{with } M'_s = \frac{\partial}{\partial s}\{EI(s)\} \cdot \kappa(x). \end{aligned} \tag{4.103}$$

where the partial variation $J'_s(\cdot)$ is assumed to be zero. The resultant integrands in Equation (4.102) and (4.103) are obviously the same as for the internal adjoint work W^*_{int} given by Equation (4.65b) and (4.67). The only difference in the equations is the integration domain. In general, the SAGF approach exclusively considers the stiffness-modified subdomain $\Omega_c \subset \Omega$, whereas variational sensitivity analysis is generally formulated regarding the entire domain Ω of the observed body.
In summary, the SAGF approach can be interpreted as the extension of the influence functions method for stiffness parameters. As variational adjoint sensitivity analysis is consistently derived for general settings of response, parameter, and underlying physical problem, the method of generalized influence functions can be seen as an extension of the SAGF approach, which embraces:

- the systematic extension for almost all parameters (see Section 4.3.5.1 for limitations)
- consideration of explicit parameter dependencies in terms of the partial variation $J'_s(s, u; \delta s)$
- straight forward application for other physics (cf. Section 4.4)

REMARK I: The target of the SAGF approach is to approximate the actual response change ΔJ due to Δs by using influence functions. In contrast, the goal of the method of generalized influence function described within this thesis is to determine sensitivities dJ/ds. However, the two purposes are closely linked if the derivatives are used in a Taylor series expansion.

REMARK II: The advantage of the SAGF approach is that the analysis in Equation (4.100) must be only executed locally within the subdomain $\Omega_c \subset \Omega$. That computation is cheap if the primal solution and the influence function are known and can thus be easily repeated for different subdomains of potential stiffness modifications. This property is reflected by adjoint sensitivity analysis by the advantage that its computational effort is almost independent of the parameter amount.

REMARK III: The SAGF approach does not consider the explicit parameter dependencies expressed through $J'_s(s, u; \delta s)$. Hence, it is not suitable for global responses as strain energy (Section 4.3.4.2) or eigenvalues (Section 4.3.4.3).

4.4 Application to another physics

Adjoint sensitivity analysis is a general approach that is not limited to structural mechanics. Hence, it is possible to transfer the method of generalized influence functions to other physical phenomenons. The key concepts of the method of generalized influence functions are:

- Determination of the influence function with the adjoint problem (cf. Section 4.2)
- Provision of additional sensitivity information by the adjoint work of the influence function, its strain, and the corresponding pseudo-quantities (cf. Section 4.3.2).
- Extension of the graphical analysis procedure by visualizing the adjoint work components (cf. Section 4.3.3).

Subsequently, the generalization of the concepts is exemplary demonstrated for steady state heat transfer problems (cf. Sections 2.3 and 3.3.4).

4.4.1 Determination of influence functions

The identification of the adjoint variable ($\hat{=}$ adjoint temperature in the case of heat problems) as influence function is in analogy to the derivations for responses in structural mechanics (cf. Section 4.2) and will be discussed below.

Nodal temperature

It is known from Green's functions approach (e.g., Stakgold et al. [133] or Section 3.4.3) that the influence function of the temperature at $\boldsymbol{x}$ as the response can be generated by the application of a concentrated unit heat source at $\boldsymbol{x}$. The connection to the adjoint variable can be seen if the jth nodal temperature $J = \phi_j \in \boldsymbol{\phi}$ is considered as response where $\boldsymbol{\phi}$ is the discrete vector of nodal temperatures. In analogy to a structural displacement

(cf. Section 4.2.1), the adjoint load

$$\frac{\partial J}{\partial \boldsymbol{\phi}} = \boldsymbol{e}_j \tag{4.104}$$

corresponds to the jth unit vector $\boldsymbol{e}_j$, which can be interpreted as a unit heat source applied at node j. Hence, the adjoint temperature has to be the influence function.

Heat flux

Another analogy with structural mechanics can be observed in the case of a nodal heat flux value in a one-dimensional heat transfer problem. Equivalent to stress resultants, heat fluxes are the components of the element residual equation $\boldsymbol{r}^e$. The nodal heat flux values $\boldsymbol{q}$ can be evaluated through

$$\boldsymbol{q} = \boldsymbol{H}_0^e \left(\boldsymbol{f}^e - \boldsymbol{k}^e \boldsymbol{\phi}^e\right) \quad \text{with} \quad \boldsymbol{H}_0^e = \begin{bmatrix} -1 & 0 \\ 0 & +1 \end{bmatrix} \tag{4.105}$$

whereby the jth heat flux $q_j \in \boldsymbol{q}$ as observed response can be determined through

$$q_j = [\boldsymbol{\eta}_0^e]^T \left(\boldsymbol{f}^e - \boldsymbol{k}^e \boldsymbol{\phi}^e\right) \quad \text{with} \quad \boldsymbol{\eta}_0^e = \left[\boldsymbol{H}_{0(j;n)}^e\right]^T \tag{4.106}$$

with $\boldsymbol{\eta}_0^e$ as the transposed jth row of $\boldsymbol{H}_0^e$. The response formulation in Equation (4.106) is the same as for stress resultants in structural analysis[1] (cf. Section 4.2.3 and in particular Equation (4.41)). Hence, all findings from the investigations of stress resultants can also be applied to heat fluxes. In particular, the element contribution of the pseudo-load can be identified as part of the partial derivative $\partial q_j / \partial s_i$, which allows the merge of $\boldsymbol{\eta}^e$ and $\boldsymbol{\eta}_0^e$ in the element-wise sensitivity term of Equation (3.22):

$$\begin{aligned} \frac{dq_j}{ds_i} &= \underbrace{[\boldsymbol{\eta}_0^e]^T \left(\frac{\partial \boldsymbol{f}^e}{\partial s_i} - \frac{\partial \boldsymbol{k}^e}{\partial s_i}\boldsymbol{\phi}^e\right)}_{\partial q_j / \partial s_i} + \sum_n \left\{ [\boldsymbol{\eta}^e]^T \left(\frac{\partial \boldsymbol{f}^e}{\partial s_i} - \frac{\partial \boldsymbol{k}^e}{\partial s_i}\boldsymbol{\phi}^e\right)\right\} \\ &= \sum_n \left\{ \left([\boldsymbol{\eta}_0^e]^T + [\boldsymbol{\eta}^e]^T\right) \left(\frac{\partial \boldsymbol{f}^e}{\partial s_i} - \frac{\partial \boldsymbol{k}^e}{\partial s_i}\boldsymbol{\phi}^e\right)\right\} \end{aligned} \tag{4.107}$$

Thus, the partial derivative $\partial q_j / \partial s_i$ can be replaced by adding a unity jump to the adjoint temperature at the elemental degree of freedom which corresponds to the response. Finally, the combination of $\boldsymbol{\eta}$ and the local correction $\boldsymbol{\eta}_0^e$ represents the influence function of heat flux response. This observation shows how well-known structural analysis approaches, such as Land's theorem and Müller-Breslau's principle, can be smoothly transferred to other application cases on the generic basis of adjoint sensitivity analysis.

[1] In truss analysis the entries of matrix $\boldsymbol{H}_0^e$ in Equation (4.105) have opposite signs (cf. Equation (4.49)). The reason is that the heat flux corresponds with the negative temperature gradient (cf. Equation (2.44)). In contrast, the truss normal force relates to the positive displacement derivative.

4.4.2 Adjoint work

Steady state heat transfer problems are similar to structural analysis problems. This becomes obvious if the variational forms in Equations (2.41) and (2.55) are compared. Refer also to Bathe [12] for a discussion on the equivalence of the principle of virtual work of structural analysis and the variational form of steady state heat transfer problems. Moreover, variational formulations of thermal problems are known as *principle of virtual thermal work* in literature, see, e.g., Romano et al. [122]. Following this methodical transfer, the concept of adjoint work (cf. Section 4.3.2) is applied to steady state heat transfer problems. In analogy to structural mechanics, the adjoint variational sensitivity formulation (cf. Equation (3.45))

$$\frac{dJ}{d\boldsymbol{s}} \cdot \delta\boldsymbol{s} = J'_s(\phi, \boldsymbol{s}; \delta\boldsymbol{s}) + W^*_{\text{int}} + W^*_{\text{ext}} \quad \text{with} \tag{4.108a}$$

$$W^*_{\text{int}} = -\int_\Omega (\boldsymbol{\nabla}\eta)^T \cdot D_{\delta\boldsymbol{s}}\boldsymbol{\kappa}\boldsymbol{\nabla}\phi \, d\Omega \quad \text{and} \tag{4.108b}$$

$$W^*_{\text{ext}} = \int_\Omega \eta \cdot D_{\delta\boldsymbol{s}} Q \, d\Omega + \int_{\Gamma_N} \eta \cdot D_{\delta\boldsymbol{s}} \left(\alpha\left(\phi_a - \phi\right) + \sigma\epsilon\left(\phi_a^4 - \phi^4\right) + \hat{q}\right) \, d\Gamma_N \tag{4.108c}$$

is used to identify the internal and external adjoint work expressions. Consistently to Equation (4.63), the integrals of the internal and external adjoint work can be separated into parts with contrary dependencies. The partial variations with respect to the parameter are identified as pseudo-quantities that are independent of the response. For instance, there is the pseudo-heat source $D_{\delta\boldsymbol{s}}Q$ or the pseudo-heat flow $D_{\delta\boldsymbol{s}}\boldsymbol{\kappa}\boldsymbol{\nabla}\phi$. In contrast, the influence function η and the adjoint heat rate $\boldsymbol{\nabla}\eta$ represent the response contribution to the sensitivity. For the linear one-dimensional case, the variational sensitivity formulation based on the weak form given by Equation (2.57) reads

$$\frac{dJ}{ds} \cdot \delta s = J'_s(s; \phi, \delta s) + W^*_{\text{int}} + W^*_{\text{ext}} \quad \text{with} \tag{4.109a}$$

$$W^*_{\text{int}} = -\int_0^l \frac{d\eta}{dx} \cdot \frac{\partial}{\partial s}\left\{\kappa A\right\} \frac{d\phi}{dx} \cdot \delta s \, dx \quad \text{and} \tag{4.109b}$$

$$W^*_{\text{ext}} = \int_0^l \eta \cdot \frac{\partial Q}{\partial s} \cdot \delta s \, dx + \int_0^l \eta \cdot \frac{\partial}{\partial s}\left\{\alpha U\left(\phi_a - \phi\right)\right\} \cdot \delta s \, dx. \tag{4.109c}$$

4.4.3 Examples

One-dimensional case

An 8 cm long rod subjected to a uniform heat source and convection at the circumferential surface is considered. The system with its material properties and boundary conditions is shown in Figure 4.22.

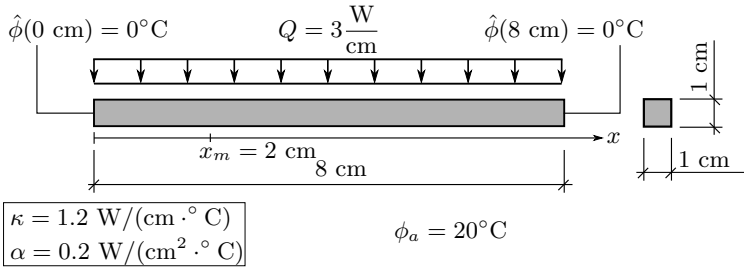

Figure 4.22: One-dimensional heat transfer problem. The rod is subjected to a uniform heat source Q and convection lengthwise on the circumferential surface.

Sensitivity analysis will be presented by the heat flux q_m at $x_m = 2$ cm as response with respect to the heat source Q, the thermal conductivity κ, and the heat transfer coefficient α as parameters. If Equation (4.109) is applied to the chosen response and parameters, the sensitivities are obtained by:

$$\frac{dq_m}{dQ} \cdot \delta Q = \int_0^l \eta \cdot 1 \cdot \delta Q \, dx \tag{4.110a}$$

$$\frac{dq_m}{d\kappa} \cdot \delta \kappa = -\int_0^l \frac{d\eta}{dx} \cdot A \frac{d\phi}{dx} \cdot \delta \kappa \, dx \tag{4.110b}$$

$$\frac{dq_m}{d\alpha} \cdot \delta \alpha = \int_0^l \eta \cdot U \, (\phi_a - \phi) \cdot \delta \alpha \, dx \tag{4.110c}$$

In analogy to the Euler-Bernoulli beam example (cf. Section 4.3.3.1), the separated visualization of the coefficients of δs within the integrals of Equation (4.110) allows a detailed analysis of the composition of the sensitivity distribution. The maps are shown in Figure 4.23 and enable the following observations:

- The sensitivity analysis with respect to the heat source is straightforward to the classical technique of influence functions. As a constant unity heat source is applied along the rod as pseudo-quantity, the sensitivity map corresponds to the influence function.
- Both the influence function and its derivative have small values for 6 cm $< x <$ 8 cm. As a consequence, the noticeable values of the respective pseudo-fields do not come into effect.
- Dominant sensitivity values can be found in areas where high values of adjoint and pseudo-field coincide. This is especially the case of sensitivity analysis with respect to κ and α for 0 cm $< x <$ 2 cm.

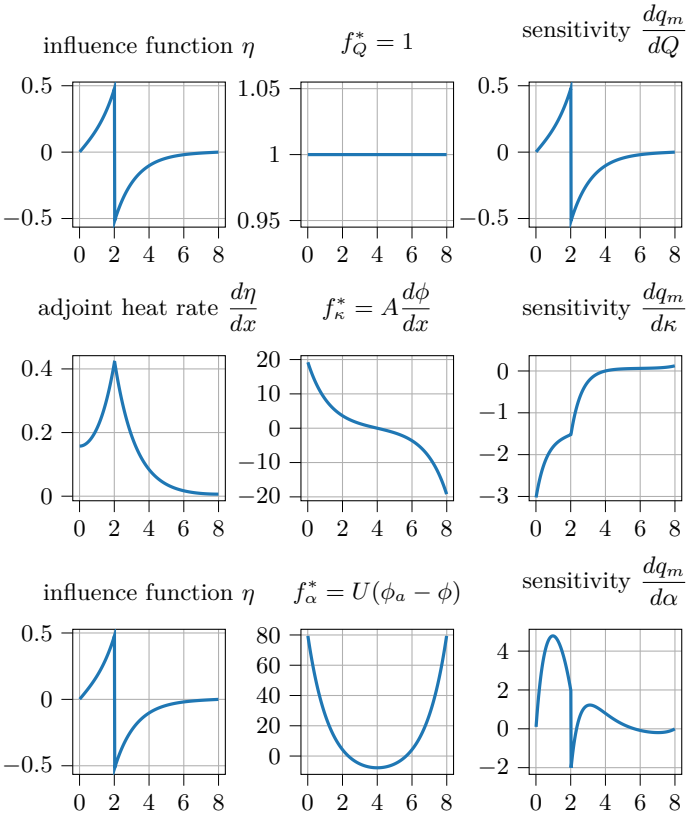

Figure 4.23: One-dimensional heat transfer problem. Composition of sensitivity courses of response q_m with respect to heat source Q (top), thermal conductivity κ (middle), and heat transfer coefficient α (bottom). The sensitivities (right) are composed according to Equation (4.110) of a quantity related to the influence function η (left) and a pseudo-quantity f_s^* (middle).

Three-dimensional case

A three-dimensional body consisting of a pipe and fin is considered. The system with its material properties and boundary conditions is shown in Figure 4.24. An isotropic material with conductivity properties described by κ is chosen. The left-hand side surface of the pipe represents the Dirichlet boundary with a prescribed temperature of $\hat{\phi} = 150°\mathrm{C}$. The remaining surface is the Neumann boundary, which is subjected to convection. Please note that

the ambient temperature differs (pipe inside: $\phi_{a,i} = 50°\text{C}$, pipe outside and fin surface: $\phi_{a,o} = 5°\text{C}$). Sensitivity analysis is presented by the average temperature on the body boundary in the green (response J_1) and in the blue-colored domain (response J_2) with respect to the heat transfer coefficient α as the parameter. The response domains are indicated in Figure 4.24.

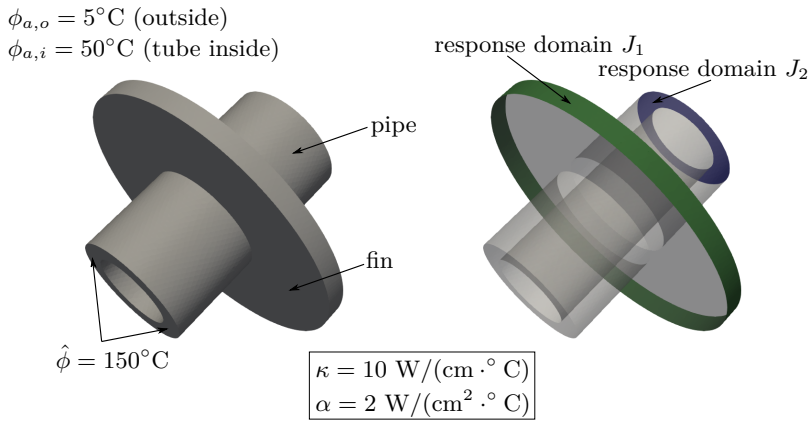

Figure 4.24: Three-dimensional heat transfer problem consisting of a pipe and a fin (left). As responses for sensitivity analysis, the average temperature on the body boundary in the green (response J_1) and in the blue-colored domain (response J_2) are considered.

The response formulation is based on nodal temperature values ϕ_i and reads

$$J = \frac{1}{n} \cdot \sum_{i=1}^{n} \phi_i \tag{4.111}$$

where n denotes the number of finite element nodes which are part of the response domain. As the response formulation has no explicit parameter dependency, the partial derivative vanishes, i.e., $\partial J / \partial s_i = 0$. According to Equation (4.108), sensitivity analysis with respect to parameter α reduces to

$$\frac{dJ}{d\alpha} \cdot \delta\alpha = \int_{\Gamma_N} \eta \cdot D_{\delta\alpha} \left(\alpha\phi_a - \alpha\phi\right) \, \Gamma_N = \int_{\Gamma_N} \eta \cdot \left(\phi_a - \phi\right) \delta\alpha \, \Gamma_N \tag{4.112}$$

which equates to the evaluation of the pseudo-quantity $f_\alpha^* = \phi_a - \phi$ on the influence function η. The sensitivity maps are shown in Figure 4.25 and enable the following observations:

- The pseudo-field is almost constant on the fin and the right part of the pipe. Hence, the sensitivity distributions in those parts are dictated by the influence functions, whereby the domains with maximal values of the influence function correspond to parts with dominating sensitivities.

- The maximal values of the pseudo-field can be found on the left part of the pipe. However, these values are almost faded due to the corresponding small values of the influence function.
- The analysis of the various maps can support the detection of the reasons for the particularities of the resulting sensitivities. For instance, the sensitivities inside the pipe are smaller in absolute values than outside. As a reason, smaller absolute values of the pseudo-quantity inside due to the higher internal pipe temperature can be identified (cf. Equation (4.112)). Since the adjoint temperature is almost the same over the entire pipe cross-section, the different pseudo-quantity values at the pipe surface are reflected accordingly in the final sensitivity.

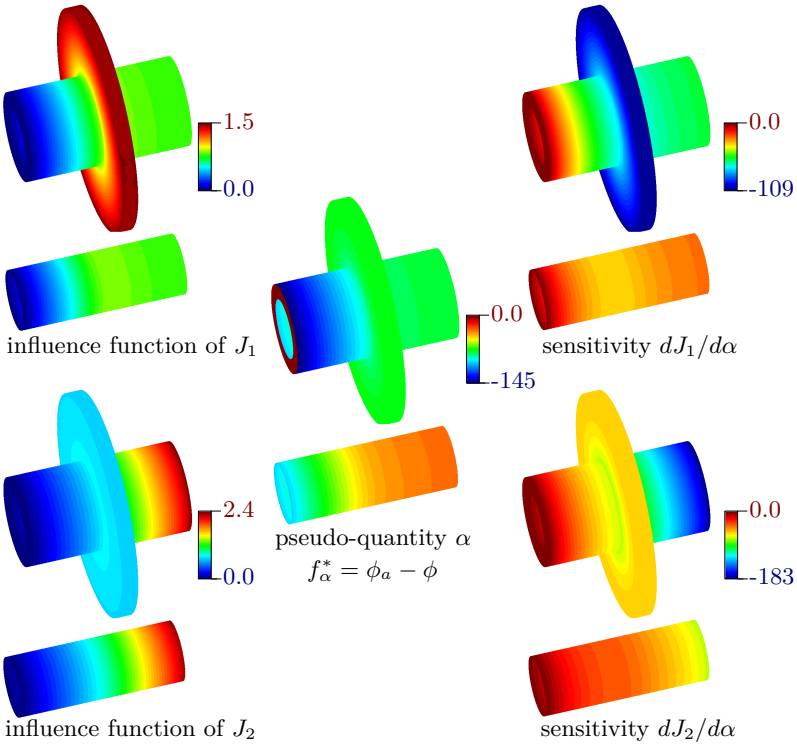

Figure 4.25: Composition of sensitivity distributions of responses J_1 (top) and J_2 (bottom) with respect to heat transfer coefficient α. The sensitivities (right) are composed according to Equation (4.112) of the influence function η (left) and the pseudo-quantity f^*_α (middle). For better visibility, the insides of the pipes are shown separately.

4.5 Summary

In this chapter, the relation between adjoint sensitivity analysis and the method of influence functions has been investigated in detail. First of all, the identification of the adjoint variable as influence function was discussed. Therefore, different viewpoints available from the literature were examined. Subsequently, the influence functions of the responses of the traditional approach (displacement, stress resultants, and support forces) have been successfully derived based on adjoint sensitivity equations. In that regard, it was shown that the evaluation of the partial derivative $\partial J/\partial s_i$ is necessary to justify the unity jump or kink of the influence function, which is not represented by the adjoint variable.
Furthermore, the concept of adjoint work was introduced and investigated. Based on variational adjoint sensitivity analysis, the work expression of the traditional influence functions approach can be extended for sensitivity analysis. A significant feature of the adjoint work concept is that analyzing the adjoint work components (pseudo-quantities and energetically conjugated counterparts of the influence function) provides valuable additional sensitivity information. Moreover, the adjoint work components can be utilized to extend the graphical analysis procedure of the traditional influence functions approach. Although the graphical analysis is complicated in the case of thin-walled and solid structures, adjoint work components can be of interest for numerical methods. Refer to Chapter 7 for an outlook in this regard.
The partial derivative $\partial J/\partial s_i$ is an essential difference between adjoint sensitivity analysis and the method of influence functions. The impact of $\partial J/\partial s_i$ on the concept has been investigated based on exemplary responses. Especially in the case of global responses (e.g., eigenvalues), the significance of the internal and external adjoint work can be strongly reduced.

Chapter 5

Sensitivity analysis based on sequenced simulation processes

A challenging group of structural models is one that requires a sequenced simulation process of several analysis stages. After stage k has finished, the analysis is stopped and the structural model is modified before the analysis of stage $k+1$ is restarted. A typical example of structural engineering is construction stage modeling. The analysis model must be adapted to the construction progress after each stage (e.g., adding new members). Another example is the design and analysis of lightweight structures (e.g., membranes or cable nets). A sequenced simulation process, which among others consists of form-finding and subsequent structural analyses, is required. The challenge in sensitivity analysis is that the quantities carried forward from one analysis stage to the next may depend on the parameters for which the sensitivities must be computed. Hence, the parameter influence in several stages has to be considered in sensitivity analysis. This chapter investigates how sensitivity analysis based on a sequenced simulation process can be realized. Section 5.1 discusses how analysis models can be initialized for the subsequent simulation stage and the necessary adjustments for sensitivity analysis. Based on these findings, additional extensions for sensitivity analysis in the case of construction stage analysis (Section 5.2) and the sequenced simulation process of lightweight structures (Section 5.3) are investigated.

5.1 Initialization of subsequent analysis stages

Sequenced simulation processes require stopping the analysis, modifying the structural analysis model (e.g., adding new members), and restarting the analysis. For the latter, retaining the state of the previous analysis stages is important. Therefore, the model of the subsequent analysis stage must be initialized accordingly. This section discusses how sensitivity analysis needs to be adjusted to adequately account for the initialization for the restart of the analysis.

5.1.1 Modeling approaches

Dieringer et al. [48] proposes two approaches to preserve the structural state of stage k and to restart the analysis of stage $k+1$:

- The approach *"restart with initial displacements"* (*InitDisp*) applies the resulting displacements $\boldsymbol{u}^{(k)}$ of stage k as initial displacements $\boldsymbol{u}_0^{(k+1)}$ for the start of stage $k+1$. The reference geometry is not updated[1], i.e., the initial reference geometry is retained in all stages $\boldsymbol{X}_{\text{init}} = \cdots = \boldsymbol{X}^{(k+1)}$.
- The approach *"restart with initial stresses"* (*InitStress*) applies the resulting stresses $\boldsymbol{S}^{(k)}$ of stage k as initial stresses $\boldsymbol{S}_0^{(k+1)}$ for the start of stage $k+1$. Furthermore, the geometry is updated, i.e., the deformed configuration $\boldsymbol{x}^{(k)}$ of stage k is taken as new reference configuration $\boldsymbol{X}^{(k+1)}$ for stage $k+1$.

The procedure of the two approaches is visualized in Figure 5.1. The illustration shows the transition from stage k to the subsequent simulation $k+1$. The initialization quantities required for the start of stage $k+1$ are highlighted in blue.
The advantages and disadvantages of the two approaches are examined in detail by Bauer [13], Dieringer [47], Dieringer et al. [48], and Philipp [118]. Their investigations show that mechanically accurate sequenced simulation processes can be achieved only with the InitDisp method. The InitStress modeling approach, on the other hand, approximates the structural behavior and should only be used for small deflections to ensure sufficient accuracy. However, the InitDisp approach is more elaborate in modeling. For instance, in the case of construction stage analysis, the reference geometry of old and new members is handled differently. This can lead to topologically separated members at the connection nodes of the construction stages. Section 5.2.1 describes this issue in more detail. It should be noted that despite the imprecision of the InitStress method, both approaches are considered in the following. The aim is to discuss the impact of different modeling approaches on the sensitivity analysis.
The initialization quantities are formulated regarding the total deformation $\boldsymbol{u}$ in the subsequent derivations. The total deformation of stage $k+1$ is determined as the difference between the initial reference configuration $\boldsymbol{X}_{\text{init}} = \boldsymbol{X}^{(1)}$ and the actual configuration $\boldsymbol{x}^{(k+1)}$:

$$\boldsymbol{u}^{(k+1)} = \boldsymbol{x}^{(k+1)} - \boldsymbol{X}_{\text{init}} \tag{5.1}$$

Optionally, it can be computed by

$$\boldsymbol{u}^{(k+1)} = \boldsymbol{u}^{(k)} + \Delta\boldsymbol{u}^{(k+1)} \tag{5.2}$$

where $\Delta\boldsymbol{u}^{(k+1)}$ is the additional deformation, which occurs in stage $k+1$. Please refer to Figure 5.1, where the total deformation is highlighted in red.

[1] This is not necessarily the case in construction stage analysis for the members added in stage $k+1$. These members can be modeled with a modified reference geometry to account for the compensation of occurred deformations. This issue is considered in Section 5.2.1.

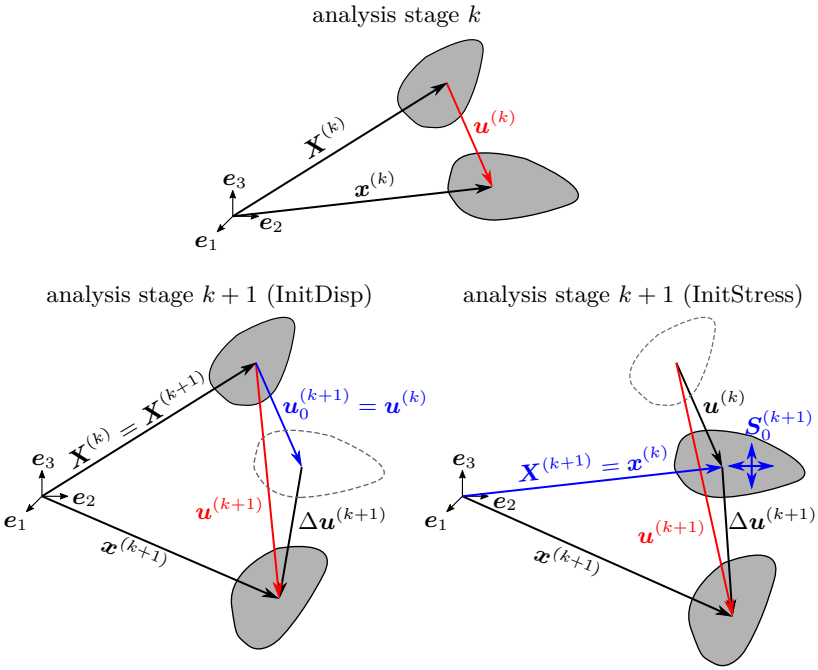

Figure 5.1: Basic modeling schemes for the initial two stages of a sequential analysis process. The second stage can be initialized by the InitDisp (left) or the InitStress (right) approach. The initialization quantities are written in blue.

5.1.2 Extension of sensitivity analysis

The basic discrete sensitivity expressions in Chapter 3.2 are derived based on the response $J(\boldsymbol{s}, \boldsymbol{u}(\boldsymbol{s}))$ (cf. Equation (3.5)) and the state equation $\boldsymbol{r}(\boldsymbol{s}, \boldsymbol{u}(\boldsymbol{s}))$ (cf. Equation (3.7)). In sequential simulation processes based on the approaches introduced in Section 5.1.1, it must be considered that the analysis is restarted based on initialization quantities. The latter are related to the deformations of the previous stages, which depend on the parameters $s_i \in \boldsymbol{s}$. These additional dependencies must be considered when formulating the response and the state equation. This section aims to derive the sensitivity equations for a response at stage $k+1$. It is expected that the deformations $\boldsymbol{u}^{(1)}(s_i)$ up to $\boldsymbol{u}^{(k+1)}(s_i)$ and the state derivatives $d\boldsymbol{u}^{(1)}/ds_i$ up to $d\boldsymbol{u}^{(k)}/ds_i$ are pre-computed.

Extension of sensitivity analysis for InitDisp

For the restart of the analysis at stage $k+1$, initial displacements $\boldsymbol{u}_0^{(k+1)}$ have to be applied. These coincide with the total displacements $\boldsymbol{u}_0^{(k+1)} = \boldsymbol{u}^{(k)}(s_i)$ and are therefore dependent on s_i. If this additional relation is considered, the response formulation and the state equation read

$$J^{(k+1)}\left(s_i, \Delta\boldsymbol{u}^{(k+1)}(s_i), \boldsymbol{u}_0^{(k+1)}\left(\boldsymbol{u}^{(k)}(s_i)\right)\right) \tag{5.3a}$$

$$\boldsymbol{r}^{(k+1)}\left(s_i, \Delta\boldsymbol{u}^{(k+1)}(s_i), \boldsymbol{u}_0^{(k+1)}\left(\boldsymbol{u}^{(k)}(s_i)\right)\right) = \boldsymbol{0} \tag{5.3b}$$

which are the basis for sensitivity analysis at stage $k+1$. The derivative of the response with respect to s_i is

$$\frac{dJ^{(k+1)}}{ds_i} = \frac{\partial J^{(k+1)}}{\partial s_i} + \frac{\partial J^{(k+1)}}{\partial \boldsymbol{u}_0^{(k+1)}}\frac{\partial \boldsymbol{u}_0^{(k+1)}}{\partial \boldsymbol{u}^{(k)}}\frac{d\boldsymbol{u}^{(k)}}{ds_i} + \frac{\partial J^{(k+1)}}{\partial \Delta\boldsymbol{u}^{(k+1)}}\frac{d\Delta\boldsymbol{u}^{(k+1)}}{ds_i} \tag{5.4}$$

if the chain rule of differentiation is applied to Equation (5.3a). The state derivative $d\Delta\boldsymbol{u}^{(k+1)}/ds_i$ can be determined equivalently to the procedure conducted in Equation (3.8). Therefore, the equilibrium condition in Equation (5.3b) is first derived concerning the parameter s_i, then the pseudo-load $\boldsymbol{F}^{*(k+1)}$ is introduced. Finally, the result is reformulated concerning the state derivative:

$$\begin{aligned} \frac{d\Delta\boldsymbol{u}^{(k+1)}}{ds_i} &= \left[\frac{\partial \boldsymbol{r}^{(k+1)}}{\partial \Delta\boldsymbol{u}^{(k+1)}}\right]^{-1} \boldsymbol{F}^{*(k+1)} \quad \text{with} \\ \boldsymbol{F}^{*(k+1)} &= -\frac{\partial \boldsymbol{r}^{(k+1)}}{\partial s_i} - \frac{\partial \boldsymbol{r}^{(k+1)}}{\partial \boldsymbol{u}_0^{(k+1)}}\frac{\partial \boldsymbol{u}_0^{(k+1)}}{\partial \boldsymbol{u}^{(k)}}\frac{d\boldsymbol{u}^{(k)}}{ds_i} \end{aligned} \tag{5.5}$$

If Equation (5.5) is substituted in (5.4) the final sensitivity equation is obtained:

$$\begin{aligned} \frac{dJ^{(k+1)}}{ds_i} =& \frac{\partial J^{(k+1)}}{\partial s_i} + \frac{\partial J^{(k+1)}}{\partial \boldsymbol{u}_0^{(k+1)}}\frac{\partial \boldsymbol{u}_0^{(k+1)}}{\partial \boldsymbol{u}^{(k)}}\frac{d\boldsymbol{u}^{(k)}}{ds_i} \\ &+ \frac{\partial J^{(k+1)}}{\partial \Delta\boldsymbol{u}^{(k+1)}}\left[\frac{\partial \boldsymbol{r}^{(k+1)}}{\partial \Delta\boldsymbol{u}^{(k+1)}}\right]^{-1} \boldsymbol{F}^{*(k+1)} \end{aligned} \tag{5.6}$$

REMARK I: When the analysis is restarted only, i.e., when the analysis model is not changed except for adding initial displacements to all degrees of freedom, the sensitivity equations for the InitDisp restart model can be simplified. Since the relations

$$\frac{\partial J^{(k+1)}}{\partial \boldsymbol{u}_0^{(k+1)}} = \frac{\partial J^{(k+1)}}{\partial \Delta\boldsymbol{u}^{(k+1)}} \quad \text{and} \quad \frac{\partial \boldsymbol{r}^{(k+1)}}{\partial \boldsymbol{u}_0^{(k+1)}} = \frac{\partial \boldsymbol{r}^{(k+1)}}{\partial \Delta\boldsymbol{u}^{(k+1)}} \tag{5.7}$$

can be identified, Equation (5.6) reduces to

$$\frac{dJ^{(k+1)}}{ds_i} = \frac{\partial J^{(k+1)}}{\partial s_i} + \frac{\partial J^{(k+1)}}{\partial \Delta \boldsymbol{u}^{(k+1)}} \left[\frac{\partial \boldsymbol{r}^{(k+1)}}{\partial \Delta \boldsymbol{u}^{(k+1)}} \right]^{-1} \frac{-\partial \boldsymbol{r}^{(k+1)}}{\partial s_i} \tag{5.8}$$

which is equal to the sensitivity expression of a single stage analysis given by Equation (3.9). The same can be found for the state derivative regarding the total displacement if Equation (5.7) is applied when Equation (5.5) is substituted in (5.18):

$$\frac{d\boldsymbol{u}^{(k+1)}}{ds_i} = \left[\frac{\partial \boldsymbol{r}^{(k+1)}}{\partial \Delta \boldsymbol{u}^{(k+1)}} \right]^{-1} \frac{-\partial \boldsymbol{r}^{(k+1)}}{\partial s_i} \tag{5.9}$$

Equations (5.8) and (5.9) show that the state derivative $d\boldsymbol{u}^{(k)}/ds_i$ has canceled out. Hence, no additional solutions of linear systems are required to determine the state derivative of previous stages. Consequently, the computational effort for sensitivity analysis is the same as for a single stage simulation. It should be noted that this observation is mainly of theoretical interest. In practical situations, the main reason for stopping and restarting an analysis is to change the model.

Extension of sensitivity analysis for InitStress

Initial stresses and a modified reference geometry are applied as initialization quantities. The updated reference configuration can be formulated with respect to the initial reference configuration as $\boldsymbol{X}^{(k+1)} = \boldsymbol{u}^{(k)}(s_i) + \boldsymbol{X}_{\text{init}}$. To determine the initial stresses for stage $k+1$, the resulting stress state of the previous stage k has to be computed. The PK2-stresses at stage k are

$$\boldsymbol{S}^{(k)} = \mathbb{C} : \boldsymbol{E}^{(k)} + \boldsymbol{S}_0^{(k)} \tag{5.10}$$

based on the Saint Venant-Kirchhoff model and the applied initial stresses for the initialization of stage k. The material tensor contains parameters that are relevant for sensitivity analysis. Hence, an explicit dependency of the initial stresses on s_i is assumed. The Green-Lagrange strains (cf. Section 2.2.1 and Equation (2.20)) are based on the reference and deformed configuration of the previous stage k, which simultaneously[2] depend on $\boldsymbol{u}^{(k)}$ and $\boldsymbol{u}^{(k-1)}$. Furthermore, the initial stresses for the restart of stage $k+1$ depend on the

[2] This can be easily seen in the case of a non-linear truss element. The resulting Green-Lagrange strain ϵ_{GL} at stage k can be computed by

$$\epsilon_{\text{GL}} = \frac{l\left(\boldsymbol{u}^{(k)}\right)^2 - L\left(\boldsymbol{u}^{(k-1)}\right)^2}{2 \cdot L\left(\boldsymbol{u}^{(k-1)}\right)^2}$$

where the current length l can be determined based on $\boldsymbol{u}^{(k)}$. The modified reference length L for stage k is computed with respect to $\boldsymbol{u}^{(k-1)}$.

initial stresses of the previous stage k, which in turn depend on the initial stresses of stage $k-1$. This results in a linkage of the initial stresses:

$$\begin{aligned}
&\boldsymbol{S}_0^{(2)}\left(s_i, \boldsymbol{u}^{(1)}\right)\\
&\boldsymbol{S}_0^{(3)}\left(s_i, \boldsymbol{u}^{(1)}, \boldsymbol{u}^{(2)}, \boldsymbol{S}_0^{(2)}\left(s_i, \boldsymbol{u}^{(1)}\right)\right)\\
&\vdots\\
&\boldsymbol{S}_0^{(k+1)}\left(s_i, \boldsymbol{u}^{(k-1)}, \boldsymbol{u}^{(k)}, \boldsymbol{S}_0^{(k)}\left(s_i, \boldsymbol{u}^{(k-2)}, \boldsymbol{u}^{(k-1)}, \boldsymbol{S}_0^{(k-1)}\left(\cdots\right)\right)\right)
\end{aligned} \tag{5.11}$$

The sensitivities of the initial stresses defined in Equation (5.11) are required below. These can be calculated using the pre-calculated state derivatives:

$$\begin{aligned}
\frac{d\boldsymbol{S}_0^{(2)}}{ds_i} &= \frac{\partial \boldsymbol{S}_0^{(2)}}{\partial s_i} + \frac{\partial \boldsymbol{S}_0^{(2)}}{\partial \boldsymbol{u}^{(1)}}\frac{d\boldsymbol{u}^{(1)}}{ds_i}\\
\frac{d\boldsymbol{S}_0^{(3)}}{ds_i} &= \frac{\partial \boldsymbol{S}_0^{(3)}}{\partial s_i} + \frac{\partial \boldsymbol{S}_0^{(3)}}{\partial \boldsymbol{u}^{(1)}}\frac{d\boldsymbol{u}^{(1)}}{ds_i} + \frac{\partial \boldsymbol{S}_0^{(3)}}{\partial \boldsymbol{u}^{(2)}}\frac{d\boldsymbol{u}^{(2)}}{ds_i} + \frac{\partial \boldsymbol{S}_0^{(3)}}{\partial \boldsymbol{S}_0^{(2)}}\frac{d\boldsymbol{S}_0^{(2)}}{ds_i}\\
&\vdots\\
\frac{d\boldsymbol{S}_0^{(k+1)}}{ds_i} &= \frac{\partial \boldsymbol{S}_0^{(k+1)}}{\partial s_i} + \frac{\partial \boldsymbol{S}_0^{(k+1)}}{\partial \boldsymbol{u}^{(k-1)}}\frac{d\boldsymbol{u}^{(k-1)}}{ds_i} + \frac{\partial \boldsymbol{S}_0^{(k+1)}}{\partial \boldsymbol{u}^{(k)}}\frac{d\boldsymbol{u}^{(k)}}{ds_i} + \frac{\partial \boldsymbol{S}_0^{(k+1)}}{\partial \boldsymbol{S}_0^{(k)}}\frac{d\boldsymbol{S}_0^{(k)}}{ds_i}
\end{aligned} \tag{5.12}$$

Since the partial derivatives $\partial_{(\bullet)}\boldsymbol{S}_0^{(j)}$ are cheap to calculate, the additional costs for the evaluation of Equation (5.12) are low for given state derivatives. If the dependency of the modified reference geometry and the initial stress on s_i is considered, the response formulation and state equation

$$J^{(k+1)}\left(s_i, \Delta\boldsymbol{u}^{(k+1)}(s_i), \boldsymbol{X}^{(k+1)}\left(\boldsymbol{u}^{(k)}(s_i)\right), \boldsymbol{S}_0^{(k+1)}(\bullet)\right) \tag{5.13a}$$

$$\boldsymbol{r}^{(k+1)}\left(s_i, \Delta\boldsymbol{u}^{(k+1)}(s_i), \boldsymbol{X}^{(k+1)}\left(\boldsymbol{u}^{(k)}(s_i)\right), \boldsymbol{S}_0^{(k+1)}(\bullet)\right) = \boldsymbol{0} \tag{5.13b}$$

are obtained. Note that $(\bullet)$ in Equation (5.13) represents the dependencies defined by Equation (5.11). The application of the chain rule of differentiation to Equation (5.13a) leads to

$$\begin{aligned}
\frac{dJ^{(k+1)}}{ds_i} =& \frac{\partial J^{(k+1)}}{\partial s_i} + \frac{\partial J^{(k+1)}}{\partial \boldsymbol{X}^{(k+1)}}\frac{\partial \boldsymbol{X}^{(k+1)}}{\partial \boldsymbol{u}^{(k)}}\frac{d\boldsymbol{u}^{(k)}}{ds_i} + \frac{\partial J^{(k+1)}}{\partial \boldsymbol{S}_0^{(k+1)}}\frac{d\boldsymbol{S}_0^{(k+1)}}{ds_i}\\
&+ \frac{\partial J^{(k+1)}}{\partial \Delta\boldsymbol{u}^{(k+1)}}\frac{d\Delta\boldsymbol{u}^{(k+1)}}{ds_i}
\end{aligned} \tag{5.14}$$

where the state derivative is determined based on Equation (5.13b):

$$\frac{d\Delta \boldsymbol{u}^{(k+1)}}{ds_i} = \left[\frac{\partial \boldsymbol{r}^{(k+1)}}{\partial \Delta \boldsymbol{u}^{(k+1)}}\right]^{-1} \boldsymbol{F}^{*(k+1)} \quad \text{with}$$
$$\boldsymbol{F}^{*(k+1)} = -\frac{\partial \boldsymbol{r}^{(k+1)}}{\partial s_i} - \frac{\partial \boldsymbol{r}^{(k+1)}}{\partial \boldsymbol{X}^{(k+1)}} \frac{\partial \boldsymbol{X}^{(k+1)}}{\partial \boldsymbol{u}^{(k)}} \frac{d\boldsymbol{u}^{(k)}}{ds_i} - \frac{\partial \boldsymbol{r}^{(k+1)}}{\partial \boldsymbol{S}_0^{(k+1)}} \frac{d\boldsymbol{S}_0^{(k+1)}}{ds_i} \tag{5.15}$$

The combination of Equations (5.14) and (5.15) yields the final sensitivity term:

$$\begin{aligned}\frac{dJ^{(k+1)}}{ds_i} =& \frac{\partial J^{(k+1)}}{\partial s_i} + \frac{\partial J^{(k+1)}}{\partial \boldsymbol{X}^{(k+1)}} \frac{\partial \boldsymbol{X}^{(k+1)}}{\partial \boldsymbol{u}^{(k)}} \frac{d\boldsymbol{u}^{(k)}}{ds_i} + \frac{\partial J^{(k+1)}}{\partial \boldsymbol{S}_0^{(k+1)}} \frac{d\boldsymbol{S}_0^{(k+1)}}{ds_i} \\ &+ \frac{\partial J^{(k+1)}}{\partial \Delta \boldsymbol{u}^{(k+1)}} \left[\frac{\partial \boldsymbol{r}^{(k+1)}}{\partial \Delta \boldsymbol{u}^{(k+1)}}\right]^{-1} \boldsymbol{F}^{*(k+1)}\end{aligned} \tag{5.16}$$

Computational aspects

Depending on the execution order of the matrix-vector products in the last line of Equations (5.6) and (5.16), a direct or adjoint procedure is carried out. In the latter case, the adjoint variable $\boldsymbol{\eta}^{(k+1)}$ is solved by the linear system of equations

$$\left[\frac{\partial \boldsymbol{r}^{(k+1)}}{\partial \Delta \boldsymbol{u}^{(k+1)}}\right]^{T} \boldsymbol{\eta}^{(k+1)} = \frac{\partial J^{(k+1)}}{\partial \Delta \boldsymbol{u}^{(k+1)}} \tag{5.17}$$

and then dot-multiplied with the pseudo-load. Otherwise, direct sensitivity analysis initiates with the solution of the state derivative given by Equations (5.5) and (5.15). Refer to Section 3.2 for a discussion of which procedure to be preferred depending on the number of responses and parameters.
In terms of computational effort, the most significant difference between Equations (5.6) respectively (5.16) and the basic sensitivity expressions derived in Section 3.2 is that the state derivatives $d\boldsymbol{u}^{(k)}/ds_i$ of the previous stages are required. To compute the state derivative $d\boldsymbol{u}^{(k+1)}/ds_i$ for the following stage, Equation (5.2) has to be derived with respect to s_i:

$$\frac{d\boldsymbol{u}^{(k+1)}}{ds_i} = \frac{d\boldsymbol{u}^{(k)}}{ds_i} + \frac{d\Delta \boldsymbol{u}^{(k+1)}}{ds_i} \tag{5.18}$$

The derivative $d\Delta \boldsymbol{u}^{(k+1)}/ds_i$ can be computed either by direct or adjoint sensitivity analysis. The choice depends on whether the number of degrees of freedom n_{DOF} or the number of parameters n_s is dominant. For $n_{\mathrm{DOF}} > n_s$ a direct procedure by solving the state derivative given by Equations (5.5) and (5.15) is to be preferred. In that case, n_s solutions of linear systems are required. Otherwise, for $n_{\mathrm{DOF}} < n_s$ an adjoint sensitivity analysis with each degree of freedom $\Delta u_j^{(k+1)} \in \Delta \boldsymbol{u}^{(k+1)}$ as response $J = \Delta u_j^{(k+1)}$ is beneficial. This procedure compromises n_{DOF} solutions of Equation (5.17). Hence, the

computational effort of sensitivity analysis can be significantly larger than for a single stage analysis. This is particularly true for large models with many degrees of freedom and $n_{\mathrm{DOF}} \approx n_s$. In such cases, neither the direct nor adjoint approach can significantly reduce the computational effort. In contrast to the calculation of the state derivative, the costs of the partial derivatives $\partial_{(\bullet)} \boldsymbol{J}^{(k+1)}$, $\partial_{(\bullet)} \boldsymbol{r}^{(k+1)}$, $\partial_{(\bullet)} \boldsymbol{u}_0^{(k+1)}$, $\partial_{(\bullet)} \boldsymbol{X}^{(k+1)}$, and $\partial_{(\bullet)} \boldsymbol{S}_0^{(k+1)}$ in the Equations (5.6) and (5.16) are comparatively low.

5.1.3 Example

To illustrate the derivations of the previous section, a two bar example is considered. The structure is also known as *von Mises* truss. The analysis model and the applied parameters are shown in Figure 5.2.

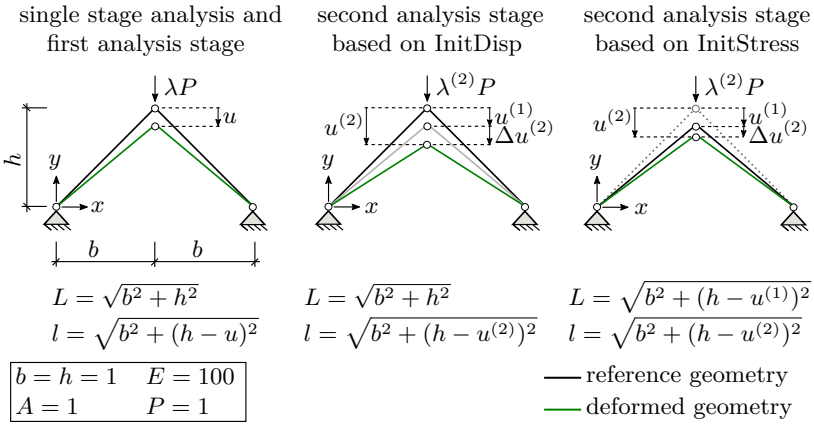

Figure 5.2: Considered von Mises truss with applied parameters (left). Deformations, reference and actual lengths of the second analysis stage are based on the InitDisp (middle) and InitStress (right) configuration update approach.

Philipp [118] utilized the example to demonstrate the restart of the structural analysis by the InitDisp and InitStress approach. Based on the derivations of Philipp [118], the example is subsequently supplemented with sensitivity analysis. The system can be analyzed with a single degree of freedom. This property is advantageous for the derivations since the equations remain clear and can be written analytically.
The residual equation of the von Mises truss with respect to the degree of freedom u reads

$$r = \frac{EA}{L^3}\left(u^3 - 3u^2 h + 2uh^2\right) - \lambda P \tag{5.19}$$

with Young's modulus E, cross section A, and external load P which is controlled by load factor λ. Based on Equation (5.19), the tangential stiffness

matrix

$$K = \frac{\partial r}{\partial u} = \frac{EA}{L^3}\left(3u^2 - 6uh + 2h^2\right) \tag{5.20}$$

is obtained. Equivalent to Philipp [118], the first analysis stage is stopped and restarted at a load factor of $\lambda = 6.5$. After the restart with the InitDisp and InitStress approach, the second analysis stage is continued until $\lambda = 13.0$. The load-displacement graph is visualized in Figure 5.3. Additionally, Table 5.1 compares the total displacement u at the considered load stages based on the two configuration update approaches with the results of a single stage analysis. At the start of analysis stage 2 both update approaches yield the reference displacement of the single step analysis. If λ is increased further, it can be observed that u based on the InitStress approach increasingly deviates from the reference result of the single stage analysis. Hence, the mechanical non-exactness of the InitStress method becomes obvious. Refer to Philipp [118] for further discussion on that issue.

Table 5.1: Structural analysis results of the von Mises truss. The displacement u is computed based on a single stage analysis and a sequenced analysis consisting of two stages. Adapted from Philipp [118].

λ	u (single stage)	$u^{(2)}$ (InitDisp)	$u^{(2)}$ (InitStress)
6.5	0.10914	0.10914 ($\pm$0.0%)	0.10914 ($\pm$0.0%)
13.0	0.32566	0.32566 ($\pm$0.0%)	0.26077 ($-$19.9%)

The aim is to compute the sensitivities of the total deformation u with respect to Young's modulus E and external load P. In the case of a single analysis stage and of the first stage of the considered sequenced analysis, the sensitivities can be computed by

$$\frac{du}{ds} = \frac{du^{(1)}}{ds} = -\frac{1}{K} \cdot \frac{\partial r}{\partial s_i}. \tag{5.21}$$

After the start of the second analysis stage the sensitivity formulation depends on whether the InitDisp or InitStress approach is utilized.
In the case of InitDisp, the displacement $u^{(1)}$ is applied as initial deformation $u_0^{(2)} = u^{(1)}$. The respective residual equation can be directly obtained by substituting the total deformation $u^{(2)} = \Delta u^{(2)} + u^{(1)}$ (cf. Equation (5.2)) into Equation (5.19), which gives

$$r^{(2)} = \frac{EA}{L^3}\left(u^{(2)3} - 3u^{(2)2}h + 2u^{(2)}h^2\right) - \lambda P. \tag{5.22}$$

The derivative $d\Delta u^{(2)}/ds_i$ is computed in a first step. For this purpose, Equation (5.22) is applied in Equation (5.5), which leads to

$$\frac{d\Delta u^{(2)}}{ds_i} = -\frac{1}{K^{(2)}} \cdot \left[\frac{\partial r^{(2)}}{\partial s_i} + \frac{\partial r^{(2)}}{\partial u_0^{(2)}} \cdot \frac{\partial u_0^{(2)}}{\partial u^{(1)}} \cdot \frac{du^{(1)}}{ds_i}\right] \tag{5.23}$$

where $K^{(2)} = \partial r^{(2)}/\partial \Delta u^{(2)}$ is the tangential stiffness matrix. The sensitivity of the total displacement is computed based on Equation (5.18), which simplifies to

$$\frac{du^{(2)}}{ds_i} = -\frac{1}{K^{(2)}} \cdot \frac{\partial r^{(2)}}{\partial s_i} - \frac{du^{(1)}}{ds_i} + \frac{du^{(1)}}{ds_i} = -\frac{1}{K^{(2)}} \cdot \frac{\partial r^{(2)}}{\partial s_i} \tag{5.24}$$

if $\partial r^{(2)}/\partial u_0^{(2)} = K^{(2)}$ and $\partial u_0^{(2)}/\partial u^{(1)} = 1$ is applied in Equation (5.23). The result is equivalent to the sensitivity equation of a single step analysis (compare Equations (5.21) and (5.24)). This finding is in line with what has already been established with regard to Equation (5.9). Hence, the final sensitivities of the sequenced analysis with InitDisp configuration update are the same as for a single stage analysis, which can seen in Table 5.2. The complete sensitivity course for $\lambda \in [0.0,\ 13.0]$ is visualized in Figure 5.3.

Table 5.2: Sensitivities computed based on a single stage analysis and a sequenced analysis consisting of two stages.

	single stage analysis		two stage analysis (InitDisp)	
λ	du/dE	du/dP	$du^{(2)}/dE$	$du^{(2)}/dP$
6.5	-0.00133	0.133	-0.00133 ($\pm$0.0%)	0.133 ($\pm$0.0%)
13.0	-0.0101	1.010	-0.0101 ($\pm$0.0%)	1.010 ($\pm$0.0%)

In the case of a restart with the InitStress approach, the reference length of the trusses is updated. The new reference length can be calculated by

$$L^{(2)} = l^{(1)} = \sqrt{b^2 + \left(h - u^{(1)}\right)^2} \tag{5.25}$$

where $l^{(1)}$ denotes the actual length resulting from analysis stage 1 at $\lambda = 6.5$. Additionally, prestress is applied to the members, which is obtained by

$$\sigma^{(2)}_{\mathrm{PK2},0} = E \cdot \epsilon_{\mathrm{GL}}\left(u^{(1)}\right) \cdot \frac{l^{(1)}}{L^{(1)}} \quad \text{with} \quad \epsilon_{\mathrm{GL}}\left(u^{(1)}\right) = \frac{1}{2}\frac{l^{(1)2} - L^{(1)2}}{L^{(1)2}} \tag{5.26}$$

based on the Saint Venant-Kirchhoff material law. Please note, the multiplier $l^{(1)}/L^{(1)}$ in Equation (5.26) is required to transform the PK2-stresses to the updated reference configuration. On that basis, the residual equation can be formulated:

$$\begin{aligned} r^{(2)} = {} & \frac{EA}{L^{(2)3}}\left(\Delta u^{(2)3} - 3\Delta u^{(2)2}\left(h - u^{(1)}\right) + 2\Delta u^{(2)}\left(h - u^{(1)}\right)^2\right) \\ & + 2A\sigma^{(2)}_{\mathrm{PK2},0}\frac{\Delta u^{(2)} + u^{(1)} - h}{L^{(2)}} - \lambda P \end{aligned} \tag{5.27}$$

The sensitivity of the total displacement (cf. Equation (5.18)) requires the derivative $d\Delta u^{(2)}/ds_i$. For this purpose, Equation (5.27) is applied in Equa-

tion (5.15), which leads to

$$\frac{d\Delta u^{(2)}}{ds_i} = -\frac{1}{K^{(2)}} \left[\frac{\partial r^{(2)}}{\partial s_i} + 2 \cdot \frac{\partial r^{(2)}}{\partial L^{(2)}} \cdot \frac{\partial L^{(2)}}{\partial u^{(1)}} \cdot \frac{du^{(1)}}{ds_i} \right. \tag{5.28a}$$

$$\left. + 2 \cdot \frac{\partial r^{(2)}}{\partial \sigma^{(2)}_{\mathrm{PK2},0}} \cdot \frac{\partial \sigma^{(2)}_{\mathrm{PK2},0}}{\partial u^{(1)}} \cdot \frac{du^{(1)}}{ds_i} + 2 \cdot \frac{\partial r^{(2)}}{\partial \sigma^{(2)}_{\mathrm{PK2},0}} \cdot \frac{\partial \sigma^{(2)}_{\mathrm{PK2},0}}{\partial s_i} \right] \tag{5.28b}$$

where $K^{(2)} = \partial r^{(2)} / \partial \Delta u^{(2)}$ is the tangential stiffness matrix. Please note, the second part of Equation (5.28b) vanishes for parameter P. Table 5.3 summarizes the sensitivities at the start and end of analysis stage 2. At $\lambda = 6.5$, the sensitivities coincide with the reference results of the single stage sensitivity analysis since $d\Delta u^{(2)}/ds_i$ vanishes. If λ is increased further, it can be observed that $du^{(2)}/ds_i$ based on the InitStress approach increasingly deviates from the reference result of the single stage analysis (cf. sensitivity course plotted in Figure 5.3). A maximal relative deviation of -55.3% at $\lambda = 13.0$ can be identified. Hence, the relative deviations of the sensitivities are significantly higher as compared to the displacements (cf. Table 5.1).

Table 5.3: Sensitivities computed based on a single stage analysis and a sequenced analysis consisting of two stages.

	single stage analysis		two stage analysis (InitStress)	
λ	du/dE	du/dP	$du^{(2)}/dE$	$du^{(2)}/dP$
6.5	-0.00133	0.133	-0.00133 ($\pm$0.0%)	0.133 ($\pm$0.0%)
13.0	-0.0101	1.010	-0.00451 ($-$55.3%)	0.451 ($-$55.3%)

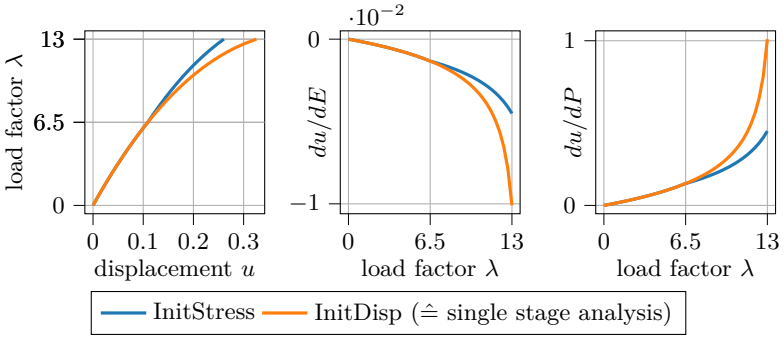

Figure 5.3: Load-displacement graph of the von Mises truss (left). Respective sensitivity courses of displacement u with respect to Young's modulus E and load P (middle and right). The analysis is restarted at $\lambda = 6.5$.

5.2 Construction stage analysis

Increasing computational power, advanced software packages, and approaches as *building information modeling* (BIM) boost the usage of *total building models* in structural analysis. These cover the load-bearing structure of an entire building. Total building models are generated with the nominal geometry of all components and it is assumed that the load (in particular, the dead load) only acts on the completed structure. These modeling assumptions do not correspond to reality. Deformations due to dead weight occur during construction, which are partially compensated for by the ongoing building process. For example, columns might be built "too long" to compensate for deformations in the earlier stages. The issue is illustrated in Figure 5.4, which shows an abstract two-stage construction process. After completing the first stage, the column is compressed by w_1 according to the dead load g_1. To meet the support at $y = 2h$ with a horizontal linear slab, the column of the second stage is erected on the deformed members of the first stage with a length of $h + w_1$. The non-consideration of such circumstances that occur during construction can lead to misjudgments of the structural behavior or even be relevant to structural safety, as reported by Fastabend et al. [55].

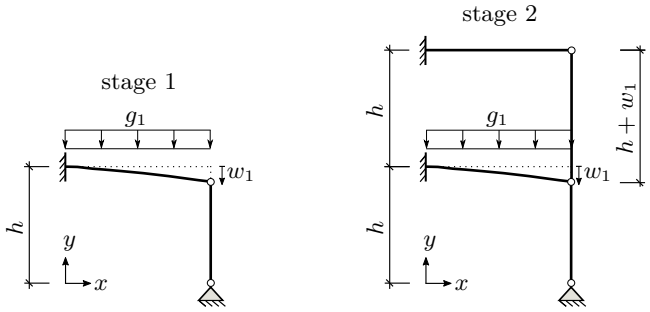

Figure 5.4: Two-stage construction sequence. The column built in the second stage is erected "too long" to compensate for the deformation of the first stage.

Construction stage analysis aims to overcome the deficits of total building models by modeling aspects such as (i) the consideration of deformations of previous construction stages, (ii) their partial compensation through the progressive construction process, (iii) change of boundary conditions, or (iv) time-dependent material behavior such as creep or shrinkage. From a computational point of view, construction stage analysis is a sequenced simulation process. After each stage, the deformed model is modified with regard to the progress of the construction.

In the literature, construction stage analysis is rarely considered, although the topic has been discussed since the 1980s, see, e.g., Choi et al. [37]. Comparative studies of different modeling approaches, including total building and construction stage models, are carried out by Kurc et al. [98], Laggner

et al. [99], and Sobek et al. [131] based on abstracted and real-world multi-story buildings. The investigations consistently show significant differences in responses, such as support forces or stress resultants, depending on the modeling approach. The references mentioned above focus on concrete structures. Research on construction stage analysis for lightweight structures can be found in Philipp [118] or Bauer [13].

There are several possibilities to model the construction stage process, i.e, the transition from one construction stage to the next. Refer to Philipp [118] for a brief introduction of different approaches and to Löwenstein [104, 105] regarding their realization in a commercial software package. In this thesis, the focus is on the method of *compensation of deformations*, where new members, whose geometry has been modified based on the deformations of previous phases, are added to a deformed and stressed structure. The investigations do not consider time-dependent effects such as creep or shrinkage. Section 5.2.1 starts with basic derivations using the modeling approaches introduced in Section 5.1.1. The aim is to investigate the fundamental challenges for sensitivity analysis. In Section 5.2.2, the focus is on the systematic realization of construction stage analysis and the corresponding sensitivity computation based on established modeling techniques in finite element codes.

5.2.1 Construction stage analysis on a fundamental basis

5.2.1.1 Modeling approach

A modified reference geometry of the new members considers the deformations of previous construction stages. The issue is illustrated in Figure 5.5. A new truss member is added at the beginning of stage $k+1$ at the actual position $\boldsymbol{x}_A^{(k)}$ of point A. The reference position of point A related to the new member is $\boldsymbol{X}_{A,\text{new}} = \boldsymbol{x}_A^{(k)}$.

In the case of the InitDisp approach, it has to be noted that attached "old" and "new" members become topologically separated. The issue becomes visible in Figure 5.5 (left). Different reference positions of point A on the existing structural domain $\boldsymbol{X}_{A,\text{init}}$ and at the connection point of the new truss member $\boldsymbol{X}_{A,\text{new}}$ can be observed. Additional nodes must be introduced to realize that particularity in a finite element model. The connection nodes are doubled to link the "old" and "new" members, whereby the new node's reference position is modified following the previous deformations. The "old" members keep their nodes at which the initial displacements are applied to account for the deformations of the previous analysis stages. The double nodes are coupled by assigning the same degree of freedom to both.

These additional modeling aspects are not necessary in the case of InitStress. There the reference geometry of "old" and "new" members is modified simultaneously and the topology is not separated. This becomes visible in Figure 5.5 (right), where the reference position of node A of the existing structural domain and the new truss member coincides. Refer to Dieringer et al. [48] and Philipp [118] for detailed discussions on this modeling issue. Furthermore, the problem is treated in the example in Section 5.2.1.3.

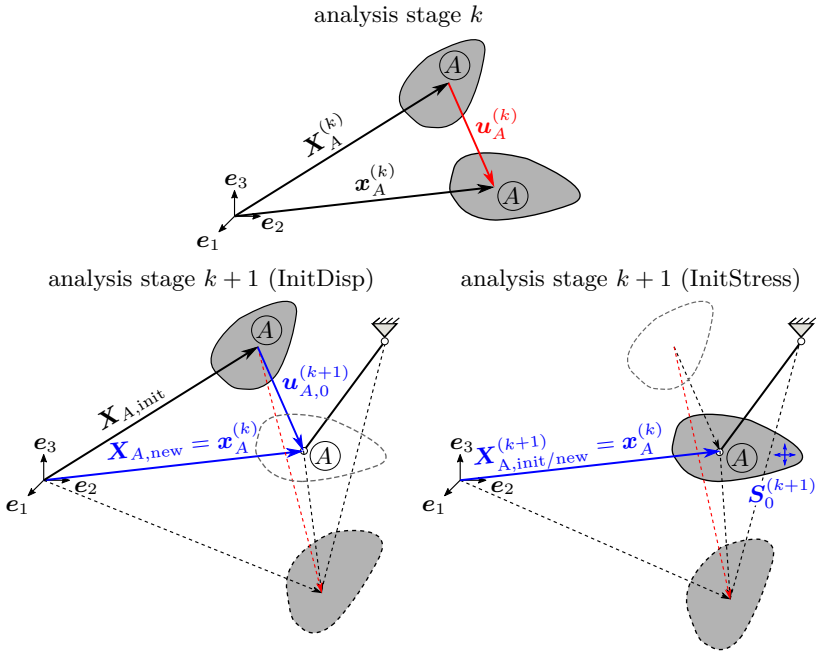

Figure 5.5: Modeling schemes for two subsequent analysis stages. At the beginning of stage $k+1$, a new truss member is added at the actual position of point A. The initialization quantities for the analysis restart are in blue.

5.2.1.2 Extension of sensitivity analysis

Section 5.1.2 discusses the necessary adaptions of sensitivity analysis for sequenced simulation processes based on two analysis restart approaches. Subsequently, the derivations are extended for construction stage analysis. It is assumed that new components are added at stage $k+1$ but not in other stages in order to keep the derivations clear. The aim is to determine sensitivities at stage $k+l$ with $l \geq 1$. It is expected that the deformations $\boldsymbol{u}^{(1)}(s_i)$ to $\boldsymbol{u}^{(k+l)}(s_i)$ and the state derivatives $d\boldsymbol{u}^{(1)}/ds_i$ to $d\boldsymbol{u}^{(k+l-1)}/ds_i$ are pre-computed.

Extension of sensitivity analysis for InitDisp

New members with the reference geometry $\boldsymbol{X}_{(k+1)}\left(\boldsymbol{u}^{(k)}(s_i)\right)$ depending on the previous deformations are added. It should be noted that the stage at which the members are added and their reference geometry is defined can be seen by a subscript. The superscript, which indicates the current observed stage, is not required in the case of InitDisp because the reference geometry

is not further modified in subsequent stages, i.e., $\boldsymbol{X}_{(k+1)} = \boldsymbol{X}_{(k+1)}^{(k+1)} = \boldsymbol{X}_{(k+1)}^{(k+l)}$ with $l \geq 1$. When new members are introduced, the number of degrees of freedom generally increases. Thus, the vector of total displacements given by Equation (5.1) must be expanded to

$$\boldsymbol{u}^{(k+l)} = \boldsymbol{x}^{(k+l)} - \begin{bmatrix} \boldsymbol{X}_{\text{init}} \\ \boldsymbol{X}_{(k+1)} \end{bmatrix} \tag{5.29}$$

where $\boldsymbol{X}_{\text{init}}$ denotes the reference geometry of the initially existing structural domain. Note that the initial displacements which are applied by the InitDisp approach are $\boldsymbol{u}_0^{(k+l)} = \boldsymbol{u}^{(k+l-1)}$ based on the total displacements defined by Equation (5.29).
For sensitivity analysis, it has to be additionally considered that the reference geometry $\boldsymbol{X}_{(k+1)}$ of the added members at stage $k+1$ depends on the deformation of the previous construction stages. Therefore, the response and equilibrium condition

$$J^{(k+l)}\left(s_i, \Delta\boldsymbol{u}^{(k+l)}(s_i), \boldsymbol{u}_0^{(k+l)}\left(\boldsymbol{u}^{(k+l-1)}(s_i)\right), \boldsymbol{X}_{(k+1)}\left(\boldsymbol{u}^{(k)}(s_i)\right)\right) \tag{5.30a}$$

$$\boldsymbol{r}^{(k+l)}\left(s_i, \Delta\boldsymbol{u}^{(k+l)}(s_i), \boldsymbol{u}_0^{(k+l)}\left(\boldsymbol{u}^{(k+l-1)}(s_i)\right), \boldsymbol{X}_{(k+1)}\left(\boldsymbol{u}^{(k)}(s_i)\right)\right) = \boldsymbol{0} \tag{5.30b}$$

are utilized. The formulations in Equation (5.30) are extensions of those in Equation (5.3). Hence, the derivation of the sensitivity equations is almost the same as presented in Section 5.1.2. The only difference is the dependency on $\boldsymbol{X}_{(k+1)}\left(\boldsymbol{u}^{(k)}(s_i)\right)$. Based on Equation (5.30), the sensitivity equation

$$\begin{aligned} \frac{dJ^{(k+l)}}{ds_i} =& \frac{\partial J^{(k+l)}}{\partial s_i} + \frac{\partial J^{(k+l)}}{\partial \boldsymbol{u}_0^{(k+l)}} \frac{\partial \boldsymbol{u}_0^{(k+l)}}{\partial \boldsymbol{u}^{(k+l-1)}} \frac{d\boldsymbol{u}^{(k+l-1)}}{ds_i} \\ &+ \frac{\partial J^{(k+l)}}{\partial \boldsymbol{X}_{(k+1)}} \frac{\partial \boldsymbol{X}_{(k+1)}}{\partial \boldsymbol{u}^{(k)}} \frac{d\boldsymbol{u}^{(k)}}{ds_i} \\ &+ \frac{\partial J^{(k+l)}}{\partial \Delta\boldsymbol{u}^{(k+l)}} \left[\frac{\partial \boldsymbol{r}^{(k+l)}}{\partial \Delta\boldsymbol{u}^{(k+l)}}\right]^{-1} \boldsymbol{F}^{*(k+l)} \end{aligned} \tag{5.31}$$

and the state derivative

$$\begin{aligned} \frac{d\Delta\boldsymbol{u}^{(k+l)}}{ds_i} =& \left[\frac{\partial \boldsymbol{r}^{(k+l)}}{\partial \Delta\boldsymbol{u}^{(k+l)}}\right]^{-1} \boldsymbol{F}^{*(k+l)} \quad \text{with} \\ \boldsymbol{F}^{*(k+l)} =& -\frac{\partial \boldsymbol{r}^{(k+l)}}{\partial s_i} - \frac{\partial \boldsymbol{r}^{(k+l)}}{\partial \boldsymbol{u}_0^{(k+l)}} \frac{\partial \boldsymbol{u}_0^{(k+l)}}{\partial \boldsymbol{u}^{(k+l-1)}} \frac{d\boldsymbol{u}^{(k+l-1)}}{ds_i} \\ &- \frac{\partial \boldsymbol{r}^{(k+l)}}{\partial \boldsymbol{X}_{(k+1)}} \frac{\partial \boldsymbol{X}_{(k+1)}}{\partial \boldsymbol{u}^{(k)}} \frac{d\boldsymbol{u}^{(k)}}{ds_i} \end{aligned} \tag{5.32}$$

are received. In contrast to the sensitivity equations of a pure restart analysis (cf. Equations (5.5) and (5.6)), not only the state derivative of the previous stage $k+l-1$ is required. Rather, the state derivative of stage k, i.e., the stage before adding the new members, is also needed.

REMARK I: Double nodes are introduced to realize the topologically separated reference geometry of "old" and "new" members in a finite element model. The nodes are coupled because they are assigned the same degrees of freedom. However, the applied initial displacements differ since the two nodes relate to different reference configurations. This particularity has to be properly considered in sensitivity analysis. For illustration, refer to Figure 5.6, which shows the initialization of node A for stage $k+l$. The terms

$$\frac{\partial(\bullet)^{(k+l)}}{\partial \boldsymbol{u}_{A,0,\mathrm{init}}^{(k+l)}} \frac{\partial \boldsymbol{u}_{A,0,\mathrm{init}}^{(k+l)}}{\partial \boldsymbol{u}_{A,\mathrm{init}}^{(k+l-1)}} \frac{d\boldsymbol{u}_{A,\mathrm{init}}^{(k+l-1)}}{ds_i}, \quad \frac{\partial(\bullet)^{(k+l)}}{\partial \boldsymbol{u}_{A,0,\mathrm{new}}^{(k+l)}} \frac{\partial \boldsymbol{u}_{A,0,\mathrm{new}}^{(k+l)}}{\partial \boldsymbol{u}_{A,\mathrm{new}}^{(k+l-1)}} \frac{d\boldsymbol{u}_{A,\mathrm{new}}^{(k+l-1)}}{ds_i}$$

as part of the partial derivative regarding the response ($\bullet \hat{=} J$) and the pseudo-load ($\bullet \hat{=} \boldsymbol{r}$) are required to consider the dependency on s_i concerning the initial displacements of double node A.

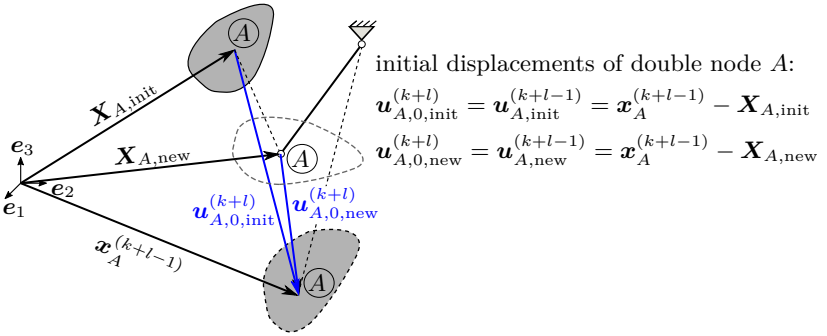

Figure 5.6: Initialization of the double node A for stage $k+l$ by initial displacements (blue).

Extension of sensitivity analysis for InitStress

New members with the reference geometry $\boldsymbol{X}_{(k+1)}^{(k+1)}\left(\boldsymbol{u}^k(s_i)\right)$ depending on the deformation of the previous stage are introduced at stage $k+1$. In contrast to the notation for the InitDisp approach, a superscript is required to indicate the currently observed stage. The total displacement of the degrees of freedom associated with the new members is defined in relation to the reference geometry at stage $k+1$. The vector of total displacements reads

$$\boldsymbol{u}^{(k+l)} = \boldsymbol{x}^{(k+l)} - \begin{bmatrix} \boldsymbol{X}_{\mathrm{init}}^{(1)} \\ \boldsymbol{X}_{(k+1)}^{(k+1)} \end{bmatrix} \tag{5.33}$$

where $\boldsymbol{X}_{\text{init}}^{(1)}$ denotes the reference geometry of the initially existing structural domain at stage 1. Accordingly, the modified reference geometry for the restart of stage $k+l$ can be determined by:

$$\boldsymbol{X}^{(k+l)}\left(\boldsymbol{u}^{(k+l-1)}(s_i), \boldsymbol{X}_{(k+1)}^{(k+1)}\left(\boldsymbol{u}^{k}(s_i)\right)\right) = \boldsymbol{u}^{(k+l-1)} + \begin{bmatrix} \boldsymbol{X}_{\text{init}}^{(1)} \\ \boldsymbol{X}_{(k+1)}^{(k+1)} \end{bmatrix} \tag{5.34}$$

The initial stresses

$$\begin{aligned} &\boldsymbol{S}_0^{(k+2)}\left(s_i, \boldsymbol{u}^{(k)}, \boldsymbol{u}^{(k+1)}\right) \\ &\vdots \\ &\boldsymbol{S}_0^{(k+l)}\left(s_i, \boldsymbol{u}^{(k+l-2)}, \boldsymbol{u}^{(k+l-1)}, \boldsymbol{S}_0^{(k+l-1)}\left(\cdots\right)\right) \end{aligned} \tag{5.35}$$

applied to the new members from stage $k+2$ show equivalent dependencies as in Equation (5.11). Accordingly, the sensitivities $d\boldsymbol{S}_0^{(j)}/ds_i$ can be computed in analogy to Equation (5.12). The response and equilibrium condition

$$J^{(k+l)}\left(s_i, \Delta\boldsymbol{u}^{(k+l)}(s_i), \boldsymbol{X}^{(k+l)}\left(\bigstar\right), \boldsymbol{S}_0^{(k+l)}\left(\bullet\right)\right) \tag{5.36a}$$

$$\boldsymbol{r}^{(k+l)}\left(s_i, \Delta\boldsymbol{u}^{(k+l)}(s_i), \boldsymbol{X}^{(k+l)}\left(\bigstar\right), \boldsymbol{S}_0^{(k+l)}\left(\bullet\right)\right) = \boldsymbol{0} \tag{5.36b}$$

are principally the same as for the pure restart analysis in Equation (5.13). Nevertheless, different dependencies must be taken into account. These are identified by symbols that refer to equations ($\bigstar$: Equation (5.34), $\bullet$: Equations (5.11) and (5.35)). Based on Equation (5.36), the sensitivity equation

$$\begin{aligned} \frac{dJ^{(k+l)}}{ds_i} =& \frac{\partial J^{(k+l)}}{\partial s_i} + \frac{\partial J^{(k+l)}}{\partial \boldsymbol{X}^{(k+l)}} \frac{\partial \boldsymbol{X}^{(k+l)}}{\partial \boldsymbol{u}^{(k+l-1)}} \frac{d\boldsymbol{u}^{(k+l-1)}}{ds_i} \\ &+ \frac{\partial J^{(k+l)}}{\partial \boldsymbol{X}^{(k+l)}} \frac{\partial \boldsymbol{X}^{(k+l)}}{\partial \boldsymbol{X}_{(k+1)}^{(k+1)}} \frac{\partial \boldsymbol{X}_{(k+1)}^{(k+1)}}{\partial \boldsymbol{u}^{(k)}} \frac{d\boldsymbol{u}^{(k)}}{ds_i} + \frac{\partial J^{(k+l)}}{\partial \boldsymbol{S}_0^{(k+l)}} \frac{d\boldsymbol{S}_0^{(k+l)}}{ds_i} \\ &+ \frac{\partial J^{(k+l)}}{\partial \Delta\boldsymbol{u}^{(k+l)}} \left[\frac{\partial \boldsymbol{r}^{(k+l)}}{\partial \Delta\boldsymbol{u}^{(k+l)}}\right]^{-1} \boldsymbol{F}^{*(k+l)} \end{aligned} \tag{5.37}$$

and the state derivative

$$\begin{aligned} \frac{d\Delta\boldsymbol{u}^{(k+l)}}{ds_i} =& \left[\frac{\partial \boldsymbol{r}^{(k+l)}}{\partial \Delta\boldsymbol{u}^{(k+l)}}\right]^{-1} \boldsymbol{F}^{*(k+l)} \quad \text{with} \\ \boldsymbol{F}^{*(k+l)} =& -\frac{\partial \boldsymbol{r}^{(k+l)}}{\partial s_i} - \frac{\partial \boldsymbol{r}^{(k+l)}}{\partial \boldsymbol{X}^{(k+l)}} \frac{\partial \boldsymbol{X}^{(k+l)}}{\partial \boldsymbol{u}^{(k+l-1)}} \frac{d\boldsymbol{u}^{(k+l-1)}}{ds_i} \\ &- \frac{\partial \boldsymbol{r}^{(k+l)}}{\partial \boldsymbol{X}^{(k+l)}} \frac{\partial \boldsymbol{X}^{(k+l)}}{\partial \boldsymbol{X}_{(k+1)}^{(k+1)}} \frac{\partial \boldsymbol{X}_{(k+1)}^{(k+1)}}{\partial \boldsymbol{u}^{(k)}} \frac{d\boldsymbol{u}^{(k)}}{ds_i} - \frac{\partial \boldsymbol{r}^{(k+l)}}{\partial \boldsymbol{S}_0^{(k+l)}} \frac{d\boldsymbol{S}_0^{(k+l)}}{ds_i} \end{aligned} \tag{5.38}$$

are received.

5.2.1.3 Example

The truss example shown in Figure 5.7 is considered. The first analysis stage is the same as discussed in Section 5.1.3, i.e., the von Mises two bar truss is stressed by an increasing load until $\lambda = 6.5$. Then, the analysis is stopped, and a third truss is added to the structure. Afterward, the second analysis stage is started by the InitDisp and InitStress approach and the load is further increased until $\lambda = 13.0$. The resulting displacements u are given in Table 5.4 and the load-displacement graph is visualized in Figure 5.9.

Table 5.4: Displacement u of a three bar truss. The third truss is added at $\lambda = 6.5$.

λ	$u^{(2)}$ (InitDisp)	$u^{(2)}$ (InitStress)
6.5	0.10914	0.10914 ($\pm$0.0%)
13.0	0.17955	0.17280 ($-$3.8%)

At $\lambda = 6.5$, a kink of the load-displacement graph can be observed due to the additional stiffness introduced by the added third truss. Furthermore, it can be identified that the system based on the InitStress restart behaves slightly stiffer than the mechanically accurate InitDisp model. Due to the third construction member, it is quite evident that the deformation that occurs during the second analysis stage is significantly smaller than in the case of the pure restart analysis in Section 5.1.3. Hence, the difference between the InitDisp and InitStress model is less pronounced. This observation aligns with the explanations of Dieringer et al. [48]. The authors argue that the two update approaches deliver comparable results if only small to moderate additional deformations occur after the analysis restart.

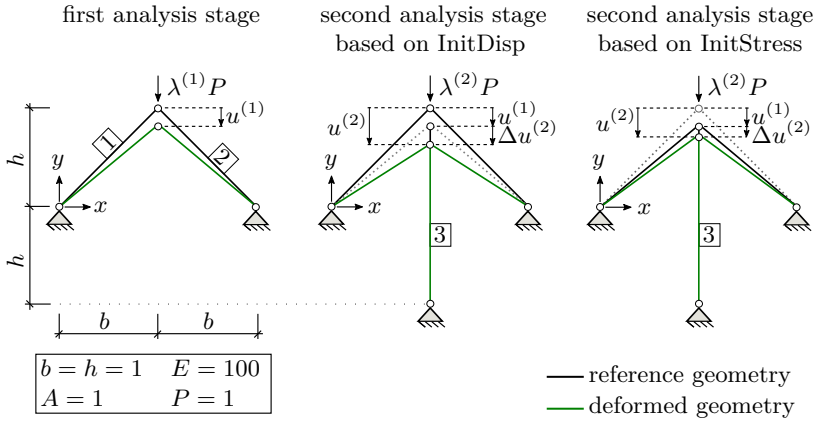

Figure 5.7: Considered two step construction sequence.

The reference length of the new member 3 (see labeling in Figure 5.7) is $L_3^{(2)} = 2 \cdot h - u^{(1)}$ to account for the deformation that occurred during the first construction stage. Since the reference geometry of the initial two trusses is not modified in the case of InitDisp, the third truss is topologically separated. The connection of the three trusses can be modeled by a double node as shown in Figure 5.8 (there the two nodes are denoted as A and B). These can be coupled by assigning the same degree of freedom $\Delta u^{(2)}$ to both. To consider the deformation of the two bar truss during the first analysis stage, an initial displacement of $u_0^{(2)} = u^{(1)}$ is assigned to node A. Once the initial displacement is applied, node A and B share again the same position. In the case of InitStress, the reference lengths $L_1^{(2)}$ and $L_2^{(2)}$ of the initial two bar truss are modified depending on $u^{(1)}$ according to Equation (5.25). Hence, a single node can realize the connection with the third truss.

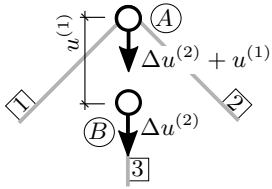

Figure 5.8: Double node to couple topologically separated trusses.

Equivalent to the von Mises truss example discussed in Section 5.1.3, the aim is to compute the sensitivities of the total deformation u. The considered parameters are the Young's modulus E of trusses 1 and 2 (see labeling in Figure 5.7) and the external load P. In the case of the first analysis stage, the sensitivities are determined by Equation (5.21). To compute the sensitivity of the total displacement of the second analysis stage according to Equation (5.18), the derivative $d\Delta u^{(2)}/ds_i$ is required. The computation of that sensitivity is very similar compared to the derivations in Section 5.1.2. However, in addition to Equations (5.23) and (5.28), the dependence of the reference length $L_3^{(2)}$ of the new member on $u^{(1)}$ (s_i) must also be taken into account.

The direct sensitivity expression reads

$$\frac{d\Delta u^{(2)}}{ds_i} = -\frac{1}{K^{(2)}} \cdot \left[\frac{\partial r^{(2)}}{\partial s_i} + \frac{\partial r^{(2)}}{\partial u_0^{(2)}} \cdot \frac{\partial u_0^{(2)}}{\partial u^{(1)}} \cdot \frac{du^{(1)}}{ds_i} + \frac{\partial r^{(2)}}{\partial L_3^{(2)}} \cdot \frac{\partial L_3^{(2)}}{\partial u^{(1)}} \cdot \frac{du^{(1)}}{ds_i} \right] \tag{5.39}$$

in the case of InitDisp, where the pseudo-load is based on Equation (5.32). If

InitStress is utilized as method for the restart of the analysis, the expression

$$\frac{d\Delta u^{(2)}}{ds_i} = -\frac{1}{K^{(2)}} \left[\frac{\partial r^{(2)}}{\partial s_i} + 2 \cdot \frac{\partial r^{(2)}}{\partial \sigma^{(2)}_{\mathrm{PK2},0}} \cdot \frac{\partial \sigma^{(2)}_{\mathrm{PK2},0}}{\partial u^{(1)}} \cdot \frac{du^{(1)}}{ds_i} + 2 \cdot \frac{\partial r^{(2)}}{\partial \sigma^{(2)}_{\mathrm{PK2},0}} \cdot \frac{\partial \sigma^{(2)}_{\mathrm{PK2},0}}{\partial s_i} + \sum_{j=1}^{3} \frac{\partial r^{(2)}}{\partial L^{(2)}_j} \cdot \frac{\partial L^{(2)}_j}{\partial u^{(1)}} \cdot \frac{du^{(1)}}{ds_i} \right] \tag{5.40}$$

is received where the pseudo-load is according to Equation (5.38). Table 5.5 summarizes the sensitivities at the start and end of analysis stage 2. At $\lambda = 6.5$, the sensitivities of the InitDisp and InitStress models coincide since $d\Delta u^{(2)}/ds_i$ vanishes. If λ is increased further, it can be observed that $du^{(2)}/ds_i$ based on the InitStress approach increasingly deviates from the reference result of the InitDisp model. However, the difference in the sensitivities based on the two models is less significant as in the case of the pure restart analysis of the von Mises truss discussed in Section 5.1.3. This becomes also obvious if the sensitivity courses plotted in Figure 5.9 are compared with those shown in Figure 5.3.

Table 5.5: Sensitivities computed based on a sequenced analysis consisting of two stages.

	restart by InitDisp		restart by InitStress	
λ	$du^{(2)}/dE$	$du^{(2)}/dP$	$du^{(2)}/dE$	$du^{(2)}/dP$
6.5	-0.00133	0.133	-0.00133 (±0.0%)	0.133 (±0.0%)
13.0	-0.00187	0.229	-0.00177 (−5.3%)	0.211 (−7.9%)

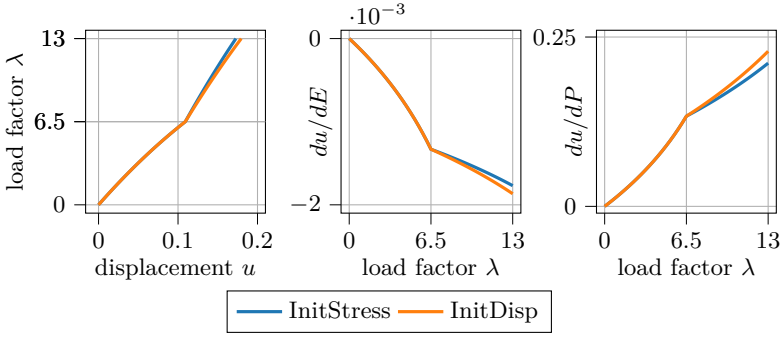

Figure 5.9: Load-displacement graph of two step construction sequence (left). Respective sensitivity courses of displacement u with respect to Young's modulus E and load P (middle and right). The second analysis stage starts at $\lambda = 6.5$.

5.2.2 Construction stage analysis with multi-freedom constraints

Section 5.2.1 discusses the fundamental challenges if sensitivities shall be computed based on construction stage models. For this purpose, (i) geometric non-linearity, (ii) a continuum mechanically motivated configuration update method for the analysis restart, and (iii) the change of the reference geometry of added members are considered. However, in many practical situations, linear structural analysis is sufficient. A systematic modeling procedure based on non-homogeneous multi-freedom constraints is described below for such cases. Furthermore, the required extensions to sensitivity analysis are discussed. Parts of this section have been directly taken from the pre-published conference paper Fußeder et al. [61] and can thus be understood as quotations.

5.2.2.1 Modeling approach

The described modeling procedure can be seen as a realization of the InitDisp-approach (cf. Section 5.1.1) by established FEM-modeling techniques. Non-homogeneous multi-freedom constraints along with the master-slave method (cf., e.g., Felippa [56]) are used. Therefore, the finite element nodes, which connect construction stage k with stage *k+1*, are realized as double nodes. These share the same geometric position but are linked to different elements. Multi-freedom constraints connect the degrees of freedom (DOFs) of the double nodes. Here, the node linked to the elements of construction stage k is chosen as master and the corresponding double node as slave. Non-homogeneous constraints are introduced to consider the deformation of construction stage k when coupling with the undeformed stage *k+1*. The coupling procedure is visualized in Figure 5.10. In the example shown, the non-homogeneous constraint is:

$$u_{\text{master},\,k+1} - u_{\text{slave},\,k+1} = u_k \tag{5.41}$$

Hence, a gap of u_k (displacement in stage k) is introduced between the master and slave DOF to account for the compensation of deformations. The applied non-homogeneity can be interpreted as pre-deformation of the master degree of freedom corresponding to the InitDisp modeling approach. However, compared to the fundamental derivations in Section 5.2.1.2, no dimension changes of the construction members added at stage $k+1$ are considered. Instead, all elements retain their originally modeled geometry throughout the entire construction stage analysis. Since no decisions need to be made on how to modify the finite element mesh based on the deformations of the previous stages, the concept is easy to implement. After the analysis of a construction stage, only the inhomogeneities of the multi-freedom constraints need to be initialized based on the determined deformations. A modeling shortfall is introduced as the method neglects stiffness changes of members whose dimensions are changed during construction to account for deformation compensation. However, since the derivations in this section are limited to linear structural analysis, in which small deformations are assumed, the non-consideration of dimensional changes can be justified. This argumentation

can be supported by Bischoff et al. [22], in which geometric deviations are rated as relatively marginal modeling errors in construction stage analysis.

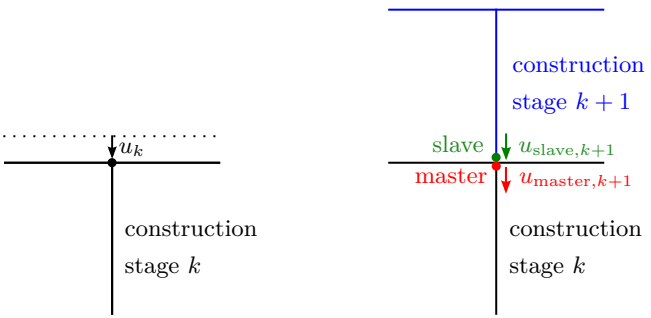

Figure 5.10: Coupling of the construction stages k and $k+1$ by a double node whose DOFs are connected by the master-slave-method. Adapted from Fußeder et al. [61].

Multiple non-homogeneous multi-freedom constraints can be systematically considered by

$$\boldsymbol{u} = \boldsymbol{T}\breve{\boldsymbol{u}} + \boldsymbol{g} \tag{5.42}$$

where $\boldsymbol{u}$ contains all degrees of freedom and $\breve{\boldsymbol{u}}$ is generated by removing all slave DOFs from $\boldsymbol{u}$. The latter is realized by a transformation matrix $\boldsymbol{T}$. The vector $\boldsymbol{g}$ contains the deformations of the master DOFs in previous construction stages. The displacements $\breve{\boldsymbol{u}}$ are determined as the solution of the linear state equation

$$\breve{\boldsymbol{r}}(\breve{\boldsymbol{u}}) = \breve{\boldsymbol{K}}\breve{\boldsymbol{u}} - \breve{\boldsymbol{F}} = \boldsymbol{0} \tag{5.43}$$

with the transformed stiffness matrix

$$\breve{\boldsymbol{K}} = \boldsymbol{T}^T\boldsymbol{K}\boldsymbol{T} \tag{5.44}$$

and transformed load vector

$$\breve{\boldsymbol{F}} = \boldsymbol{T}^T\left(\boldsymbol{F} - \boldsymbol{K}\boldsymbol{g}\right). \tag{5.45}$$

5.2.2.2 Extension of sensitivity analysis

To enable sensitivity analysis for application on models that consider the construction stage modeling as described in Section 5.2.2.1, the response formulation in Equation (3.5) must be extended for the state vector $\boldsymbol{u}$ as given in Equation (5.42). The reason is that the entries of $\boldsymbol{g}$ can also depend on the input parameters $\boldsymbol{s}$, which must be considered in sensitivity analysis. The adapted response is:

$$J(\boldsymbol{s}, \underbrace{\boldsymbol{T}\breve{\boldsymbol{u}}(\boldsymbol{s}) + \boldsymbol{g}(\boldsymbol{s})}_{\boldsymbol{u}(\boldsymbol{s})}) \tag{5.46}$$

To compute the derivative of Equation (5.46) with respect to parameter $s_i \in \boldsymbol{s}$ the chain rule of differentiation has to be utilized:

$$\frac{dJ}{ds_i} = \frac{\partial J}{\partial s_i} + \left[\frac{\partial J}{\partial \boldsymbol{u}}\right]^T \boldsymbol{T}\frac{d\breve{\boldsymbol{u}}}{ds_i} + \left[\frac{\partial J}{\partial \boldsymbol{u}}\right]^T \frac{d\boldsymbol{g}}{ds_i} \tag{5.47}$$

The derivative of the state variables $\breve{\boldsymbol{u}}$ with respect to s_i is determined by applying Equation (5.43) to Equation (3.8)

$$\frac{d\breve{\boldsymbol{u}}}{ds_i} = \breve{\boldsymbol{K}}^{-1}\left[\frac{\partial \breve{\boldsymbol{F}}}{\partial s_i} - \frac{\partial \breve{\boldsymbol{K}}}{\partial s_i}\breve{\boldsymbol{u}}\right] \tag{5.48}$$

The state derivative can be reformulated in terms of Equations (5.44) and (5.45) as

$$\frac{d\breve{\boldsymbol{u}}}{ds_i} = \breve{\boldsymbol{K}}^{-1}\boldsymbol{T}^T \underbrace{\left[\frac{\partial \boldsymbol{F}}{\partial s_i} - \frac{\partial \boldsymbol{K}}{\partial s_i}\boldsymbol{u} - \boldsymbol{K}\frac{d\boldsymbol{g}}{ds_i}\right]}_{\boldsymbol{F}^*} \tag{5.49}$$

where the bracket term can be considered as extended pseudo-load $\boldsymbol{F}^*$. The insertion of Equation (5.49) into (5.47) leads to

$$\frac{dJ}{ds_i} = \frac{\partial J}{\partial s_i} + \left[\frac{\partial J}{\partial \boldsymbol{u}}\right]^T \boldsymbol{T}\breve{\boldsymbol{K}}^{-1}\boldsymbol{T}^T\boldsymbol{F}^* + \left[\frac{\partial J}{\partial \boldsymbol{u}}\right]^T \frac{d\boldsymbol{g}}{ds_i} \tag{5.50}$$

as sensitivity equation. A direct sensitivity analysis is executed if the state derivative given by Equation (5.49) is first solved and then inserted into Equation (5.47). An adjoint formulation of Equation (5.50) can be achieved by introducing the adjoint variable $\breve{\boldsymbol{\eta}}$ as the solution of the following linear system of equations (the reduced stiffness $\breve{\boldsymbol{K}}$ is symmetric, i.e., $\breve{\boldsymbol{K}} = \breve{\boldsymbol{K}}^T$):

$$\breve{\boldsymbol{\eta}}^T = \left[\frac{\partial J}{\partial \boldsymbol{u}}\right]^T \boldsymbol{T}\breve{\boldsymbol{K}}^{-1} \Leftrightarrow \breve{\boldsymbol{K}}\breve{\boldsymbol{\eta}} = \boldsymbol{T}^T\frac{\partial J}{\partial \boldsymbol{u}} \tag{5.51}$$

According to Equation (5.51), the adjoint variable $\breve{\boldsymbol{\eta}}$ can be identified as the nodal displacements (with missing slave DOFs) due to the adjoint load $\boldsymbol{T}^T\partial J/\partial \boldsymbol{u}$. The comparison of the right-hand side of Equation (5.51) with the reduced load vector in Equation (5.45) shows that $\breve{\boldsymbol{\eta}}$ is solved with homogeneous multi-freedom constraints, i.e., $\boldsymbol{g} = \boldsymbol{0}$. Hence, the adjoint variables are independent of the construction process. The adjoint displacement vector containing all DOFs (also the slave freedoms) can be determined by adaption of the transformation rule according to Equation (5.42):

$$\boldsymbol{\eta} = \boldsymbol{T}\breve{\boldsymbol{\eta}} \tag{5.52}$$

After inserting Equations (5.51) and (5.52) in Equation (5.50) the final adjoint sensitivity term is achieved:

$$\frac{dJ}{ds_i} = \frac{\partial J}{\partial s_i} + \boldsymbol{\eta}^T\left[\frac{\partial \boldsymbol{F}}{\partial s_i} - \frac{\partial \boldsymbol{K}}{\partial s_i}\boldsymbol{u} - \boldsymbol{K}\frac{d\boldsymbol{g}}{ds_i}\right] + \left[\frac{\partial J}{\partial \boldsymbol{u}}\right]^T \frac{d\boldsymbol{g}}{ds_i} \tag{5.53}$$

When comparing the classical adjoint sensitivity analysis (cf. Equation (3.15)) with the extended approach for construction stage analysis (Equation (5.53)), it can be observed that the only differences are the terms including the derivative $d\boldsymbol{g}/ds_i$. The vector $d\boldsymbol{g}/ds_i$ contains the sensitivities of the displacements of the master DOFs of previous construction stages. Direct or adjoint sensitivity analysis can be beneficial to compute $d\boldsymbol{g}/ds_i$. The choice depends on whether the number of master DOFs or the number of parameters s_i is dominant. In the latter case, an adjoint sensitivity analysis according to Equation (5.53) with the displacement of each of the master DOFs as response J is to be preferred. However, the sensitivity analyses of these additional responses involve solving the adjoint problem given by Equation (5.51). In the other case, the state derivative provided by Equation (5.49), which contains the derivatives of all master DOFs with respect to s_i, is directly solved. Regardless of whether direct or adjoint computations are utilized to solve $d\boldsymbol{g}/ds_i$, the computational effort of sensitivity analysis for construction stage models can be significantly larger than for the corresponding holistic models. This is particularly the case for problems with a high number of coupling nodes and a simultaneously high number of parameters, where neither the direct nor the adjoint approach can significantly reduce the computational effort.

5.2.2.3 Example: Idealized eight-story building

The idealized eight-story building shown in Figure 5.11 is considered. The example is intended to investigate the differences in sensitivities based on a total building model and a construction stage model. The structure under consideration is taken from an example presented by Bischoff et al. [21]. Refer also to Fußeder et al. [62], where the example demonstrates how sensitivity analyses regarding load parameters can assess the load redistribution after removing a temporary auxiliary truss.

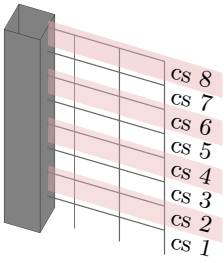

Figure 5.11: Structure to be built in eight construction stages (cs).

Rigid connections between the slabs and the core are modeled. Moment hinges link slabs and columns. It is considered that the rigid core is already erected. The frame structure is subsequently built in eight construction phases. This means that three columns and one slab are erected in each step. The

coupling of the construction stages is modeled as described in Section 5.2.2.1. Figure 5.12 compares the bending moment and normal force distribution due to the dead weight of the total building and the construction stage model. The following differences can be observed:

- The total building model shows a considerably higher maximal clamping moment.
- The largest bending moment is located at different points in the structure (slab over 8th floor vs. slab over 4th floor).
- The construction stage model shows larger column normal forces in absolute values. This observation is a typical deficit of total building models. These generally underestimate the loading of weak vertical load-bearing elements (in this case, the columns compared to the stiff core) as Bischoff et al. [21] and Fastabend et al. [55] for instance report.

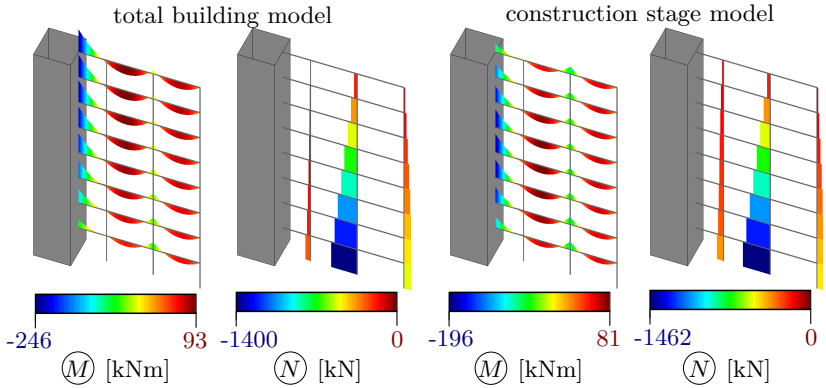

Figure 5.12: Moment M and normal force N due to dead load based on different models. Adapted from Fußeder et al. [61].

Sensitivity analyses are performed to improve the understanding of the composition of the decisive bending moments and to enhance the transparency of the different structural models. For this purpose, the clamping moments of the slab above the 4th floor (decisive moment of the construction stage model, called M_{CS4}) and above the 8th floor (decisive moment of the total building model, called M_{CS8}) are chosen as responses. The responses are labeled in Figure 5.13. Sensitivities are computed with respect to the slabs' dead load, where the dead load of each slab is considered as an individual parameter. The situation after all eight construction stages have been built is considered for the investigations. The sensitivities are computed with Equation (5.53) in the case of the construction stage model and with Equation (3.15) for the total building model. The sensitivity maps are shown in Figure 5.13. Please note that the load sensitivities are illustrated by a constant plot over the length of

the respective slab (see Section 6.1 for details concerning the visualization). Based on the maps, the following observations can be made:

- In the total building model, the dead load of all slabs influences the traced moments. This observation reveals a fundamental shortcoming of total building models in which the dead load of earlier stages (cs 1 - 3 in case of M_{CS4} resp. cs 1 - 7 in case of M_{CS8}) leads to deformations and stresses in later stages.
- In the construction stage model, only the dead load of the members, built in the same or a later construction stage as the slab in which the response is located, influences the respective response. For instance, only the dead load of the slab above the 8th floor has an influence on M_{CS8} (see Figure 5.13, right). The model error of the total building model mentioned above is resolved by coupling the stages with inhomogeneous multi-freedom constraints.
- The total building model underestimates the impact of the dead load of the slab over the 4th floor on M_{CS4} (-1.9 vs. -2.6, see first and second sub-figure from left in Figure 5.13). This observation reflects the mentioned shortcoming of total building models. The lower absolute value of the sensitivity indicates that the dead load of the slab above the 4th floor is also carried by the components added in later stages.
- The sensitivity of the clamping moment M_{CS8} with respect to the dead load of the slab over the eighth floor is the same for both modeling approaches (-3.0, see third and fourth sub-figure from left in Figure 5.13). As the dead load of all slabs influences M_{CS8} in the case of the total building model, the moment is significantly larger compared to the construction stage model.

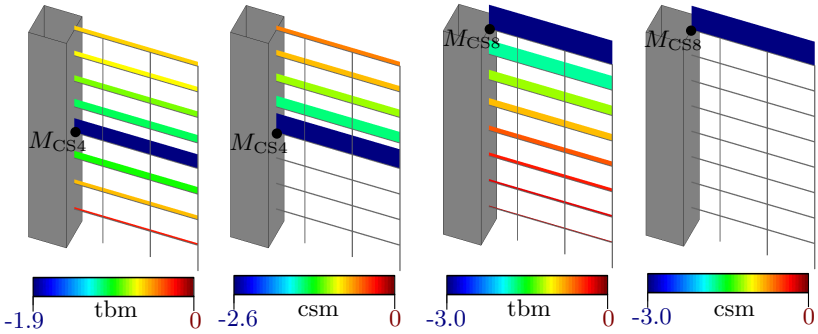

Figure 5.13: Sensitivities of the responses M_{CS4} and M_{CS8} concerning the dead load of the slabs based on a total building model (tbm) and a construction stage model (csm). Adapted from Fußeder et al. [61].

Significant differences can also be observed for other parameters when comparing the results of the two modeling approaches. Figure 5.14 shows an example of the sensitivities of the normal force N of a column on the first floor regarding the Young's modulus of the slabs. The sensitivities differ both in terms of distribution and intensity. In the total building model, the Young's modulus of the slabs of the top floors has the most significant influence on N. In contrast, the stiffness of the middle floors is the most important in the case of the construction stage model. Please note the unit dependence of the derivatives, which is the reason for the small numbers of the derivatives concerning the Young's modulus (cf. Section 6.2 for information).

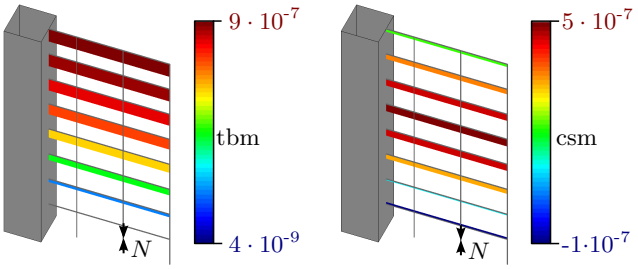

Figure 5.14: Sensitivities of the response N with respect to the Young's modulus of the slabs based on a total building model (tbm, left) and a construction stage model (csm, right). Adapted from Fußeder et al. [61].

5.3 Simulation process of hybrid lightweight structures

This section aims to apply sensitivity analysis to hybrid lightweight structures. These include elastic elements such as beams and tensile elements like membranes or cables. An example is shown in Figure 5.15. The umbrella structure consists of elastic beams that stretch the membrane. For detailed information on the structure, refer to Dieringer [47] and Michalski [112]. Lightweight structures cannot be designed by a single simulation. Instead, several analysis stages such as form-finding, structural analysis, and cutting pattern generation are required. Refer to Goldbach [72] for a comprehensive discussion on the multi-stage design process of lightweight structures. This section limits the focus to the connection between form-finding and structural analysis. Concerning sensitivity analysis, two significant challenges are faced. First, the material and cross-sectional properties of the elastic elements influence the form-found shape. Hence, the impact of those variables during the form-finding process has to be considered in sensitivity analysis. This issue is addressed in Section 5.3.1. Second, form-finding results must be transferred, and the subsequent structural analysis must be appropriately initialized to combine the two analyses. The necessary adjustments for sensitivity analysis are described in Section 5.3.2.

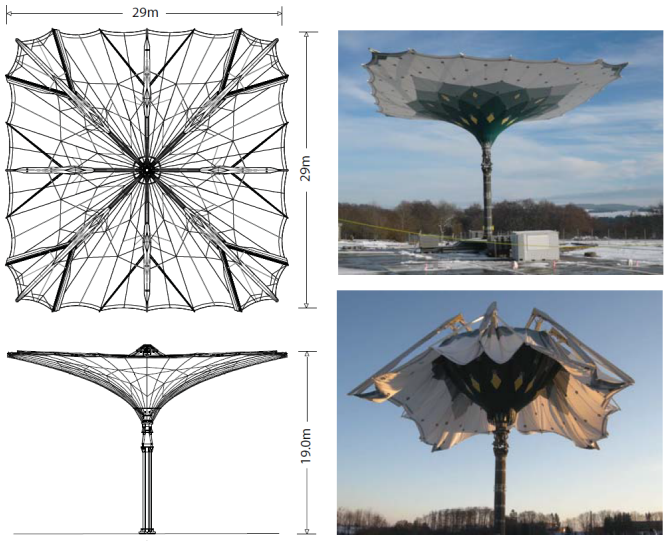

Figure 5.15: A foldable umbrella as an example of a hybrid lightweight structure. Taken from Michalski [112].

5.3.1 Form-finding with the Updated Reference Strategy

The main focus of this section is to discuss the adaption of sensitivity analysis to form-finding. Therefore, form-finding is only briefly presented so that the sensitivity derivations can be understood. For further reading, refer to Bletzinger et al. [25] and Linhard et al. [102] on the topic in general and to Dieringer et al. [48] on form-finding of hybrid structures in particular.
Form-finding aims to determine the geometry for which a given stress state is in equilibrium, considering given boundary conditions. This means the opposite task must be solved compared to regular structural analysis. There, the stress state is calculated based on load-dependent displacements. This is why form-finding is also denoted as *inverse problem*.
Form-finding is initiated by prescribing the desired stress state in terms of Cauchy stresses $\boldsymbol{\sigma}_0$. On this basis, the equilibrium is formulated by the principle of virtual work in the current configuration, which is

$$\delta W_{\mathrm{c}} = -\int_{\Omega} \boldsymbol{\sigma}_0 : \delta \boldsymbol{e}\, d\Omega = 0 \tag{5.54}$$

if external loads are excluded[3]. It appears that the tangential stiffness matrix becomes singular when Equation (5.54) is discretized (cf. Section (2.2.5)) to solve it. The reason is the non-uniqueness of the discrete form-finding geometry because finite element nodes can be moved tangentially on the domain surface without changing the structure's geometry. An illustrative discussion of the issue is given by Wüchner [137]. A regularization is required to solve the form-finding problem. Therefore, Bletzinger et al. [24] proposes an homotopy approach which extends Equation (5.54) as

$$\delta W_{\mathrm{hom}} = \lambda \cdot \delta W_{\mathrm{c}} + (1-\lambda) \cdot \delta W_{\mathrm{PK2}} \tag{5.55}$$

where the principle of virtual work in the reference configuration

$$\delta W_{\mathrm{PK2}} = -\int_{\Omega_0} \boldsymbol{S}_0 : \delta \boldsymbol{E}\, d\Omega_0 = 0 \tag{5.56}$$

is chosen as a stabilization term. The influence of the latter is controlled by the homotopy factor $\lambda \in [0;\, 1[$. For the solution of the form-finding problem based on Equation (5.55), Bletzinger et al. [24] proposes the *Updated Reference Strategy* (*URS*). A value for λ and an initial reference geometry $\boldsymbol{X}$ are chosen. Furthermore, the PK2 stresses are prescribed by the desired Cauchy stresses $\boldsymbol{S}_0 = \boldsymbol{\sigma}_0$. Based on this setting, Equation (5.55) is solved by the finite element method, which is denoted as form-finding step. Generally, one form-finding step is insufficient to ensure that the resulting stresses equate to the desired stress state. Therefore, an iterative procedure is required. For a subsequent form-finding step $k+1$ the resulting geometry $\boldsymbol{x}^{(k)}$ of the previous step is chosen as new reference geometry $\boldsymbol{X}^{(k+1)} = \boldsymbol{x}^{(k)}$. The procedure is

[3] This a typical assumption in the case of mechanically prestressed membrane or cable net structures.

repeated until convergence where the resulting Cauchy stresses $\boldsymbol{\sigma}$ equate the prescribed prestresses $\boldsymbol{S}_0$. Equivalence of the stresses is achieved when the reference and actual configuration coincides $\boldsymbol{X}^{(k+1)} = \boldsymbol{x}^{(k+1)} = \boldsymbol{x}^{(\text{final})}$.
In the special case of hybrid lightweight structures, the virtual work

$$\delta W_{\text{elastic}} = -\int_{\Omega_0} (\mathbb{C} : \boldsymbol{E}) : \delta \boldsymbol{E} \, d\Omega_0 = 0 \tag{5.57}$$

of the elastic members must be added to Equation (5.55). The PK2 stresses of the elastic members are not prescribed. Instead, they are calculated using the Saint Venant-Kirchhoff model based on the displacements occurring during form-finding. It is important to note that, unlike the form-finding elements, the reference geometry of the elastic members is not changed during the form-finding process.

Sensitivity of form-found geometry

For the derivations in Section 5.3.2, the sensitivity of the form-found geometry, expressed by the state derivative $d\boldsymbol{x}^{(\text{final})}/ds_i$, is required. It is important to note that the form-finding problem is independent of the material properties of the form-finding elements because their stress state is prescribed. The situation is different with the material and geometry parameters of the elastic members (e.g., Young's modulus or cross-sectional area). These parameters are introduced to the form-finding problem via Equation (5.57) and influence the form-finding result. In addition, parameters that affect the boundary conditions, such as the spatial position of the supports, influence the form-found geometry.
Each form-finding step with the URS is an entire finite element analysis. Hence, the URS can be interpreted as a sequenced simulation process. After form-finding step k has finished, the actual configuration $\boldsymbol{x}^{(k)}$ is taken as reference configuration $\boldsymbol{X}^{(k+1)}$ for step $k+1$. If $\boldsymbol{x}^{(k)}$ is dependent on s_i, the equilibrium condition

$$\boldsymbol{r}^{(k+1)}\left(s_i, \boldsymbol{x}^{(k+1)}(s_i), \boldsymbol{X}^{(k+1)}\left(\boldsymbol{x}^{(k)}(s_i)\right)\right) = \boldsymbol{0} \tag{5.58}$$

has to be considered, which is derived with respect to s_i

$$\frac{d\boldsymbol{r}^{(k+1)}}{ds_i} = \frac{\partial \boldsymbol{r}^{(k+1)}}{\partial s_i} + \frac{\partial \boldsymbol{r}^{(k+1)}}{\partial \boldsymbol{x}^{(k+1)}} \frac{d\boldsymbol{x}^{(k+1)}}{ds_i} + \frac{\partial \boldsymbol{r}^{(k+1)}}{\partial \boldsymbol{X}^{(k+1)}} \frac{\partial \boldsymbol{X}^{(k+1)}}{\partial \boldsymbol{x}^{(k)}} \frac{d\boldsymbol{x}^{(k)}}{ds_i} = \boldsymbol{0} \tag{5.59}$$

and reformulated as

$$\frac{d\boldsymbol{x}^{(k+1)}}{ds_i} = -\left[\frac{\partial \boldsymbol{r}^{(k+1)}}{\partial \boldsymbol{x}^{(k+1)}}\right]^{-1} \left[\frac{\partial \boldsymbol{r}^{(k+1)}}{\partial s_i} + \frac{\partial \boldsymbol{r}^{(k+1)}}{\partial \boldsymbol{X}^{(k+1)}} \frac{\partial \boldsymbol{X}^{(k+1)}}{\partial \boldsymbol{x}^{(k)}} \frac{d\boldsymbol{x}^{(k)}}{ds_i}\right] \tag{5.60}$$

to compute the state derivative by direct sensitivity analysis. Equation (5.60) has to be solved after each form-finding step to receive the sensitivity of the

form-found geometry $\boldsymbol{x}^{(\text{final})} = \boldsymbol{x}^{(k+1)}$:

$$\begin{aligned}
\frac{d\boldsymbol{x}^{(1)}}{ds_i} &= -\left[\frac{\partial \boldsymbol{r}^{(1)}}{\partial \boldsymbol{x}^{(1)}}\right]^{-1} \frac{\partial \boldsymbol{r}^{(1)}}{\partial s_i} \\
\frac{d\boldsymbol{x}^{(2)}}{ds_i} &= -\left[\frac{\partial \boldsymbol{r}^{(2)}}{\partial \boldsymbol{x}^{(2)}}\right]^{-1} \left[\frac{\partial \boldsymbol{r}^{(2)}}{\partial s_i} + \frac{\partial \boldsymbol{r}^{(2)}}{\partial \boldsymbol{X}^{(2)}} \frac{\partial \boldsymbol{X}^{(2)}}{\partial \boldsymbol{x}^{(1)}} \frac{d\boldsymbol{x}^{(1)}}{ds_i}\right] \\
&\vdots \\
\frac{d\boldsymbol{x}^{(k+1)}}{ds_i} &= -\left[\frac{\partial \boldsymbol{r}^{(k+1)}}{\partial \boldsymbol{x}^{(k+1)}}\right]^{-1} \left[\frac{\partial \boldsymbol{r}^{(k+1)}}{\partial s_i} + \frac{\partial \boldsymbol{r}^{(k+1)}}{\partial \boldsymbol{X}^{(k+1)}} \frac{\partial \boldsymbol{X}^{(k+1)}}{\partial \boldsymbol{x}^{(k)}} \frac{d\boldsymbol{x}^{(k)}}{ds_i}\right]
\end{aligned} \tag{5.61}$$

The computation of the state derivative with Equation (5.61) regarding one form-finding step requires the solution of n_s linear systems where n_s denotes the number of parameters. Hence, in total $n_s \cdot (k+1)$ evaluations of linear equation systems are necessary to compute the sensitivities of the form-found geometry with the direct approach. In cases where n_s exceeds the number of degrees of freedom n_{DOF} an adjoint approach is beneficial, which requires $n_{\text{DOF}} \cdot (k+1)$ solutions of linear systems. The necessary equations are not presented here but can be derived in analogy to Section 3.2.

5.3.2 Form-finding and consecutive structural analysis

During form-finding with the URS, the reference configuration of the form-finding members is updated in each step. In contrast, the elastic members keep their reference configuration and follow the form-finding process by elastic deformations. These must be retained for the subsequent structural analysis. Therefore, Dieringer et al. [48] propose using the InitDisp or InitStress approach presented in Section 5.1.1.

Extension of sensitivity analysis for InitDisp

If the InitDisp approach is used, the elastic deformations during form-finding are applied as initial displacements. This procedure initializes the structural analysis to be mechanically accurate. However, it has the disadvantage that the reference geometry of elastic and form-finding members are topologically separated. The same modeling issues arise as discussed for construction stage analysis in Section 5.2.1.2.

For sensitivity analysis, it has to be considered that the initial displacements $\boldsymbol{u}_0$ and the reference geometry of the form-finding members $\boldsymbol{X}_{\text{ffm}}$ depend on the form-finding solution $\boldsymbol{x}^{(\text{final})}(s_i)$. The response and equilibrium condition

$$J\left(s_i, \boldsymbol{u}(s_i), \boldsymbol{u}_0\left(\boldsymbol{x}^{(\text{final})}(s_i)\right), \boldsymbol{X}_{\text{ffm}}\left(\boldsymbol{x}^{(\text{final})}(s_i)\right)\right) \tag{5.62a}$$

$$\boldsymbol{r}\left(s_i, \boldsymbol{u}(s_i), \boldsymbol{u}_0\left(\boldsymbol{x}^{(\text{final})}(s_i)\right), \boldsymbol{X}_{\text{ffm}}\left(\boldsymbol{x}^{(\text{final})}(s_i)\right)\right) = \boldsymbol{0} \tag{5.62b}$$

are formally equivalent to those of construction stage analysis defined by Equation (5.30). Hence, the response sensitivity

$$\begin{aligned}\frac{dJ}{ds_i} =& \frac{\partial J}{\partial s_i} + \frac{\partial J}{\partial \boldsymbol{u}_0}\frac{\partial \boldsymbol{u}_0}{\partial \boldsymbol{x}^{(\text{final})}}\frac{d\boldsymbol{x}^{(\text{final})}}{ds_i} + \frac{\partial J}{\partial \boldsymbol{X}_{\text{ffm}}}\frac{\partial \boldsymbol{X}_{\text{ffm}}}{\partial \boldsymbol{x}^{(\text{final})}}\frac{d\boldsymbol{x}^{(\text{final})}}{ds_i} \\ &+ \frac{\partial J}{\partial \boldsymbol{u}}\left[\frac{\partial \boldsymbol{r}}{\partial \boldsymbol{u}}\right]^{-1}\boldsymbol{F}^* \quad \text{with} \\ \boldsymbol{F}^* =& -\frac{\partial \boldsymbol{r}}{\partial s_i} - \frac{\partial \boldsymbol{r}}{\partial \boldsymbol{u}_0}\frac{\partial \boldsymbol{u}_0}{\partial \boldsymbol{x}^{(\text{final})}}\frac{d\boldsymbol{x}^{(\text{final})}}{ds_i} - \frac{\partial \boldsymbol{r}}{\partial \boldsymbol{X}_{\text{ffm}}}\frac{\partial \boldsymbol{X}_{\text{ffm}}}{\partial \boldsymbol{x}^{(\text{final})}}\frac{d\boldsymbol{x}^{(\text{final})}}{ds_i}\end{aligned} \tag{5.63}$$

is equivalent to Equation (5.31) where $d\boldsymbol{x}^{(\text{final})}/ds_i$ is computed by Equation (5.61).

Extension of sensitivity analysis for InitStress

When using the InitStress approach, the reference geometry of the form-finding and elastic elements is adjusted based on $\boldsymbol{x}^{(\text{final})}(s_i)$. Furthermore, the internal stress state due to the deformations of the elastic members during form-finding is considered by initial stresses. The advantage is that the members remain connected and no double nodes are required as in the case of InitDisp. But, as noted earlier, the InitStress approach delivers no mechanically consistent analysis initialization.
For sensitivity analysis, it has to be considered that the initial stresses $\boldsymbol{S}_0$ and the reference geometry of all elements depend on the form-finding solution $\boldsymbol{x}^{(\text{final})}(s_i)$. The response and equilibrium condition are:

$$J\left(s_i, \boldsymbol{u}(s_i), \boldsymbol{X}\left(\boldsymbol{x}^{(\text{final})}(s_i)\right), \boldsymbol{S}_0\left(s_i, \boldsymbol{x}^{(\text{final})}(s_i)\right)\right) \tag{5.64a}$$

$$\boldsymbol{r}\left(s_i, \boldsymbol{u}(s_i), \boldsymbol{X}\left(\boldsymbol{x}^{(\text{final})}(s_i)\right), \boldsymbol{S}_0\left(s_i, \boldsymbol{x}^{(\text{final})}(s_i)\right)\right) = \boldsymbol{0} \tag{5.64b}$$

As for InitDisp, formally equivalent formulations as for construction stage analysis (Equation (5.36)) are received. Hence, the response sensitivity

$$\begin{aligned}\frac{dJ}{ds_i} =& \frac{\partial J}{\partial s_i} + \frac{\partial J}{\partial \boldsymbol{X}}\frac{\partial \boldsymbol{X}}{\partial \boldsymbol{x}^{(\text{final})}}\frac{d\boldsymbol{x}^{(\text{final})}}{ds_i} + \frac{\partial J}{\partial \boldsymbol{S}_0}\left[\frac{\partial \boldsymbol{S}_0}{\partial s_i} + \frac{\partial \boldsymbol{S}_0}{\partial \boldsymbol{x}^{(\text{final})}}\frac{d\boldsymbol{x}^{(\text{final})}}{ds_i}\right] \\ &+ \frac{\partial J}{\partial \boldsymbol{u}}\left[\frac{\partial \boldsymbol{r}}{\partial \boldsymbol{u}}\right]^{-1}\boldsymbol{F}^* \quad \text{with} \\ \boldsymbol{F}^* =& -\frac{\partial \boldsymbol{r}}{\partial s_i} - \frac{\partial \boldsymbol{r}}{\partial \boldsymbol{X}}\frac{\partial \boldsymbol{X}}{\partial \boldsymbol{x}^{(\text{final})}}\frac{d\boldsymbol{x}^{(\text{final})}}{ds_i} - \frac{\partial \boldsymbol{r}}{\partial \boldsymbol{S}_0}\left[\frac{\partial \boldsymbol{S}_0}{\partial s_i} + \frac{\partial \boldsymbol{S}_0}{\partial \boldsymbol{x}^{(\text{final})}}\frac{d\boldsymbol{x}^{(\text{final})}}{ds_i}\right]\end{aligned} \tag{5.65}$$

is equivalent to Equation (5.37) where $d\boldsymbol{x}^{(\text{final})}/ds_i$ is computed by Equation (5.61).

5.3.3 Example

The example shown in Figure 5.16 is considered as an abstracted hybrid lightweight structure. The trusses 1 and 2 represent the elastic members,

whereas the cable 3 is the form-finding member. The form-finding goal is to determine the y-coordinate of node A (see labeling in Figure 5.16) such that a Cauchy stress of $\sigma_0 = 10$ acts in the cable. After form-finding, a structural analysis with an external load P is executed. Please note that P is not acting during form-finding. The aim is to compute the sensitivities of displacement u with respect to the Young's modulus E of the elastic trusses (members 1 and 2) and the load P.

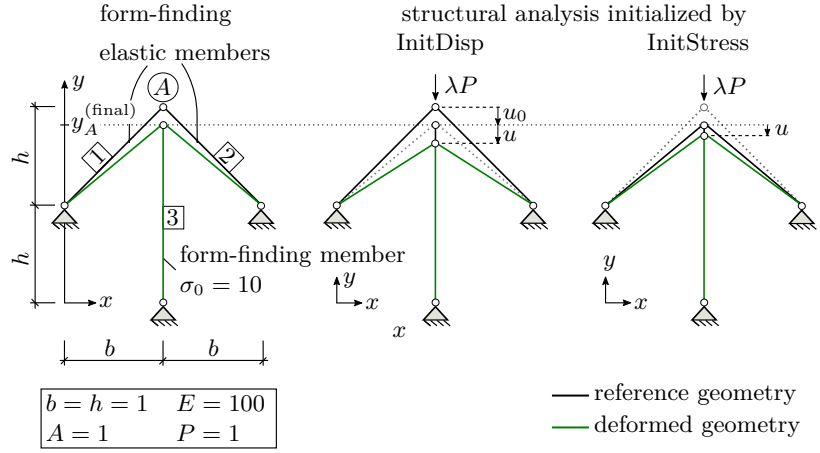

Figure 5.16: Form-finding and consecutive structural analysis of an abstracted hybrid structure.

If the URS as introduced in Section 5.3.1 is used, $y_A^{(\mathrm{final})} = 1.806$ is obtained as the form-found position of node A. For form-finding step $k+1$, the actual position $y_A^{(\mathrm{k})}$ is taken as new reference position $Y_A^{(\mathrm{k+1})}$ of the node A. Hence, Equation (5.61) reads

$$\frac{dy_A^{(k+1)}}{ds_i} = -\left[\frac{\partial r^{(k+1)}}{\partial y_A^{(k+1)}}\right]^{-1}\left[\frac{\partial r^{(k+1)}}{\partial s_i} + \frac{\partial r^{(k+1)}}{\partial Y_A^{(k+1)}}\frac{\partial Y_A^{(k+1)}}{\partial y_A^{(k)}}\frac{dy_A^{(k)}}{ds_i}\right] \tag{5.66}$$

to compute the sensitivities of the form-found position of node A. The results are given in Table 5.6. A positive sensitivity regarding the Young's modulus is obtained, which indicates that an increased stiffness leads to a shift of the form-found position of node A in the positive y-direction.

Table 5.6: Form-found position of node A and the corresponding sensitivities.

$y_A^{(\mathrm{final})}$	$dy_A^{(\mathrm{final})}/dE$	$dy_A^{(\mathrm{final})}/dP$
1.806	0.00299	0.0

The subsequent structural analysis is initialized with the InitDisp and InitStress approach. Note that the initialization of the analysis and, consequently, the sensitivity equations correspond to those of the example presented in Section 5.2.1.3 for construction stage analysis. In the case of InitDisp, the reference length of the cable element is $L_3 = y_A^{(\text{final})}$ according to the form-finding result. Since the reference geometry of the elastic elements is not modified, a double node is introduced to realize the topologically separated elements. The modeling is equivalent to construction stage analysis and can be seen in Figure 5.8. An initial displacement of $u_0 = 2h - y_A^{(\text{final})}$ is applied to account for the deformation of the elastic members during form-finding. If the dependency of L_3 and u_0 on the form-found geometry in Equation (5.63) is considered, the expression

$$\frac{du}{ds_i} = -\frac{1}{K}\left[\frac{\partial r}{\partial s_i} + \frac{\partial r}{\partial u_0}\frac{\partial u_0}{\partial y_A^{(\text{final})}}\frac{dy_A^{(\text{final})}}{ds_i} + \frac{\partial r}{\partial L_3}\frac{\partial L_3}{\partial y_A^{(\text{final})}}\frac{dy_A^{(\text{final})}}{ds_i}\right] \tag{5.67}$$

is received to compute the sensitivities. In the case of InitStress, the reference length of all three members is modified in dependency on the form-found geometry $y_A^{(\text{final})}$. Furthermore, an initial stress is applied to the elastic members. The prestress can be computed according to Equation (5.26). For sensitivity analysis, the dependency of the reference lengths L_j and the elastic element's prestress on $y_A^{(\text{final})}$ has to be considered and the expression

$$\begin{aligned}\frac{du}{ds_i} = -\frac{1}{K}\Bigg[&\frac{\partial r}{\partial s_i} + 2\frac{\partial r}{\partial \sigma_{\text{PK2},0}}\frac{\partial \sigma_{\text{PK2},0}}{\partial y_A^{(\text{final})}}\frac{dy_A^{(\text{final})}}{ds_i} \\ &+2\frac{\partial r}{\partial \sigma_{\text{PK2},0}}\frac{\partial \sigma_{\text{PK2},0}}{\partial s_i} + \sum_{j=1}^{3}\frac{\partial r}{\partial L_j}\frac{\partial L_j}{\partial y_A^{(\text{final})}}\frac{dy_A^{(\text{final})}}{ds_i}\Bigg]\end{aligned} \tag{5.68}$$

is obtained based on Equation (5.65). Structural and sensitivity analysis are conducted for $\lambda \in [0.0,\ 10.0]$. The outcomes are shown in Figure 5.17 and Table 5.7. The results allow similar observations to the truss examples in Sections 5.1.3 and 5.2.1.3. It can be observed that u and its sensitivities du/ds_i, which are based on the InitStress approach, increasingly deviate from the reference result of the InitDisp model for increasing λ.

Table 5.7: Sensitivities of structural analysis result u after previous form-finding.

	restart by InitDisp		restart by InitStress	
λ	du/dE	du/dP	du/dE	du/dP
0	0.0	0.0	0.0 (±0.0%)	0.0 (±0.0%)
10	-0.00126	0.159	-0.000899 (−28.7%)	0.129 (−18.9%)

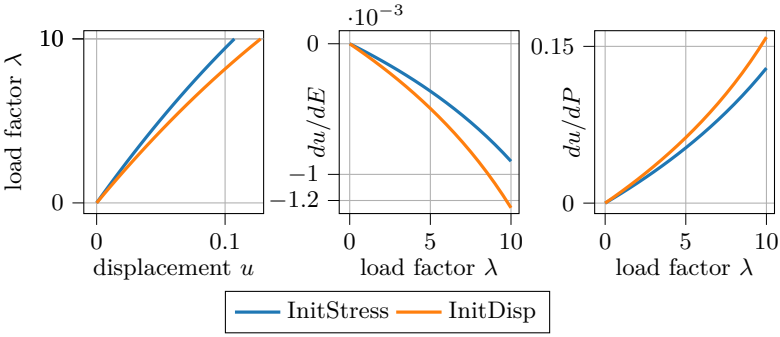

Figure 5.17: Load-displacement graph of structural analysis after previous form-finding (left). Respective sensitivity courses of displacement u with respect to Young's modulus E and load P (middle and right).

5.4 Summary

This chapter discussed how sensitivity analyses can be carried out on the basis of sequential simulation processes. These consist of a series of analyses, where the model is modified after the completion of a stage and must be correctly initialized for the subsequent analysis. To realize the restart of the next stage, two approaches from the literature were used. These employ either initial displacements or initial stresses in combination with a modified reference geometry to initialize the analysis. For sensitivity analysis, it has to be considered that the response and the equilibrium condition depend on the initialization quantities. As the latter depend on the structural analysis results of the previous stage, the chain rule of differentiation must be consistently applied to the interlinked dependencies. A particular computational challenge in this context is the requirement of the state derivatives du_j/ds_i of the preliminary stage. Determining the necessary du_j/ds_i requires entire sensitivity analyses, including the solution of linear equation systems. Depending on whether the number of u_j or s_i is dominating, a direct or adjoint approach is to be preferred. However, regardless of the method used to determine du_j/ds_i, the additional computational effort can be significant compared to a standard one-step analysis problem.

Chapter 6

Application of sensitivity analysis in structural design

The "*Grundlagen zur Festlegung von Sicherheitsanforderungen für bauliche Anlagen*" (*GruSiBau*, DIN [46]) is the German base document for standardization of structural design and forms the basis for codes such as the *EN 1990* (*Eurocode 0*, CEN [42]). Among other requirements, the GruSiBau demands a review of the structural design and calculation. The structural analysis must be checked to cover the actual influences and boundary conditions and that appropriate analysis models are used (cf. DIN [46], §7.2.1). In order to meet these requirements, it is necessary to deal carefully with the used analysis models. On the one hand, relevant model parameters must be identified to consider them in the calculation. On the other hand, the model itself must be examined. In the 1980s, when the GruSiBau was published, simple structural models were typically used, and the necessary investigations could be performed with intuitional engineering understanding. However, complex models can nowadays be calculated using modern numerical analysis methods. Advanced exploration approaches are required if the models are too complex to assess intuitively. For this reason, computational sensitivity analysis is proposed as an auxiliary structural design tool. The practical application of sensitivity analysis in this context is demonstrated below. The first part of the section demonstrates how sensitivities can be further processed for practical usage. Subsequently, a systematic analysis and decision chain to identify essential model parameters is proposed. To conclude the chapter, the proposed methods and procedures are demonstrated using examples from structural engineering. Note that parts of this section are directly taken from the previously published works Fußeder et al. [64, 66, 67] and can thus be understood as quotations. The author also contributed to the revision of the GruSiBau with a chapter on sensitivity analysis. An initial proposal of the document for discussion in the specialist community was published by DIBt [45] in 2022. The sensitivity analysis part of the GruSiBau revision is based on investigations that are also presented in the following. For readability reasons, explicit reference is not always made below to the sources mentioned.

6.1 Sensitivity maps

Section 3.2 describes the ability of adjoint sensitivity analysis to calculate sensitivities for many parameters per response in a computationally efficient way. For a purposeful exploration of essential model parameters from the resulting large amount of sensitivity information, graphical processing as sensitivity maps is recommended. Chapter 4 discusses in detail the relationship between the method of influence functions and adjoint sensitivity analysis. Based on this connection, the sensitivity maps of adjoint sensitivity analyses can be interpreted in analogy to influence functions. This property is examined in Section 4.3.3. There, it is discussed how the graphical analysis procedure of the influence functions approach can be extended. Subsequently, it is described how sensitivities concerning different parameter types can be visualized and read in this context. Similar sensitivity maps are regularly used in sensitivity analyses concerning many parameters. See Heimbach et al. [86] or Henning et al. [87] for examples from different application areas.

The influence function itself can be considered as a sensitivity map for the parameter "load intensity," whereby the functional value of the influence function at the position of the load corresponds to the sensitivity with respect to the load parameter (cf. Section 4.1.1). In that regard, Figure 6.1 (top) shows the sensitivity map of bending moment $J \hat{=} M_m$ at location x_m as response with respect to load F at position ξ as parameter, i.e., $\eta(\xi) = dM_m/dF(\xi)$. This type of graphical presentation can be transferred to the sensitivities concerning general parameters in an equivalent manner as Figure 6.1 additionally shows by two examples.

The map in the middle of Figure 6.1 displays the sensitivities of M_m with respect to the bending stiffness of the four construction members EI_{1-4}. The sensitivity analysis according to Equation (3.15) provides a scalar derivative value dM_m/dEI_i for the bending stiffness $s_i \hat{=} EI_i$ of the ith construction member, which is illustrated by a constant representation over the length of the ith component in the sensitivity map. By analogy to the influence function, the derivative of the response function concerning the parameter can be read at the location of the parameter. All construction members' bending stiffness has the same influence on the response, but the sensitivities of elements 2 and 3 have a negative sign. This map type is the discrete equivalent of the final sensitivity maps presented in Section 4.3.3.1.

Parameters of the nodes of a finite element mesh often have components in the spatial directions (e.g., nodal position or pre-deformation). Thus, sensitivities of such nodal parameters also have components in the respective directions, which can be visualized as a vector arrow at the corresponding finite element node. As an example of this type of illustration, the lower map in Figure 6.1 shows the sensitivities of M_m with respect to the spatial position $\boldsymbol{X}_i$ of nodes 1 - 5. These sensitivities express the consequences of deviations between the structure's actual and planned geometry. It can be seen that only four of the considered nodes influence the response. The horizontal position of the support in the middle is the most influential one (red arrow).

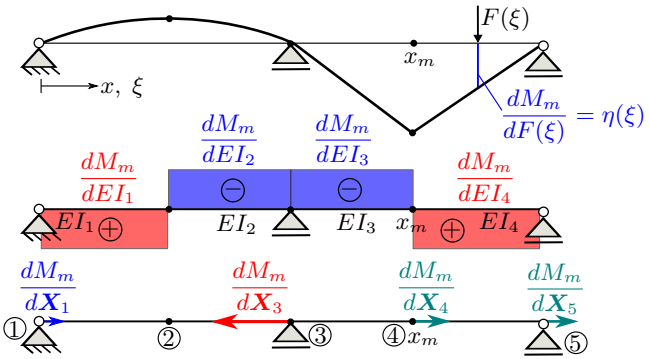

Figure 6.1: Sensitivity maps of the response "bending moment M_m" with respect to the parameters "load intensity $F(\xi)$" (top), "bending stiffness EI_{1-4}" (middle), and the parameters "spatial position $\boldsymbol{X}_i$ of nodes 1-5" (below). Adapted from Fußeder et al. [67].

6.2 Normalization of sensitivities

With their value and sign, local sensitivities provide two valuable pieces of information. In principle, the magnitude of the sensitivities can be used to compare the effect of model parameters on the response or to quantify the effect of a parameter variation. However, this is made more difficult because the value of a derivative depends on the units of the response J and the parameter s_i. In order to achieve comparability between the sensitivities of a response concerning different parameter types or between sensitivities of different responses with respect to the same parameter, a normalization with

$$e_i = \frac{dJ}{ds_i} \cdot \frac{s_i}{J(\boldsymbol{s})} \ [\%] \tag{6.1}$$

can be done. A normalized sensitivity of $e_i = 1.0$ indicates that a parameter variation of 1.0% leads to a response variation of 1.0%. Smith et al. [130] gives an extensive discussion on the significance of normalized and unmodified sensitivities.

However, applying Equation (6.1) is not readily possible for all typical questions in structural engineering. In the first instance, parameters exist whose value is unsuitable for normalization. An example is the spatial position of a finite element node. The entire finite element model can be moved in space without changing itself and its behavior, while the nodal coordinates' values constantly vary during movement. Thus, the actual values of the nodal coordinates are not unique for usage in Equation (6.1).

Furthermore, parameters with a reference value of $s_i = 0$ are problematic. A practical situation is investigating the effect of possible support settlements.

No magnitudes of support settlements for normalization are available if the sensitivity analysis is based on the initial model with unmoved supports. To enable a quantification of the parameter variation effect for the depicted parameter types, a slightly modified normalization approach is recommended:

$$d_i = \frac{dJ}{ds_i} \cdot \frac{\delta_{s_i}}{J(\boldsymbol{s})} \cdot 100 \ [\%] \tag{6.2}$$

Instead of the actual parameter value, Equation (6.2) incorporates a characteristic variation δ_{s_i} in the unit of the parameter. Suppose an exemplary finite element model based on the unit of length meters. A sensitivity concerning a nodal position or support settlement of $d_i = 1.0$ for $\delta_{s_i} = 0.001$ m indicates that the response variation is 1.0% if the nodal position or settlement varies by 0.001 m. The result of Equation (6.2) is highly dependent on the choice of δ_{s_i}. This circumstance complicates the comparison of the relevance of different parameters. It is important to note that Equations (6.1) and (6.2) are based on Taylor series expansions. Hence, their results only approximate if the functional relation between J and s_i is non-linear.
The sign of the sensitivity indicates whether an increase in the parameter value leads to an increased (positive derivative) or decreased (negative derivative) value of the response function. This information can be helpful when the *semi-probabilistic partial safety factor concept* (PSF concept) introduced by DIN [46] and Ellingwood et al. [50] is applied. The sign shows whether a basis variable has a favorable or unfavorable impact on a design quantity and how the partial safety factors have to be applied accordingly. Section 6.6 presents an example for this purpose.

6.3 The effect of the applied load on the sensitivities

Attention must be drawn to the load case and its level applied during sensitivity analysis. On the one hand, the term ($\hat{=}$ Equation (3.15), repeated for clarity)

$$\frac{dJ}{ds_i} = \frac{\partial J}{\partial s_i} + \boldsymbol{\eta}^T \left[\frac{\partial \boldsymbol{F}}{\partial s_i} - \frac{\partial \boldsymbol{K}}{\partial s_i} \boldsymbol{u} \right]$$

shows that the sensitivities are, in general, dependent on the actual model state. This can be seen as the displacement vector $\boldsymbol{u}$ is part of the pseudo-load. On the other hand, the actual value of the response $J(\boldsymbol{s}, \boldsymbol{u}(\boldsymbol{s}))$ is affected by the load, too. As the response value and derivative are part of Equations (6.1) and (6.2), the normalized sensitivities also depend on the load case. This must be considered when normalized sensitivities are used for investigations in structural design where different load combinations and certain load levels (e.g., mean, characteristic, or design load level) are of interest.
Subsequently, the steel arch bridge introduced in Appendix A.3 is considered. The structure is subjected to self-weight G and a traffic load Q in the bridge center. This example aims to study the effect of the applied load on the derivatives and normalized sensitivities. For this purpose, the bridge is comparatively analyzed at mean and design load level. The mean self-weight

G_μ is computed with the nominal dimensions of the members and a specific weight of 0.0785 MN/m^3. The characteristic self-weight G_k is selected as the mean[1] value, to which a partial safety factor of $\gamma_G = 1.35$ is applied to calculate the design value. For the traffic load, a Gumbel distribution with a mean of Q_μ=0.01 MN/m and a coefficient of variation of 25% is assumed. The design value Q_d is determined based on the 98% fractile as characteristic value Q_k and a partial safety factor of $\gamma_Q = 1.5$. Hence, the load combinations

$$F_\mu = G_\mu \text{ “+” } Q_\mu \quad \text{and} \quad F_d = \gamma_G \cdot G_k \text{ “+” } \gamma_Q \cdot Q_k \tag{6.3}$$

are received. The following observations are made for bending moment M as response with respect to (i) the intensity of the traffic load Q, (ii) the vertical nodal position of the connection node 1 of tension chord/main girder, and (iii) the Young's modulus of the member “component 1” in the arch crown as parameters (see labeling in Figure 6.2).

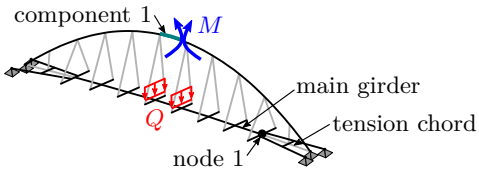

Figure 6.2: Arch-type bridge with indication of the response “bending moment M” and the observed model members. Adapted from Fußeder et al. [67].

The detailed computation of the normalized sensitivities at the two load stages is shown in Table 6.1 and enables the following observations:

- Significant differences in the derivative values dJ/ds_i due to their unit dependency can be observed. Hence, comparing the effects of the different parameter types based on the derivatives is not readily possible (line 2 in Table 6.1).
- The derivative concerning the traffic load intensity is the same in linear statics for both load stages. In contrast, the derivatives regarding the nodal position and the Young's modulus are different due to their dependency on the current state (cf. Equation (3.15)).
- The absolute variations $dJ/ds_i \cdot \delta_{s_i}$ (line 4 in Table 6.1) are more significant at design load level, either due to a higher value of δ_{s_i} (load) or higher derivative values (other parameters).
- Depending on whether the change in the derivative, parameter variation, or the shift in the response value dominates, the relative variations, i.e.,

[1] According to EN 1990 (CEN [42]), this is possible due to the low variability of the specific weight of steel, whose coefficient of variation is $< 1\%$ (cf. JCSS model code, Vrouwenvelder [136, Part 2.1]).

the entirely normalized sensitivities (line 5 in Table 6.1), show irregular alternations for the two load levels.

The comparison of absolute and relative variations shows that a judgment based exclusively on normalized sensitivity values can lead to misinterpretations. The qualitative observation of line 5 in Table 6.1 indicates that the impact of the nodal position is less at the design load stage. However, this evaluation is only relatively valid, as the absolute change in the response value under design load is more significant with the same parameter variation (cf. line 4). These circumstances must be considered when critical values for sensitivities are defined. Therefore, whether the relative or the absolute parameter effect is more suitable for the specific design problem must be carefully decided. The influence of the variations δ_{s_i} on the observable sensitivity measures must also be considered.

Table 6.1: Composition of normalized sensitivities for load impact with mean values ($J(F_\mu)$=0.89 MNm) and design values ($J(F_d)$=1.73 MNm). The load combinations F_μ and F_d are defined by Equation (6.3). Taken from Fußeder et al. [67].

line	parameter s_i	traffic load Q		node 1		Young's modulus	
	unit	MN/m		m		MPa	
#	load comb.	F_μ	F_d	F_μ	F_d	F_μ	F_d
1	value of s_i	0.01	0.025	/		210 000	
2	dJ/ds_i	42.3		0.24	0.34	7.3e-7	1.5e-6
3	δ_{s_i}	0.0001	0.00025	0.01		2 100	
4	$dJ/ds_i \cdot \delta_{s_i}$	0.0042	0.011	0.0024	0.0034	0.0015	0.0031
5	$\frac{dJ}{ds_i}\frac{\delta_{s_i}}{J(\boldsymbol{s})} \cdot 100\%$	0.48	0.61	0.27	0.20	0.17	0.18

6.4 Proposal of a systematic analysis and decision chain

The proposed analysis and decision chain is an extended version of the one presented in Fußeder et al. [64, 66] and is shown in Figure 6.3. It compromises the consecutive stages: (i) problem definition, (ii) identification, and (iii) assessment and control. The stages are described in more detail below.

6.4.1 Problem definition

A key challenge in applying sensitivity analysis is defining the responses and model parameters for which sensitivities should be computed. Almost every structure has a unique character with different challenges in planning and construction. Moreover, a structure can be modeled in different ways and must be modeled differently depending on the problem, i.e., what phenomenon (local stress vs. eigenmode) has to be analyzed. Refer to Bischoff et al. [21] for

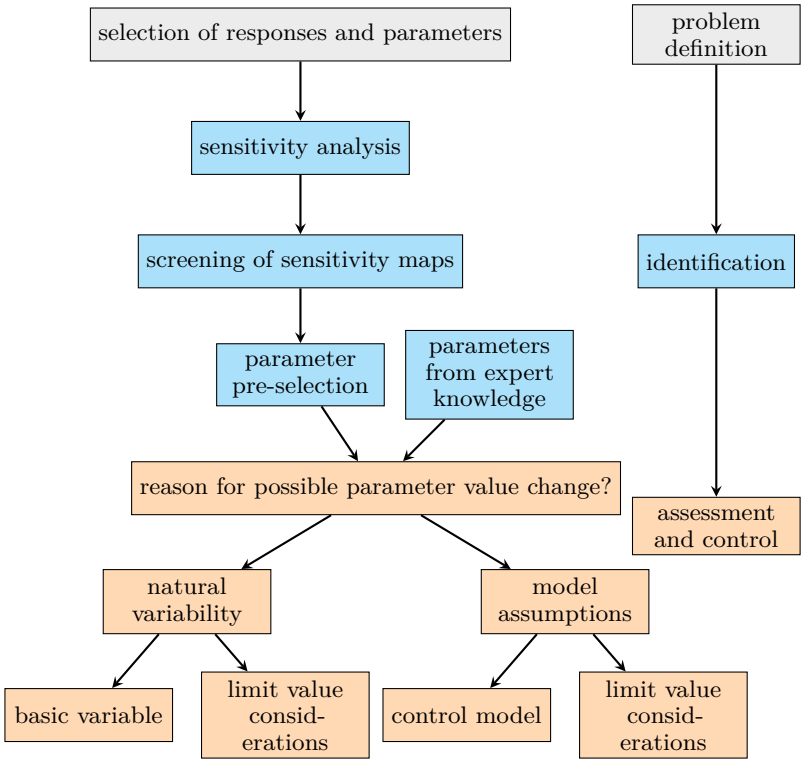

Figure 6.3: Analysis and decision chain to treat structural sensitivities.

a discussion of this issue. Therefore, a universally valid definition of responses and model parameters for sensitivity analysis is impossible.

When selecting the parameters, adjoint sensitivity analysis can be used to calculate the sensitivities concerning numerous parameters per response in a computationally efficient manner (cf. Section 3.2). Hence, no limited parameter selection is required, and the computation of sensitivities concerning various entities is possible. For instance, stiffness or material parameters of construction members or finite elements, load parameters, geometric parameters, or parameters of the boundary conditions can be analyzed. This enables a broad overview of the influenceability of specific responses. In particular, information about the influence of the parameters, which are listed in CEN [42, §4] (EN 1990) as potential basic variables, can be received. These are (i) actions and environmental influences, (ii) material and product properties, and (iii) geometrical data. Furthermore, parameters that contribute to the model uncertainty should be considered. According to the *Model Code* of the *JCSS*, the negligence of aspects like 3D-effects, inhomogeneities, interactions,

boundary effects, simplification of connection behavior, and imperfections are the primary sources of the uncertainty of the structural analysis model (cf. Vrouwenvelder [136, Part 3.9]). Some of these aspects are directly or indirectly related to model parameters, which can be assessed with a sensitivity analysis. For example, the importance of spring stiffness parameters of connections or boundary conditions can be analyzed. Finally, model- or project-specific parameters should be traced as well.
When selecting responses, those that are part of a limit state function or a partial safety factor (PSF) design inequality in probabilistic or semi-probabilistic design are particularly interesting. However, modern computational tools can perform almost automatic structural design. No PSF design inequality, including a specific model response, is explicitly chosen when such tools are used. In the case of complex structures with various construction members, a selection strategy can be to choose the design quantity (e.g., stress resultant) of the construction member with the highest utilization level. In that regard, Section 6.6 presents an exemplary roof construction where the decisive bending moments of certain construction members are chosen as responses for sensitivity analysis.

6.4.2 Identification

The identification stage aims to obtain a pre-selection of potentially significant parameters. Therefore, sensitivity analyses are performed for the selected model responses and parameters. For a purposeful exploration of the results, graphical processing as sensitivity maps is recommended (cf. Section 6.1). Furthermore, it is beneficial to normalize the results (cf. Section 6.2) to enhance the comparability between the sensitivities of a specific response with respect to different parameter types or between sensitivities of various responses. The sensitivity maps are then reviewed in a screening phase, providing an overview of essential parameters or structural components. By this, a parameter selection for further assessment is received. The selection is supplemented by parameters that are considered significant based on expert knowledge (e.g., experience from other projects).

6.4.3 Assessment and control

This phase aims to evaluate the significance of the pre-selected parameters and to decide whether and how they should be further considered in the structural design. The first step is to evaluate the reasons for possible changes in the values of the pre-selected parameters. Conceivable causes can be natural variability, lack of knowledge, or subjective assumptions during the structure modeling. Depending on this assessment, various actions are possible.
In the case of natural variability, the identified parameter should be considered as a basic variable in subsequent probabilistic or semi-probabilistic analyses. If the PSF concept is utilized, the parameter influence can be captured by the explicit safety components (characteristic value, partial safety factor, or additive safety element). The sign of the sensitivity shows whether a basis variable has a favorable or unfavorable impact on a design quantity. On that

basis, it can be determined how the explicit safety components need to be applied. Hence, sensitivity analysis assists in controlling the completeness of the utilized basis variables and the correct usage of the explicit safety components. Section 6.6 presents an example for this purpose. If the utilized standards do not provide explicit safety components for a specific parameter, limit value considerations due to unfavorable modification of the parameter value could be made instead.

Suppose there is an appreciable or conspicuous sensitivity regarding a parameter whose value is due to certain model assumptions or modeling decisions. In that case, the results of sensitivity analyses can serve as the basis for controlling or modifying the model. It can be checked whether the sensitivity is the consequence of a specific, possibly even erroneous modeling which is less pronounced or not present in the case of a modified model (e.g., the sensitivity concerning the bending stiffness of a hinged column is not zero because the connection modeling with the slab is erroneous).

6.5 Application example: steel arch bridge

The steel arch bridge described in Appendix A.3 is examined. The load combination F_μ defined by Equation (6.3) is applied when performing the sensitivity analysis. The example demonstrates the analysis and decision chain introduced in Section 6.4. In particular, the systematic use of the sensitivity maps presented in Section 6.1 to obtain a fast overview of significant parameters during the identification phase is shown. The example is also presented in Fußeder et al. [66].

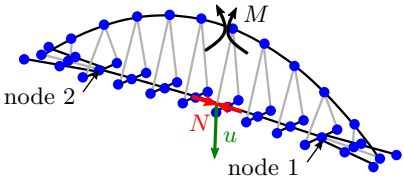

Figure 6.4: Static system of an arch-type bridge. Considered responses: bending moment M, normal force N, and deflection u. Blue points indicate observed nodes. The connection node main girder/tension chord is denoted by "node 1/2."

Problem description

The observed responses are (i) bending moment M, (ii) normal force N, and (iii) vertical deflection u, whose respective positions can be seen in Figure 6.4. The parameters are (a) the Young's modulus of the beam construction members (black-colored members in Figure 6.4) and (b) the spatial node position of the construction members connections (blue points in Figure 6.4).

Identification

After the sensitivity analysis is completed, normalization is applied. The sensitivities concerning the Young's modulus are normalized according to Equation (6.1) whereas for the nodal positions Equation (6.2) with $\delta_{s_i} = 0.01$ m (unit of length of the model is meters) is utilized. The screening of the maps with normalized sensitivities (abbreviation: n.s.) shown in Figure 6.5 leads to the following observations:

- The considered parameters have less influence on normal force (max. n.s. 0.03) than on bending moment (max. n.s. 0.27) and deflection (max. n.s. 0.30).
- The influence of the Young's modulus (|max. n.s.| 0.17 and 0.13) and the node positions (max. n.s. 0.27 and 0.30) is comparable for bending moment and deflection.
- The Young's modulus in the area of the arch crown has a comparatively large influence on all three responses.
- In addition to the spatial position of the support nodes of the arch, only the vertical position of the connection node of the tension chord to the main girder (cf. node 1/2 in Figure 6.4) has a comparatively large influence on the observed responses. This is indicated by the comparably large vector arrows at the position of those nodes.

Assessment and control

The following assessments can be concluded from the observations made during the identification phase:

- The normalized sensitivities concerning the Young's modulus have only a moderately high maximum value of 0.17. Furthermore, the coefficient of variation of the Young's modulus of steel is relatively small. For instance, the Model Code of the JCSS recommends a coefficient of variation of 3% (cf. Vrouwenvelder [136, Part 3]). In combination with the low coefficient of variation, the normalized sensitivity indicates that the Young's modulus is not a significant model parameter in this case.
- The normalized sensitivity concerning the vertical node position of the tension chord/main girder connection node shows a remarkable order compared to the other observed nodes. However, a good dimensional tolerance can be expected due to the prefabrication of the steel components at a factory. Hence, the vertical position of the connection does not tend to be a safety-relevant parameter. This assertion is supported by the magnitude of the normalized sensitivity, which is 0.3 for the deflection u. Based on a linearized estimate, the deflection varies by 0.3% when the deviation of the connection node is 1 cm. However, even if the connection node is not relevant from a safety point of view, the modeling of the analysis model should be checked in the vicinity of the connection (e.g., stiffness of the adjacent elements, prestress force of the tension chord, or possible eccentricity).

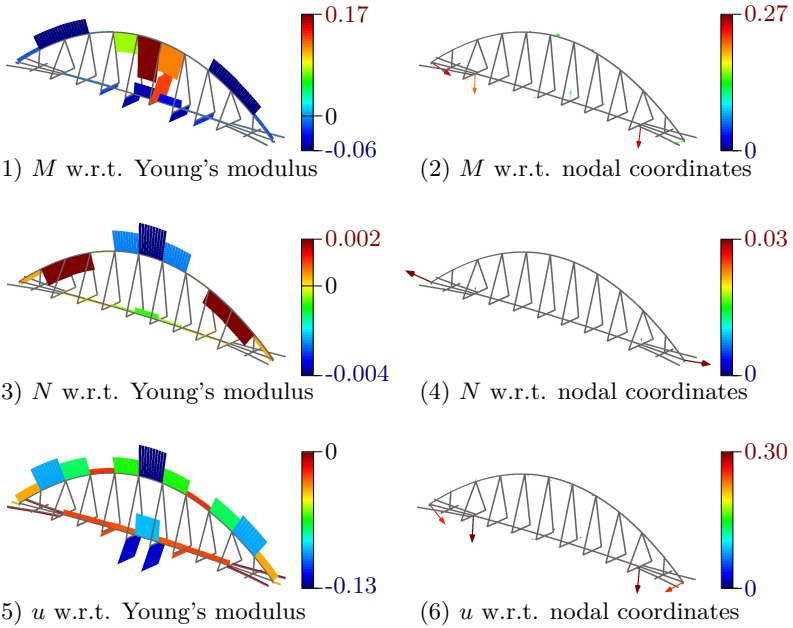

(1) M w.r.t. Young's modulus (2) M w.r.t. nodal coordinates

(3) N w.r.t. Young's modulus (4) N w.r.t. nodal coordinates

(5) u w.r.t. Young's modulus (6) u w.r.t. nodal coordinates

Figure 6.5: Sensitivity maps of different responses with respect to (abbreviation. w.r.t.) the parameters "Young's modulus of construction members" (left) and the parameters "spatial position of FE nodes". Modified from Fußeder et al. [66].

6.6 Application example: wooden roof construction

The roof construction shown in Figure 6.6 is considered. The example is also presented in Fußeder et al. [66, 67]. The bearing structure is a girder grid that consists of wooden beams in combination with single steel and concrete girders. The grid is planked by a wooden plate and is pointwise-supported by columns (indicated by blue and orange points in Figure 6.6). Refer to Appendix A.4 for more details on the roof construction.
Some support columns reach only the prestressed concrete plate of the floor below but not the foundation. The deformation of the prestressed concrete plate due to creep and shrinkage represents an additional load case for the analysis of the roof structure. As no total building model is used, the settlements are modeled by prescribed displacements in the analysis model. Given the expected support settlements of up to 30 mm, a thorough treatment of these is crucial for the design, according to expert assessment. It is assumed that the support settlements act in particular on the surrounding stiff steel facade strip (see green colored bars in Figure 6.6). It will be shown how sensitivity analysis can support handling such a challenge. For this purpose,

the analysis and decision chain presented in Section 6.4 is utilized, and the information obtained are applied to the structural design with the partial safety factor concept.

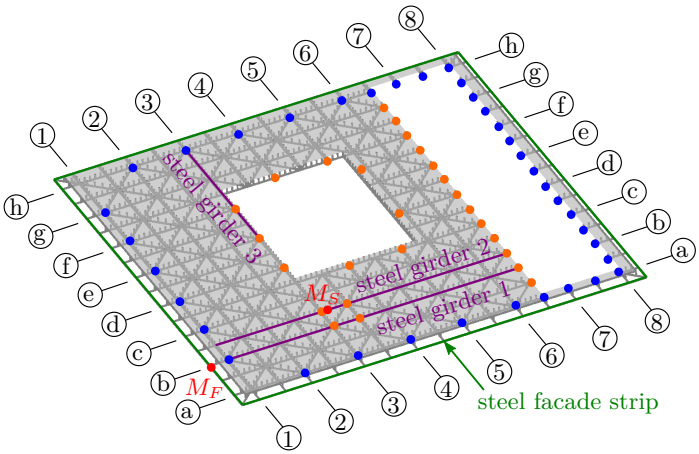

Figure 6.6: Roof construction: covered girder grid made of wood with highlighted important construction members and supports (blue and orange points). Refer to Appendix A.4 for more details. Adapted from Fußeder et al. [67].

Problem definition

Sensitivity analysis will be demonstrated using three quantities as responses. These are (i) the sum of the vertical displacements of all finite element nodes of the facade strip, (ii) the decisive bending moment of the facade strip M_F, and (iii) the decisive bending moment M_S of steel girder 2 (see identifiers in Figure 6.6). The bending moments are needed for the structural design of the facade strip and the steel girder. They are located at a specific position within the roof. On the contrary, the displacement response is a more global performance measure of the structure whose sensitivities can be used to screen potential essential parameters of the overall roof construction. The model parameters of particular interest are the settlement magnitudes of the supports, marked by blue points in Figure 6.6. In addition, the sensitivities concerning the second moment of inertia I_y of all beam elements of the girder grid are computed. These sensitivities can be used as comparative values to further assess the actual relevance of the support settlements. Please note that each beam finite element's second moment of inertia is treated as an individual parameter. To obtain the sensitivity of a complete construction member, the sensitivities of the finite elements contained in the member must be added.

The settlement magnitude $\hat{u}_j$ of the support corresponding to the jth degree of freedom is a prescribed entry of the displacement vector $\boldsymbol{u}$. Note that such parameters were not considered when deriving the pseudo-load in Equation (3.14). The consideration of the explicit existence of the parameter $s_i = \hat{u}_j = u_j$ as the jth entry of the displacement vector leads to

$$-\frac{\partial \boldsymbol{r}}{\partial s_i} = -\boldsymbol{K}\frac{\partial \boldsymbol{u}}{\partial s_i} = -\boldsymbol{K}\frac{\partial \boldsymbol{u}}{\partial u_j} = -\boldsymbol{K}\boldsymbol{e}_j \tag{6.4}$$

as pseudo-load for prescribed displacements when Equation (3.12) is derived, where $\boldsymbol{e}_j$ is the jth unit vector. Equation (6.4) is independent of the actual system state $\boldsymbol{u}$ due to a specific external load case. Moreover, the result of Equation (6.4) can be identified as the load case corresponding to a support settlement of the jth degree of freedom by a value of "1" (cf. Section 4.2.2). Thus, the sensitivity computed by the dot product of the influence function ($\hat{=}$ adjoint variable $\boldsymbol{\eta}$, see Section 4.1) and the pseudo-load (Equation (6.4)) is equal to the resulting response value due to a unit displacement of the support.
The sensitivities concerning the second moment of inertia are normalized according to Equation (6.1) whereas for the prescribed displacements Equation (6.2) with $\delta_{s_i} = 0.001$ m (unit of length is meters) is utilized. During sensitivity analysis and the computation of the response values, the model is stressed by permanent action G (dead load and weight of finishes), wind W, and snow S with their design values for the ultimate limit state according to the EN 1990 (Eurocode 0, CEN [42]). Refer to Appendix A.4 for more details on the load cases. The actions are applied with the following combination rule:

$$\gamma_G \cdot G \text{ "+" } \gamma_Q \cdot W \text{ "+" } \gamma_Q \cdot \psi_0 \cdot S \text{ with } \gamma_G = 1.35,\ \gamma_Q = 1.5 \text{ and } \psi_0 = 0.5 \tag{6.5}$$

Please note that the supports are kept in their unmoved position. Thus, the normalized sensitivities concerning the prescribed displacements make it possible to quantify the effect of the support settlements in addition to the impact of the action combination according to Equation (6.5).

Identification, assessment and control

The screening of the maps with normalized sensitivities shown in Figure 6.7 leads to the following observations:

- The nodal displacements of the facade are influenced by all traced support settlements and the second moment of inertia of a large part of the elements. The settlements and the second moment of inertia are particularly significant near the intersection points of axes a/2, b/1, g/1, and h/2. This observation indicates that these regions are potentially important and should be carefully considered by the design. Noteworthy are also the higher I_y-sensitivities of the steel girders compared to the wooden ones.

- Noticeable sensitivities of the bending moment M_F concerning the support settlements are restricted to six supports (intersection points of axes 1/b-d and a/2-4). The normalized sensitivities with values up to 9.19 are relatively high (the moment changes by 9.19% compared to its value due to the load combination in Equation (6.5) if the corresponding support sinks by 1 mm). The influence of M_F concerning the second moment of inertia is also locally restricted. In particular, the sensitivities of the elements close to the intersection points of the axes a/2 and b/1 are noticeable.

- The bending moment M_S is influenced only locally by a limited number of support settlements (intersection points of axes 1/b-d and a/2-5) and the second moment of inertia of the steel girders 1 and 2. Although the maximum absolute value of the normalized support settlement sensitivities is much smaller compared to M_F (0.57 vs. 9.19), the influence is not negligible given support settlements of up to 30 mm.

- As the sensitivity normalization of the support settlements and second moment of inertia is carried out differently (cf. problem definition in the previous section), the parameter types' influence cannot be directly compared. A connection can be established by estimating the needed parameter variation to achieve the same effect on the response. For instance, the sensitivity of M_S concerning the support settlement at position 1/b indicates a change in the negative response function value of -0.57% if the support sinks by 1 mm. The normalized sensitivity of M_S with respect to I_y of steel girder 2 is -0.43 (calculated by adding the sensitivities of all finite elements of steel girder 2). Hence, a response change of -0.57% can be achieved by a 1.3% increase of I_y.

The sensitivity analysis confirms the experts' estimation of the significance of the support settlements. It is essential to consider the settlements in structural design. EN 1990 classifies that support settlements belong to the basic variable group "actions and environmental influences." More specifically, they are treated as indirect permanent actions. See CEN [42, §4.1.1] and for more information the corresponding chapter in the designers' guide (Gulvanessian et al. [79]). The treatment of the settlements as basic variables in semi-probabilistic design is shown in the following section.

In addition to applying a partial safety factor to the settlements, the determination of their magnitude should also be carefully considered. The utilized magnitudes correspond to the displacements at the respective positions of the rising columns in the analysis model of the prestressed concrete floor. After checking whether the computational analysis model of the prestressed concrete floor is suitable for determining the required deformations, a detailed study can be carried out to investigate in what range they can vary. The basis for this study is the knowledge about the settlements, which have the most significant effect on the bending moments given by the sensitivity analysis.

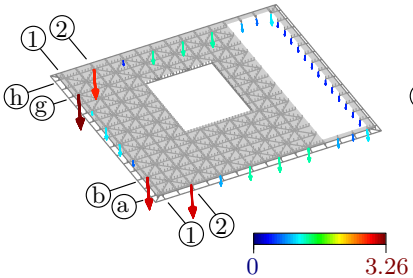

(1) displacement (facade) w.r.t. $\hat{u}$

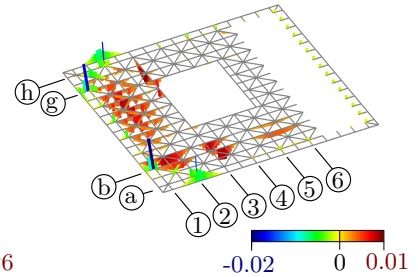

(2) displacement (facade) w.r.t. I_y

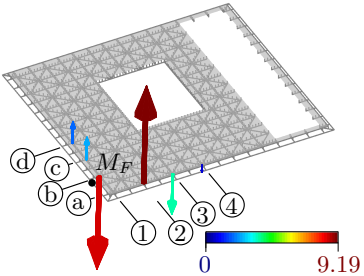

(3) M_F (facade) w.r.t. $\hat{u}$

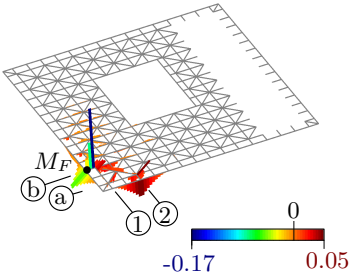

(4) M_F (facade) w.r.t. I_y

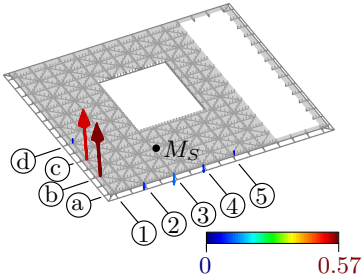

(5) M_S (steel girder 2) w.r.t. $\hat{u}$

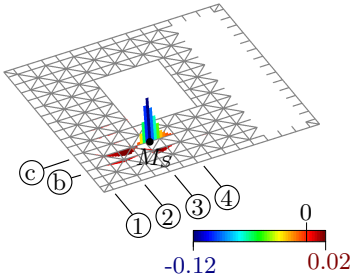

(6) M_S (steel girder 2) w.r.t. I_y

Figure 6.7: Sensitivity maps of roof construction. Responses: nodal displacements of facade strip and design moments M_F and M_S with respect to (abbreviation: w.r.t.) parameters: prescribed displacements $\hat{u}$ (sign convention: positive/negative sensitivities are shown by downwards/upwards directed vector arrows) and second moment of inertia I_y of beam elements. Adapted from Fußeder et al. [67].

Sensitivity-assisted structural design

The previous section identifies and discusses the high relevance of the support settlements regarding the bending moments M_F and M_S. For the design of the facade strip and steel girder with the partial safety factor concept, the sensitivity maps in sub-figures (3) and (5) of Figure 6.7 indicate which of the traced support settlements under consideration have a noteworthy influence. Furthermore, they show by the direction of the vector arrows that there are both supports whose sinking has an unfavorable and supports with a favorable effect. As the moments M_F and M_S are negative, unfavorably acting settlements are indicated by negative sensitivities. Hence, the sensitivities provide information about which of the settlements need to be taken into account and how the corresponding partial safety factors must be applied. To quantify these findings, the design values of the bending moments are determined in three ways:

- Design 1: basic action combination according to Equation (6.5) without approach of settlements
- Design 2: basic action combination according to Equation (6.5) and approach of settlements, with a partial safety factor applied to all settlements (cf. Table 6.2)
- Design 3: basic action combination according to Equation (6.5) and approach of settlements, where only unfavorably acting settlements are subjected to a partial safety factor (cf. Table 6.2)

Table 6.2: Applied values and partial safety factors (PSF) of prescribed displacements (p.s.) to compute the design value of M_F and M_S. Taken from Fußeder et al. [67].

position	a/2	a/3	a/4	a/5	1/b	1/c	1/d
p.s. values [mm]	30	30	30	30	10	10	10
design 2							
PSFs (M_F and M_S)	1.35	1.35	1.35	1.35	1.35	1.35	1.35
design 3							
sign sensitivity (M_F)	−	+	+	−	+	−	−
PSFs (M_F)	1.35	1.0	1.0	1.35	1.0	1.35	1.35
sign sensitivity (M_S)	+	+	+	−	−	−	−
PSFs (M_S)	1.0	1.0	1.0	1.35	1.35	1.35	1.35

The resulting moments for design cases 1 to 3 can be found in Table 6.3. Their remarkable differences underline the relevance of carefully considering the support settlements. Especially in the case of M_F, the increase of the response value is highly significant for structural design and safety. As the sensitivities of M_F are much greater than the respective ones of M_S (cf. Figure 6.7),

the differences in the design values of M_S are consequently lower when the settlements are considered. Nevertheless, the increase of 9% between designs 1 and 3 is not negligible and should be considered.

Table 6.3: Design moments (absolute values) due to different treatment of prescribed displacements of supports. Taken from Fußeder et al. [67].

moment	design 1	design 2	design 3
M_F [kNm]	242.6	557.1 (+130%)	748.2 (+208%)
M_S [kNm]	2 384.6	2 518.5 (+6%)	2 590.1 (+9%)

6.7 Summary

The chapter illustrated the application of adjoint sensitivity analysis in structural design. Sensitivity maps were used for the purposeful identification of essential model parameters. When interpreting sensitivities, their unit dependence must be considered. Normalization can be applied to the derivatives to compare sensitivities concerning different responses and parameters. In structural design, various load cases and load levels are of interest. In order to avoid misjudgments regarding the importance of the parameters, the dependence of the sensitivities and their normalized value on the load must be taken into account. Furthermore, a workflow for systematically using sensitivities was introduced and demonstrated based on two examples.

Chapter 7

Conclusions and outlook

An essential outcome of this thesis is the method of generalized influence functions. It is based on the close relationship between the influence function approach and adjoint sensitivity analysis. The methodological connection comprises identifying the influence function as part of adjoint sensitivity analysis and the formal equivalence of the influence function technique and adjoint sensitivity analysis. It was already known from the literature that the adjoint variable equates to the influence function. This knowledge was verified and extended by the thesis. In particular, it was shown that examining the entire sensitivity equation - and not just the adjoint variable - is necessary to identify the influence function. The concept of adjoint work was introduced to extend the method of influence functions to non-load parameters. Since the adjoint work is based on variational adjoint sensitivity analysis, an equivalence to the principle of virtual work, which is based on the variational form of the underlying problem, is achieved. Moreover, the adjoint work can be considered as an extension of the work balance of the influence function method. The adjoint work consists of expressions including the influence function, its strain, and energetically conjugated pseudo-quantities. The adjoint work components show contrary dependencies concerning the response and the parameters. Thus, their individual assessment and visualization can provide additional sensitivity information. For example, the influence function and its strain indicate potentially significant zones in a structure regardless of the parameters.

Based on the stated findings, the thesis proposed that the influence function method can be generalized by (i) determining the influence function for different types of responses by the adjoint problem, (ii) considering different types of parameters by the concept of adjoint work, and (iii) visualizing the adjoint work components. The three key concepts were also transferred to steady state heat transfer. However, the method shows shortcomings regarding responses with a dominant explicit parameter dependency $\partial J/\partial s_i$ and specific parameter types (in particular shape parameters). Furthermore, the graphical analysis of the adjoint work components complicates in the case of thin-walled and solid structures. Although the proposed generalization

concept is not equally suitable for all cases, the investigations show that it can be used for many typical structural engineering and design issues. Responses such as stress resultants, local stresses, support forces, or displacements are particularly important. For these responses, the thesis demonstrated that $\partial J/\partial s_i$ is nonexistent or can be merged with the adjoint variable. Hence, the influence function and the other adjoint work components are significant for the final sensitivities, leading the method of generalized influence function to be a promising approach for sensitivity analysis in structural engineering.

The thesis introduced the concept of adjoint work. Furthermore, the usage of the adjoint work components was demonstrated for the qualitative assessment of analysis models. Therefore, a consequent next step is their quantitative application for numerical methods. The internal adjoint work consists of the adjoint strain and the pseudo-stress. The combination of both delivers the derivatives with respect to parameters such as cross-sectional area or thickness, which are required for gradient-based size optimization. In the case of linear responses concerning the state variables, only the pseudo-stress is state-dependent. By using the adjoint strain as a kind of gradient information, size optimization can be performed independently from the applied load. This could be a concept for optimizing structures subjected to many load cases and should be further investigated. Similarly, adjoint strains could also be of interest to determine suitable sensor locations on existing structures, which is essential for model updating to create a digital twin. Suppose the case that the suitability of location A for placing a strain gauge to detect stiffness changes (e.g., due to degradation or cracks) at location B needs to be investigated. The strain at A is chosen as the response. Comparable low adjoint strains at B indicate that the sensitivity concerning a stiffness-related parameter (e.g., Young's modulus) will also be low there. Thus, A would not be a reliable sensor location. Exploring this idea could be another promising area for future research related to the method of generalized influence functions.

The second methodological focus of the thesis was the extension of sensitivity analysis for sequenced simulation processes. Two approaches from the literature were used to initialize the model for subsequent analysis stages. These apply either initial displacements or stresses to retain the state of the previous analysis. The major challenge concerning sensitivity analysis is that the initialization quantities are determined based on the parameter-dependent state variables of the previous stage. Hence, considering all parameter dependencies in the sensitivity analysis is crucial. In the thesis, the sensitivity equations were determined for the pure restart of an analysis, construction stage analysis, and the design process of lightweight structures. The derived expressions of the analyzed cases consistently show that considerable computational effort is necessary to solve them. This is the main challenge with sensitivity analyses based on sequenced simulation processes. Hence, the sensitivity analyses examined are only suitable to a limited extent for structures for which the primary analysis is already very costly. One example is the construction stage analysis of three-dimensional high-fidelity models of high-rise buildings. The value of the presented methods can rather be seen for preliminary investigations of these structures based on less extensive

models. This was demonstrated for an idealized multi-story building. The properties of the different modeling approaches could be investigated in detail by comparing the sensitivities of a total building model and a construction stage model. Furthermore, the presented sensitivity analysis is of interest for structures that are complex in their construction process and structural behavior but have only a moderate number of degrees of freedom and parameters of interest. In addition to the high computational costs required to carry out sensitivity analyses, the implementation effort in a finite element code is a further significant difficulty. Complex process and data structures are required to consider the additional partial derivatives of the response and the residual equation and to transfer sensitivity information from one analysis stage to the next.
The work focused on exploring the fundamentals for extending sensitivity analysis for sequenced simulation processes and identifying associated challenges. This was achieved by deriving and demonstrating the basic sensitivity equations based on comprehensive academic examples. Thus, the next step is to further develop the investigated fundamentals for larger-scale structures. In this context, it is essential to investigate how the computational costs can be reduced.

Finally, the thesis demonstrated the usage of sensitivity analysis for structural engineering and design. Application-oriented aspects such as normalization, graphical processing, and the load-dependency of sensitivities were examined. Furthermore, a systematic analysis and decision chain for using sensitivities in structural design was introduced and demonstrated exemplarily. The workflow is not intended to be prescriptive and entirely fitting for all applications, models, and design scenarios. Instead, the decision and analysis chain should be understood as a systematized synthesis of aspects that could be important for dealing with model parameters.
Among the structures considered in the thesis, the rooftop example highlighted the benefit of computational sensitivity analysis in structural design. The most critical support settlements for the design quantities were purposefully identified and applied accordingly in the partial safety factor concept. In principle, information regarding the influence of the support settlements could also be obtained by classical parameter studies, i.e., by repeated analysis with a different moved support each time. However, in addition to the tremendous effort, there is a risk that relevant support settlements are overlooked and thus not further considered. This risk can be reduced by adjoint sensitivity analysis since all supports can be systematically considered. In addition, the graphically prepared sensitivities allow a quick overview and can be a helpful auxiliary way to document and communicate decisions during structural design.
In order to further increase the acceptance of sensitivity analysis in daily structural engineering, future work should focus on real-world examples. A portfolio of examples with individual challenges in structural design, similar to the shown rooftop, should be collected. On this basis, the proposed analysis and decision chain can be tested and refined, and the overall benefit of sensitivity analysis in structural engineering and design can be demonstrated.

Appendix **A**

Description of analyzed structures

A.1 Cable net bridge

The observed cable net bridge shown in Figure A.1 is a real-world structure planned by the engineering office *Breinlinger Ingenieure*. The bridge crosses the Danube (Donau) river by Inzigkofen in Southwest Germany with a span of 45 m. The flexible bridge shows deformations up to 0.25 m through regular pedestrian loading. Hence, geometric non-linear analysis has to be utilized. The behavior of the bridge during load increase is thoroughly studied in Fußeder et al. [65]. The cable net can be crossed by a steel grid pavement supported by the two central bearer cables. The cables are made of steel with a Young's modulus of 160 000 MN/m^2 and different diameters, whereas the central bearer cables have a diameter of 24 mm. For structural analysis, the bridge is subjected to prestress (defined by form-finding, varying among cables), self-weight, and a uniform line load of $p_z = 0.9$ kN/m applied to the central bearer cables (cf. Figure A.1, right).

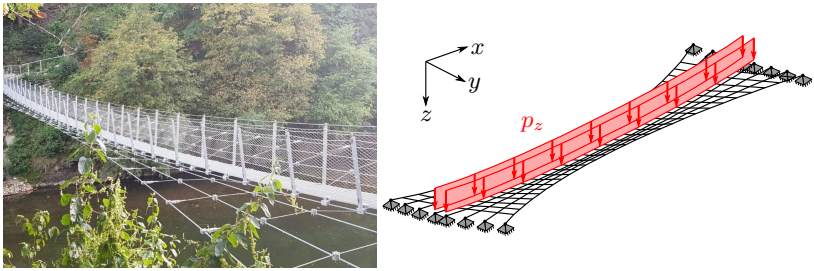

Figure A.1: Photo of cable net bridge taken from Breinlinger Ingenieure [28] and its analysis model. Adapted from Fußeder et al. [65].

A.2 Four-point sail membrane structure

The observed structure is a four-point sail membrane shaped like a hyperbolic paraboloid (hypar). The structure has a base area of 6×6 m and a height of 3 m and is shown in Figure A.2.

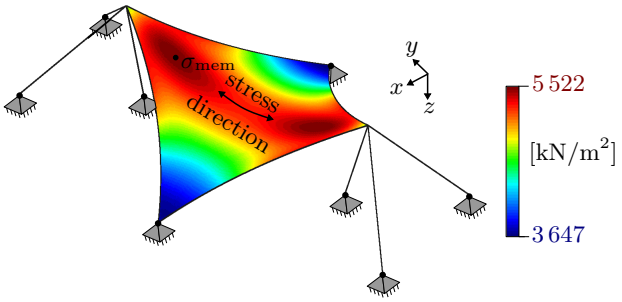

Figure A.2: Observed membrane structure with the shape of a hyperbolic paraboloid. The plot shows the Cauchy stress distribution in the direction pointing between the high points of the sail.

The membrane and its edge cables are fixed at the low points. At the high points, the structure is supported by elastic trusses braced by prestressed cables. The Updated Reference Strategy by Bletzinger et al. [24] is used for form-finding. Therefore, an isotropic prestressing for the membrane of 4.0 kN/m and an edge cable force of 40 kN is utilized. The membrane with a thickness of 1 mm is modeled with a linear elastic isotropic material law defined by a Young's modulus of E=600 kN/m (pre-integrated over the thickness) and a Poisson's ratio of ν=0.4. In addition, a stress-strain tensor modification is applied as described in Nakashino et al. [116] based on the tension field theory to incorporate wrinkle deformation due to tension loss in the membrane. The edge and support cables have a Young's modulus of 205 000 MN/m^2 and a diameter of 12 mm. For structural analysis, the hypar is subjected to prestress and a uniformly distributed snow load acting in the positive z-direction. Figure A.2 shows the Cauchy stress distribution in the direction pointing between the high points of the sail under a snow load of 0.5 kN/m^2. The position of the maximal stress is indicated by σ_{mem}.

A.3 Steel arch bridge

The observed arch-type bridge shown in Figure A.3 is based on the construction presented by Krapf [95]. The pedestrian and bicycle bridge crosses the Neckar and connects the Stuttgart districts of Mühlhausen and Hofen. The construction is a steel arch bridge with a suspended composite deck. For the sake of simplicity, not the entire bridge deck is modeled. Instead, only the steel substructure is considered. The components included in the analysis model have the following properties:

- The arch spans 79.2 m and is designed as a steel box girder with a width/height of 60/55 cm (crown) and 1.6/1.0 m (abutment).
- The box-shaped main girder is made of steel, has a constant height of 40 cm, and a variable width of 1.5 to 3.25 m.
- The box-shaped transverse girders are made of steel, have a height of 30 to 40 cm, a width of 30 cm, and are arranged at a distance of 7.20 m.
- The main girder and the arch abutment are connected by a tension chord consisting of two 70 mm thick steel cables.
- The bridge deck is suspended on 35 mm thick steel cables attached between the arch and the transverse girder.
- A Young's modulus of 210 000 MN/m^2 is selected for all steel parts. The specific weight is 0.0785 MN/m^3.

The bridge is stressed by self-weight and a traffic load of Q =0.01 MN/m.

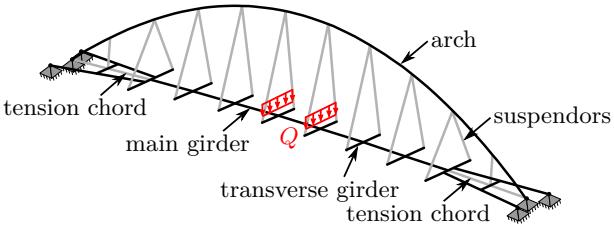

Figure A.3: Static system of an arch-type bridge. Beam elements are colored in black and cable elements in gray.

A.4 Wooden roof construction

A top view of the roof construction is shown in Figure A.4. The bearing structure is a girder grid that consists of wooden beams in combination with single steel and concrete girders. The different girder types and a sketch of their cross-sections are indicated by different colors in Figure A.4.

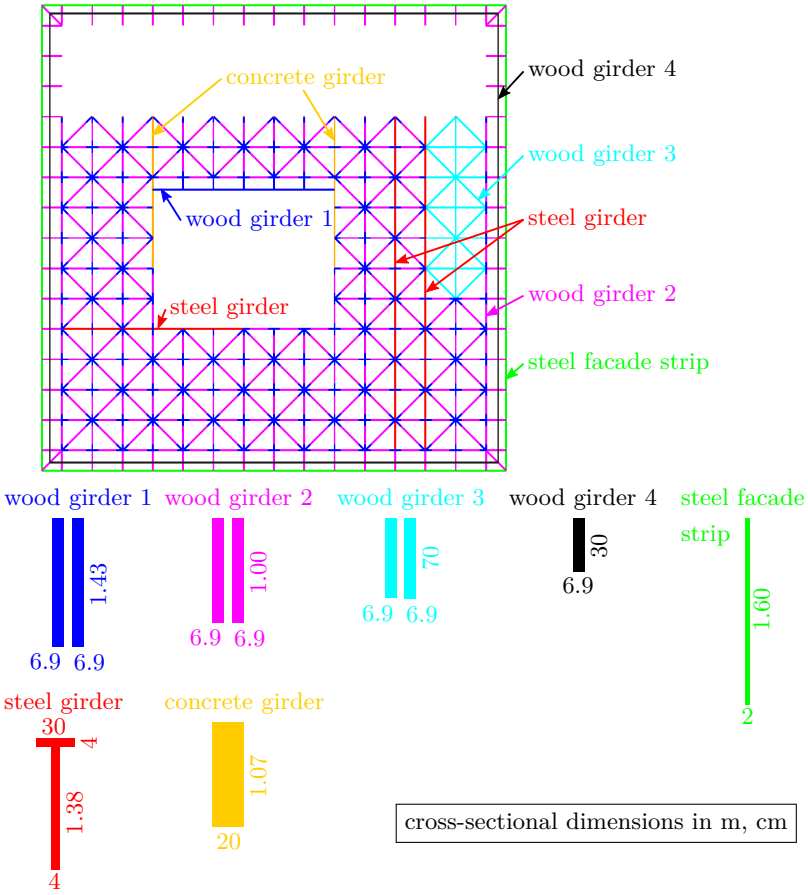

Figure A.4: Overview of the utilized girder cross-sections in a roof construction.

The grid is planked with a 0.057 m thick wood cladding, which is modeled with an orthotropic material law to account for the different properties of wood regarding the fiber direction. All wood members are made of glued laminated timber *GL 32 c*, the steel girders of *S355*, and the concrete girders

of *C30/37*. The properties of the construction material are chosen according to the respective standards.
The structure is stressed by different load cases, which are illustrated in Figure A.5. The permanent action consists of the self-weight of the construction members and additional load due to finishes (e.g., technical facility equipment or ceiling liners). The actions from finishes are considered by uniform surface loads (different at the outer balcony area) and point loads. The latter consider connecting constructions, which are applied at the connection nodes of the steel facade segments (blue points in Figure A.5) and the connection nodes of the girder grid members (5 kN each, not shown in Figure A.5 for clarity). The variable action consists of snow and wind.

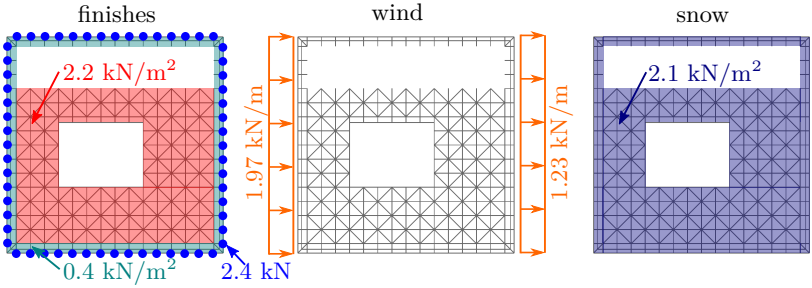

Figure A.5: Load cases applied to the roof construction. The given magnitudes are characteristic values.

Appendix **B**

Structural elements

B.1 Euler-Bernoulli beam

The Euler-Bernoulli beam theory neglects shear deformations of the cross-section. Therefore, the theory assumes that initially straight lines perpendicular to the beam's center line remain straight during deformation and stay perpendicular to the deformed center line. Due to this assumption, the rotation angle φ of the cross-section can be related to the derivative of the vertical bending deformation w:

$$\varphi = -w' \tag{B.1}$$

The curvature κ of the bending deformation

$$\kappa = \frac{d\varphi}{dx} = -w'' \tag{B.2}$$

can be used to calculate the bending moment M by Hooke's law

$$M = EI\kappa \tag{B.3}$$

where EI is the bending stiffness consisting of Young's modulus E and second moment of inertia I. The differential equation for a beam is

$$\left(EIw''\right)'' = p \tag{B.4}$$

where p is a distributed load acting along the beam. The corresponding weak form for a two-sided clamped beam reads:

$$\begin{aligned} &A(w, \delta w) = a(w, \delta w) - F(\delta w) = 0 \quad \text{with} \\ &a(w, \delta w) = \int_0^l EIw'' \cdot \delta w''\, dx \quad \text{and} \quad F(\delta w) = \int_0^l p \cdot \delta w\, dx \end{aligned} \tag{B.5}$$

B.2 Geometrically non-linear truss

Based on the reference length L and actual length l of a truss element, the Green-Lagrange strain reads:

$$\epsilon_{\mathrm{GL}} = \frac{1}{2}\frac{l^2 - L^2}{L^2} \tag{B.6}$$

The energetically conjugated Second Piola-Kirchhoff stress can be determined by the Saint Venant-Kirchhoff material model as

$$\sigma_{\mathrm{PK2}} = E \cdot \epsilon_{\mathrm{GL}} \tag{B.7}$$

where E is the Young's modulus. Based on the Green-Lagrange strain and the Second Piola-Kirchhoff stress, the variational form can be formulated as

$$\begin{aligned} A(\boldsymbol{u}; \delta\boldsymbol{u}) &= a(\boldsymbol{u}; \delta\boldsymbol{u}) - \boldsymbol{P}^T \delta\boldsymbol{u} = 0 \quad \text{with} \\ a(\boldsymbol{u}; \delta\boldsymbol{u}) &= \int_{\Omega_0} \sigma_{\mathrm{PK2}} \cdot \frac{\partial \epsilon_{\mathrm{GL}}}{\partial \boldsymbol{u}} \delta\boldsymbol{u} \, d\Omega_0 \end{aligned} \tag{B.8}$$

where $\boldsymbol{P}$ denotes point forces applied at the end-points of the truss and $\Omega_0 = A \cdot L$ is the reference truss domain with cross-section A. Since the strain and stress are constant along the truss, Equation (B.8) simplifies to

$$\begin{aligned} A(\boldsymbol{u}; \delta\boldsymbol{u}) &= AL \cdot \sigma_{\mathrm{PK2}} \cdot \frac{\partial \epsilon_{\mathrm{GL}}}{\partial l} \left[\frac{\partial l}{\partial \boldsymbol{u}}\right]^T \delta\boldsymbol{u} - \boldsymbol{P}^T \delta\boldsymbol{u} \\ &= \delta\boldsymbol{u}^T \left(A \cdot \frac{l}{L} \cdot \sigma_{\mathrm{PK2}} \cdot \frac{\partial l}{\partial \boldsymbol{u}} - \boldsymbol{P} \right) = \delta\boldsymbol{u}^T \boldsymbol{r} \end{aligned} \tag{B.9}$$

where the vector of unbalanced forces

$$\boldsymbol{r} = \boldsymbol{f}_{\mathrm{int}} - \boldsymbol{f}_{\mathrm{ext}} = A\frac{l}{L}\sigma_{\mathrm{PK2}}\frac{\partial l}{\partial \boldsymbol{u}} - \boldsymbol{P} \tag{B.10}$$

consisting of internal forces $\boldsymbol{f}_{\mathrm{int}}$ and external forces $\boldsymbol{f}_{\mathrm{ext}}$ can be identified. Please note that nodal forces are typically not treated as element quantities in a finite element formulation. Hence, the elemental residual equation (denoted by index e) consists merely of the internal force vector:

$$\boldsymbol{r}^e = \boldsymbol{f}^e_{\mathrm{int}} = A \cdot \frac{l}{L} \cdot \sigma_{\mathrm{PK2}} \cdot \frac{\partial l}{\partial \boldsymbol{u}} \tag{B.11}$$

B.3 Prestressed membrane

The considered membrane element is assumed to be extremely thin with negligible bending resistance. To withstand out-of-plane loading, the membrane is prestressed. Due to this assumptions, the PK2 stress tensor $\boldsymbol{S}$ reduces to the in-plane normal stresses S^{11}, S^{22} and the in-plane shear stresses $S^{12} = S^{21}$ which are composed of elastic stress $\boldsymbol{S}_{\mathrm{el}}$ and prestress $\boldsymbol{S}_0$. As a constant and deformation-independent thickness t is assumed, the stresses can be pre-integrated. Hence, the PK2 stress resultants read

$$\boldsymbol{n} = \boldsymbol{n}_{\mathrm{el}} + \boldsymbol{n}_0 = t \cdot \begin{bmatrix} S^{11}_{\mathrm{el}} \\ S^{11}_{\mathrm{el}} \\ S^{12}_{\mathrm{el}} \end{bmatrix} + t \cdot \begin{bmatrix} S^{11}_{0} \\ S^{11}_{0} \\ S^{12}_{0} \end{bmatrix} \tag{B.12}$$

in Voigt notation. The elastic PK2 stress resultants can be related to the Green-Lagrange strains $\boldsymbol{E} = \boldsymbol{\epsilon}$ by the constitutive equation. By consideration of isotropic material and strains that are given in a local Cartesian basis (further denoted by $\bar{\bullet}$), the PK2 stress resultants read

$$\bar{\boldsymbol{n}}_{\mathrm{el}} = \begin{bmatrix} \bar{n}^{11}_{\mathrm{el}} \\ \bar{n}^{22}_{\mathrm{el}} \\ \bar{n}^{12}_{\mathrm{el}} \end{bmatrix} = t \cdot \bar{\boldsymbol{C}}^{\mathrm{iso}} \cdot \begin{bmatrix} \bar{\epsilon}_{11} \\ \bar{\epsilon}_{22} \\ 2\bar{\epsilon}_{12} \end{bmatrix} = t \cdot \bar{\boldsymbol{C}}^{\mathrm{iso}} \cdot \bar{\boldsymbol{\epsilon}} \tag{B.13}$$

where

$$\bar{\boldsymbol{C}}^{\mathrm{iso}} = \frac{E}{1-\nu^2} \begin{bmatrix} 1 & \nu & 0 \\ \nu & 1 & 0 \\ 0 & 0 & \dfrac{1-\nu}{2} \end{bmatrix} \tag{B.14}$$

is the material matrix. Based on those definitions, the weak form is

$$A(\boldsymbol{u}; \delta\boldsymbol{u}) = a(\boldsymbol{u}; \delta\boldsymbol{u}) - F(\boldsymbol{u}; \delta\boldsymbol{u}) = 0 \quad \text{with} \tag{B.15a}$$

$$a(\boldsymbol{u}; \delta\boldsymbol{u}) = \int_{A_0} (\bar{\boldsymbol{n}}_{\mathrm{el}} + \bar{\boldsymbol{n}}_0) : \frac{\partial \bar{\boldsymbol{\epsilon}}}{\partial \boldsymbol{u}} \delta\boldsymbol{u} \, dA_0 \quad \text{and} \tag{B.15b}$$

$$F(\boldsymbol{u}; \delta\boldsymbol{u}) = \int_{A_0} \boldsymbol{p}_0 \cdot \delta\boldsymbol{u} \, dA_0 + \int_{\Gamma_{N0}} \hat{\boldsymbol{t}}_0 \cdot \delta\boldsymbol{u} \, d\Gamma_{N0} \tag{B.15c}$$

where A_0 is the membrane's reference surface with the Neumann boundary edges $d\Gamma_{N0}$. The membrane is loaded by an external load $\boldsymbol{p}_0$ on the surface and an external load $\hat{\boldsymbol{t}}_0$ on the edges. For further reading on the membrane theory, refer to Bischoff et al. [20] and Philipp et al. [117].

Bibliography

[1] R. A. Adams and J. J. F. Fournier. *Sobolev spaces*. Pure and Applied Mathematics. Oxford: Elsevier, 2003. ISBN: 9780120441433.

[2] H. M. Adelman and R. T. Haftka, eds. *Sensitivity Analysis in Engineering*. NASA-CP-2457, Proceedings of the NASA Symposium. Hampton, VA: NASA Langley Research Center, Sept. 1986.

[3] H. M. Adelman and R. T. Haftka. "Sensitivity Analysis of Discrete Structural Systems". In: *AIAA Journal* 24.5 (1986), pp. 823–832. DOI: https://doi.org/10.2514/3.48671.

[4] F. N. Airaudo, R. Löhner, R. Wüchner, and H. Antil. "Adjoint-based determination of weaknesses in structures". In: *Computer Methods in Applied Mechanics and Engineering* 417 (2023), p. 116471. DOI: https://doi.org/10.1016/j.cma.2023.116471.

[5] I. Antonau, S. Warnakulasuriya, K.-U. Bletzinger, F. M. Bluhm, M. Hojjat, and R. Wüchner. "Latest developments in node-based shape optimization using Vertex Morphing parameterization". In: *Structural and Multidisciplinary Optimization* 65.7 (2022), p. 198. DOI: 10.1007/s00158-022-03279-w.

[6] J. S. Arora. "An exposition of the material derivative approach for structural shape sensitivity analysis". In: *Computer Methods in Applied Mechanics and Engineering* 105.1 (1993), pp. 41–62. DOI: https://doi.org/10.1016/0045-7825(93)90115-E.

[7] J. S. Arora and E. J. Haug. "Methods of Design Sensitivity Analysis in Structural Optimization". In: *AIAA Journal* 17.9 (1979), pp. 970–974. DOI: 10.2514/3.61260.

[8] C. Balaji. *Essentials of Radiation Heat Transfer*. Springer International Publishing, 2021. ISBN: 978-3-030-62616-7. DOI: 10.1007/978-3-030-62617-4.

[9] F.-J. Barthold. "Zur Kontinuumsmechanik inverser Geometrieprobleme". Habilitation, Braunschweiger Schriften zur Mechanik 44-2002. TU Braunschweig, 2002. DOI: http://dx.doi.org/10.17877/DE290R-13502.

[10] F.-J. Barthold and E. Stein. "A continuum mechanical-based formulation of the variational sensitivity analysis in structural optimization. Part I: analysis". In: *Structural Optimization* 11 (1996), pp. 29–42. DOI: https://doi.org/10.1007/BF01279652.

[11] Y. Başar and D. Weichert. *Nonlinear Continuum Mechanics of Solids*. Springer Berlin Heidelberg, 2000. DOI: 10.1007/978-3-662-04299-1.

[12] K.-J. Bathe. *Finite element procedures in engineering analysis*. Englewood Cliffs, New Jersey: Prentice-Hall, 1982. ISBN: 0-13-317305-4.

[13] A. M. Bauer. "CAD-Integrated Isogeometic Analysis and Design of Lightweight Structures". Ph.D. Thesis. Munich: Technical University of Munich, 2020.

[14] A. D. Belegundu. "Interpreting Adjoint Equations in Structural Optimization". In: *Journal of Structural Engineering* 112.8 (1986), pp. 1971–1976. DOI: 10.1061/(ASCE)0733-9445(1986)112:8(1971).

[15] A. D. Belegundu. "Lagrangian Approach to Design Sensitivity Analysis". In: *Journal of Engineering Mechanics* 111.5 (1985), pp. 680–695. DOI: 10.1061/(ASCE)0733-9399(1985)111:5(680).

[16] A. D. Belegundu. "Müller-Breslau's Principle in Adjoint Design Sensitivity Analysis". In: *Mechanics of Structures and Machines* 17.3 (1989), pp. 333–347. DOI: 10.1080/089054508915645.

[17] A. D. Belegundu. "The adjoint method for determining influence lines". In: *Computers & Structures* 29.2 (1988), pp. 345–350. DOI: https://doi.org/10.1016/0045-7949(88)90269-6.

[18] T. Belytschko, W. K. Liu, B. Moran, and K. I. Elkhodary. *Nonlinear finite elements for continua and structures*. 2nd ed. West Sussex: John Wiley and Sons, 2014. ISBN: 978-1-118-63270-3.

[19] C. H. Bischof, H. M. Bücker, B. Lang, A. Rasch, and J. W. Risch. "Extending the functionality of the general-purpose finite element package SEPRAN by automatic differentiation". In: *International Journal for Numerical Methods in Engineering* 58.14 (2003), pp. 2225–2238. DOI: https://doi.org/10.1002/nme.942.

[20] M. Bischoff, K.-U. Bletzinger, W. A. Wall, and E. Ramm. "Models and Finite Elements for Thin-Walled Structures". In: *Encyclopedia of Computational Mechanics*. Ed. by E. Stein, R. de Borst, and T. J. R. Hughes. John Wiley & Sons, Ltd, 2004. ISBN: 9780470091357. DOI: https://doi.org/10.1002/0470091355.ecm026.

[21] M. Bischoff and S. Kimmich. "Computerstatik am Gesamtsystem - Modellierung ohne Grenzen?" In: *Tagungsband Baustatik-Baupraxis 11, Universität Innsbruck / TU Graz* (2011).

[22] M. Bischoff, S. Roth, and F. Geiger. "Ein Baufortschrittsmodell auf der Basis von Verschiebungssteifigkeitsmatrizen". In: *Tagungsband Baustatik-Baupraxis 13, Ruhr-Universität Bochum* (2017).

[23] K.-U. Bletzinger, M. Firl, and F. Daoud. "Approximation of derivatives in semi-analytical structural optimization". In: *Computers & Structures* 86.13 (2008), pp. 1404–1416. DOI: https://doi.org/10.1016/j.compstruc.2007.04.014.

[24] K.-U. Bletzinger and E. Ramm. "A General Finite Element Approach to the form Finding of Tensile Structures by the Updated Reference Strategy". In: *International Journal of Space Structures* 14.2 (1999), pp. 131–145. DOI: 10.1260/0266351991494759.

[25] K.-U. Bletzinger and E. Ramm. "Structural optimization and form finding of light weight structures". In: *Computers & Structures* 79.22 (2001), pp. 2053–2062. DOI: https://doi.org/10.1016/S0045-7949(01)00052-9.

[26] J. Bonet and R. D. Wood. *Nonlinear Continuum Mechanics for Finite Element Analysis*. 2nd ed. Cambridge University Press, 2008. DOI: 10.1017/CBO9780511755446.

[27] R. de Borst, M. A. Crisfield, J. J. C. Remmers, and C. V. Verhoosel. *Non-Linear Finite Element Analysis of Solids and Structures*. John Wiley & Sons, Ltd, 2012. ISBN: 9781118375938. DOI: https://doi.org/10.1002/9781118375938.

[28] Breinlinger Ingenieure. *Donau-Erlebnissteg*. https://www.breinlinger.de/project/donau-erlebnissteg/, visited on 2023-02-10.

[29] A. Cabada. *Green's Functions in the Theory of Ordinary Differential Equations*. New York, NY: Springer New York, 2014. ISBN: 978-1-4614-9505-5. DOI: 10.1007/978-1-4614-9506-2.

[30] D. G. Cacuci, M. Ionescu-Bujor, and I. M. Navon. *Sensitivity and uncertainty analysis, Volume II: Applications to large-scale systems*. Boca Raton: CRC Press, 2005. ISBN: 9780429204562. DOI: https://doi.org/10.1201/9780203483572.

[31] D. G. Cacuci and R. Fang. "Predictive Modeling of a Paradigm Mechanical Cooling Tower: I. Adjoint Sensitivity Model". In: *Energies* 9 (2016), p. 718. DOI: 10.3390/en9090718.

[32] J. B. Cardoso and J. S. Arora. "Variational Method for Design Sensitivity Analysis in Nonlinear Structural Mechanics". In: *AIAA Journal* 26.5 (1988), pp. 595–603. DOI: 10.2514/3.9939.

[33] O. Carl. "Statische und dynamische Sensitivitätsanalysen von geschädigten Tragwerken mit Greenschen Funktionen". Ph.D. Thesis. Siegen: Universität Siegen, 2011.

[34] O. Carl, F. Hartmann, and C. Zhang. "Schnelle Berechnung von Änderungen und Varianten bei komplexen Tragsystemen (3D-Modellen)". In: *Stahlbau* 86.3 (2017), pp. 217–224. DOI: 10.1002/stab.201710468.

[35] G. Cheng and Y. Liu. "A new computation scheme for sensitivity analysis". In: *Engineering Optimization* 12.3 (1987), pp. 219–234. DOI: 10.1080/03052158708941096.

[36] S. Cho and H.-S. Jung. “Design sensitivity analysis and topology optimization of displacement–loaded non-linear structures”. In: *Computer Methods in Applied Mechanics and Engineering* 192.22 (2003), pp. 2539–2553. DOI: https://doi.org/10.1016/S0045-7825(03)00274-3.

[37] C.-K. Choi and E.-D. Kim. “Multistory Frames Under Sequential Gravity Loads”. In: *Journal of Structural Engineering* 111.11 (1985), pp. 2373–2384. DOI: 10.1061/(ASCE)0733-9445(1985)111:11(2373).

[38] K. K. Choi and N.-H. Kim. *Structural Sensitivity Analysis and Optimization 1: Linear Systems*. Mechanical Engineering Series. New York, NY: Springer, 2004. ISBN: 978-0-387-23232-4. DOI: https://doi.org/10.1007/b138709.

[39] H.-S. Chung and J. J. Alonso. “Using gradients to construct response surface models for high-dimensional design optimization problems”. In: *39th Aerospace Sciences Meeting and Exhibit*. Reno, NV, Jan. 2001. DOI: 10.2514/6.2001-922.

[40] F. Cirak. “Adaptive Finite-Element-Methoden bei der nichtlinearen Analyse von Flächentragwerken”. Ph.D. Thesis. Stuttgart: Universität Stuttgart, 1998.

[41] F. Cirak and E. Ramm. “A posteriori error estimation and adaptivity for linear elasticity using the reciprocal theorem”. In: *Computer Methods in Applied Mechanics and Engineering* 156.1 (1998), pp. 351–362. DOI: https://doi.org/10.1016/S0045-7825(97)00220-X.

[42] Comité Européen de Normalisation (CEN). *EN 1990: Eurocode: Basis of structural design (EN 1990:2002 + A1:2005 + A1:2005/AC:2010)*. Brussels, 2002/2010.

[43] P. Dadvand, R. Rossi, M. Gil, X. Martorell, J. Cotela, E. Juanpere, S. R. Idelsohn, and E. Oñate. “Migration of a generic multi-physics framework to HPC environments”. In: *Computers & Fluids* 80 (2013), pp. 301–309. DOI: https://doi.org/10.1016/j.compfluid.2012.02.004.

[44] P. Dadvand, R. Rossi, and E. Oñate. “An Object-oriented Environment for Developing Finite Element Codes for Multi-disciplinary Applications”. In: *Archives of Computational Methods in Engineering* 17.3 (2010), pp. 253–297. DOI: 10.1007/s11831-010-9045-2.

[45] Deutsches Institut für Bautechnik. *Vorschlag für die Fortschreibung „Grundlagen zur Festlegung von Sicherheitsanforderungen für bauliche Anlagen“*. Berlin, 2022. eprint: https://www.dibt.de/fileadmin/dibt-website/Dokumente/Allgemein/Vorschlag_Grusibau_2_0.pdf.

[46] Deutsches Institut für Normung e.V. *Grundlagen zur Festlegung von Sicherheitsanforderungen für bauliche Anlagen*. Berlin, Köln: Beuth, 1981. ISBN: 3-410-11474-2.

[47] F. H. Dieringer. "Numerical Methods for the Design and Analysis of Tensile Structures". Ph.D. Thesis. Munich: Technical University of Munich, 2014.

[48] F. H. Dieringer, B. F. Philipp, R. Wüchner, and K.-U. Bletzinger. "Numerical Methods for the Design and Analysis of Hybrid Structures". In: *International Journal of Space Structures* 28.3-4 (2013), pp. 149–160. DOI: 10.1260/0266-3511.28.3-4.149.

[49] M. Ehre, R. Flock, M. Fußeder, I. Papaioannou, and D. Straub. "Certified Dimension Reduction for Bayesian Updating with the Cross-Entropy Method". In: *SIAM/ASA Journal on Uncertainty Quantification* 11.1 (2023), pp. 358–388. DOI: 10.1137/22M1484031.

[50] B. Ellingwood, T. V. Galambos, J. G. MacGregor, and C. A. Cornell. *Development of a Probability Based Load Criterion for American National Standard A58: Building Code Requirements for Minimum Design Loads in Buildings and Other Structures*. U.S. Department of Commerce, National Bureau of Standards, 1980.

[51] A. Emiroğlu. "Multiphysics Simulation and CAD-Integrated Shape Optimization in Fluid-Structure Interaction". Ph.D. Thesis. Munich: Technical University of Munich, 2019.

[52] A. Emiroğlu, M. Fußeder, R. Wüchner, and K.-U. Bletzinger. "A discrete adjoint approach to the operational eigenvalue sensitivities of nonlinear structural systems". Expected to be submitted in 2024.

[53] R. M. Errico. "What Is an Adjoint Model?" In: *Bulletin of the American Meteorological Society* 78.11 (1997), pp. 2577–2591. DOI: 10.1175/1520-0477(1997)078<2577:WIAAM>2.0.CO;2.

[54] D. Estep, M. Holst, and M. Larson. "Generalized Green's Functions and the Effective Domain of Influence". In: *SIAM Journal on Scientific Computing* 26.4 (2005), pp. 1314–1339. DOI: 10.1137/S1064827502416319.

[55] M. Fastabend, T. Schäfers, M. Albert, and H.-G. Lommen. "Zur sinnvollen Anwendung ganzheitlicher Gebäudemodelle in der Tragwerksplanung von Hochbauten". In: *Beton- und Stahlbetonbau* 104.10 (2009), pp. 657–663. DOI: 10.1002/best.200900022.

[56] C. A. Felippa. *Introduction to Finite Element Methods*. 2016.

[57] F. Fernandez and D. A. Tortorelli. "Semi-analytical sensitivity analysis for nonlinear transient problems". In: *Structural and Multidisciplinary Optimization* 58.6 (2018), pp. 2387–2410. DOI: 10.1007/s00158-018-2096-y.

[58] V. M. Ferrándiz, P. Bucher, R. Zorrilla, R. Rossi, A. Cornejo, S. Warnakulasuriya, J. Cotela, ..., and J. Gárate. *KratosMultiphysics/Kratos: Release 9.4.2*. Version v9.4.2. Oct. 2023. DOI: https://doi.org/10.5281/zenodo.8422380.

[59] M. Firl and K.-U. Bletzinger. “Shape optimization of thin walled structures governed by geometrically nonlinear mechanics”. In: *Computer Methods in Applied Mechanics and Engineering* 237-240 (2012), pp. 107–117. DOI: 10.1016/j.cma.2012.05.016.

[60] J. Fourier. *The Analytical Theory of Heat*. Reprint of Fourier’s 1822 monograph. New York: Dover Publications, Inc., 1955.

[61] M. Fußeder and K.-U. Bletzinger. “Computational Sensitivity Analysis for Construction Stage Models”. In: *Proceedings of the IABSE Symposium, Prague 2022: Challenges for Existing and Oncoming Structures*. Prague, Czech Republic: International Association for Bridge and Structural Engineering (IABSE), 2022. DOI: 10.2749/prague.2022.1676.

[62] M. Fußeder and K.-U. Bletzinger. “Tragwerksplanung - Sensitivitätsanalysen unterstützen die Auslegung statischer Systeme und können Sicherheitsrisiken aufdecken”. In: *Der Prüfingenieur* 59 (2021), pp. 48–55.

[63] M. Fußeder, A. Kodakkal, and K.-U. Bletzinger. “The method of generalized influence functions - a computational engineering tool for sensitivity analysis”. Submitted in 2023 for Lecture Notes in Applied and Computational Mechanics, expected to be published in 2024.

[64] M. Fußeder, M. Teichgräber, D. Straub, and K.-U. Bletzinger. *Schlussbericht des Forschungsprojektes GruSiBau 2.0*. Research report. Deutsches Institut für Bautechnik, 2020.

[65] M. Fußeder, R. Wüchner, and K.-U. Bletzinger. “Computational Sensitivity Analysis in the Design Process of Pre-Stressed Lightweight Structures”. In: *Proceedings of the IASS Annual Symposium 2020/21 and the 7th International Conference on Spatial Structures*. Ed. by S. Behnejad, G. Parke, and O. Samavati. Guilford, UK: International Association for Shell and Spatial Structures (IASS), 2021.

[66] M. Fußeder, R. Wüchner, and K.-U. Bletzinger. “Sensitivitätsanalyse mit verallgemeinerten Einflussfunktionen zur Tragwerksbewertung bei Modellparametervariationen”. In: *Bauingenieur* 96.06 (2021), pp. 191–200. DOI: 10.37544/0005-6650-2021-06-33.

[67] M. Fußeder, R. Wüchner, and K.-U. Bletzinger. “Towards a computational engineering tool for structural sensitivity analysis based on the method of influence functions”. In: *Engineering Structures* 265 (2022), p. 114402. DOI: https://doi.org/10.1016/j.engstruct.2022.114402.

[68] A. Geiser, I. Antonau, and K.-U. Bletzinger. “Aggregated formulation of geometric constraints for node-based shape optimization with vertex morphing”. In: *Proceedings of the 14th International Conference on Evolutionary and Deterministic Methods for Design, Optimization and Control*. Ed. by N. Gauger, K. Giannakoglou, M. Papadrakakis, and J. Periaux. Eccomas Proceedia, 2021, pp. 80–94. DOI: 10.7712/140121.7952.18383.

[69] A. Ghali and A. M. Neville. *Structural Analysis: A Unified Classical and Matrix Approach, Seventh Edition*. Boca Raton: CRC Press, 2017. ISBN: 9781498725064.

[70] M. B. Giles and N. A. Pierce. "Adjoint equations in CFD: duality, boundary conditions and solution behaviour". In: *Proceedings of the 13th Computational Fluid Dynamics Conference*. 1997. DOI: 10.2514/6.1997-1850.

[71] M. B. Giles and N. A. Pierce. "An Introduction to the Adjoint Approach to Design". In: *Flow, Turbulence and Combustion* 65.3 (2000), pp. 393–415. DOI: 10.1023/A:1011430410075.

[72] A.-K. Goldbach. "The CAD-Integrated Design Cycle for Structural Membranes". Ph.D. Thesis. Munich: Technical University of Munich, 2021.

[73] T. Grätsch. "L_2–Statik Eine auf dem Skalarprodukt basierende Darstellung der modernen Statik unter besonderer Betrachtung der Methode der finiten Elemente". Ph.D. Thesis. Kassel: Universität Kassel, 2002.

[74] T. Grätsch and K.-J. Bathe. "Influence functions and goal-oriented error estimation for finite element analysis of shell structures". In: *International Journal for Numerical Methods in Engineering* 63.5 (2005), pp. 709–736. DOI: 10.1002/nme.1298.

[75] T. Grätsch and F. Hartmann. "Finite element recovery techniques for local quantities of linear problems using fundamental solutions". In: *Computational Mechanics* 33 (2003), pp. 15–21. DOI: 10.1007/s00466-003-0478-4.

[76] T. Grätsch and F. Hartmann. "Pointwise error estimation and adaptivity for the finite element method using fundamental solutions". In: *Computational Mechanics* 37 (2006), pp. 394–407. DOI: 10.1007/s00466-005-0711-4.

[77] T. Grätsch, F. Hartmann, and C. Katz. "Einflussfunktionen und finite Elemente". In: *Bauingenieur* 78 (2003), pp. 489–497.

[78] F. Guhr and F.-J. Barthold. "Variational sensitivity analysis and shape optimisation applied to a non-local, ductile damage model". In: *Computational Mechanics* 73 (2024), pp. 507–531. DOI: 10.1007/s00466-023-02377-w.

[79] H. Gulvanessian, J.-A. Calgaro, and M. Holický. *Designers' Guide to Eurocode: Basis of Structural Design: EN 1990*. Second edition. ICE Publishing, 2012. DOI: 10.1680/bsd.41714.

[80] R. T. Haftka and H. M. Adelman. "Recent developments in structural sensitivity analysis". In: *Structural optimization* 1.3 (1989), pp. 137–151. DOI: 10.1007/BF01637334.

[81] F. Hartmann. *Green's Functions and Finite Elements*. Berlin, Heidelberg: Springer, 2013. ISBN: 978-3-642-29522-5. DOI: 10.1007/978-3-642-29523-2.

[82] F. Hartmann and P. Jahn. *Statics and Influence Functions – From a Modern Perspective, Second Edition*. Cham: Springer, 2021. ISBN: 978-3-030-55888-8. DOI: 10.1007/978-3-030-55889-5.

[83] F. Hartmann and T. Kunow. "Sensitivity Analysis of Computer Models of Structures with Green's Functions". In: *Proceedings of the Ninth International Conference on Computational Structures Technology*. Ed. by B. H. V. Topping and M. Papadrakakis. Kippen: Civil-Comp Press, 2008. ISBN: 978-1-905088-23-2.

[84] E. J. Haug and J. S. Arora. "Design sensitivity analysis of elastic mechanical systems". In: *Computer Methods in Applied Mechanics and Engineering* 15.1 (1978), pp. 35–62. DOI: https://doi.org/10.1016/0045-7825(78)90004-X.

[85] E. J. Haug, K. K. Choi, and V. Komkov. *Design sensitivity analysis of structural systems 1st Edition*. Mathematics in science and engineering. Orlando: Academic Press, 1986. ISBN: 9780080960005.

[86] P. Heimbach and V. Bugnion. "Greenland ice-sheet volume sensitivity to basal, surface and initial conditions derived from an adjoint model". In: *Annals of Glaciology* 50.52 (2009), pp. 67–80. DOI: 10.3189/172756409789624256.

[87] C. Henning and T. Ricken. "Transition of the variational sensitivity analysis to polymorphic uncertainty quantification to soil investigations". In: *Advances in Engineering Materials, Structures and Systems: Innovations, Mechanics and Applications*. Ed. by A. Zingoni. CRC Press, 2019, pp. 297–301. ISBN: 9780429426506. DOI: 10.1201/9780429426506-51.

[88] R. Hertle. "Über konstruktive Fehler spricht man nicht - oder doch? Forensic Engineering: eine (noch) verkannte Disziplin". In: *Der Prüfingenieur* 63 (2023), pp. 55–62.

[89] M. Hohenbichler and R. Rackwitz. "Sensitivity and importance measures in structural reliability". In: *Civil Engineering Systems* 3.4 (1986), pp. 203–209. DOI: 10.1080/02630258608970445.

[90] G. Holzapfel. *Nonlinear Solid Mechanics - A Continuum Approach for Engineering*. Chichester: John Wiley & Sons, Inc, 2000. ISBN: 978-0-471-82319-3.

[91] H.-C. Huang and A. S. Usmani. *Finite element analysis for heat transfer: theory and software*. London: Springer, 1994. DOI: 10.1007/978-1-4471-2091-9.

[92] B. Iooss and P. Lemaître. "A Review on Global Sensitivity Analysis Methods". In: *Uncertainty Management in Simulation-Optimization of Complex Systems*. Ed. by G. Dellino and C. Meloni. Vol. 59. Operations Research/Computer Science Interfaces Series. Boston, MA: Springer, 2015, pp. 101–122. ISBN: 978-1-4899-7547-8. DOI: 10.1007/978-1-4899-7547-8_5.

[93] H. J. Kelley. “Method of Gradients”. In: *Optimization Techniques*. Ed. by G. Leitmann. Vol. 5. Mathematics in Science and Engineering. Elsevier, 1962, pp. 205–254. DOI: https://doi.org/10.1016/S0076-5392(08)62094-9.

[94] J. M. Kiendl. “Isogeometric Analysis and Shape Optimal Design of Shell Structures”. Ph.D. Thesis. Munich: Technical University of Munich, 2011.

[95] A. Krapf. “Neckarsteg Stuttgart - Eine filigrane Stahlbogenbrücke mit Verbundüberbau für Fußgänger und LKW-Verkehr”. In: *Tagungsband Baustatik-Baupraxis 11, Universität Innsbruck / TU Graz* (2011).

[96] S. Krenk. *Non-linear Modeling and Analysis of Solids and Structures*. Cambridge University Press, 2009. DOI: 10.1017/CBO9780511812163.

[97] T. Kunow. “Modellfehler und Greensche Funktionen in der Statik”. Ph.D. Thesis. Kassel: Universität Kassel, 2008.

[98] O. Kurc and A. Lulec. “A comparative study on different analysis approaches for estimating the axial loads on columns and structural walls at tall buildings”. In: *The Structural Design of Tall and Special Buildings* 22.6 (2013), pp. 485–499. DOI: 10.1002/tal.699.

[99] T. M. Laggner, D. Schlicke, N. V. Tue, and W.-D. Denk. “Statische Analyse mit linear elastischen 3D–Gebäudemodellen”. In: *Beton- und Stahlbetonbau* 116.5 (2021), pp. 360–369. DOI: 10.1002/best.202000055.

[100] J. Liedmann and F.-J. Barthold. “Variational sensitivity analysis of elastoplastic structures applied to optimal shape of specimens”. In: *Structural and Multidisciplinary Optimization* 61.6 (2020), pp. 2237–2251. DOI: 10.1007/s00158-020-02492-9.

[101] J. H. Lienhard IV and J. H. Lienhard V. *A Heat Transfer Textbook, Fifth Edition*. Version 5.10. Cambridge, MA: Phlogiston Press, 2020.

[102] J. Linhard and K.-U. Bletzinger. ““Tracing” the Equilibrium – Recent Advances in Numerical Form Finding”. In: *International Journal of Space Structures* 25.2 (2010), pp. 107–116. DOI: 10.1260/0266-3511.25.2.107.

[103] G.-R. Liu and S. S. Quek. *The finite element method: a practical course*. Oxford: Butterworth-Heinemann, 2014. ISBN: 978-0-08-098356-1. DOI: https://doi.org/10.1016/C2012-0-00779-X.

[104] J. G. Löwenstein. “Bauen unter Gravitation”. In: *Tagungsband Baustatik-Baupraxis 13, Ruhr-Universität Bochum* (2017).

[105] J. G. Löwenstein. “Bauen unter Gravitation - Verformungsausgleich im Baufortschritt”. In: *mb AEC Software GmbH: mb-news 4* (2014), pp. 14–19.

[106] Z. Luo, X. Wang, and D. Liu. "Prediction on the static response of structures with large-scale uncertain-but-bounded parameters based on the adjoint sensitivity analysis". In: *Structural and Multidisciplinary Optimization* 61.1 (2020), pp. 123–139. DOI: 10.1007/s00158-019-02349-w.

[107] P. Marti. *Baustatik: Grundlagen - Stabtragwerke - Flächentragwerke*. Ernst und Sohn Verlag, 2012. ISBN: 9783433601068. DOI: 10.1002/9783433601068.

[108] H. Masching. "Parameter Free Optimization of Shape Adaptive Shell Structures". Ph.D. Thesis. Munich: Technical University of Munich, 2016.

[109] H. Masching and K.-U. Bletzinger. "Parameter free structural optimization applied to the shape optimization of smart structures". In: *Finite Elements in Analysis and Design* 111 (2016), pp. 33–45. DOI: 10.1016/j.finel.2015.12.008.

[110] D. Materna. "Structural and Sensitivity Analysis for the Primal and Dual Problems in the Physical and Material Spaces". Ph.D. Thesis. Dortmund: TU Dortmund University, 2009.

[111] Y. A. Melnikov. *Influence functions and matrices*. New York: Routledge, 2017. ISBN: 9780203750889. DOI: https://doi.org/10.1201/9780203750889.

[112] A. Michalski. "Simulation leichter Flächentragwerke in einer numerisch generierten atmosphärischen Grenzschicht". Ph.D. Thesis. Munich: Technical University of Munich, 2010.

[113] Z. Milka. "Finite element solution of a stationary heat conduction equation with the radiation boundary condition". In: *Applications of Mathematics* 38.1 (1993), pp. 67–79.

[114] D. P. Mok, W. A. Wall, M. Bischoff, and E. Ramm. "Algorithmic aspects of deformation dependent loads in non–linear static finite element analysis". In: *Engineering Computations* 16.5 (1999), pp. 601–618. DOI: 10.1108/02644409910277951.

[115] J. E. Mottershead, M. Link, and M. I. Friswell. "The sensitivity method in finite element model updating: A tutorial". In: *Mechanical Systems and Signal Processing* 25.7 (2011), pp. 2275–2296. DOI: https://doi.org/10.1016/j.ymssp.2010.10.012.

[116] K. Nakashino and M. C. Natori. "Efficient Modification Scheme of Stress-Strain Tensor for Wrinkled Membranes". In: *AIAA Journal* 43.1 (2005), pp. 206–215. DOI: 10.2514/1.7143.

[117] B. F. Philipp, M. Breitenberger, I. D'Auria, R. Wüchner, and K.-U. Bletzinger. "Integrated design and analysis of structural membranes using the Isogeometric B-Rep Analysis". In: *Computer Methods in Applied Mechanics and Engineering* 303 (2016), pp. 312–340. DOI: https://doi.org/10.1016/j.cma.2016.02.003.

[118] B. F. Philipp. "Methodological Treatment of Non-linear Structural Behavior in the Design, Analysis and Verification of Lightweight Structures". Ph.D. Thesis. Munich: Technical University of Munich, 2017.

[119] N. A. Pierce and M. B. Giles. "Adjoint Recovery of Superconvergent Functionals from PDE Approximations". In: *SIAM Review* 42.2 (2000), pp. 247–264. DOI: 10.1137/S0036144598349423.

[120] M. J. Poldneff, I. S. Rai, and J. S. Arora. "Design variations of nonlinear elastic structures subjected to follower forces". In: *Computer Methods in Applied Mechanics and Engineering* 110.3 (1993), pp. 211–219. DOI: https://doi.org/10.1016/0045-7825(93)90161-P.

[121] M. J. Poldneff, I. S. Rai, and J. S. Arora. "Implementation of design sensitivity analysis for nonlinear elastic structures". In: *AIAA Journal* 31.11 (1993), pp. 2137–2142. DOI: 10.2514/3.11901.

[122] G. Romano, M. Diaco, and R. Barretta. "Variational Formulation of the First Principle of Continuum Thermodynamics". In: *Continuum Mechanics and Thermodynamics* 22 (2009), pp. 177–187. DOI: 10.1007/s00161-009-0119-z.

[123] T. Rother. *Green's Functions in Classical Physics*. Cham: Springer International Publishing, 2017. ISBN: 978-3-319-52436-8. DOI: 10.1007/978-3-319-52437-5.

[124] T. Rumpel and K. Schweizerhof. "Hydrostatic fluid loading in non-linear finite element analysis". In: *International Journal for Numerical Methods in Engineering* 59.6 (2004), pp. 849–870. DOI: 10.1002/nme.892.

[125] Y. S. Ryu, M. Haririan, C. C. Wu, and J. S. Arora. "Structural design sensitivity analysis of nonlinear response". In: *Computers & Structures* 21.1 (1985), pp. 245–255. DOI: https://doi.org/10.1016/0045-7949(85)90247-0.

[126] A. Saltelli, K. Chan, and E. M. Scott, eds. *Sensitivity Analysis*. Wiley Series in Probability and Statistics. Chichester: Wiley, 2000. ISBN: 0-471-99892-3.

[127] J. L. T. Santos. "Sizing Design Sensitivity Analysis of Linear Steady Heat Transfer Systems Using Established Finite Element Codes". In: *Numerical Heat Transfer, Part B: Fundamentals* 15.1 (1989), pp. 49–71. DOI: 10.1080/10407798909342398.

[128] S. Schwarz. "Sensitivitätsanalyse und Optimierung bei nichtlinearem Strukturverhalten". Ph.D. Thesis. Stuttgart: Universität Stuttgart, 2001.

[129] K. Schweizerhof and E. Ramm. "Displacement dependent pressure loads in nonlinear finite element analyses". In: *Computers & Structures* 18.6 (1984), pp. 1099–1114. DOI: 10.1016/0045-7949(84)90154-8.

[130] E. D. Smith, F. Szidarovszky, W. J. Karnavas, and A. T. Bahill. "Sensitivity Analysis, a Powerful System Validation Technique". In: *The Open Cybernetics & Systemics Journal* 2.1 (2008), pp. 39–56. DOI: 10.2174/1874110X00802010039.

[131] W. Sobek, S. Hagenmayer, M. Duder, and T. Winterstetter. "Die "Highlight Munich Business Towers" in München – Tragwerksplanung und statische Nachweise". In: *Bautechnik* 83.4 (2006), pp. 247–253. DOI: https://doi.org/10.1002/bate.200610022.

[132] I. M. Sobol'. "Global sensitivity indices for nonlinear mathematical models and their Monte Carlo estimates". In: *Mathematics and Computers in Simulation* 55.1 (2001), pp. 271–280. DOI: https://doi.org/10.1016/S0378-4754(00)00270-6.

[133] I. Stakgold and M. Holst. *Green's Functions and Boundary Value Problems*. Hoboken, NJ, USA: John Wiley & Sons, Inc, 2011. ISBN: 9780470906538. DOI: 10.1002/9780470906538.

[134] R. Tomović. *Sensitivity Analysis of Dynamic Systems*. New York: McGraw-Hill Book Co., 1963.

[135] D. A. Tortorelli and Z. Wang. "A systematic approach to shape sensitivity analysis". In: *International Journal of Solids and Structures* 30.9 (1993), pp. 1181–1212. DOI: https://doi.org/10.1016/0020-7683(93)90012-V.

[136] T. Vrouwenvelder. "The JCSS probabilistic model code". In: *Structural Safety* 19.3 (1997), pp. 245–251. DOI: https://doi.org/10.1016/S0167-4730(97)00008-8.

[137] R. Wüchner. "Mechanik und Numerik der Formfindung und Fluid-Struktur-Interaktion von Membrantragwerken". Ph.D. Thesis. Munich: Technical University of Munich, 2006.

[138] B. A. Wujek and J. E. Renaud. "Automatic differentiation for more efficient system analysis and optimization". In: *Engineering Optimization* 31.1 (1998), pp. 101–139. DOI: 10.1080/03052159808941367.

[139] O. C. Zienkiewicz and R. L. Taylor. *The Finite Element Method: The basis*. 5th ed. Vol. 1. Oxford: Butterworth-Heinemann, 2000. ISBN: 0-7506-5049-4.

Bisherige Titel der Schriftenreihe

Band	Titel
1	Frank Koschnick, *Geometrische Lockingeffekte bei Finiten Elementen und ein allgemeines Konzept zu ihrer Vermeidung*, 2004.
2	Natalia Camprubi, *Design and Analysis in Shape Optimization of Shells*, 2004.
3	Bernhard Thomee, *Physikalisch nichtlineare Berechnung von Stahlfaserbetonkonstruktionen*, 2005.
4	Fernaß Daoud, *Formoptimierung von Freiformschalen - Mathematische Algorithmen und Filtertechniken*, 2005.
5	Manfred Bischoff, *Models and Finite Elements for Thin-walled Structures*, 2005.
6	Alexander Hörmann, *Ermittlung optimierter Stabwerkmodelle auf Basis des Kraftflusses als Anwendung plattformunabhängiger Prozesskopplung*, 2006.
7	Roland Wüchner, *Mechanik und Numerik der Formfindung und Fluid-Struktur-Interaktion von Membrantragwerken*, 2006.
8	Florian Jurecka, *Robust Design Optimization Based on Metamodeling Techniques*, 2007.
9	Johannes Linhard, *Numerisch-mechanische Betrachtung des Entwurfsprozesses von Membrantragwerken*, 2009.
10	Alexander Kupzok, *Modeling the Interaction of Wind and Membrane Structures by Numerical Simulation*, 2009.

Band Titel

11 Bin Yang, *Modified Particle Swarm Optimizers and their Application to Robust Design and Structural Optimization*, 2009.

12 Michael Fleischer, *Absicherung der virtuellen Prozesskette für Folgeoperationen in der Umformtechnik*, 2009.

13 Amphon Jrusjrungkiat, *Nonlinear Analysis of Pneumatic Membranes - From Subgrid to Interface*, 2009.

14 Alexander Michalski, *Simulation leichter Flächentragwerke in einer numerisch generierten atmosphärischen Grenzschicht*, 2010.

15 Matthias Firl, *Optimal Shape Design of Shell Structures*, 2010.

16 Thomas Gallinger, *Effiziente Algorithmen zur partitionierten Lösung stark gekoppelter Probleme der Fluid-Struktur-Wechselwirkung*, 2011.

17 Josef Kiendl, *Isogeometric Analysis and Shape Optimal Design of Shell Structures*, 2011.

18 Joseph Jordan, *Effiziente Simulation großer Mauerwerksstrukturen mit diskreten Rissmodellen*, 2011.

19 Albrecht von Boetticher, *Flexible Hangmurenbarrieren: Eine numerische Modellierung des Tragwerks, der Hangmure und der Fluid-Struktur-Interaktion*, 2012.

20 Robert Schmidt, *Trimming, Mapping, and Optimization in Isogeometric Analysis of Shell Structures*, 2013.

21 Michael Fischer, *Finite Element Based Simulation, Design and Control of Piezoelectric and Lightweight Smart Structures*, 2013.

22 Falko Hartmut Dieringer, *Numerical Methods for the Design and Analysis for Tensile Structures*, 2014.

23 Rupert Fisch, *Code Verification of Partitioned FSI Environments for Lightweight Structures*, 2014.

Band Titel

24 Stefan Sicklinger, *Stabilized Co-Simulation of Coupled Problems Including Fields and Signals*, 2014.

25 Madjid Hojjat, *Node-based parametrization for shape optimal design*, 2015.

26 Ute Israel, *Optimierung in der Fluid-Struktur-Interaktion - Sensitivitätsanalyse für die Formoptimierung auf Grundlage des partitionierten Verfahrens*, 2015.

27 Electra Stavropoulou, *Sensitivity analysis and regularization for shape optimization of coupled problems*, 2015.

28 Daniel Markus, *Numerical and Experimental Modeling for Shape Optimization of Offshore Structures*, 2015.

29 Pablo Suárez, *Design Process for the Shape Optimization of Pressurized Bulkheads as Components of Aircraft Structures*, 2015.

30 Armin Widhammer, *Variation of Reference Strategy - Generation of Optimized Cutting Patterns for Textile Fabrics*, 2015.

31 Helmut Masching, *Parameter Free Optimization of Shape Adaptive Shell Structures*, 2016.

32 Hao Zhang, *A General Approach for Solving Inverse Problems in Geophysical Systems by Applying Finite Element Method and Metamodel Techniques*, 2016.

33 Tianyang Wang, *Development of Co-Simulation Environment and Mapping Algorithms*, 2016.

34 Michael Breitenberger, *CAD-integrated Design and Analysis of Shell Structures*, 2016.

35 Önay Can, *Functional Adaptation with Hyperkinematics using Natural Element Method: Application for Articular Cartilage*, 2016.

Band Titel

36 Benedikt Philipp, *Methodological Treatment of Non-linear Structural Behavior in the Design, Analysis and Verification of Lightweight Structures*, 2017.

37 Michael Andre, *Aeroelastic Modeling and Simulation for the Assessment of Wind Effects on a Parabolic Trough Solar Collector*, 2018.

38 Andreas Apostolatos, *Isogeometric Analysis of Thin-Walled Structures on Multipatch Surfaces in Fluid-Structure Interaction*, 2018.

39 Altuğ Emiroğlu, *Multiphysics Simulation and CAD-Integrated Shape Optimization in Fluid-Structure Interaction*, 2019.

40 Mehran Saeedi, *Multi-Fidelity Aeroelastic Analysis of Flexible Membrane Wind Turbine Blades*, 2017.

41 Reza Najian Asl, *Shape optimization and sensitivity analysis of fluids, structures, and their interaction using Vertex Morphing Parametrization*, 2019.

42 Ahmed Abodonya, *Verification Methodology for Computational Wind Engineering Prediction of Wind Loads on Structures*, 2020.

43 Anna Maria Bauer, *CAD-integrated Isogeometric Analysis and Design of Lightweight Structures*, 2020.

44 Andreas Winterstein, *Modeling and Simulation of Wind Structure Interaction of Slender Civil Engineering Structures Including Vibration Systems*, 2020.

45 Franz-Josef Ertl, *Vertex Morphing for Constrained Shape Optimization of Three-dimensional Solid Structures*, 2020.

46 Daniel Baumgärtner, *On the Grid-based Shape Optimization of Structures with Internal Flow and the Feedback of Shape Changes into a CAD Model*, 2020.

47 Mohamed Khalil, *Combining Physics-based models and machine learning for an Enhanced Structural Health Monitoring*,2021.

Band Titel

48 Long Chen, *Gradient Descent Akin Method*, 2021.

49 Aditya Ghantasala, *Coupling Procedures for Fluid-Fluid and Fluid-Structure Interaction Problems Based on Domain Decomposition Methods*, 2021.

50 Ann-Kathrin Goldbach, *The Cad-Integrated Design Cycle for Structural Membranes*, 2022.

51 Iñigo Pablo López Canalejo„ *A Finite-Element Transonic Potential Flow Solver with an Embedded Wake Approach for Aircraft Conceptual Design*, 2022.

52 Mayu Sakuma, *An Application of Multi-Fidelity Uncertainty Quantification for Computational Wind Engineering*, 2022.

53 Suneth Warnakulasuriya, *Development of methods for Finite Element-based sensitivity analysis and goal-directed mesh refinement using the adjoint approach for steady and transient flows*, 2022.

54 Klaus Bernd Sautter, *Modeling and Simulation of Flexible Protective Structures by Coupling Particle and Finite Element Methods*, 2022.

55 Efthymios Papoutsis, *On the incorporation of industrial constraints in node-based optimization for car body design*, 2023.

56 Thomas Josef Oberbichler, *A modular and efficient implementation of isogeometric analysis for the interactive CAD-integrated design of lightweight structures*, 2023.

57 Tobias Christoph Teschemacher, *CAD-integrated constitutive modelling, analysis, and design of masonry structures*, 2023.

58 Shahrokh Shayegan, *Enhanced Algorithms for Fluid-Structure Interaction Simulations – Accurate Temporal Discretization and Robust Convergence Acceleration*, 2023.

Band Titel

59 Ihar Antonau, *Enhanced computational design methods for large industrial node-based shape optimization problems*, 2023.

60 Rishith Ellath Meethal, *Hybrid modelling and simulation approaches for the solution of forward and inverse problems in engineering by combining finite element methods and neural networks*, 2023.

61 Máté Péntek, *Method Development for the Numerical Wind Tunnel in Applied Structural Engineering*, 2023.

62 Anoop Kodakkal, *High Fidelity Modeling and Simulations for Uncertainty Quantification and Risk-averse Optimization of Structures Under Natural Wind Conditions*, 2024.

63 Philipp Bucher, *CoSimulation and Mapping for large scale engineering applications*, 2024.

64 Martin Fußeder, *Methodological and Application-Oriented Advances in Sensitivity Analysis with a Focus on Structural Engineering*, 2024.